Summer 2019

Consequences of in vitro and in vivo environmental cues on localized delivery of MSCs

Anthony John Burand Jr.
University of Iowa

CONSEQUENCES OF *IN VITRO* AND *IN VIVO* ENVIRONMENTAL CUES ON LOCALIZED DELIVERY OF MSCS

by

Anthony John Burand Jr.

A thesis submitted in partial fulfillment
of the requirements for the Doctor of Philosophy
degree in Biomedical Engineering in the
Graduate College of
The University of Iowa

August 2019

Thesis Supervisor: Assistant Professor James A. Ankrum

To my wife Lauren, family, friends, and mentors. It has been a long journey to get here. Thank you for your dedication and support. Without it, I would not be here.

Education is not the learning of facts, it's rather the training of the mind to think.

~Albert Einstein

ACKNOWLEDGEMENTS

I want to thank my advisor, Dr. James Ankrum for all the training and support he has given me over the course of my Ph.D. I know there was a risk and cost involved with taking me on as a graduate student, but I appreciate being given a chance to learn and grow as a researcher under his guidance. Since I was his first graduate student, I have appreciated having the space and opportunity to try a lot of different projects and though them to develop my understanding of the cell therapy field, expand my troubleshooting skills, hone my experimental planning abilities, develop effective methods to teach trainees, and to learn how to manage a laboratory. While this thesis describes the core of my work, I have had the opportunity to substantially contribute on other projects not described in this thesis including MSC manufacturing, single cell barcoding, biomaterials and scaffolds, and *in vitro* modeling of diabetic environments, human adipose tissue, and human islets. I know the breadth of experience is unique and not available in many labs, so I am thankful for my time in his lab. Without his help, this journey in my higher education would not have been possible.

I also want to thank my Ph.D. examining committee members, Dr. Ling Yang, Dr. Edward Sander, Dr. Jon Houtman, and Dr. Kristin Worthington. I am grateful for your time reading and critiquing my research plan, willingness to help me with experiments, provide materials and instruments, and support in my endeavor to complete my degree. You have all contributed insights which facilitated the development of my thesis research. I also want to thank all those who have collaborated with me to help make my time here a success, including Dr. Al Klingelhutz, Dr. Yumi Imai, Dr. Markus Kuehn, Dr. Aliasger Salem, Dr. Julien Sebag, Dr. Donna Santillan, Dr. Alejandro Pezzulo, Dr. Sam Stephens, Dr. Brandon Davies, Dr. Matthew Potthoff, and Dr. Mary Wilson. All of who have provided me with lab space, equipment, and other resources during my Ph.D. There are many others who have helped me generate and develop ideas for my research. I would also like to thank Dr. Raghavan who was a part of my qualifying exam committee.

I would like to thank all my lab mates in the Ankrum lab especially Lauren Boland, Alex Brown, Devlin Boyt, Michael Schrodt, and Yoshi Nagumo. Thank you for all the help with experiments and feedback on my research. Your assistance and comradery have been invaluable

to my success. I also want to thank all my trainees, including Alex Brown, Riley Deutsch, and Lin Di who have put a lot of time into learning and carrying out experiments for me.

I am also thankful and honored by the financial support I received through my training grant. During the 2018-2019 years, my research has been supported by the NIH Ruth L. Kirschstein National Research Service Award (NRSA) Interdisciplinary Training in Pain Research (NS045549). This training grant gave me substantial experience in pain mechanisms via course work and pain seminars as well as experience with patients in the pain clinic at the University of Iowa Hospitals and Clinics.

I am thankful for all my family and friends who are here and who are no longer with us, in Iowa, Minnesota, and elsewhere, for all their support and encouragement during these long five years. I have appreciated all your prayers for me, visits, and listening ears. Thank you to Greg Hanson who has been my mentor for the past few years. I have appreciated his willingness to meet with me to discuss the Bible, hang out, and help my wife and I in our life journey. I want to give a thank you to my in-laws who have taken an interest in my research and really made me feel a part of their family. I especially want to thank my parents and younger brother, Kim, Tony, and Jonas, who helped me make this transition to graduate school and have been there whenever I have needed them. I am immensely grateful for all you have done for me that has made me the person I am today.

Finally, I want to express my appreciation to my wife, Lauren. She has been so supportive and been with me through the hard times. She has stayed up late helping me prepare papers, qualifying exam, comprehensive exam and doing laboratory work, as well as spent countless hours editing my writing and listening to me practice research talks. She has listened to my joys and frustrations and encouraged me to keep going even when I have been discouraged. I am very excited to complete this stage in my education and get to enjoy our life and new baby, Grace Marguerite, together.

ABSTRACT

Mesenchymal stromal cells (MSCs) are being explored for treatment of inflammatory, ischemic, autoimmune, and degenerative diseases. More and more of these diseases require MSCs to be delivered locally to the diseased site rather than systemically injected into patients. However, little is understood about whether cell cryopreservation or prelicensing will affect the efficacy of the locally injected product or how the local injection environment affects MSC expression of trophic factors and interactions with patient immune cells. Several groups have disagreed on whether cryopreservation hinders MSC potency and therefore it is important to understand the effects of cryopreservation on MSC function and in what contexts cryopreservation can be used. Therefore, a better understanding of MSC phenotype after local injection is needed so that cryopreservation and prelicensing can be optimized to modulate cell potency for more efficacious MSC products.

Currently, it has been shown that *in vivo* there are rapid drastic shifts in gene expression by MSCs which have been locally injected. One of the most prominent gene changes is in the enzyme COX-2 which leads to the production of bioactive lipids called prostaglandins, namely PGE2. PGE2 has several functions depending on the context in which other cells encounter it. In order to model the gene changes that occur *in vivo*, *in vitro* cell aggregates termed spheroids have been utilized to study the effects of local injection of MSCs. MSC spheroids have shown more potency than their 2D counterparts in shifting macrophage polarization and rescue of cells from ischemic damage.

This thesis examines how process variables like cryopreservation and prelicensing affect the efficacy of the MSC product in the context of local injection. Additionally, it shows how spheroid formation alters therapeutic factor expression and activity and how drug treatment and biomaterials can be utilized to modify potency of these cells. In Chapter 2, we demonstrate that cryopreservation in the context of an ischemia/reperfusion injury in the eye does not significantly decrease MSCs effectiveness in salvaging neuronal cells. However, IFN-γ, a commonly used prelicensing cytokine to increase MSC potency, led to a decrease in the effectiveness of MSCs in this model. Chapters 3 and 4 define the changes that occur to several of MSCs' trophic factors including immunomodulatory and growth factors and how these alterations affect MSC interactions with macrophages and T cells. Because validation and tracking of locally injected

products can be cost-prohibitive for many research groups, Chapter 5 lays out a low-cost method to track fluorescently labeled cells in local injections to skin to aid in minimization of variability in results obtained from animal wound healing models.

These findings demonstrate that initial preparation of MSC therapeutics is critical to their efficacy in local injection. Therefore, careful testing of potency for large-scale MSC production pipelines should be evaluated to ensure the efficacy of the resulting product. Additionally, spheroids exhibit differences in the mechanisms of action due to alterations in their secretome which can be partly overcome with co-administration of steroids such as budesonide. Therefore, steroid co-administration with MSCs being considered for local application should be further explored for use in local delivery of MSCs for the treatment of inflammatory conditions. Finally, this research demonstrates the need to further understand the mechanisms by which spheroids alter their gene and trophic factor production to better tailor MSC therapies for disease specific localized injection.

PUBLIC ABSTRACT

Mesenchymal stem cells (MSCs) have shown promise in treating a number of diseases such as stroke, diabetic wounds, and Crohn's disease in both animal models and recent clinical trials. Many of these diseases require MSCs to be injected locally into the diseased tissue rather than into the blood stream. After local injection into the patient, MSCs form clumps of cells and behave differently than MSCs grown as sheets in the laboratory. However, most research being performed only tests how cells perform as sheets and little is known about how the assembly of these cells into 3D structures alters their interaction with the patient's own cells after injection into the body. The goal of my research is to understand how changes in MSCs due to their new structure affect their ability to treat inflammation and regenerate damaged tissue. Additionally, my research looks to understand how our manufacturing of the cells before injection into patients affects their effectiveness. I have found that appropriate preservation of these cells in frozen cell banks does maintains their performance in a model of acute ischemic eye injury. However, treatment of MSCs with inflammatory molecules normally found to enhance MSC performance, leads to a decreased performance of the cells in my acute ischemic eye injury model. I found that the therapeutic factors produced by the MSCs are dramatically altered when I model local injection and these changes negatively impact MSCs' interactions with immune cells. I proposed use of a co-administered steroid, budesonide, with the locally injected MSCs to rescue some lost effectiveness of the MSCs in suppressing immune cells like T cells. By understanding how locally injected MSCs alter their characteristics and interactions with immune cells as well as how the MSC function is affected by manufacturing and preservation parameters, we will be able to develop better MSC therapies to regenerate damaged tissue in patients.

TABLE OF CONTENTS

LIST OF TABLES xi

LIST OF FIGURES xii

CHAPTER 1: INTRODUCTION 1

1.1. OVERVIEW 1

1.2. INTRODUCTION TO MESENCHYMAL STROMAL CELLS AND THEIR USE IN TREATING DISEASE 2

1.3. BIOMANUFACTURING OF MESENCHYMAL STROMAL CELLS PRIOR TO TRANSPLANT 8

1.4. LOCAL INJECTION OF MESENCHYMAL STROMAL CELLS 14

1.5. TRACKING AND VALIDATION OF LOCAL DELIVERY OF MESENCHYMAL STROMAL CELLS 21

1.6. CHAPTER SUMMARY 23

1.7. REFERENCES 26

CHAPTER 2: *IN VITRO* PROCESSING MODULATES MESENCHYMAL STROMAL CELL POTENCY PRE-TRANSPLANT 33

2.1. OVERVIEW 33

2.2. CRYOPRESERVATION DOES NOT NEGATIVELY IMPACT MSC POTENCY IN ISCEMIA/REPERFUSION INJURY 34

2.3. PRELICENSING MSCS WITH IFN-γ HINDERS FUNCTION IN ISCHEMIA/REPERFUSION INJURY 64

2.4. REFERENCES 72

CHAPTER 3: AGGREGATION OF MESENCHYMAL STROMAL CELLS MODULATES THEIR FUNCTION 78

3.1. OVERVIEW 78

3.2. MSCS ACTIVATE A PGE2-EP RECEPTOR AUTOCRINE FEEDBACK LOOP 79

3.3. MSC AGGREGATES ALTER THROPHIC FACTOR EXPRESSION, INCREASE ER STRESS, DECREASE METABOLIC FUNCTION, AND INCREASE SUSCIPTABILITY TO PALMITATE DAMAGE 83

3.4. REFERENCES 102

CHAPTER 4: AGGREGATED MESENCHYMAL STROMAL CELLS DEMONSTRATE ALTERED INTERATIONS WITH IMMUNE CELLS.....105

4.1. OVERVIEW 105

4.2. AGGREGATED HUMAN MESENCHYMAL STROMAL CELLS LOSE THE ABILITY TO SUPPRESS T CELLS BUT REGAIN IT VIA SYNERGY WITH BUDESONIDE 106

4.3. REFERENCES 146

CHAPTER 5: LOCALLY INJECTIONED CELLS LABELED WITH A FLUORESCENT DYE CAN BE TRACTED WITH A LOW-COST INTRAOPERATIVE TECHNIQUE 151

5.1. OVERVIEW 151

5.2. A LOW-COST TECHNIQUE FOR INTRAOPERATIVE IMAGING OF CELL DELIVERY AND RETENTION IN A MODEL OF DELAYED WOUND HEALING 152

5.3. REFERENCES 175

APPENDIX A: TECHNIQUES FOR CREATING AND ANALYZING MESENCHYMAL STROMAL CELL SPHEROIDS *IN VITRO* 176

A.1. OVERVIEW 176

A.2. METHODS FOR FORMING SPHEROID MSCS 177

A.3. METHODS FOR EXTRACTING RNA FROM SPHEROID MSCS 194

A.4. RAPID ESTIMATION OF MSC SIZE AND CELL NUMBER USING IMAGEJ.....204

A.5. REFERENCES.....213

APPENDIX B: CELLULAR ENGINEERING METHODS CAN ALTER MSC PHENOTYPE 214

B.1. OVERVIEW.....214

B.2. MSC PHENOTYPE CAN BE MODULATED WITH BIOMATERIALS 215

B.3. REFERENCES.....224

LIST OF TABLES

Table 1. Growth factor array data for 40 growth factors. 61

Table 2. List of human primers. 141

Table 3. Comparison of imaging modalities. 169

Table 4. Selection of compatible fluorescent tracers (pros/cons). 172

Table A.1. Troubleshooting spheroid formation methods. 184

Table A.2. Comparison of common *in vitro* spheroid forming techniques. 190

Table A.3. Troubleshooting spheroid RNA extraction methods. 197

Table A.4. Comparison of Trizol and direct lysis techniques. 203

LIST OF FIGURES

Figure 1. Cryopreservation marginally affects MSC viability and metabolic activity. 44

Figure 2. Cryopreserved MSC maintain immunosuppressive potential. 47

Figure 3. Cryopreservation minimally impacts baseline or stimulated growth factor secretion by MSC. 50

Figure 4. Locally administered MSCs form aggregates in a simulated vitreous. 52

Figure 5. Cryopreserved MSC prevent RGC loss after ischemia/reperfusion injury *in vivo*. 53

Figure 6. Cryopreserved MSC do not persist in the eye following ischemia/reperfusion injury. 55

Figure 7. IDO production remains consistent after cryopreservation. 63

Figure 8. IFN-γ priming enhances IDO expression of cryopreserved MSCs *in vitro* but is detrimental to MSC performance in an ischemia/reperfusion injury *in vivo*. 68

Figure 9. Tailoring MSCs to fit the disease. 71

Figure 10. *In vitro* MSC spheroid aggregation leads to upregulation of PGE2 receptors 2/4 to detect synthesized PGE2. 81

Figure 11. MSC spheroids alter gene expression over time. 88

Figure 12. Spheroid MSCs upregulate ER stress genes. 89

Figure 13. ROS is not significantly upregulated in spheroid MSCs. 90

Figure 14. Spheroid formation lowers metabolic function in MSCs. 92

Figure 15. Palmitate negatively affects spheroid MSC viability. 94

Figure 16. Palmitate affects spheroid MSCs metabolic function more than adherent MSCs. 95

Figure 17. Spheroid MSCs show altered uptake of palmitate. 96

Figure 18. MSC spheroid gene expression varies over time. 99

Figure 19. Adherent and spheroid MSC expression or ER stress genes and ROS. 100

Figure 20. Similar numbers of adherent and spheroid MSCs attach to tissue culture plastic. 101

Figure 21. Mechanism of spheroid MSC-budesonide synergistic suppression of T cells. 107

Figure 22. Isolated umbilical cord cells meet the minimal MSC criteria. 110

Figure 23. MSC spheroids do not suppress activated PBMCs. 114

Figure 24. Spheroid MSCs alter macrophage phenotype. 115

Figure 25. Spheroid MSCs show decreased viability compared to adherent MSCs. 116

Figure 26. Spheroid dose and contact factors do not explain lack of PBMC suppression. 118

Figure 27. Spheroid MSCs display an altered immunomodulatory profile. 119

Figure 28. Budesonide synergizes with spheroids to suppress PBMC proliferation. 122

Figure 29. Spheroid MSCs with budesonide affect PBMC production of cytokines. 124

Figure 30. Budesonide treatment of spheroid MSCs does not restore kynurenine production. . 125

Figure 31. Spheroid produced PGE2 levels alone are not sufficient to suppress PBMCs..... 127

Figure 32. Spheroid PGE2 synergizes with budesonide via EP2/4 receptors on T cells. 128

Figure 33. Budesonide and EP inhibitors do not affect PBMC proliferation alone. 130

Figure 34. Magnification can be set on the Dino-Lite system to optimize working distance (WD), field of view (FOV), and fluorescent intensity. 159

Figure 35. DiR/mCherry stained MSCs display a dose dependent fluorescent signal *in vitro* via both Odyssey and Dino-Lite imaging. 160

Figure 36. Dino-Lite and Odyssey quantification of MSC fluorescence shows a similar dose dependence *in vivo*. 162

Figure 37. Injection depth impacts MSC fluorescent intensity and distribution of signal. 164

Figure 38. Dino-Lite imaging to document and characterize quality of cell application *in vivo*. 165

Figure 39. Fluorescently labeled MSCs can be tracked multiple days *in vivo*. 167

Figure 40. Workflow to tailor cell labeling and handheld microscope parameters to study needs. 170

Figure A.1. Spheroids can be made through several methods. 187

Figure A.2. Assays must be optimized for use with spheroid MSCs. 191

Figure A.3. RNA yield from spheroid MSCs can be improved through cell disruption. 199

Figure A.4. MSC donor, cell number, and spheroid size lead to variability in RNA yield. 200

Figure A.5. Direct lysis of spheroid MSCs can be used to extract RNA. 202

Figure A.6. Pseudoislets exhibit a narrower size distribution compared with cultured-intact islets. 207

Figure A.7. ImageJ macro measures spheroid size from Leica z-stack .lif files. 209

Figure A.8. Macro defined spheroid boundaries can be manually reviewed by the user. 210

Figure A.9. Auto-threshold misidentification of cell mass can be corrected with a manual threshold. 211

Figure B.1. Spheroid MSCs do not alter secretion of factors in response to IFN-γ. 220

Figure B.2. Alginate encapsulation of MSCs modulates their phenotype. 221

CHAPTER 1: INTRODUCTION

1.1. OVERVIEW

The purpose of this chapter is to give the reader an overview of MSCs, their local application to treat disease, and the challenges associated with optimizing MSCs for localized injection. This includes a description of their immunomodulatory and regenerative properties, how MSC products are produced for clinical applications, challenges involving creating a MSC product for local injection, and how changes to MSC phenotype upon local injection alter their potency. Additionally, I briefly describe the common techniques used to ensure appropriate delivery of locally injected MSCs both in the clinic and in basic research. This chapter ends with a general summary of the chapters and appendices of the thesis detailing the primary focus and findings of this thesis.

Contributors: Anthony J. Burand Jr, Lauren Boland, Devlin Boyt, Michael Schrodt, and James A. Ankrum

1.2. INTRODUCTION TO MESENCHYMAL STROMAL CELLS AND THEIR USE IN TREATING DISEASE

A brief history of mesenchymal stromal cells

Mesenchymal stromal or "stem" cells (MSCs) have been studied for over 40 years and have become increasingly prevalent in research over the past decade. Alexander J. Friedenstein is credited with the official discovery of this cell type, isolating, culturing, and differentiating MSCs from bone marrow.[1] Since his initial discovery, a basic definition of these cells has been established as cells that adhere to tissue culture plastic, show positive expression for the surface markers CD73, CD90, and CD105, do not express CD45, CD34, CD14, CD11b, CD79α, CD19, and HLA-DR, and can differentiate into osteoblasts, adipocytes, and chondroblasts.[2] While originally discovered in bone marrow aspirate, MSCs have been isolated from most human tissues and organ systems including white adipose tissue, dental pulp, Wharton's jelly in umbilical cords, muscle, and even peripheral blood. MSCs are often associated with vasculature within these different organ systems and exhibit pericyte behavior through their support of blood vessel structures.[3] However, they also can exist outside the vascular space. Although a consensus has been reached regarding minimal features of MSC identification, full phenotypic characterization and *in vivo* study of MSCs is an active and ever-evolving area of investigation in the MSC field.

Two key properties of MSCs have been harnessed for use in pre-clinical and clinical trials: their differentiation capacity and their trophic factor production. It has been well established that MSCs can differentiate into osteoblasts, adipocytes, chondroblasts, and myocytes.[2,4,5] Therefore, many groups have sought to use these cells for repair of bone defects, cartilage replacement, studying fat *in vitro*, heart muscle repair, among other applications. Initial interest in the therapeutic use of MSC capitalized on their osteogenic ability for use in treatment of bone disorders, such as osteogenesis imperfecta and osteoporosis. While this has continued to be an area of MSC research, most clinical applications depend on trophic factor generation by MSCs in their undifferentiated state. MSCs produce a host of antimicrobial molecules, growth factors, immunomodulatory proteins, angiogenic molecules, and anti-apoptotic factors. Collectively these trophic factors are comprised of small molecules, micro-RNAs, proteins, peptides, and exosomes. The trophic factors that MSCs produce have been shown to modulate

the host healing response to ischemic injury, as well as modulate immune cell inflammation. Although *in vitro* and *in vivo* preclinical models have demonstrated the essential role of these trophic factors, there remains a substantial fraction of patients who do not respond to MSCs therapies. The potential methods by which MSCs modulate pro-regenerative and angiogenic outcomes in the host are numerous. However, substantial questions regarding which mechanisms are essential to mediate MSC therapeutic benefits and how these mechanisms are altered by the biomanufacturing/development of MSC products and the host environment into which the cells are transplanted remains to be answered.

Cells isolated from bone marrow, umbilical cords, and adipose tissue all meet the minimal criteria for classification as MSCs. Recently, however, several groups have shown that MSCs isolated from different tissue sources exhibit differences in gene expression, protein expression, and function that is not captured by the minimal criteria. Sacchetti *et al.* found that bone marrow, muscle, periosteum, and cord blood derived MSCs have gene expression profiles from total exome sequencing that cluster separately when condensed into principle component plots (PCA analysis), indicating unique tissue specific features of MSCs.[6] Furthermore, they found that particular gene sets were enriched in MSCs isolated from particular tissue sources. For example, cord blood MSCs show higher numbers of transcripts related to cell cycle regulation, while muscle derived MSCs expressed genes related to muscle development even after 2 weeks in culture.[6] These findings reveal that the phenotype of MSCs is tissue-specific and that extended culture time does not erase the "memory" of the original tissue source. Similarly, Wagner *et al.* showed differential expression of genes involved in ECM, cell signaling, cell growth, and transcription factors, when comparing adipose-, cord blood-, and bone marrow-derived MSCs.[4] Interestingly, of the genes either two-fold upregulated or down regulated, all MSCs showed similar expression profiles but the degree to which these genes were expressed was influenced by tissue source. In addition, the researchers assessed MSCs from a single bone marrow source processed under two different culturing methods and found that the two MSC products had different gene expression profiles. Under one culture condition, bone marrow MSCs showed a gene profile similar to cord blood MSCs. In the other culture condition, the same donor cells more closely clustered with adipose-derived MSCs by hierarchical clustering. These findings highlight the growing understanding in the MSC field that tissue source, donor, and isolation process all have substantial effects on MSC phenotype. Given the range of factors

that influence MSC phenotype, as well as the growing use in clinical trials of MSCs isolated from a variety of tissue sources, it has become increasingly important to understand, control, and optimize the influence of these modifying factors on MSC therapeutic potency.

There have been several key discoveries made in the past decade which have enhanced our understanding of how MSCs exert trophic effects to suppress inflammation and promote growth and regeneration of damaged tissues. Despite the increased knowledge about MSCs, there are still challenges ensuring the effectiveness of the therapy for patients.

Advantages of using living mesenchymal stromal cells as therapeutics

The use of proteins and small molecules harvested from MSCs, known as MSC conditioned media, is an appealing alternative to cell-based therapies as it does not require live cell transplant into patients and the composition of the therapeutic product can be tightly controlled and easily regulated. While conditioned media products have been shown to be advantageous and promote regeneration of tissues, they suffer from two major deficiencies. One deficiency is that conditioned media alone only partly replicates the therapeutic potential of transplanted cells, due to the absence of essential immune-modifying contact factors (i.e. programmed death ligand 1 or PD-L1) expressed on the surface of MSCs.[7–9] Secondly, while live cells can continue to produce trophic factors after injection, conditioned media products can be quickly cleared from the body and can therefore require multiple therapeutic applications. In the case of diabetic wounds, the site of injury is easily accessible and therefore multiple applications of conditioned media may be reasonable. However, for disease indications where the site of injury is not superficially exposed, such as stroke or myocardial infarction (MI), multiple applications of conditioned media may require multiple surgical procedures, which may unnecessarily increase a patient's susceptibility to injury and infection. Therefore, the choice of live cell therapy versus conditioned media is highly dependent on the specific pathophysiology or the disease being treated and warrants an increased understanding of the disease-specific considerations in order to optimize therapeutic efficacy.

The ability of living MSCs to sense and respond to the local human microenvironment is both a notable strength and predominant weakness of this therapeutic modality, as will be discussed in greater detail in Chapter 1.4. While there are significant advantages to therapeutic products which respond to inflammatory and damage-associated molecular patterns (DAMPs),

these cues can also alter MSC therapeutic efficacy. For example, while MSCs are often observed to be anti-inflammatory, when treated with the inflammatory mediator TNF-α alone, MSCs were shown to upregulate several pro-inflammatory chemokines and cytokines resulting in monocyte recruitment and a failure to reduce myocardial scarring after ischemic myocardial injury. However, when these pro-inflammatory mediators were blocked via treatment with an NF-κB inhibitor loaded into microparticles, MSC recruitment of monocytes and myocardial scarring decreased. Therefore, it is essential to gain an understanding of how specific components of a microenvironment modify MSC therapeutic mechanisms in order to engineer strategies to enhance MSC performance in damaging environments.

Mesenchymal stromal cell treatment of ischemia/reperfusion injury

Ischemia/reperfusion (I/R) injury is the underlying pathology of many of the leading causes of death in the United States, including stroke, diabetes, and heart disease. Current therapies for the treatment of I/R typically inhibit the early fallout of I/R injury, thereby limiting tissue damage, but are unable to help restore or regenerate tissue function post-injury. Without tissue regeneration, these injured tissues have depressed native function resulting in increased morbidity and mortality in patients. Therefore, there is a significant need to develop regenerative therapies that can reduce the debilitating effects of ischemia/reperfusion injury. One property that makes MSCs desirable as a cell therapy for the treatment of I/R is their ability to produce secreted factors that modify the response of other cells in their environment. Several researchers have shown that MSCs reduce apoptosis in I/R injured cells such as renal cells, endothelial cells, and neurons, demonstrating MSC rescue of host cells from apoptosis. Additionally, MSCs promote regeneration of damaged tissue, including proliferation of fibroblasts and keratinocytes. Therefore, knowledge of MSC methods of action and ways to engineer MSC trophic factor production is critical in enhancing their use in I/R injury.

In addition to the treatment of I/R injury, MSCs have been investigated in clinical trials for the treatment of many immunopathologies and/or diseases with an immunopathological component, as is the case in I/R. MSCs utilize immunomodulatory factors such as indoleamine-2,3-dioxygenase, an intercellular enzyme that metabolizes tryptophan to the powerful immunomodulatory factor kynurenine (KYN), to suppress the proliferation and effector function of T helper cells (Th1/2) possibly through the promotion of T cell anergy.[10] Additionally, KYN

produced by MSCs can increase the number and suppressive function of FOXP3+ regulatory T cells, a specialized T cell that promotes peripheral tolerance. When IDO activity is blocked using a competitive inhibitor such as 1-methyl-tryptophan, some of the suppressive effects in MSCs are lost. However, there is evidence that suggests a more complex regulation of T cells outside of the IDO-KYN axis alone. Francois *et al.* demonstrated that in peripheral blood mononuclear cells, which contain T cells, B cells, NK cells, monocytes, and dendritic cells, MSCs suppressed inflammatory response from T cells. However, if CD14+ cells of the monocyte lineage were depleted, MSCs were less effective at suppressing T cell proliferation and inflammatory cytokine production.[11] This loss of MSC suppression varied dependent on the MSC donor used in the assay. This finding suggests that the mechanisms by which MSCs regulate immune cell activation can occur through third-party effects, i.e. MSCs alter the phenotype of one immune cell type which then alters the behavior of the final effector immune cell of interest. Additionally, although the IDO-KYN axis has been extensively investigated as the major pathway by which MSCs modify immune cell activation, inherent differences in MSC donors and tissue sources may select for MSCs that favor certain pathways of suppression. In addition to IDO, MSCs can produce many other immunomodulatory factors including IL-6, TGF-β, PGE2, and TSG-6, which have been shown to play roles in dendritic cell maturation, macrophage polarization, and NK activity. Communication across immune cell subpopulations is highly complex. Therefore, the ability of MSCs to affect multiple immune cell populations through a host of different factors gives them a notable benefit for their use in the treatment of complex immune/inflammatory diseases.

In addition to MSCs' immunomodulatory ability, MSCs can support tissue regeneration. MSCs produce high levels of vascular growth factors, such as VEGF, which can induce budding and growth of new vasculature. The development of new vasculature after tissue injury is a critical feature to reestablishing native tissue function. Neuroprotective factors produced by MSCs like BNDF, PGE2, and PDGF, have been shown to increase neuronal survival though activation of anti-apoptotic pathways.[12–14] Additionally, MSCs have been shown to decrease neural inflammation, as well as block the activation and proliferation of astrocytes.[15] In the context of wound healing, MSCs promote wound closure through enhancing fibroblast and keratinocyte proliferation. The ability of MSCs to support revascularization and to promote survival of the primary cells of the tissue (i.e. parenchymal cells) is an integral feature of their

therapeutic potency, particularly in the treatment of diseases in which the innate regenerative ability of the injured tissues is limited.

The pathology of ischemic injury is complex, involving spatiotemporally distinct stages. Although the initial ischemic event results in lack of blood flow to the tissue, the coordinated response to this event involves the parenchymal cells of the tissue (e.g. neurons, keratinocytes, or cardiomyocytes), resident immune cells (e.g. macrophages and microglia), peripherally recruited immune cells, vasculature, as well as stromal cells (e.g. fibroblasts and MSCs). Lack of blood flow to the region leads to cell death and often over-activation of macrophages which can cause prolonged damage.[16–19] MSCs are a highly attractive cell therapy for the treatment of ischemic disease because their multimodal influence on other cell types enables them to stabilize existing vasculature, blunt immune cell activation, and promote cell survival or regeneration, thus addressing multiple aspects of I/R pathology.

1.3. BIOMANUFACTURING OF MESENCHYMAL STROMAL CELLS PRIOR TO TRANSPLANT

Use of autologous and allogeneic mesenchymal stromal cell products

To scale MSC products for treatment of patients in the clinic, two schools of practice are currently employed for obtaining MSCs for treatment: autologous and allogeneic therapies. Autologous or "from self" therapies involve the isolation of cells directly from the patient. After isolation, MSCs are expanded *ex vivo* to generate enough cells for a dose and then transplanted back into the same patient. Because cells are taken directly from the patient, there is no mismatch of MHC class I and II proteins encoded by the HLA alleles, which are major drivers of transplant rejection. The absence of HLA mismatch is the distinct advantage of using an autologous approach in that the risk of rejection by the host immune system is completely mitigated. While there are only three major class I and five class II alleles in the human genome, the thousands of possible variants for each makes it difficult and at times impossible to find good transplant matches for patients, even when familial sources are available. However, there are several disadvantages to autologous MSC therapies, including lengthy expansion times, the need for specialized facilities to extract as well as culture the cells, and the scalability of the therapy. Given the need to individually isolate, expand, and validate patient cells on site in GMP culture facilities, autologous MSC therapies are often quite expensive. In addition to the high cost, the lack of immediate availability (due to extended time for cell expansion) makes the application of autologous therapies for the treatment of many ischemic and inflammatory diseases not possible. In diseases such as stroke, myocardial infarction, GvHD, and critical limb ischemia, significant tissue damage can occur over a short window of time and is often irreversible, therefore application of a therapy is needed quickly. Another difficulty with autologous therapies is that if a patient's MSCs are not effective or potent due to cellular stress or lower production of trophic factors, the patient's own cells may not be effective to treat their disease. Notably, several diseases, including obesity and type 2 diabetes, have been shown to dampen the therapeutic efficacy of MSCs when applied autologously.[20,21] Therefore, although autologous MSCs have distinct advantages, careful consideration must be paid to the timeline of therapeutic administration, as well as the influence of patient comorbidities on the effectiveness of the intervention.

In order to minimize MSC therapy costs, ensure cell potency, and provide immediately accessible off-the-shelf therapies, many industry leaders have turned to allogeneic MSC sources. Here, MSCs are isolated from donors, *ex vivo* expanded, and then "banked" via cryopreservation until provided to clinics at point-of-care. This approach allows companies the time to expand large numbers of MSCs from a few select individuals to treat a broad range of patients. Additionally, the extended lead time between isolation and clinical need in allogeneic approaches allows for more rigorous validation of key features that could identify and select for highly potent and phenotypically consistent MSCs. In fact, screening of immunomodulatory performance through *in vitro* potency assays and the development of predictive metrics for MSC performance has become a critical focus for both industry and regulatory bodies as the use of MSC therapy has expanded. A major concern with an allogeneic strategy of MSC therapy is the potential threat of immune rejection. However, because MSCs suppress immune cells, MSCs can evade the host immune system and provide a therapeutic effect even though they would otherwise be recognized as foreign. Longitudinal studies of patients treated in clinical trials of MSC therapy have shown development of allo-antibodies[22] to donor MSC antigens, signifying a host-mediated alloreactive response against mismatched MSCs; however, this finding does not correlate with decreased therapeutic efficacy, indicating at present, that alloreactivity does not dictate the safety or effectiveness of MSC therapy.[23–25] Overall, despite the difficulties of implementing allogeneic MSC therapy, this course of treatment remains the most feasible option, clinically.

Isolation of mesenchymal stromal cells

MSC can be isolated from several tissue sources, but the most common sites are bone marrow, adipose tissue, and umbilical cord due to the relative abundance of the cells in these locations and the ease of acquiring these tissues. Historically, bone marrow MSCs have been most widely used in clinical trials and are the leading MSC product candidates for FDA approval and clinical use (e.g. Prochymal by Osiris and Rexlemestrocel-L by Mesoblast). Isolation and purification from non-MSC cellular contaminants are particularly important given the heterogeneous cell populations of bone marrow, adipose tissue, and umbilical cords, with parenchymal cells, leucocytes, erythrocytes, granulocytes, platelets, and hematopoietic stem cells often making up the non-MSC component of these tissues. For bone marrow MSC isolation,

MSCs are extracted though puncture of the iliac crest and then the aspirate is plated into MSC selection media before *ex vivo* expansion.[26,27] Adipose-derived MSCs are typically isolated from tissues removed during surgical procedures with post-processing of the tissue typically performed enzymatically followed by crude fractionation. Finally, umbilical cord MSCs are isolated from Wharton's Jelly through tissue explant or enzymatic digestion. Once cells are extracted a variety of processing steps occur, including *ex vivo* expansion under particular media additives, including both fetal bovine serum and xeno-free supplements such as human serum, platelet lysate, and synthetic chemically defined serum. Most GMP manufacturing facilities utilize either human derived serum products or synthetic serum to avoid any potential contamination with xenogeneic proteins and other pathogens and to get rapid growth of cells. Additionally, to increase initial purity of the isolated product, MSC enrichment methods such as CD271 microbeads or FACS sorting can be used to increase the initial proportion of MSCs in bone marrow aspirate from <0.1% of total cells to 5-10% or higher. While pre-enrichment can substantially increase the initial purity of the harvested sample, it is expensive and therefore is typically not widely used. Although there is a similar pattern of isolation strategy across the three tissue sources, methods and reagents used post-isolation vary widely and can critically alter the final cell product.

Expansion of mesenchymal stromal cells

A high yield of MSCs from donors is often important for two reasons. First, patients need to be treated with tens of millions of MSCs in order to receive a therapeutic benefit. A commonly used dose in graft vs host disease is 1 million cells per kg, which for an average weight individual in the United States is approximately 80 million MSCs. If multiple administrations of MSCs are required, this cell requirement can quickly grow. The difference between the initial amount of cells isolated (e.g. ~100,000 cells from bone marrow collection) and the clinical dose required necessitates at least a hundred-fold increase in cell number.[28] Secondly, a major advantage in allogeneic therapy is the ability to use one donor for the treatment of multiple patients, which greatly decreases the overall cost of the therapy thereby enabling a larger breadth of patients to ultimately be treated. The importance of high cell yields for patient treatment demands that care be applied in the choice of expansion parameters used.

There are several methods to expand MSCs with the most common being through expansion on tissue culture plastic, particularly in academic research settings. While tissue culture plastic is often sufficient for research purposes, this method is time intensive and costly. Therefore, bioreactor systems are often used to perform large scale expansions more quickly. Some of the more common bioreactor technologies include multi-layered culture flasks, stir tank bioreactors, hollow fiber bioreactors, and packed bed bioreactors.[29] A common feature of these bioreactor systems is to enhance surface area for cell growth while also decreasing costly reagent use. Additionally, all of these set-ups have been shown to produce a 6-10-fold increase in cell number within 5-7 days of culture, which is greater than what can be done monolayer. Technologies including multilayered flasks and small stir tank-microcarrier bead systems, require minimal specialized culture vessels while packed bed, hollow fiber, and industrial sir tank require >100,000 USD specialized bioreactors making them not accessible to many researchers and small startup companies. However, in largescale production, partly automated bioreactors including industrial stir tank and packed bed reactors can minimize the requirements for operators and significantly streamline the production process. While optimizing MSC expansion and yield has been a desirable goal for industry in order to decrease cost of therapy, several concerns regarding the preservation of therapeutic efficacy in over-expanded MSC products have arisen.

Although termed “stem cells”, MSCs are a multipotent adult stem cell population which makes them subject to replicative senescence upon over-expansion. In retrospective studies of clinical trials of MSC therapy for GvHD, there has been a clear survival advantage for patients receiving low passaged MSCs compared to those who received high passaged MSCs.[30] Several groups have shown that overly expanded MSCs have lower secretion rates of critical immunomodulatory factors like kynurenine, as well becoming pro-inflammatory cells characterized by a senescence-associated secretory phenotype (SASP).[31] These notable alterations in MSC phenotype may account for the drop of therapeutic efficacy observed in GvHD clinical trials. These findings indicate that therapeutic efficacy is directly tied to the degree of MSC expansion, therefore it is critical to determine the optimal balance between expansion and cell efficacy.

Cryopreservation of mesenchymal stromal cells

A crucial component of allogeneic, off-the-shelf MSC therapies is the ability to reliably store cells prior to clinical use, which involves intermediate cryostorage. Cryopreservation enables a broader range of patients and diseases to be treated, because point-of-care usage is not delayed by expansion of cells, as is the case in autologous therapy. Cell therapies need to be produced within good manufacturing practice (GMP) facilities. To enable on-site development of either autologous or allogeneic therapies, hospitals need to invest a substantial sum of money in developing these facilities, which often makes using a commercialized allogeneic source more financially feasible. There is both an economical argument for the benefit of off-the-shelf MSC therapies, as well as a logistical need in the treatment of ischemic diseases due to the short treatment window required. As discussed previously, ischemic diseases require immediate treatment after injury to salvage function of damaged tissue and MSCs are uniquely equipped to treat ischemic disease given their pro-regenerative, immunomodulatory, and angiogenic properties. In the case of stroke, treatment must be administered in less than 6 hours after the onset of the ischemic event or significant irreversible damage is incurred. Therefore, MSC therapy for ischemic disease necessitates having an off-the-shelf (i.e. cryopreserved) product to be immediately available. However, cryopreserved MSCs must be both viable and potent coming out of cryopreservation, otherwise the inherent advantage of off-the-shelf MSCs is lost.

Several groups have disagreed on whether cryopreservation hinders MSC potency. [32,33] MSCs used in treatment of GvHD tend to have more favorable outcomes when applied fresh rather than directly out of cryopreservation.[34] Other groups have shown that upon thaw, cryopreserved MSCs can have low viability (<70%), decreased IDO activity possibly due to cryopreservation activation of heat-shock proteins, and can be cleared by CD8 T cells significantly faster than their fresh counterparts.[32,33] In contrast, cryopreservation techniques which demonstrate high viability post-thaw maintain MSC IDO activity and suppression of activated T cell proliferation.[35] Additionally, I have shown that there is a slight deficiency in viability and metabolic function of cryopreserved MSCs. However, both cryopreserved and fresh MSCs produce trophic factors and suppress activated peripheral blood mononuclear cells (PBMCs) equally.[36] A stark contrast exists in the methods and reagents used to cryopreserve MSCs in studies showing a detrimental effect versus benign effect. Therefore, the method of

cryopreservation appears to play a critical role in ensuring that MSCs are highly functional and potent post-thaw.

Priming mesenchymal stromal cells to enhance function

High variability in the efficacy of MSC products has been proposed as a major reason for inconsistencies between results in preclinical models and clinical trial outcomes. In order to address this inconsistency, several methods are being explored to improve allogeneic MSC potency and to maintain this potency post-transplant. Many techniques, including viral transduction, priming MSCs with small molecules or cytokines, using biomaterials to manipulate the mechanical properties of the transplant environment, hypoxic conditioning, and nutrient starvation have been explored to enhance MSC potency.[37–39] By far the most common method used is priming or "pre-licensing" MSCs with combinations of inflammatory cytokines, including IFN-γ, TNF-α, IL-6, and IL-1β. MSCs pre-licensed with IFN-γ (PL-MSCs) have been shown to increase production of immunomodulatory factors such as IDO, kynurenine, PGE2, HGF and TGF-β.[40,41] Additionally, PL-MSCs have been shown to increase suppression of T cells and induce T regulatory (Treg) differentiation.[40,42] Several groups have also used PL-MSCs in pre-clinical models and have shown improved outcomes in critical limb ischemia and GvHD leading to lower limb amputation and increased tolerance to bone marrow transplant, respectively.[43,44] Together this data suggests that pre-licensing of MSCs is a powerful technique to push MSCs toward a tolerogenic, pro-regenerative phenotype.

1.4. LOCAL INJECTION OF MESENCHYMAL STROMAL CELLS

Benefits to local delivery of mesenchymal stromal cells

Local delivery of MSCs is being explored for several diseases including Crohn's disease, multiple sclerosis, rheumatoid arthritis, and diabetic wounds to improve MSC efficacy and reduce undesirable outcomes. While systemic infusion into patients has been used for many years, many clinical trials place MSC products directly at the sites of injury or damage to increase efficacy and avoid possible emboli formation seen with systemic infusion. Despite these potential benefits, in many cases, it is unclear if localized delivery of MSCs is advantageous over systemic administration. Although local injection is frequently used (~50% of clinical trials), little is known about how processing of MSCs prior to transplant affects their efficacy after localized injection into patients.[45] While considerations of MSC isolation, expansion, preservation, and priming are critical to function of MSC therapeutics, this optimization process must be coupled with an understanding of functional changes that occur after injection so that MSC products being used in local injection can be tailored to better suit the patient microenvironment.

Mesenchymal stromal cells aggregate during local injection

As previously eluded to, MSCs are dynamic and their behavior can be modulated by their microenvironment. *In vivo* microenvironments are significantly different from traditional *in vitro* cell culture environments, differing in cell assembly into 3D structures, oxygen availability, nutrient supply, molecular cues, and extracellular matrix. These differences can lead to significant changes in cell behavior *in vivo* compared to what is predicted by *in vitro* experiments. Route of injection can drastically change the environmental cues seen by MSCs.[46] While many applications of MSCs use systemic infusion, there is a growing use of local injections to better target MSCs to tissues where they are needed due to low homing capacity of MSCs to sites of damage. MSCs locally targeted are spatially confined and therefore are forced to interact with each other. As has been shown, when MSCs are placed in these confined areas, they coalesce together to form a 3D aggregate, termed a spheroid.[47] Bartosh *et al.* demonstrated that upon injection of his GFP labeled MSCs into a mouse peritoneal cavity, the MSCs formed aggregates. Spheroid MSCs upregulate surface receptors to aid in attachment to each other such

as integrin subunit α2 and intercellular adhesion molecule 1 (ICAM-1). In addition, spheroid MSCs also upregulate extracellular matrix components to promote cell-cell adhesion through laminin and small leucine-rich proteoglycans.[48] 3D organization of cells has been shown in other organoid systems to alter their phenotype, therefore, further research into phenotypic changes are critical to ensure MSCs behave in a therapeutic manner.

Alterations in aggregated mesenchymal stromal cell phenotype

A commonly overlooked assumption in MSC therapy is that MSCs will exhibit a similar phenotype *in vivo* and *in vitro*. However, this assumption is invalid when MSCs are locally administered due to formation of cell aggregates.[47] MSCs delivered locally to the peritoneal space in mice had a significantly altered phenotype expressing high levels of COX2, TGS-6, and STC1 upon initial aggregation and after 72 hours post-injection *in vivo*.[47] Additionally, other groups have shown that locally delivered MSCs persist longer *in vivo* compared to those systemically administered. Spheroids have a vastly different phenotype compared to their 2D cultured counterparts and respond differently to environmental stimuli.[49] Because of the significant shift in gene and protein expression, it is important to understand how these changes in MSC secretome will affect the cell behavior.

Since MSC phenotype changes occur after local injection, there is a critical need to model these *in vivo* changes that occur post-injection *in vitro* because *in vitro* assays can test specific questions about MSC phenotype alteration and interactions with particular cell types which are obscured *in vivo*. Phenotypic changes in MSCs locally delivered *in vivo* have been replicated in 3D MSC culture systems. Bartosh *et al.* demonstrated that MSC gene expression profile changes were similar to those from *in vitro* cell spheroids created through use of a hanging droplet technique.[50] Therefore, the locally injected MSC phenotype is more accurately modeled through 3D spheroids as compared to culture as a monolayer.

Due to this unique microenvironment created from densely packed MSCs forming their own 3D structure, there are several gene expression changes, which contribute to the unique phenotype of spheroid MSCs. Upon *in vitro* spheroid formation, there are transcriptional changes, which affect secreted molecules, cell surface receptors, extracellular matrix molecules, and transcription factors.[48] Several groups have shown that upon spheroid formation, gene and protein expression significantly change. Many factors are upregulated such as VEGF, TGF-β,

TSG-6, STC-1, and HGF.[47,49] All of these factors have demonstrated direct and indirect neuroprotective effects, such as support of vasculature, anti-apoptotic effects, and suppression of inflammatory cytokine production.[51,52] In addition, PGE2 is a bioactive lipid synthesized by the inducible protein COX-2. COX-2 is significantly upregulated with spheroid formation and subsequently PGE2.[53] PGE2 demonstrates several pleotropic actions including growth factor regulation and anti-apoptotic effects.[13,54]In studies with neurons, the addition of PGE2 led to higher viability after hypoxic, glutamate, and hemin challenges, indicating these neurons possess EP receptors, which allow for PGE2 detection.[55–58] Several transcription factors are upregulated upon spheroid formation including SATB1 known to facilitate chromatin remodeling in lymphocytes, nuclear receptor related 1 protein encoded by the gene NR4A2 which acts as an anti-inflammatory regulator in microglia, and ETV1, a transcription factor which has diverse roles in angiogenesis, cell proliferation, and cell differentiation.[48] Therefore, spheroid MSCs upregulate many trophic factor pathways which may further enhance their effectiveness.

While spheroid MSCs produce many immunomodulatory factors, they also produce cytokines such as IL-1, IL-7, IL-8, IL-11, and IL-24[48] which are known to have both pro- and anti-inflammatory signaling roles as well as chemoattractant and hematopoietic support functions. Additionally, while known for its immunosuppressive function, PGE2, the most upregulated factor in spheroids known to date, has been shown to have roles in promoting inflammatory responses of immune cells. Therefore, while spheroid MSCs produce a wide range of immunomodulatory factors, the presence of inflammatory factors warrants further research to elucidated spheroid MSCs' anti-inflammatory properties.

Therapeutic consequences of mesenchymal stromal cell aggregation

In addition to altered immunomodulatory and growth factor production, locally injected MSCs also demonstrate an ability to persist *in vivo* longer than their 2D counter parts.[46,47] Several factors could contribute to this finding including 3D structure providing a favorable microenvironment for MSCs and spheroid MSC production of anti-apoptotic factors.[51] Additionally, MSCs transplanted *in vivo* often are exposed to harsh environments which lead to upregulation of reactive oxygen species (ROS) leading to cell apoptosis. STC-1 is a protein, produced by spheroid MSCs, shown to scavenge for reactive oxygen species (ROS). This may explain why spheroids demonstrate superior resilience during ROS challenge and why spheroid

MSCs persist longer after local injection.[47,51,59] Because locally injected MSCs remain viable for longer periods of time, it is critical that their post-transplant phenotype be engineered to remain efficacious over the longer duration of the cell therapy.

Spheroid MSCs have been shown to improve I/R injury outcomes through their production of anti-apoptotic, immunomodulatory, and growth factors. Human adipose derived stromal cells were shown to increase angiogenic factors such as VEGF, HGF, and FGF2 in response to spheroid formation.[60] *In vitro* and *in vivo* spheroid cells decreased apoptosis of endothelial cells, increased vascular density, and growth factor availability in the limb leading to fewer spontaneous limb losses in the mouse model of hindlimb ischemia.[60] In a rodent model of cerebral stroke, MSC spheroids decreased stroke infarct volume and neuron apoptosis more so than 2D cultured cells.[61] Finally, compared to 2D cultured MSCs, spheroids MSCs showed increased TSG-6 and other growth factors. This alteration in phenotype better reduced kidney injury score and injury biomarkers creatinine and blood oxygen nitrogen in a mouse model of kidney ischemia. This may be due to a combination of spheroid reduction of renal cell apoptosis as well as promotion of new vascular growth.[62] Together this data suggests that in addition to the direct effects of PGE2, there may be several other important factors produced by spheroid MSCs which can be beneficial in ischemic conditions.

While spheroid MSCs produce some pro-inflammatory cytokines, spheroids overall have been shown to be suppressive of macrophages, likely through a PGE2 dependent mechanism. PGE2 can act as a potent immunomodulatory molecule both repolarizing macrophages and suppressing activation of other immune cell components.[47,48] Bartosh *et al.* have shown that addition of PGE2 to macrophages causes suppression of the M1 pro-inflammatory and conversion to the M2 phenotype.[47,63] By fractionating spheroid conditioned media, they found that only the fractions containing molecules under 3 kD which were not denatured by heat demonstrated suppression of TNF-α production by macrophages leading to the observation that suppression effects were due to high levels of PGE2.[64] They observed a similar suppressive effect by the addition of conditioned media from spheroids, which contain high levels of PGE2. Additionally, direct blockade of PGE2 production decreased spheroid suppression of macrophages demonstrating that PGE2 is a potent suppressor needed for spheroid function.[47] Therefore, PGE2 appears to be a critical component for spheroid MSC manipulation of

macrophage phenotype, but further research must be done to determine PGE2's role in spheroid MSCs' interactions with other immune cells.

Production of PGE2 in aggregated mesenchymal stromal cells

Understanding the role PGE2 plays in the spheroid secretome is of paramount importance because it may impact immunomodulatory and pro-regenerative function of MSCs, and many clinically administered pain and anti-inflammatory medications affect PGE2 production. While PGE2 alone has been shown to promote survival of neurons in addition to skewing macrophages towards an anti-inflammatory phenotype, it has also been shown to drive T cell inflammation.[13,65] Therefore, if PGE2 is critical to spheroid MSC function or lack of function, steps must be taken to control its production. Additionally, many patients with I/R injuries such as stroke receive NSAID therapy. Since NSIADs are potent inhibitors of COX-2 activity, this class of drugs could have a significant impact on spheroid MSCs' therapeutic benefit for these diseases. Therefore, a better understanding of the mechanism by which PGE2 is upregulated will aid in control of this aspect of spheroid MSC phenotype.

PGE2 is produced through a complex set of enzymatic modifications which is regulated through inflammatory autocrine signaling in spheroid MSCs. Arachidonic acid, the precursor to PGE2, is cleaved from phospholipids or diacylglycerol (DAG) via phospholipase C/A2. The cyclooxygenase domain on COX-1/2 converts arachidonic acid to PGG2 and then the peroxidase domain reduces the product to PGH2. PGH2 can then be converted to PGE2 via the PGE isomerase encoded by mPGES/cPGES.[66] In addition to PGE2, PGH2 can be converted into thromboxane A2, prostacyclin, PGD2, and PGF2α by other synthases.[67] While upregulation of COX-2 can lead to upregulation of these prostaglandins, without upregulation of the specific synthases, many prostaglandins cannot be formed.[68] Ylostalo *et al*. found that specifically in spheroid MSCs, PGE2 and PGD2 synthases were upregulated by microarray analysis.[64] If the spheroids where treated with IRAK or IL-1R inhibitors, targets of IL-1α/β, PGE2 production was decreased and the spheroid conditioned media lost its suppressive effect. In a similar way, blocking the binding of IL-1 to its receptor through anti-IL-1 or IL-1ra, knocking down mRNA levels of IL-1 through siRNAs, or blocking cleavage of IL-1 to its active form through caspase inhibition all decreased IL-1 production and subsequently PGE2. Therefore, they hypothesized that IL-1R signals through NFκB to activate production of immunomodulatory and ROS

scavenging factors PGE2, TSG-6, and STC1.[47] In further studies, they found that NFκB signaling upregulates the genes PLA2G4A/C, which encode PLA2, a protein that cleaves arachidonic acid from phospholipids providing more substrate to COX-2 and mPGES to produce PGE2.[64] There are several proteins critical to the PGE2 production pathway including NFκB, IL-1, and COX-2 which can be targeted to control PGE2 levels in spheroid MSCs.

PGE2 signaling mechanisms

Spheroid MSC PGE2 can signal to a variety of cells through PGE2 receptors (EP receptors), which leads to suppression of certain immune cell populations. PGE2 has four receptors (EP1-4), which are seven segment transmembrane G-coupled protein receptors. MSCs have been shown to express all four receptors, but little is known about regulation of these receptors in spheroids. PGE2 receptor EP1 signals through G_q to activate PLC. Downstream of PLC can take either the IP3 signaling pathway to induce calcium release from the endoplasmic reticulum or the DAG pathway to activate PKC. EP2 and EP4 can signal through G_s to activate adenylate cyclase, which produces cAMP. Increases in cAMP can then activate PKA downstream and eventually cause phosphorylation of CREB, which then will translocate to the nucleus and modulate gene expression. Alternatively, EP4 can also signal through PI3K to phosphorylate Akt and then drive downstream activation of the transcription factor NFKB. EP3 is a negative regulator of cAMP by signaling through G_s to inhibit adenylate cyclase activity. EP2/4 signaling has been shown to increase production of growth factors such as VEGF and HGF, immunomodulatory factors PGE2 and TGF-β, and anti-apoptotic factors. There are several transcriptional factors downstream of the EP receptors that are likely responsible for this modulation of gene expression, including CREB, NFκB, and β-catenin.[47,69,70] Microglial cells possess high amounts of the EP2/4 receptors, which has been shown to dampen the inflammatory phenotype upon receptor signaling.[64,71] In macrophages, the addition of PGE2 can suppress TNF-α secretion while upregulating IL-10.[47,65] While current research has shown positive effects of PGE2 on suppression of inflammatory macrophages, PGE2 signaling is complex and effects are modified by cell type and relative expression of different PGE2 receptor subsets.

In addition to immunomodulatory signaling, PGE2 signaling can alter production of growth factors produced by cells. Most commonly, PGE2 signaling leads to CREB translocation where it can bind to hundreds of thousands of cAMP response elements (CRE) on the human

genome, however due to methylation patterns, the promoters and enhancer regions which CREB binds can be wildly different between cell types.[72] CRE targets have been found on many genes encoding growth factors, anti-apoptotic factors, attachment factors, proteins that regulate metabolic function, and transcription factors, in addition to immunomodulatory factors.[69,72] Several groups implicate these factors in improved outcomes for critical limb ischemia (CLI), stroke injury, and myocardial infarction (MI) in animal models.[43,73,74] Because of the variety of cell-specific downstream targets of PGE2 and its interaction with other signals present *in vivo*, it is unclear how MSC spheroid PGE2 will affect the function of host cells.

While MSC secreted factors can modulate host cells, they can also modulate their own phenotype. PGE2 receptors EP1-4 have been shown to be expressed in MSCs. Lee *et al*. demonstrated for 2D MSCs that EP2 blockade lead to decrease in proliferation of MSCs and cell-cell contact for 2D MSCs decreased their production COX-2, mPGES, PGE2, and EP2 while increasing EP3. They demonstrated that through the addition of a gap junction inhibitor they could partly restore PGE2, COX-2, and mPGES expression.[75] However, this change in PGE2 levels left immunomodulatory and growth factor expression unaffected.[75] Additionally, PGE2 autocrine signaling may drive spheroid MSCs production of several growth factors, including VEGF, TGFβ3, HGF, BMP2, BMP6, GDF15, LIF, and IGFBP5, as these genes are downstream of EP receptor signaling.[49] These growth factors have a wide variety of functions from angiogenesis, differentiation, anti-scarring, wound repair, recruitment of epithelial cells, immunomodulation, neuroprotection, pro-survival signaling, and cell proliferation. The role of PGE2 autocrine signaling in spheroids has not been elucidated yet, but there exists the possibility of a similar autocrine feedback loop.

1.5. TRACKING AND VALIDATION OF LOCAL DELIVERY OF MESENCHYMAL STROMAL CELLS

Problems confirming mesenchymal stromal cell delivery and retention in local injection

When MSCs are locally administered, validation of the location and number of cells delivered is important. For both clinicians and researchers, the technique to locally inject MSCs must be learned and its execution will vary from person to person making delivery of these therapies different. In the clinical setting, often clinicians will have technologies such as CT or fluoroscopes to aid in the placement of the delivery needle. However, some procedures do not warrant use of these guidance technologies. In most research settings, there is no validation of cell application making interpretation of negative data difficult.

There can be several factors which influence where locally injected MSCs finally end up. Since tissue is dense, cells must be injected into interstitial spaces in order to get the cells to be retained in the tissue. Cells injected here often can flow into the surrounding sites making the treatment area variable depending on the injection technique. Additionally, when not properly injected into interstitial spaces or when the volume delivered exceeds the space available, cell product can leak back out via the delivery path of the needle. When this occurs, the full dose of MSCs is not delivered and in the absence of methods to measure the cell number, it will be impossible to determine if a therapeutic dose has been delivered. Therefore, there is a need especially in research to verify cell placement and dose and correlate these parameters with subject outcomes.

Labeling and tracking of mesenchymal stromal cell delivery

There have been several methods to track and verify delivery of MSCs to injection sites in animal models, but each method has limitations on its use labeling MSCs for tracking. A few common labeling methods include nanoparticles, chemical dyes, bioluminescent enzymes, and fluorescent proteins. For years, cells have been visualized by microscopy using membrane integrating or intracellular dyes. Since tissue does not adsorb light in the far-red spectrum, dyes that emit light in this range can be used for tracking of cells in animal models. Similarly, cells can be modified to express fluorescent proteins which emit in the far-red. The main disadvantage of dyes is that they can be transferred to their surroundings over time while only cells modified

with the fluorescent protein gene can express this protein. Additionally, most dyes will degrade over time, while fluorescent proteins will be made over the lifetime of the cell. However, fluorescent proteins have been shown to have some immunogenicity and their effect on cell clearance must be assessed. Since most MSCs do not engraft long-term, it is not imperative that these labeling technologies last indefinitely *in vivo*.

Further, the imaging system must be both accurate and accessible for implementation in cell tracking. Clinically, the use of MRI with cells loaded with iron oxide nanoparticles has been validated, but this technique has not been widespread in its use due to accessibility to preclinical researchers and high cost of the technique. Nanoparticles have been developed to be easily up taken by cells and detectable by MRI to overcome the limitations of fluorescent based imaging systems. The most common contrast agent used is iron oxide although other agents have been tried such as gadolinium, probes that induce chemical exchange saturation transfer (CEST), and ^{19}F labeling.[76,77] This system has been shown to be able to detect less than 100 cells. To date, there have not been any other cell tracking methods approved for use in humans.[78] In addition to MRI, cells injected into the skin or subcutaneous fat of animals have been observed using conventional microscope camera, but to view cells injected below the dermal layers requires whole body fluorescent imaging systems, such as IVIS. Tissue still absorbs a nominal amount of far-red light and therefore, there is a much larger number of cells needed, compared to MRI, in order for these scanners to detect the cells. Imaging tools for use in pre-clinical cell tracking must be assessed based on the researcher needs on field of imaging, sensitivity to cell number, timespan which cells will be tracked, and cost of the technique. There will be additional discussion of a low-cost technique for research purposes in Chapter 5.

1.6. CHAPTER SUMMARY

As described above, increased use of localized injection to deliver MSCs necessitates MSC production changes in order to supply a reliably efficacious product for patients. These requirements must be validated for effects on potency, not solely for MSC viability and proliferation. Additionally, because of the unique environment in which local injection places MSCs, changes in cell potency and interaction with surrounding cells must be understood in order to determine conditioning regiments which will enhance the therapy's effectiveness for treating particular disease states in patients. My thesis will focus on how cryopreservation and prelicencing of MSCs can affect their application in local injection. Additionally, I will discuss how the aggregation of MSCs alters their phenotype and how these alterations affect interactions with immune cells. Finally, I will discuss a low-cost technique to track locally administered MSC in a mouse model of diabetic wounds to make cell tracking practical for more researchers.

In Chapter 2, the effect of cryopreservation and prelicencing will be explored in the context of preparation for local injection. While some have found that cryopreservation can have a substantial negative impact on MSC potency, I will demonstrate that with my cryopreservation protocol, I am able to preserve MSC potency and function in a local injection in a retinal ischemia/reprofusion model. Finally, while IFN-γ treatment has been widely explored as a method to increase potency of MSCs prior to transplant, I will show that in the context of my retinal ischemia/reprofusion model, prelicencing of MSCs with IFN-γ is detrimental to their *in vivo* function. This indicates that prelicencing regiments should be assessed for local injections on a case by case basis as this treatment does not broadly ensure increases in effectiveness of MSCs.

While some effects of MSC aggregation are known, the impact of PGE2 autocrine signaling, cellular stress, kinetics of gene expression changes, changes in metabolic function, and spheroid interaction with type-2 diabetic environments have been minimally explored despite their implications to the effectiveness of locally administered MSC therapies. Chapter 3 demonstrates that the environment to which MSCs are transplanted into has a substantial effect on the cells' function and production of trophic factors. Here, I will show that MSC aggregation affects not only their gene expression, but also their secretome, metabolic function, stress state, and susceptibility to palmitate, a long chain fatty acid highly present in obese patients, damage.

Additionally, in Chapter 4, I will demonstrate that local injection has a wide range of effects on MSC immunomodulatory factor expression and activity. These changes lead to impairment of MSCs ability to suppress T cell proliferation and alter how MSCs modify macrophage phenotype.

One of the challenges of local injection is validation of delivery of cells to the treatment site. Often in research there is little or no control or documentation of the local injection of MSCs into animals. This has the potential to lead to high variability in results between research groups. Therefore, in Chapter 5, I will provide a method for cheaply and quickly assessing injection of MSCs into dermal tissue. This method can be used to track MSCs over time in the skin as well providing information on retention of the cells at the application site. Additionally, I will discuss a variety of cell labeling options and imaging modalities which can also be used to provide similar tracking and injection validation.

In Appendix A, I go over methods for culturing and analyzing spheroid cells. There are several different methods to form spheroids including hanging droplet, low-attachment plates, alginate encapsulation, spheroid plates, polyethylene glycol-dextran (PEG-DEX) biphasic solutions, and injection of cells into a gelatin-alginate gel. I found that because cells in spheroids are densely packed, they require a method of dispersion in order to be analyzed in several common techniques such as western blot, RNA extraction, membrane staining, immunohistochemistry, and metabolic function assessment. In addition, because MSCs are stressed and lose viability in the spheroids, cell lysate and RNA extraction protocols require more cells when applied to spheroids. I optimized a method for spheroid RNA extraction using Trizol and a tissue homogenizer. Finally, since spheroids often must be transferred between cell culture vessels for analysis and co-cultures with other cells, there can be damage to spheroids leading to variable number of cells being transferred. To mitigate this variability, I demonstrate the effectiveness of an ImageJ script to estimate spheroid size, which can be used to estimate cell number.

There are several ways to engineer MSCs to drive their anti-inflammatory or pro-regenerative phenotype for local injection. In Appendix B, I will show that prelicensing MSC aggregates with IFN-γ does not alter their production of some trophic factors. However, biomaterials can modify cell phenotype. Specifically, encapsulation of MSCs with alginate can manipulate their phenotype to closely resemble spheroid MSCs or adherent MSCs through

chemically modifying alginate with gelatin. This is an area of cell engineering which requires further investigation in application to locally delivered MSCs.

1.7. REFERENCES

1. Friedenstein, A. J. *et al.* Precursors for fibroblasts in different populations of hematopoietic cells as detected by the in vitro colony assay method. *Exp. Hematol.* **2**, 83–92 (1974).
2. Dominici, M. *et al.* Minimal criteria for defining multipotent mesenchymal stromal cells. The International Society for Cellular Therapy position statement. *Cytotherapy* **8**, 315–317 (2006).
3. de Souza, L. E. B., Malta, T. M., Kashima Haddad, S. & Covas, D. T. Mesenchymal Stem Cells and Pericytes: To What Extent Are They Related? *Stem Cells Dev.* **25**, 1843–1852 (2016).
4. Wagner, W. *et al.* Comparative characteristics of mesenchymal stem cells from human bone marrow, adipose tissue, and umbilical cord blood. *Exp. Hematol.* **33**, 1402–1416 (2005).
5. Guo, X. *et al.* Cardiomyocyte differentiation of mesenchymal stem cells from bone marrow: new regulators and its implications. *Stem Cell Res. Ther.* **9**, 44 (2018).
6. Sacchetti, B. *et al.* No Identical "Mesenchymal Stem Cells" at Different Times and Sites: Human Committed Progenitors of Distinct Origin and Differentiation Potential Are Incorporated as Adventitial Cells in Microvessels. *Stem Cell Reports* **6**, 897–913 (2016).
7. Bernardo, M. E. & Fibbe, W. E. Mesenchymal Stromal Cells: Sensors and Switchers of Inflammation. *Cell Stem Cell* **13**, 392–402 (2013).
8. English, K. *et al.* Cell contact, prostaglandin E2 and transforming growth factor beta 1 play non-redundant roles in human mesenchymal stem cell induction of CD4 + CD25 High forkhead box P3 + regulatory T cells. *Clin. Exp. Immunol.* **156**, 149–160 (2009).
9. Hackstein, H. *et al.* Contact-dependent abrogation of bone marrow-derived plasmacytoid dendritic cell differentiation by murine mesenchymal stem cells. *Biochem. Biophys. Res. Commun.* **476**, 15–20 (2016).
10. Munn, D. H. & Mellor, A. L. Indoleamine 2,3 dioxygenase and metabolic control of immune responses. *Trends Immunol.* **34**, 137–143 (2013).

11. François, M., Romieu-Mourez, R., Li, M. & Galipeau, J. Human MSC Suppression Correlates With Cytokine Induction of Indoleamine 2,3-Dioxygenase and Bystander M2 Macrophage Differentiation. *Mol. Ther.* **20**, 187–195 (2012).
12. Wilkins, A. *et al.* Human bone marrow-derived mesenchymal stem cells secrete brain-derived neurotrophic factor which promotes neuronal survival in vitro. *Stem Cell Res.* **3**, 63–70 (2009).
13. Andrade da Costa, B. L. da S., Kang, K. D., Rittenhouse, K. D. & Osborne, N. N. The localization of PGE2 receptor subtypes in rat retinal cultures and the neuroprotective effect of the EP2 agonist butaprost. *Neurochem. Int.* **55**, 199–207 (2009).
14. Osborne, A., Sanderson, J. & Martin, K. R. Neuroprotective Effects of Human Mesenchymal Stem Cells and Platelet-Derived Growth Factor on Human Retinal Ganglion Cells. *Stem Cells* **36**, 65–78 (2018).
15. Uccelli, A., Benvenuto, F., Laroni, A. & Giunti, D. Neuroprotective features of mesenchymal stem cells. *Best Pract. Res. Clin. Haematol.* **24**, 59–64 (2011).
16. Frantz, S. & Nahrendorf, M. Cardiac macrophages and their role in ischaemic heart disease. *Cardiovasc. Res.* **102**, 240–248 (2014).
17. Eming, S. A., Martin, P. & Tomic-canic, M. Wound repair and regeneration: Mechanisms, signaling, and translation. *Wound Heal.* **6**, (2014).
18. Patel, A. R., Ritzel, R., Mccullough, L. D. & Liu, F. Microglia and ischemic stroke: a double-edged sword. *Int J Physiol Pathophysiol Pharmacol* **5**, 73–90 (2013).
19. Kaur, C., Foulds, W. S. & Ling, E.-A. Hypoxia-ischemia and retinal ganglion cell damage. *Clin. Ophthalmol.* **2**, 879–889 (2008).
20. Capilla-González, V. *et al.* PDGF Restores the Defective Phenotype of Adipose-Derived Mesenchymal Stromal Cells from Diabetic Patients. *Mol. Ther.* **26**, 2696–2709 (2018).
21. Acosta, L. *et al.* Adipose Mesenchymal Stromal Cells Isolated From Type 2 Diabetic Patients Display Reduced Fibrinolytic Activity. *Diabetes* **62**, 4266–4269 (2013).
22. Berglund, A. K., Fortier, L. A., Antczak, D. F. & Schnabel, L. V. Immunoprivileged no more: measuring the immunogenicity of allogeneic adult mesenchymal stem cells. *Stem Cell Res. Ther.* **8**, 288 (2017).

23. Sun, Q. *et al.* Allogeneic mesenchymal stem cells as induction therapy are safe and feasible in renal allografts: pilot results of a multicenter randomized controlled trial Open Access Journal of Translational Medicine. *J. Transl. Med.* **16**, 52 (2018).
24. Galipeau, J. & Sensébé, L. Mesenchymal Stromal Cells: Clinical Challenges and Therapeutic Opportunities. *Cell Stem Cell* **22**, 824–833 (2018).
25. Mautner, K., Carr, D., Whitley, J. & Bowers, R. Allogeneic Versus Autologous Injectable Mesenchymal Stem Cells for Knee Osteoarthritis. *Tech. Orthop.* **00**, 1 (2019).
26. Jenei-Lanzl, Z. *et al.* Estradiol inhibits chondrogenic differentiation of mesenchymal stem cells via nonclassic signaling. *Arthritis Rheum.* **62**, 1088–1096 (2010).
27. Grässel, S., Stöckl, S. & Jenei-Lanzl, Z. Isolation, Culture, and Osteogenic/Chondrogenic Differentiation of Bone Marrow-Derived Mesenchymal Stem Cells. **879**, (2012).
28. Mageed, A. S., Pietryga, D. W., DeHeer, D. H. & West, R. A. Isolation of large numbers of mesenchymal stem cells from the washings of bone marrow collection bags: Characterization of fresh mesenchymal stem cells. *Transplantation* **83**, 1019–1026 (2007).
29. Mizukami, A. *et al.* Technologies for large-scale umbilical cord-derived MSC expansion: Experimental performance and cost of goods analysis. *Biochem. Eng. J.* (2018). doi:10.1016/j.bej.2018.02.018
30. von Bahr, L. *et al.* Long-Term Complications, Immunologic Effects, and Role of Passage for Outcome in Mesenchymal Stromal Cell Therapy. *Biol. Blood Marrow Transplant.* **18**, 557–564 (2012).
31. Kizilay Mancini, Ö. *et al.* A Proinflammatory Secretome Mediates the Impaired Immunopotency of Human Mesenchymal Stromal Cells in Elderly Patients with Atherosclerosis. *Stem Cells Transl. Med.* **6**, 1132–1140 (2017).
32. Chinnadurai, R. *et al.* Cryopreserved MSCs are susceptible to T-cell mediated apoptosis which is partly rescued by IFNγ licensing Raghavan. *Stem Cells* **34**, 2429–2442 (2016).
33. François, M. *et al.* Cryopreserved mesenchymal stromal cells display impaired immunosuppressive properties as a result of heat-shock response and impaired interferon-γ licensing. *Cytotherapy* **14**, 147–152 (2012).
34. Moll, G. *et al.* Do Cryopreserved Mesenchymal Stromal Cells Display Impaired Immunomodulatory and Therapeutic Properties? *Stem Cells* **32**, 2430–2442 (2014).

35. Luetzkendorf, J. *et al.* Cryopreservation does not alter main characteristics of Good Manufacturing Process–grade human multipotent mesenchymal stromal cells including immunomodulating potential and lack of malignant transformation. *Cytotherapy* **17**, 186–198 (2015).
36. Gramlich, O. W. *et al.* Cryopreserved Mesenchymal Stromal Cells Maintain Potency in a Retinal Ischemia/Reperfusion Injury Model: Toward an off-the-shelf Therapy. *Sci. Rep.* **6**, 26463 (2016).
37. Li, M. *et al.* Mesenchymal stem cell-conditioned medium accelerates wound healing with fewer scars. *Int. Wound J.* **14**, 64–73 (2017).
38. Prasanna, S. J., Gopalakrishnan, D., Shankar, S. R. & Vasandan, A. B. Pro-Inflammatory Cytokines, IFNγ and TNFα, Influence Immune Properties of Human Bone Marrow and Wharton Jelly Mesenchymal Stem Cells Differentially. *PLoS One* **5**, e9016 (2010).
39. Rosová, I., Dao, M., Capoccia, B., Link, D. & Nolta, J. a. Hypoxic Preconditioning Results in Increased Motility and Improved Therapeutic Potential of Human Mesenchymal Stem Cells. *Stem Cells* **26**, 2173–2182 (2008).
40. Ryan, J. M., Barry, F., Murphy, J. M. & Mahon, B. P. Interferon-γ does not break, but promotes the immunosuppressive capacity of adult human mesenchymal stem cells. *Clin. Exp. Immunol.* **149**, 353–363 (2007).
41. Sivanathan, K. N. *et al.* Interleukin-17A-Induced Human Mesenchymal Stem Cells Are Superior Modulators of Immunological Function. *Stem Cells* **33**, 2850–2863 (2015).
42. Sheng, H. *et al.* A critical role of IFNγ in priming MSC-mediated suppression of T cell proliferation through up-regulation of B7-H1. *Cell Res.* **18**, 846–857 (2008).
43. Li, Y. *et al.* Primed 3D injectable microniches enabling low-dosage cell therapy for critical limb ischemia. *Proc. Natl. Acad. Sci.* **111**, 13511–13516 (2014).
44. Polchert, D. *et al.* IFN-γ activation of mesenchymal stem cells for treatment and prevention of graft versus host disease. *Eur. J. Immunol.* **38**, 1745–1755 (2008).
45. Moll, G. *et al.* Intravascular Mesenchymal Stromal/Stem Cell Therapy Product Diversification: Time for New Clinical Guidelines. *Trends Mol. Med.* **25**, 149–163 (2019).
46. Braid, L. R., Wood, C. A., Wiese, D. M. & Ford, B. N. Intramuscular administration potentiates extended dwell time of mesenchymal stromal cells compared to other routes. *Cytotherapy* **20**, 232–244 (2018).

47. Bartosh, T. J., Ylöstalo, J. H., Bazhanov, N., Kuhlman, J. & Prockop, D. J. Dynamic compaction of human mesenchymal stem/precursor cells into spheres self-activates caspase-dependent IL1 signaling to enhance secretion of modulators of inflammation and immunity (PGE2, TSG6, and STC1). *Stem Cells* **31**, 2443–2456 (2013).
48. Bartosh, T. J. *et al.* Aggregation of human mesenchymal stromal cells (MSCs) into 3D spheroids enhances their antiinflammatory properties. *Proc. Natl. Acad. Sci.* **107**, 13724–13729 (2010).
49. Xie, L., Mao, M., Zhou, L., Zhang, L. & Jiang, B. Signal Factors Secreted by 2D and Spheroid Mesenchymal Stem Cells and by Cocultures of Mesenchymal Stem Cells Derived Microvesicles and Retinal Photoreceptor Neurons. *Stem Cells Int.* **2017**, 1–13 (2017).
50. Bartosh, T. J. & Ylostalo, J. H. Preparation of Anti-Inflammatory Mesenchymal Stem/Precursor Cells (MSCs) Through Sphere Formation Using Hanging-Drop Culture Technique. *Curr. Protoc. Stem Cell Biol.* **28**, 2B.6.1-2B.6.23 (2014).
51. Kim, S. J. *et al.* Stanniocalcin-1 Protects Retinal Ganglion Cells by Inhibiting Apoptosis and Oxidative Damage. *PLoS One* **8**, e63749 (2013).
52. Ma, S. *et al.* Immunobiology of mesenchymal stem cells. *Cell Death Differ.* **21**, 216–225 (2014).
53. Sreeramkumar, V., Fresno, M. & Cuesta, N. Prostaglandin E2 and T cells: friends or foes? *Immunol. Cell Biol.* **90**, 579–586 (2012).
54. Parga, J. A. *et al.* Prostaglandin EP2 Receptors Mediate Mesenchymal Stromal Cell-Neuroprotective Effects on Dopaminergic Neurons. *Mol. Neurobiol.* **55**, 4763–4776 (2018).
55. Docheva, D., Haasters, F. & Schieker, M. Mesenchymal Stem Cells and Their Cell Surface Receptors. *Curr. Rheumatol. Rev.* **4**, 1–6 (2008).
56. Bilak, M. *et al.* PGE2 receptors rescue motor neurons in a model of amyotrophic lateral sclerosis. *Ann. Neurol.* **56**, 240–248 (2004).
57. Mohan, S., Narumiya, S. & Doré, S. Neuroprotective role of prostaglandin PGE2 EP2 receptor in hemin-mediated toxicity. *Neurotoxicology* **46**, 53–59 (2015).

58. Yamagishi, R., Aihara, M. & Araie, M. Neuroprotective effects of prostaglandin analogues on retinal ganglion cell death independent of intraocular pressure reduction. *Exp. Eye Res.* **93**, 265–270 (2011).
59. Costa, M. H. G., McDevitt, T. C., Cabral, J. M. S., da Silva, C. L. & Ferreira, F. C. Tridimensional configurations of human mesenchymal stem/stromal cells to enhance cell paracrine potential towards wound healing processes. *J. Biotechnol.* **262**, 28–39 (2017).
60. Bhang, S. H. *et al.* Angiogenesis in ischemic tissue produced by spheroid grafting of human adipose-derived stromal cells. *Biomaterials* **32**, 2734–2747 (2011).
61. Guo, L. *et al.* Three-Dimensional Spheroid-Cultured Mesenchymal Stem Cells Devoid of Embolism Attenuate Brain Stroke Injury After Intra-Arterial Injection. *Stem Cells Dev.* **23**, 978–989 (2014).
62. Xu, Y., Shi, T., Xu, A. & Zhang, L. 3D spheroid culture enhances survival and therapeutic capacities of MSCs injected into ischemic kidney. *J. Cell. Mol. Med.* **20**, 1203–1213 (2016).
63. Vasandan, A. B. *et al.* Human Mesenchymal stem cells program macrophage plasticity by altering their metabolic status via a PGE2-dependent mechanism. *Sci. Rep.* **6**, 38308 (2016).
64. YlÖstalo, J. H., Bartosh, T. J., Coble, K. & Prockop, D. J. Human Mesenchymal Stem/Stromal Cells Cultured as Spheroids are Self-activated to Produce Prostaglandin E2 that Directs Stimulated Macrophages into an Anti-inflammatory Phenotype. *Stem Cells* **30**, 2283–2296 (2012).
65. MacKenzie, K. F. *et al.* PGE2 Induces Macrophage IL-10 Production and a Regulatory-like Phenotype via a Protein Kinase A-SIK-CRTC3 Pathway. *J. Immunol.* **190**, 565–577 (2013).
66. Park, J. Y., Pillinger, M. H. & Abramson, S. B. Prostaglandin E2 synthesis and secretion: The role of PGE2 synthases. *Clin. Immunol.* **119**, 229–240 (2006).
67. Nørregaard, R., Kwon, T.-H. & Frøkiær, J. Physiology and pathophysiology of cyclooxygenase-2 and prostaglandin E2 in the kidney. *Kidney Res. Clin. Pract.* **34**, 194–200 (2015).
68. Ricciotti, E. & FitzGerald, G. A. Prostaglandins and Inflammation. *Arterioscler. Thromb. Vasc. Biol.* **31**, 986–1000 (2011).

69. Luan, B. *et al.* CREB pathway links PGE2 signaling with macrophage polarization. *Proc. Natl. Acad. Sci.* 201519644 (2015). doi:10.1073/pnas.1519644112
70. Kalinski, P. Regulation of Immune Responses by Prostaglandin E2. *J. Immunol.* **188**, 21–28 (2012).
71. Quan, Y., Jiang, J. & Dingledine, R. EP2 Receptor Signaling Pathways Regulate Classical Activation of Microglia. *J. Biol. Chem.* **288**, 9293–9302 (2013).
72. Zhang, X. *et al.* Genome-wide analysis of cAMP-response element binding protein occupancy, phosphorylation, and target gene activation in human tissues. *Proc. Natl. Acad. Sci. U. S. A.* **102**, 4459–64 (2005).
73. Wu, Y., Chen, L., Scott, P. G. & Tredget, E. E. Mesenchymal Stem Cells Enhance Wound Healing Through Differentiation and Angiogenesis. *Stem Cells* **25**, 2648–2659 (2007).
74. Timmers, L. *et al.* Reduction of myocardial infarct size by human mesenchymal stem cell conditioned medium. *Stem Cell Res.* **1**, 129–137 (2008).
75. Lee, B.-C. *et al.* PGE2 maintains self-renewal of human adult stem cells via EP2-mediated autocrine signaling and its production is regulated by cell-to-cell contact. *Sci. Rep.* **6**, 26298 (2016).
76. Hoehn, M. *et al.* Cell tracking using magnetic resonance imaging. *J. Physiol.* **584**, 25–30 (2007).
77. Ahrens, E. T. & Bulte, J. W. M. Tracking immune cells in vivo using magnetic resonance imaging. *Nat. Rev. Immunol.* **13**, 755–763 (2013).
78. Bulte, J. W. M. In Vivo MRI Cell Tracking: Clinical Studies. *Am. J. Roentgenol.* **193**, 314–325 (2009).

CHAPTER 2: *IN VITRO* PROCESSING MODULATES MESENCHYMAL STROMAL CELL POTENCY PRE-TRANSPLANT

2.1. OVERVIEW

This chapter demonstrates that cryopreservation and prelicensing with inflammatory cytokines are critical parameters in developing an off-the-shelf MSC therapy for localized delivery. Specifically, we highlight a method of cryopreservation which preserves MSC viability, trophic factor production, and function in a local injection model of ischemic/reperfusion in the eye. Finally, we show that while commonly utilized prelicensing methods with IFN-γ can benefit MSC production of trophic factors like IDO, when IFN-γ prelicensed cells are locally injected into the model of ischemia in the eye they are less effective in their rescue of retinal ganglion neurons.

This chapter is an adaptation of two peer-reviewed articles published on May 23, 2016 and November 10, 2016 in *Scientific Reports* and *Stem Cells* respectively. Adapted with permission.

Gramlich OW, **Burand AJ**, Brown AJ, Deutsch RJ, Kuehn MH, Ankrum JA. Cryopreserved Mesenchymal Stromal Cells Maintain Potency in a Retinal Ischemia/Reperfusion Injury Model: Toward an Off-the-Shelf Therapy. **Sci Rep.** 2016 May 23;6:26463. doi: 10.1038/srep26463. PubMed PMID: 27212469; PubMed Central PMCID: PMC4876464

Burand AJ, Gramlich OW, Brown AJ, Ankrum JA. Function of Cryopreserved Mesenchymal Stromal Cells With and Without Interferon-γ Prelicensing is Context Dependent. **Stem Cells.** 2017 May;35(5):1437-1439. doi:10.1002/stem.2528. Epub 2016 Nov 10. PubMed PMID: 27758056; PubMed Central PMCID: PMC5397371

2.2. CRYOPRESERVATION DOES NOT NEGATIVELY IMPACT MSC POTENCY IN ISCEMIA/REPERFUSION INJURY

Abstract

The ability to use mesenchymal stromal cells (MSC) directly out of cryostorage would significantly reduce the logistics of MSC therapy by allowing on-site cryostorage of therapeutic doses of MSC at hospitals and clinics. Such a paradigm would be especially advantageous for the treatment of acute conditions such as stroke and myocardial infarction, which are likely to require treatment within hours after ischemic onset. Recently, several reports have emerged that suggest MSC viability and potency are damaged by cryopreservation. Herein we examine the effect of cryopreservation on human MSC viability, immunomodulatory potency, growth factor secretion, and performance in an ischemia/reperfusion injury model. Using modifications of established cryopreservation methods, we developed MSC that retain >95% viability upon thawing, remain responsive to inflammatory signals, and are able to suppress activated human peripheral blood mononuclear cells. Most importantly, when injected into the eyes of mice 3 hours after the onset of ischemia and 2 hours after the onset of reperfusion, cryopreserved performed as well as fresh MSC to rescue retinal ganglion cells. Thus, our data suggests when viability is maintained throughout the cryopreservation process, MSC retain their therapeutic potency in both *in vitro* potency assays and an *in vivo* ischemia/reperfusion model.

Introduction

Mesenchymal stromal/stem cells (MSC) have been explored in hundreds of clinical trials for the treatment of dozens of conditions.[1,2] While MSC can be harvested from nearly any tissue[3], they are a rare cell type[4] and thus typically require significant *ex vivo* expansion to generate therapeutic doses of cells. Allogeneic MSC are used in most clinical trials as MSC are immune evasive, allowing them to avoid immediate immune detection and clearance[2]. Allogeneic MSC are typically expanded in culture, cryopreserved, and banked for future use, creating the opportunity for an 'off-the-shelf' therapy.

Many proposed applications of MSC therapy would require on demand access to therapeutic doses of MSC and therefore necessitate access to cryopreserved MSC stocks. Acute conditions including acute graft versus host disease (GvHD), acute kidney injury, acute lung

injury, and sudden onset ischemic events such as myocardial infarction, acute limb ischemia, retinal and optic neuropathies, and stroke would all benefit from rapid MSC administration within hours after the onset of symptoms. The mechanism of action of MSC in these conditions is thought to be mediated through both modulation of inflammatory reactions as well as secretion of protective growth factors[5]. Even if a disease indication could accommodate a post-thaw recovery period ranging from hours to days, logistically, use of MSC immediately post-thaw would still be preferable, since post-thaw recovery needs to be carried out by experienced technicians in dedicated facilities. This not only leads to quality control issues but also adds significant infrastructure requirements that will prevent the use of MSC therapies in many hospitals. Therefore, identification of conditions that preserve MSC function throughout cryopreservation as well as disease indications that allow MSC to be applied directly post-thaw is critical to the development of truly 'off-the-shelf' MSC therapies.

Although multiple groups have investigated the impact of cryopreservation on the phenotype of MSC, studies to date have yielded conflicting results and many questions remain. Most importantly, do changes in phenotype caused by cryopreservation have a meaningful impact on therapeutic efficacy? Luetzkendorf *et al*. examined changes in MSC proliferation, viability, and immunosuppressive potential after cryopreservation[6]. In this study cryopreserved MSC showed no difference in proliferation or viability post-thaw. When co-cultured with PHA-stimulated peripheral blood mononuclear cells (PBMC), MSC' immunosuppressive potency after thaw varied depending on MSC donor. Two donors exhibiting enhanced suppression after cryopreservation, one donor exhibited reduced potency, and a fourth donor had highly variable function**6**. Galipeau and colleagues recently reported freshly thawed MSC exhibit significantly diminished viability compared to cells that had been in culture for greater than 7 days[7]. In addition, freshly thawed MSC showed reduced response to interferon-γ (IFN-γ). Notably, maintenance in culture for 7 days restored MSC sensitivity to IFN-γ and indoleamine 2,3-dioxygenase (IDO) expression, suggesting the observed impairment was transient. The reduced viability and expression of immunomodulatory factors in freshly thawed MSC also resulted in reduced suppression of activated T cells and, in some cases, actually led to hyper-proliferation of T cells in co-culture assays. The authors hypothesized that these phenomena are due to the presence of large numbers of dead cells[7]. The same group subsequently reported that the actin cytoskeleton of freshly thawed MSC is disrupted, leading to reduced adhesion to endothelium

and poor engraftment following intravenous infusion. Again, recovery in culture for 48 hours restored this aspect of MSC function[8]. Moll *et al.* recently compared the propensity of freshly thawed MSC to activate the complement cascade and induce an instant blood mediated inflammatory reaction (IBMIR)[9]. In their study, freshly thawed MSC were more susceptible to destruction by IBMIR and complement activation. They also demonstrated that freshly thawed MSC had lower levels of IDO transcripts after IFN-γ stimulation and had diminished immunosuppressive potency in co-cultures with activated PBMCs isolated from whole blood. In contrast to the Galipeau paper[7] and in agreement with the Leutzkendorf paper[6], the viability of freshly thawed MSC was observed to be similar to the viability of MSC harvested from continuous cultures, likely a consequence of differences in MSC donors and/or cryopreservation/thaw procedures used in the respective labs. In addition to *in vitro* analysis, Moll *et al.* also compared the clinical response of acute GvHD patients receiving intravenous injections of thawed MSC versus MSC collected from continuous cultures. Overall patients receiving fresh MSC, particularly early passage fresh MSC, had a much improved clinical response compared to patients receiving cryopreserved MSC[9].

Herein we seek to determine the effect of cryopreservation on human MSC's suitability to treat acute ischemic and inflammatory conditions. MSC phenotype, including viability, growth potential, growth factor secretion, expression of immunomodulatory factors, and ability to suppress activated inflammatory cells are analyzed in passage and donor matched MSC with and without cryopreservation. Finally, we test an 'off-the-shelf' MSC therapy treatment paradigm in a retinal ischemia/reperfusion injury model designed to replicate a clinical scenario.

Materials and Methods

MSC cultures and cryopreservation

Pre-characterized human MSC were provided by the Texas A&M Health Science Center College of Medicine Institute for Regenerative Medicine at Scott & White through a grant from NCRR of the NIH, Grant # P40OD011050, resource ID SCR_005522. Two donors of MSC, #7083 and #8002L, were obtained from Texas A&M and both were accompanied by a complete analysis of MSC surface marker expression and differentiation capacity in accordance with the ISCT minimal criteria for MSC[10]. Specifically, MSC from both donors were >95% positive for CD73a, CD90, and CD105, <2% positive for CD11, CD14, CD19, CD34, CD45, CD79a, and

HLA-II, and capable of multilineage differentiation. MSC were plated at a density of 5,000 cells/cm^2 in MEM-alpha supplemented with 15% fetal bovine serum (Premium Select, Atlanta Biologicals), 1% penicillin/streptomycin, and 1% L-glutamine unless otherwise stated. Cells were passaged when cells reached 70-80% confluence, which typically corresponded to 2.5 population doublings. All MSC were between population doubling levels of 6-11 at the time of use (Passage 3-5). MSC were cryopreserved using CryoStor CS5 cryopreservation media (Sigma, St. Louis, MO) and a CoolCell controlled rate freezing container (Biocision, San Rafael, CA). Briefly, MSC were harvested from cultures, pelleted, and resuspended in 4°C Cryostor CS5 at a concentration of 1x10^6/ml and aliquoted into cryovials. Vials were then placed in a CoolCell pre-chilled to 4°C and placed in a -80°C freezer for at least 90 minutes. Vials were then rapidly transferred to a pre-chilled liquid nitrogen storage box and maintained in liquid nitrogen vapor for 7-30 days before thawing. For thawing, all vials were removed from liquid nitrogen and placed directly in a 37°C water bath until a small ice pellet remained. Cells were then gently pipetted into 4 ml pre-warmed media, centrifuged at 500 x g for 5 min and resuspended in 1 ml pre-warmed media for use in downstream applications. For *in vivo* transplantation, cryopreserved MSC (cryo-MSC) were thawed, resuspended in room temperature PBS -/- (without calcium and magnesium), counted, centrifuged, and resuspended in ice cold PBS -/- at a concentration of 10x10^6/ml and placed on ice. All intraocular MSC injections occurred within 1 hour of thawing. 'Fresh' MSC in this study were all maintained in culture for at least 7 days. Cryo-MSC were used immediately after thawing unless otherwise noted. All experiments used donor and passage matched MSC to isolate the effect of cryopreservation on MSC phenotype and function.

In vitro vitreous assay

The *in vitro* vitreous was constructed using a combination of alginate and gelatin in a hydrogel. Briefly, 3% (w/v) sodium alginate (Sigma) and gelatin (Sigma) was dissolved in PBS to create a thick gel in which cells could be injected. The solution of heated to 75°C to dissolve any remaining powder. 1 mL of this solution was added to a low-attachment 24-well plate (Corning) and allowed to cool. MSCs were resuspended at 10 million cells/mL and 3 µL of cell solution was injected using a 20 µL pipette. 250 µL of media was added to the top of the gel to supply nutrients to the cells. Cells were then allowed to incubate in the gel for 3 days at 37°C. In

order to stain the cell nuclei, 250 µL of a 6 µL Hoechst per mL of media solution was added to the top of the gel and incubated at 37°C for 30 minutes.

Viability and metabolic activity assays

For viability analysis, terminal deoxynucleotidyl transferase dUTP nick end labeling (TUNEL) staining was performed on fresh MSC and MSC thawed directly from cryopreservation. In both cases, cells were washed twice, resuspended in PBS, and either analyzed immediately or after 1 hour of storage on wet ice. TUNEL staining was performed using the Apo-Direct Apoptosis Detection Kit (BD Biosciences, Franklin Lakes, NJ) according to the manufacturer's instructions. Briefly, cells were fixed in 2.5% neutral buffered formalin (Sigma, St. Louis, MO) for 60 minutes, washed three times, fixed, and permeabilized in 70% ethanol at -20°C for 3 days. Post thawing, double strand breaks were stained by incubation with FITC-dUTP followed by staining of all nuclei with propidium iodide (PI). The samples were analyzed by an Accuri C6 flow cytometer, with positive and negative control cells used for gating and color compensation. Fluorescent images of all samples were also acquired as validation. For viability analysis of fresh and cryo-MSC in the days after thawing, 30,000 MSC were seeded into a 24-well plate in triplicate for each experiment and cultured for 24, 48, and 72 hours. At each time point, media was removed from wells and 200 µL of staining media containing Hoechst and PI (Invitrogen, Carlsbad, CA) was added to each well. After 20 minutes of staining at 37°C, four random fields were imaged to detect PI positive nuclei and total nuclei. Cells incubated with 1 µM staurosporine (Tocris, San Diego, CA) for 3 hours served as a dead control to verify the staining procedure and set the acquisition settings. Images were captured using an inverted phase contrast and fluorescent microscope with a 10x objective (DMI6000B, Leica Microsystems, Wetzlar, Germany). ImageJ (NIH) was used for nuclei counting.

Metabolic activity in the days following thawing was measured using an XTT assay (ATCC, Manassas, VA) after 24, 48, and 72 hours. Here, 15,000 MSC were placed in wells of a 96-well plate in 100 µL of culture media. Both fresh MSC, cultured for >7 days, and cryo-MSC were plated in duplicate or triplicate for each time point and metabolic activity was measured according to the manufacturer's instructions. Wells with half the cell starting density with XTT, media only with XTT, and MSC alone without XTT were used as controls for each experiment (n=4).

Growth factor array

Growth factor secretion from fresh and cryo-MSC was assessed using the Human Growth Factor Array Q1 (RayBiotech, Norcross, GA). Here, either 200,000 fresh or cryo-MSC were cultured in 2 mL of 1% (v/v) FBS, 1% (v/v) Penicillin/Streptomycin, and 1% (v/v) L-glutamine supplemented MEM-α media in T25 flasks for 48 hours with or without 100 ng/mL human IFN-γ (PeproTech, Rocky Hill, NJ) and 50 ng/mL human TNF-α (Invitrogen, Carlsbad, CA). Media was collected and frozen at -20°C along with cell lysate for western blot and IDO activity analysis. The array was performed per the manufacturer's instructions using the growth factor standards provided in the kit and the media was loaded into the array with no dilution and at a 4x dilution. The slide was read, and data extracted by RayBiotech. The total concentration of each growth factor in basal media and MSC conditioned media was interpolated using the standard curves for each factor. To determine growth factor concentration contributed by the MSC, the concentration of growth factor in the basal media was subtracted from the concentration measured in the MSC conditioned media.

Western blot

Cell lysates were collected from MSC by washing T25 plates in chilled PBS three times to remove media followed by addition of 80 µL chilled RIPA buffer with protease inhibitor cocktail (Santa Cruz Biotechnology, item# sc-24948A) and agitation with a cell scrapper. Tubes were incubated on ice for 15 minutes and lysate was clarified by pelleting precipitate at 8,000 x g at 4ºC for 10 minutes. Prior to loading, total protein content was measured by microBCA (Thermo Scientific, Waltham, MA). 10-20 µg of protein was loaded into each well of a precast Bolt 4-12% Bis-Tris gels. After transfer, the membranes were blocked with 5% non-fat dry milk and stained with their respective primary antibodies (1:1000 rabbit anti-IDO (12006S, Cell Signaling, Danvers, MA), 1:20,000 mouse anti-β-actin (1406030, Ambion, Thermo Scientific, Waltham, MA)). Horseradish peroxidase conjugated antibodies (1:10,000 goat anti-rabbit (A2315), 1:10,000 goat anti-mouse (H2014), Santa Cruz Biotechnology, Dallas, TX) were used as a secondary followed by incubation with SuperSignal West Femto chemiluminescent substrate (Thermo Scientific, Waltham, MA). Western blot images were visualized using an Odyssey C-Digit scanner and processed using Image Studio software (LI-COR Biosciences, Lincoln, NE).

All Westerns were repeated 2-3 times and representative blots are displayed. Full length blots are provided in Supplemental Information.

IDO activity assay

Media collected from fresh or cryo-MSC stimulated with or without human IFN-γ/TNF-α was analyzed for kynurenine content as a marker of IDO activity[11]. L-kynurenine (Sigma Aldrich, St. Louis, MO) was dissolved in culture media and used to create a standard curve. 100 µL of conditioned media or standards were placed in a 96-well plate. 50 µL of 30% (w/v) trichloroacetic acid was added to each well to precipitate out proteins. The plate was heated for 30 minutes at 52°C to facilitate the conversion of N-formylkynurenine to kynurenine and then centrifuged at 1,200 x g for 15 minutes. 75 µL of supernatant from each sample or standard was mixed with 75 µL of Ehrlich's reagent (0.8% (w/v) 4-(Dimethylamino)benzaldehyde in acetic acid) and incubated at room temperature for 10 minutes. The plate was then read at 492 nm and the concentration of kynurenine in each sample was interpolated from the standard curve.

PBMC co-cultures

MSC immunosuppressive capability was assessed by direct co-culture with isolated PBMCs from leukapheresis reduction cones obtained from the DeGowin Blood Center at the University of Iowa Hospital and Clinics. MSC to PBMC ratios (1:3, 1:6, and 1:12) were established by seeding 250,000 PBMCs in wells containing 83,300 MSC, 41,600 MSC, or 20,800 MSC of a 48-well plate. MSC were plated 1 hour prior to addition of PBMCs in RPMI supplemented with 10% (v/v) FBS, 1% (v/v) Penicillin/Streptomycin, and 1% (v/v) L-glutamine. PBMCs were labeled with CellTrace CFSE Cell Proliferation Kit (Invitrogen, Carlsbad, CA) at a final dye concentration of 1 µM. The PBMCs were then stimulated with 250,000 Human T-activator CD3+/CD28+ Dynabeads (Invitrogen, Carlsbad, CA) in each well and cultured for 6 days. PBMC only with or without Dynabeads served as activated and un-activated controls respectively for all experiments. After 6 days, PBMCs were dispersed by gentle pipetting, collected, centrifuged at 500 x g for 5 minutes, and resuspended in 100 µL RPMI before analysis on an Accuri C6 flow cytometer. Unstimulated control PBMCs were used to set the gating threshold for each experiment (n=4).

Retinal ischemia/reperfusion injury and MSC transplantation

All animal experiments were carried out in accordance with the ARVO Statement for the Use of Animals in Ophthalmology and Vision Research and were approved by the IACUC committee of the University of Iowa. Unilateral retinal damage was induced by Ischemia/Reperfusion (I/R) injury as described earlier[12–14]. Briefly, male and female two-month old C57BL6/J (The Jackson Laboratory, Bar Harbor, ME) were anaesthetized by intraperitoneal injection of Xylazin/Ketamine (10 mg/kg and 100 mg/kg, respectively). Eyes received 0.5 % proparacaine eye drops for topical analgesia, pupils were dilated with 0.5% tropicamide (both Akorn, Lake Forest, IL), and corneas were kept moist until animals had fully recovered (GenTeal, Alcon, Fort Worth, TX). The anterior chamber was cannulated with a sterile 30-gauge needle, which was connected to a saline reservoir by a perfusion line. Intraocular pressure (IOP) was elevated to 80 mmHg in left eyes by setting the saline reservoir to an equivalent height (108 cm) above the mouse's head. Retinal ischemia was confirmed by blanching of the fundus and stasis within retinal vessels using fundus imaging. After one hour of IOP elevation, the cannula was carefully removed, and reperfusion was evident by resumption of retinal blood and recovery of pulsation.

Two hours after I/R, animals underwent isoflurane sedation and I/R eyes were treated with either fresh MSC (I/R + Fresh MSC, N=10) or cryo-MSC (I/R + Cryo-MSC, N=17). $3x10^4$ MSC in 3 µl PBS were transplanted into the vitreous cavity using a Hamilton syringe equipped with a 33-gauge needle. A vehicle control group received an equivalent volume of PBS (I/R + PBS, N=10). The right eyes of all mice received no manipulation and served as controls. Animals were euthanized at either three or seven days after I/R injury by CO_2 inhalation followed by cervical dislocation.

Detection of transplanted MSC

Eyes of animals having received cryopreserved MSC were harvest three (N=5) days after transplantation, fixed in 4% paraformaldehyde for 2 hours, sucrose embedded and processed for traversal sectioning. Eyes (N=7) obtained seven days after MSC transplantation were split in half; DNA was extracted from freshly isolated retinas for RT-PRC experiments from one half of the eye while the other half was processed for immunostaining. 7 µm sections were blocked in 1 % BSA/PBS for 30 min, washed and incubated with goat anti-human Tra 1-85 antibodies (1:50

in 0.3 % Triton X-100/PBS, R&D Systems, Minneapolis, MN) overnight. Slides were washed with PBS and an Alexa Flour 488 donkey anti-goat secondary antibodies (1:400 in PBS) was applied for 3 hours. After final rinses, nuclei were visualized using DAPI. Sections were coverslipped and images were taken using an Olympus BX41 microscope.

Detection of human DNA

Genomic DNA was extracted from the posterior retina of five eyes seven days after MSC transplant using DNeasy columns (Qiagen, Valencia, CA). 250 ng of this DNA was used in a quantitative PCR reaction using primers specific for human genomic DNA (forward: GAGAGCGTTTGGAAATTGGA, Reverse: TGGCTGCTGTTTCATGTCTC). Samples were amplified in a quantitative PCR reaction for 45 cycles using a CFX96 thermal cycler (BioRad, Hercules, CA). Data were compared against a standard curve was constructed using genomic DNA extracted from a known quantity of human MSC (17 to 16,750 cells). A positive control containing DNA from 1,675 MSC and a negative control (water only) were included. All measurements were taken in triplicate.

Analysis of retinal ganglion cell survival

All animals were euthanized seven days after I/R injury by CO_2 inhalation followed by cervical dislocation. Eyes were enucleated and fixed in 4% paraformaldehyde for 2 hrs. As previously described [15,16], retinas were immunostained for γ-synuclein, a marker for retinal ganglion cells (RGC), and the number of surviving RGC was determined. Briefly, retinas where incubated overnight with mouse anti-γ-synuclein primary antibody solution (1:400, Abnova Corporation, Walnut, CA, USA), followed by several rinses in PBS and incubation with an Alexa Fluor 488 donkey anti-mouse secondary antibody (1:300, Life technologies, Grand Island, NY). After another PBS wash, retinas were whole-mounted, cover slipped and imaged. Twelve images (318×318 µm, 40 X magnifications) were taken at predetermined mid-peripheral locations using a Nikon Eclipse i80 confocal microscope (Nikon Instruments Inc, Melville, NY). γ-synuclein positive RGC were counted in a masked fashion by an independent observer using the cell counter plugin in ImageJ software (NIH).

Statistical analysis

For statistical comparisons *in vitro* between fresh and cryo-MSC, One-way ANOVA with Sidak correction for multiple comparisons with significance set at $p<.05$ was used in Prism 6 (GraphPad, San Diego, CA). For *in vivo* experiments, averaged RGC data was analyzed using Tukey's honest significant difference (HSD) post hoc tests (with unequal *N*) in Statistica software (Dell, Round Rock, TX). P-values< .05 are considered as statistically significant. All data are given as mean ± standard deviation (SD).

Results

Cryopreservation marginally impairs MSC viability and metabolic activity

Cryopreservation is an inherently stressful process for cells, and it is not surprising to see detrimental effects on the viability and growth kinetics of cells immediately after thawing. Viability of MSC after thawing has been one of the most variable metrics in recent papers examining the use of cryo-MSC, ranging from as low as 50%[7] to greater than 90% viability[6,9]. These disparate finding could be related to the fact that pores form in membranes following exposure to DMSO[17] that could lead to false staining with traditional cell death markers including PI and Annexin V. Thus, here we sought to characterize the viability and growth kinetics of MSC following cryopreservation by directly labeling double stranded DNA breaks characteristic of cell death in MSC in the hour immediately post-thaw. In addition, we measured viability and metabolic activity 24, 48, and 72 hours after thawing to determine if cryopreservation has any lasting impact on MSC. Staining for double strand breaks with TUNEL immediately after thawing and after 1 hour of storage on ice revealed that MSC viability is not significantly reduced by cryopreservation when carried out as described herein (0.1-0.2% of cells stained positive by TUNEL in all groups, Figure 1A). In contrast, when viability was assessed by PI staining cryo-MSC displayed a minor, but statistically significant, reduction in viability both 24 and 48 hours after thawing (2.8% and 1.9% reduction respectively, $n=5$, $p<.05$, Figure 1B). Differences in viability were no longer significant 72 hours after thawing (1.3% reduction, Figure 1B). Similarly, while cryo-MSC displayed slightly lower metabolic activity than fresh MSC at 24 (18% lower), 48 (17% lower), and 72 hours (4% lower) after thawing, as measured by XTT, differences were not statistically significant at any time point (Figure 1C). Overall,

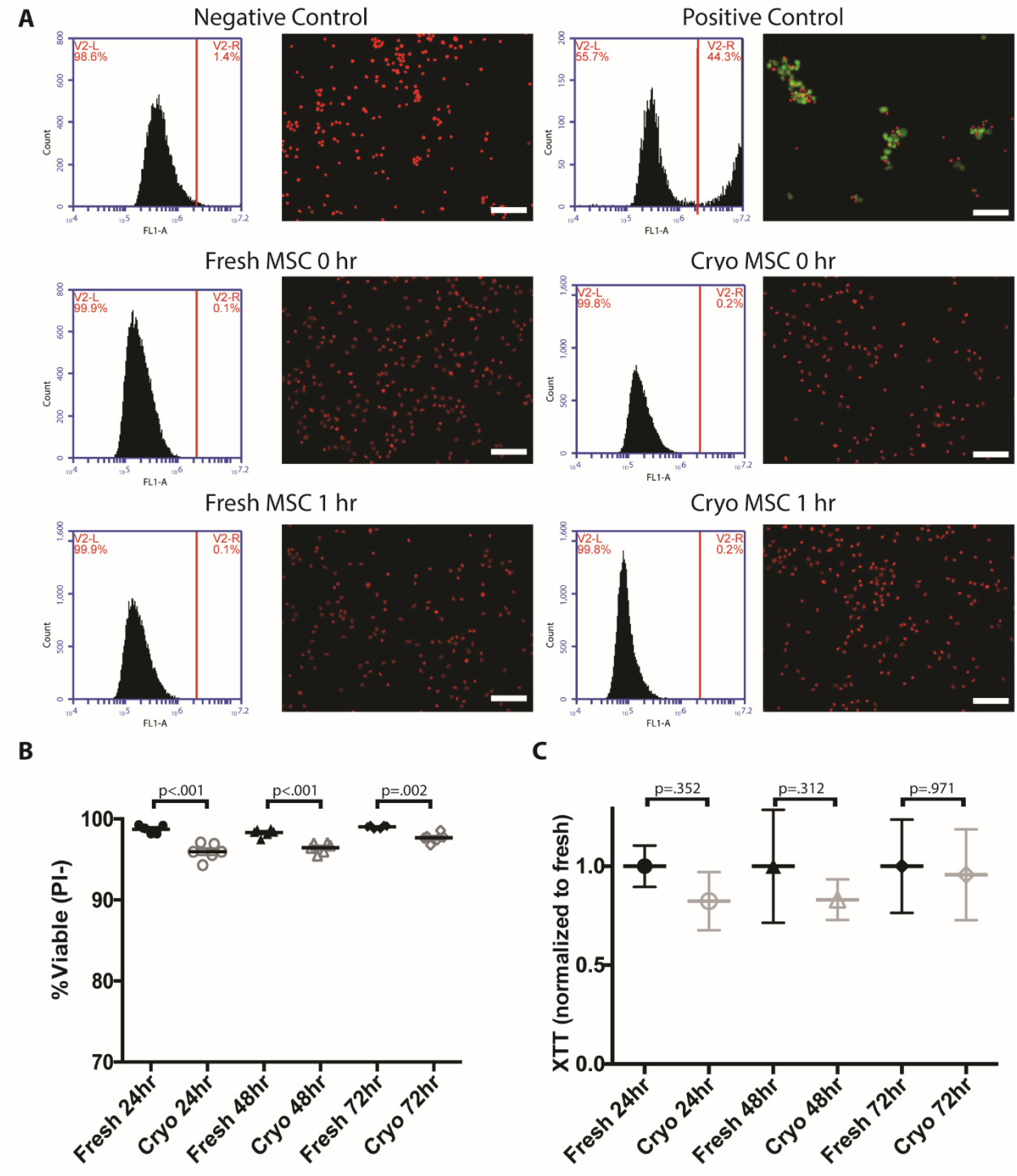

Figure 1. Cryopreservation marginally affects MSC viability and metabolic activity.

(A) MSC harvested from culture or thawed directly out of cryostorage were assayed for double strand DNA breaks by TUNEL staining. MSC were analyzed immediately after thawing or after 1 hour of storage on wet ice by flow cytometry and fluorescence imaging. The percent of positive and negative stained cells is reported in the upper right and left corners of each plot

Figure 1 – Continued

respectively. Cells were fixed, stained with PI (red) and FITC-dUTP (green). Double positive cells were considered dead. (Scale Bar = 100 µm) (B) Viability of MSC plated after thawing was compared to donor and passage matched MSC from fresh cultures 24, 48, and 72 hours after thawing. Cells were stained with Hoechst 33342 and PI and imaged with a fluorescence microscope. Cells double positive for Hoechst 33342 and PI were considered dead. (One-way ANOVA with Sidak correction for multiple comparisons, $p<.05$ considered significant, n=5) (C) The metabolic activity of MSC after cryopreservation was compared to donor and passage matched MSC from continuous cultures using XTT (mean ± SD, One-way ANOVA with Sidak correction for multiple comparisons, $p<.05$ considered significant, n=6). All experiments performed with MSC from donors 8002L and 7083 at passages P3-P5.

cryopreservation and cell handling, as performed in this study, appears to only marginally reduce MSC viability and metabolic activity.

Cryopreserved MSC maintain immunomodulatory potential

Sterile inflammation following ischemia/reperfusion injury leads to the destruction of cells in the tissue that would otherwise survive the ischemic insult. MSC can prevent this untargeted damage by inducing neutrophil apoptosis through the expression of IDO, which produces kynurenine metabolites known to be toxic to neutrophils.[18,19] In addition, MSC express a variety of factors that have been demonstrated to directly suppress T cell activation and proliferation[20]. Thus, we sought to determine if MSC's immunomodulatory potency was impaired during cryopreservation.

We have previously described that IDO expression varies significantly by MSC donor and passage[21], and consequently all experiments here were completed with donor and passage matched MSC. MSC exposed to IFN-γ immediately after thawing expressed similar levels of IDO as MSC maintained in fresh cultures (Figure 2A). Full IDO western blots are shown in Figure 7. Very little IDO was detectable in either fresh or cryo-MSC after 24 hours of cytokine stimulation, but IDO levels increased similarly in both groups 48 and 72 hours after stimulation. In addition, both fresh and cryo-MSC stimulated for 48 hours with either IFN-γ or IFN-γ and TNF-α displayed high levels of IDO protein expression (Figure 2B) and concomitant IDO activity as measured by kynurenine production (Figure 2C). Next, to determine if cryo-MSC maintain their ability to suppress T cell activation, we performed a co-culture experiment with primary human PBMCs. Unstimulated PBMCs and PBMCs stimulated with CD3/CD28 dynabeads served as unactivated and activated controls, respectively (Figure 2D). Both fresh and cryo-MSC were able to suppress proliferation of PBMCs when cultured at MSC:PBMC ratios of 1:3, 1:6 and 1:12 (Figure 2E). Mean PBMC proliferation rates in the presence of fresh MSC were 21%, 35%, and 57%, respectively, whereas PBMC in the presence of cryo-MSC proliferated at 31%, 43%, and 59%, respectively (Figure 2F). None of the differences were statistically significant (1:3 and 1:6 n=4, 1:12 n=3). Thus, in our hands, cryopreservation did not significantly impair MSC's immunomodulatory potential.

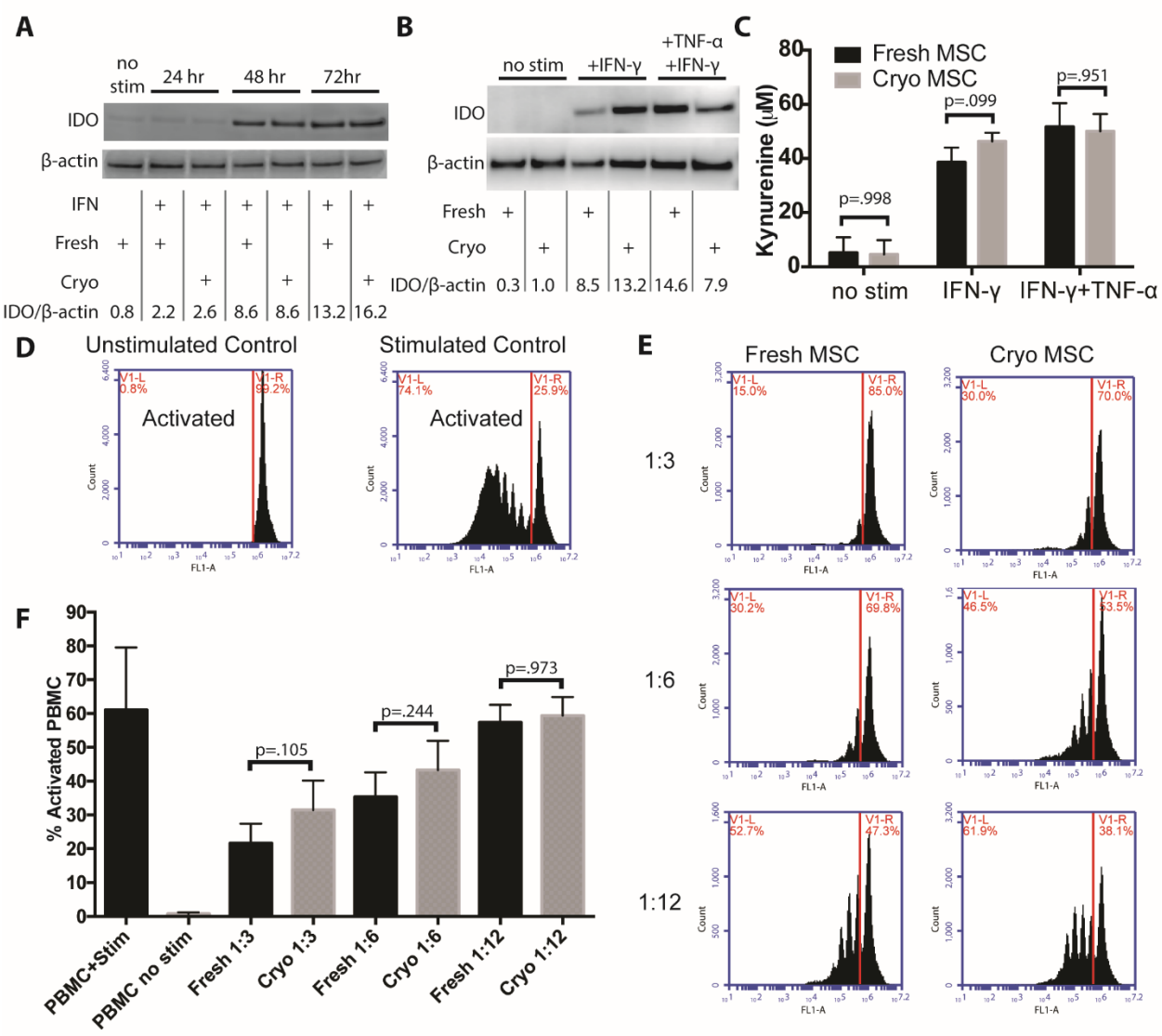

Figure 2. Cryopreserved MSC maintain immunosuppressive potential.

(A) Representative Western blot of IDO protein in fresh and cryo-MSC after exposure to IFN-γ for 24, 48, or 72 hours. β-actin provided as a loading control. (B) Representative Western blot of IDO in fresh and cryo-MSC after exposure to IFN-γ or TNF-α/IFN-γ for 48 hours. β-actin provided as a loading control. (C) IDO activity as measured by the concentration of kynurenine in the conditioned media collected from fresh or cryo-MSC exposed to IFN-γ or TNF-α/IFN-γ for 48 hours (mean ± SD, One-way ANOVA with Sidak correction for multiple comparisons, $p<.05$ considered significant, n=6). (D) Example unstimulated and stimulated PBMC controls used for gating and setting the activation threshold. PBMCs stained with CFSE remain as a single population in unstimulated conditions but upon stimulation with CD3/CD28 dynabeads become activated and proliferate. (E) Example flow cytometry histograms of stimulated CFSE

Figure 2 – Continued

stained PBMCs co-cultured with fresh or cryo-MSC at MSC:PBMC ratios of 1:3, 1:6 or 1:12. (F) Quantification of the percent of activated PBMCs in each co-culture condition compared to unstimulated and stimulated controls. No statistical differences between fresh MSC and cryo-MSC at each ratio. (mean ± SD, One-way ANOVA with Sidak correction for multiple comparisons, $p<.05$ considered significant, 1:3 and 1:6 n=4, 1:12 n=3). All experiments performed with MSC from donors 8002L and 7083 at passages P3-P5.

Effect of cryopreservation on MSC secretome

In addition to blunting a T cell mediated inflammatory response, the ability of MSC to support cell survival in ischemia/reperfusion could also involve the synthesis of growth factors that prevent cell death and aid the reestablishment of the vasculature. Indeed, VEGF secreted from MSC has previously been shown to reduce neuronal loss in a rat stroke model[22] and PDGF secreted from MSC has been implicated as being neuroprotective for retinal ganglion cells[23]. Thus, we sought to identify any potential changes in the MSC growth factor secretome that arises due to cryopreservation. The quantity and composition of the MSC secretome is heavily dependent on MSC donor and over 10-fold differences in expression and secretion levels have been observed by multiple groups when comparing individual donors subjected to identical culture conditions[21,24–26]. Thus, we analyzed fresh and cryopreserved passage matched MSC derived from a single donor, #7083, in order to isolate the impact of cryopreservation on the MSC secretome. Fresh or cryo-MSC, from donor #7083, were plated in reduced serum (1% FBS) growth media with or without a cytokine cocktail selected to mimic *in vivo* inflammatory conditions. After 48 hours, the media was collected and analyzed for the presence of 40 growth factors. A complete table of growth factor concentrations for fresh and cryo-MSC with and without cytokine stimulation is provided in Table 1. Of the 40 screened factors, only 14 were detectable in at least 2 of the 4 conditions tested, and their concentrations are displayed in Figure 3A, C. In addition, as a statistical measure of the impact of cryopreservation on the production of each growth factor, the effect size, displayed as fold change compared to fresh MSC is plotted in Figure 3B, D. Overall, the profile and magnitude of growth factor expression was similar when comparing cryo-MSC to fresh MSC in both the unstimulated (Figure 3A, B) and stimulated conditions (Figure 3C, D). Expression of PDGF which is known to be anti-apoptotic and pro-angiogenic, was slightly elevated in cryo-MSC compared to the fresh MSC while VEGF levels remained similar in both groups. Cytokine stimulation resulted in marked increase in secretion of both stem cell factor receptor (SCF R/c-kit) and TGF-β1 in both fresh and cryo-MSC. BMP-7 exhibited the most striking difference between cryo-MSC and fresh MSC. It was robustly expressed in both unstimulated and stimulated cryo-MSC but was undetectable in both forms of fresh MSC. Overall, differences in secreted factors between fresh and cryo-MSC were subtle and the impact of these differences must be considered in the context of specific

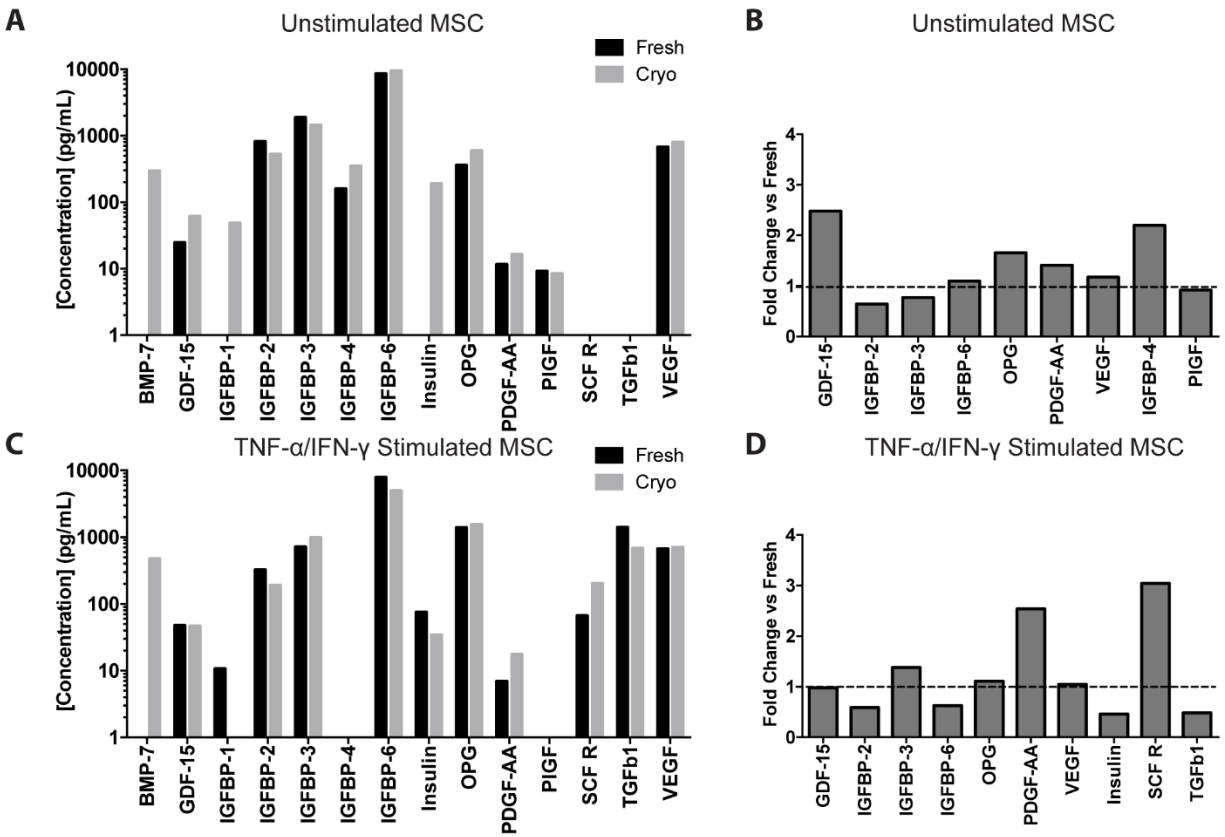

Figure 3. Cryopreservation minimally impacts baseline or stimulated growth factor secretion by MSC.

Fresh and cryo-MSC, both passage 4 MSC from donor 7083, were cultured for 48 hours in reduced serum media with or without stimulation by TNF-α/IFN-γ, the media was collected, and screened for 40 growth factors. Of the 40 proteins, 14 were detectable in at least 2 of the tested conditions and are reported here. Values represent measured concentration after background subtraction (unconditioned control media). A full table of values is available in Supplemental Figure 1. (A) The concentration of each growth factor produced by fresh and cryo-MSC over 48 hours in unstimulated conditions. (B) Fold change in concentration in unstimulated MSC, [Cryo]/[Fresh] (C): The concentration of each growth factor produced by fresh and cryo-MSC over 48 hours in stimulated conditions. (D) Fold change in concentration in stimulated MSC, [Cryo]/[Fresh]. Dashed line at 1 corresponds to no-change between groups.

therapeutic applications. Thus, we turned to an *in vivo* model of retinal ischemia reperfusion injury to determine if MSC's therapeutic potency was impaired by cryopreservation.

Fresh MSC and cryo-MSC equally rescue retinal ganglion cells following I/R injury

MSC aggregates form in vitreous like conditions

We next wanted to determine if the vitreous of the eye would be conducive to formation of MSC aggregates. Therefore, we injected MSCs into our simulated vitreous constructed from an alginate-gelatin solution (Figure 4A). The vitreous is mainly composed on hyaluronic acid, collagen, and water.[27] While our *in vitro* vitreous did not contain these components, both alginate and gelatin have similar chemical structures and physical properties. We found that in this environment, we did get aggregation of MSCs indicating that the vitreous may promote formation of spheroids (Figure 4B).

Cryo-MSCs maintain potency in a retinal ischemia/reperfusion mouse model

In order to assess whether cryo-MSC retain their neuroprotective potential *in vivo* we employed retinal ischemia/reperfusion (I/R) as a model of central nervous system (CNS) injury (Figure 5A). As expected, 1 hour of ischemia induced significant retinal damage as measured by retinal ganglion cell (RGC) loss. Eyes in the vehicle-only control group displayed a loss of approx. 88% of RGC seven days after I/R injury when compared to the non-ischemic contralateral eyes (I/R + PBS: 309 ± 308 RGC mm^2; non-ischemic: 2413 ± 413 RGC mm^2; $p<.001$, Figure 5B,C). Loss of RGC was significantly ameliorated in the presence of fresh MSC. Transplantation of these cells resulted in survival of 829 ± 405 RGC mm^2 ($p=.019$). Moreover, transplantation of cryo-MSC provided an equivalent effect on RGC survival (845 ± 320 RGC mm^2) and is also statistically significant when compared to the RGC density of the vehicle group ($p=.024$).

Rescue of RGC did not appear to depend on engraftment or persistence of MSC in the eye. Staining the human cell surface antigen Tra 1-85 has been used successfully to identify human cells, including MSC, in xenogenic transplant experiments[28,29]. By staining retina sections for Tra 1-85, a small portion of surviving MSC could be consistently detected in I/R eyes three days after transplantation (Figure 6A,B). The remnant of MSC were found either in the vitreous, on the surface of the nerve fiber layer, or partially integrated, in the retinal ganglion cell layer

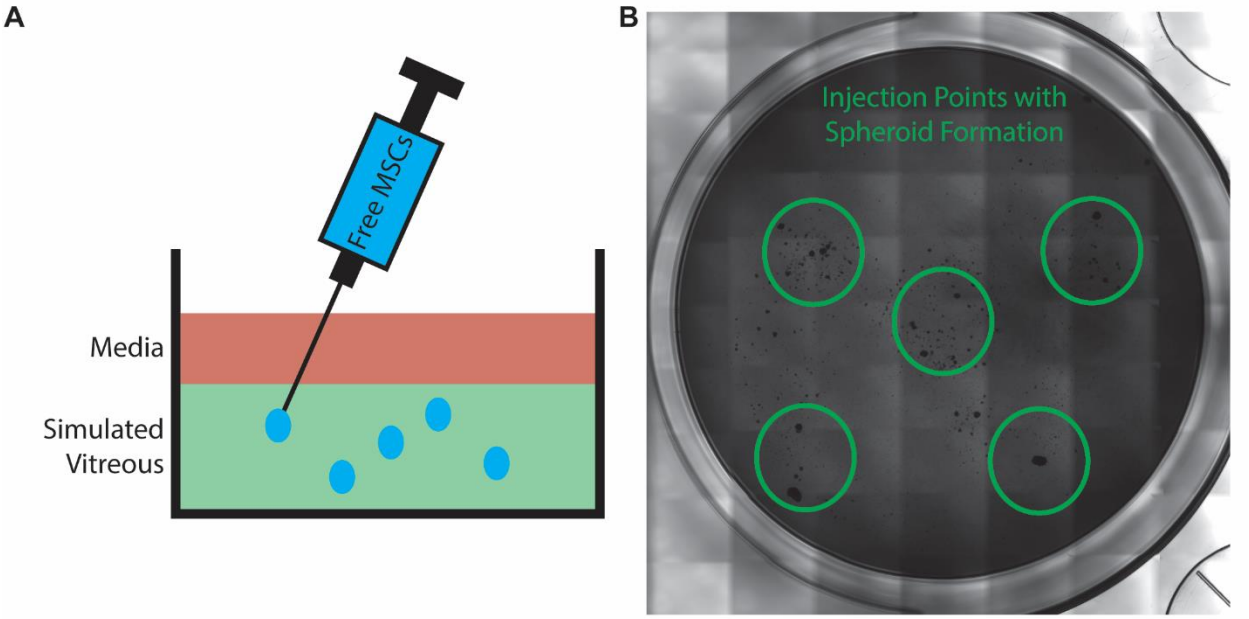

Figure 4. Locally administered MSCs form aggregates in a simulated vitreous.
(A) Schematic showing MSCs were injected into an alginate-gelatin gel and allowed to aggregate. (B) After 3 days, brightfield imaging tile scan was taken showing MSC spheroid formation.

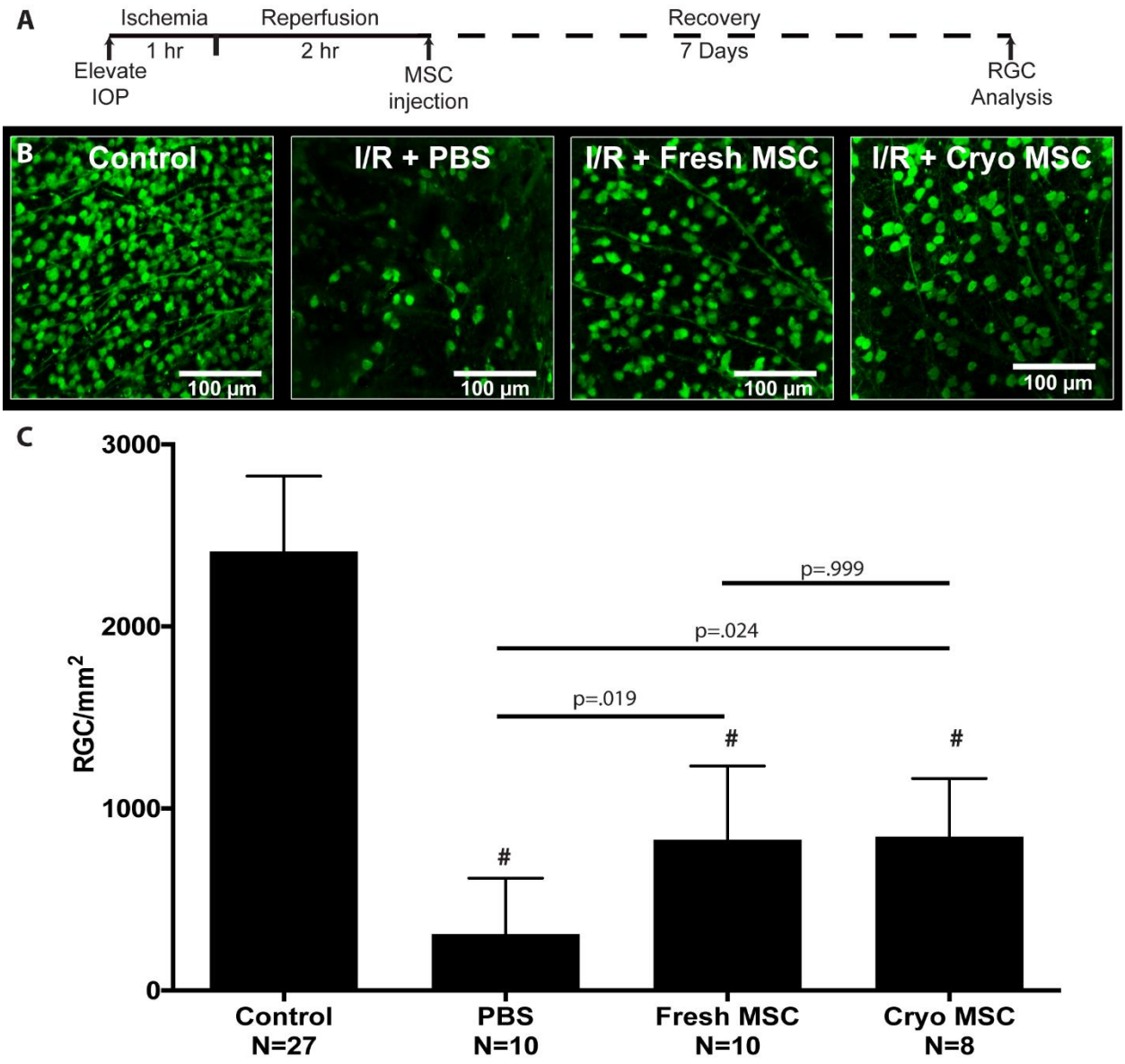

Figure 5. Cryopreserved MSC prevent RGC loss after ischemia/reperfusion injury *in vivo*. (A) Injury and treatment timeline for all retinal ischemia/reperfusion model. Intraocular pressure (IOP) was elevated to blanch the fundus for 1 hour, after which perfusion was restored. 2 hours after reperfusion, eyes were injected with one of the MSC groups or PBS as a vehicle control. 7 days later, animals were sacrificed, and eyes were analyzed for RGC counts. (B) Representative images of γ-synuclein immunostaining of whole-mounted retina from non-ischemic retinas (control) and retinas after I/R treated with vehicle (I/R + PBS), fresh MSC (I/R +Fresh MSC) or cryo-MSC (I/R + Cryo-MSC). (C) Quantitative analysis of RGC survival in eyes after I/R revealed a significant rescue effect after transplantation of both fresh MSC and cryo-MSC (mean

Figure 5 – Continued

± SD, One-way ANOVA with Tukey honest significant difference post hoc test to correct for multiple comparisons, $p<.05$ considered significant). # denotes $p< 0.001$ in comparison to healthy control. Both cryo-MSC and fresh MSC were from donor 7083.

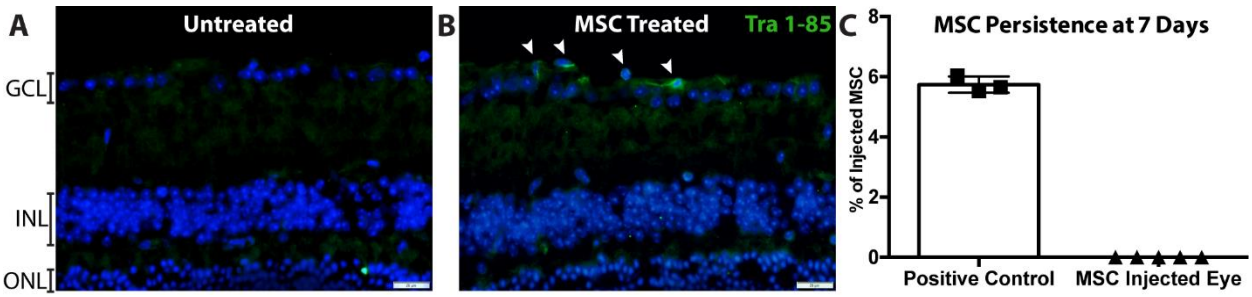

Figure 6. Cryopreserved MSC do not persist in the eye following ischemia/reperfusion injury. Human cells, identified by human specific Tra 1-85 immunostaining and counterstained with DAPI were undetectable in (A) untreated eyes and rare in (B) treated eyes at 3 days, white arrows indicate positive cells atop the ganglion cell layer. (C) Quantitative PCR for human genomic DNA remaining in mouse retina seven days after transplantation. Human DNA was not detected in any of the tested eyes (n=5, mean ± SD). Data normalized as % of injected as 30,000 MSC were delivered to each eye. Donor 7083 used for all mice. Pos: positive control is DNA extracted from 1,670 MSC, corresponding to 5.6% of the total injected MSC). GCL: Ganglion cell layer, INL: Inner Nuclear Layer, ONL: Outer Nuclear Layer.

(Figure 6B). After 7 days, no MSCs were detected and furthermore, no signs of tumor formation were observed in any of the eyes by histological analysis (n=7). To confirm MSC did not persist in the eye and no human derived tumors had formed, RT-PCR was performed. PCR amplification of genomic DNA extracted from the retinas of treated eyes did not indicate the presence of human DNA within the mouse tissue 7 days after transplantation (Figure 6C). These data indicate that all of the tested samples contained fewer than 17 cells, which was the lowest concentration included in the standard curve and support our immunohistochemical findings suggesting that MSC do not persist in the retina at 7 days. The absence of human genomic DNA also demonstrates the absence of MSC derived tumors. Thus, our data not only demonstrate that use of human MSC is safe and effective in this mouse model of retinal I/R injury but are also congruent with our *in vitro* data indicating that cryopreservation does not significantly diminish the function of MSC.

Discussion

Successful application of MSC to treat numerous conditions in animal models has led to a rapid increase in clinical trials exploring MSC therapy[2]. The safety of MSC therapy in clinical trials to date has only hastened the exploration of MSC for more and more conditions[30]. While most studies using animal models and even small clinical trials have utilized fresh MSC cultured on-site, cryopreservation of MSC is essential to the widespread application of MSC-based therapies. Cryopreservation allows for MSC to be prepared by specialized facilities, in large batches under the application of accepted quality control measures. Preservation and storage are already routine for other tissue engineered products: Organogenesis' Apligraf can be stored for 15 days at 20-23°C and Orthofix's Trinity Elite bone allograft can be stored for weeks at -80°C allowing off-the-shelf use as the need arises and eliminating the need for on-site GMP cell culture facilities.

Importantly, the availability of cryo-MSC enables administration of large doses of cells without time delay caused by culture expansion. While development of cryopreservation techniques for MSC that minimize loss of therapeutic function is a critical step to advancing MSC-therapy for all applications, many acute-onset conditions such as ischemic events or acute GvHD would specifically benefit from an off-the-shelf MSC therapy. Tissue damage in these conditions is often rapid and without immediate treatment, the desired therapeutic effect may not

be fully realized. For example, in the retinal ischemia/reperfusion model employed herein almost all damage occurs within the first 72 hours after the insult and little additional damage is observed 7 days after reperfusion[12].

To date, studies focused on the impact of cryopreservation on MSC function have yielded mixed results.[31] Cryopreservation of MSC has become routine and MSC stored for extended periods of time have been shown to have low tumorigenic potential[32], maintain growth kinetics upon thawing[33], and remain capable of multilineage differentiation.[33–36] When MSC were examined for their ability to differentiate to form bone, cryopreservation did not significantly impact the differentiation capacity of the cells in *in vitro* assays[33] or after *in vivo* transplantation.[34–36] Subcutaneously implanted scaffolds in primate[34] and murine[35,36] models have revealed no statistical difference between fresh and cryo-MSC's osteogenic potential. In contrast, studies focused on the use of MSC for their secreted trophic factors have reported detrimental effects from cryopreservation. Most notably, MSC have been reported to have poor viability after cryopreservation which reduces the number of cells capable of responding to inflammatory cues[7]. In addition, cellular debris in one study induced hyperproliferation of T cells in co-culture experiments[7]. While MSC function in *in vitro* potency assays are informative, the critical question is whether cryopreservation impairs MSC function *in vivo*. Until now, data comparing the efficacy of cryo-MSC compared to fresh MSC *in vivo* and in humans has been limited. A post-hoc analysis of clinical outcomes in acute GvHD patients receiving intravenous injection of fresh or cryo-MSC revealed patients receiving fresh MSC tended to respond better than patients receiving cryo-MSC[9].

We sought to determine whether cryopreservation would impact the therapeutic potency of MSC intended to combat I/R injury in the setting of localized delivery. Multiple mechanisms lead to cell death in the context of ischemia/reperfusion injury in the CNS. In addition to hypoxic insult, reperfusion of the ischemic tissue results in the generation of damaging reactive oxygen species and an influx of inflammatory cells that cause sterile inflammation[37]. While inflammation benefits clearance of damaged cells, activated neutrophils in sterile inflammation often contribute to damage, and viable cells are indiscriminately killed while cellular debris is cleared. Sterile inflammation has been well documented to significantly contribute to tissue damage following ischemic events in a variety of tissues[38]. For example, inhibition of neutrophil function by knocking out Nlrp3 prevented inflammasome activation and significantly reduced

the extent of tissue damage in a model of acute renal ischemia[39]. In addition, antigen presenting cells such as dendritic cells are exposed to antigens from dying cells and damage associated molecular patterns (DAMPs) released by necrotic cells that serve as adjuvants[40]. These activated dendritic cells can then migrate to lymph nodes where they stimulate a T cell response to antigens in the ischemic tissue.[41] Thus, preservation of both cell viability and MSC immunomodulatory properties is critical to the successful use of cryo-MSC to treat ischemia/reperfusion injury.

Numerous cryopreservation techniques and cryoprotectants have been used to preserve MSC with variable effects on the phenotype of cells post-thaw. Recent reviews by Yong *et al*.[31] and Marquez-Curtis et al.[42] provide an in depth overview of emerging cryopreservation technology. As viability of cells post-thaw appeared to be a predictor of MSC function in past studies, we used a cryopreservation media and method that has worked well in our lab and others[43] for maximizing post-thaw recovery. MSC were frozen in serum-free, xeno-free CryoStor CS5 media containing 5% DMSO at a concentration of $1x10^6$/ml using a controlled-rate freezing cell at 1°C/min. This process consistently yields MSC with >95% viability post-thaw. Cryo-MSC had an overall similar profile of secreted growth factors compared to passage and donor matched fresh MSC. MSC preserved and thawed using our protocol responded to exposure to IFN-γ by synthesizing IDO and converting tryptophan to kynurenine at the same rate as fresh MSC. In addition, these cryo-MSC remained suppressive of anti-CD3/anti-CD28 activated PBMCs in co-culture assays. While these findings stand in contrast to previous studies that reported impaired immunosuppressive properties using cryopreservation techniques that yielded 40-50% dead cells after thawing[7], they are consistent with the notion that post-thaw viability is critical for post-thaw immunomodulatory function. Thus, viability, and not cryopreservation per se, appears to be a predictor of MSC function. Our study demonstrates that when viability is maintained, MSC remain functional in *in vitro* potency assays regardless if they are fresh or cryopreserved. This is in agreement with a recent study from RoosterBio which reported cryopreservation in CryoStor CS5 results in MSC with high viability, IDO activity, and similar cytokine secretion compared to fresh MSC.[43]

Finally, we demonstrated cryo-MSC remain therapeutic when locally injected immediately after thawing in a retinal model of I/R. Retinal I/R leads to rapid destruction of RGCs, neurons on the surface of the retina that transmit signals received from photoreceptor

cells via bipolar and amacrine cells to visual processing centers of the brain through long axons that form the optic nerve[44]. The inner layer of the retina, were the RGC cell bodies reside, have been demonstrated to be particularly sensitive to hypoxia[45], thus the ability to salvage RGC in the setting of I/R is critical if some degree of vision is to be preserved. In addition, retinal I/R injury not only resembles various ophthalmologic disorders causing visual impairment such as ischemic optic neuropathies and glaucoma, but also recapitulates many aspects of CNS injury, in particular stroke[46–48]. The analogy in the pathobiology with respect to hypoxia, oxidative stress and inflammation makes the animal model of retinal I/R extremely suitable to determine whether transplantation of cryo-MSC into the ischemic retina improves RGC survival as an off-the-shelf therapy. The rapid onset of reactive oxygen species and inflammatory cells in the ischemic tissue following reperfusion requires any mitigating treatment to be applied quickly if ganglion cells are to be salvaged. Thus, cell therapy strategies that require *in vitro* culture prior to infusion are not suitable for treating I/R injury. In our model, we demonstrated that MSC could be taken directly from cryostorage, thawed, washed, and locally injected into the ischemic tissue without impairing the therapeutic potency of the MSC. These findings are similar to those of earlier studies that suggested that retinal transplantation of MSC improves RGC survival after injury [23,49]. However, these studies relied on experimental designs that employed fresh MSC transplanted prior to injury. Herein we significantly extend these findings by demonstrating that transplantation of human MSC taken directly from cryostorage and injected two hours after reperfusion is significantly protective. This is a crucial difference from a translational point of view as our model recapitulates a clinical scenario, in which patients seek treatment in the hours following an ischemic event, receive reperfusion therapy, and would then be able to receive an off-the-shelf therapy to prevent secondary damage from the I/R injury. Our finding that MSC can be cryopreserved without an apparent loss in efficacy suggests that storage and use of MSC in a clinical setting may be feasible for I/R injury to the eye and CNS.

Conclusion

The success of MSC clinical therapy will ultimately depend on the availability of a rapidly accessible source of reliably effective cells. Cryopreservation greatly simplifies the logistics of cell therapy, by allowing centralized GMP facilities to grow and phenotype MSC. In addition, cryopreservation allows MSC to be used on-demand, eliminating the need to wait for

cells to be expanded or acclimated in culture prior to use. However, cryopreserved cells only have therapeutic utility if their potency is preserved in the process. The work presented here outlines a simple and effective method for cryopreserving MSC that maintains >95% viability, expression of immunomodulatory factors and growth factors, and the ability of MSC to suppress activated immune cells. In addition, we demonstrate cryo-MSC perform as well as fresh MSC in a retinal model of I/R injury. Thus, we observed no major detriment in MSC phenotype or potency in *in vitro* and *in vivo* assays following cryopreservation making cryo-MSC a feasible off-the-shelf therapy for some indications. Further studies are warranted targeting additional disease indications and delivery routes to fully elucidate conditions and modes of delivery that are compatible with freshly thawed cryo-MSC.

Acknowledgments

Financial support for this work was provided in part by the NIDDK Diabetic Complications Consortium (DiaComp,www.diacomp.org), grant DK076169 to J.A.A. and start-up funding provided by the Fraternal Order of Eagles Diabetes Research Center to J.A.A. M.H.K. was supported in part by Merit Review Award Number I01 RX001163-02 from the United States (U.S.) Department of Veterans Affairs Rehabilitation R&D (Rehab RD) Service

Author Contributions

O.W.G., A.J. Burand, A.J. Brown, M.H.K., and J.A.A designed research and wrote the manuscript; O.W.G., A.J. Burand, J.A.A., and A.J. Brown performed research; O.W.G., M.H.K., J.A.A., R.J.D., A.J. Burand, and A.J. Brown analyzed data.

Author Conflicts of Interest

The authors declare no conflicts of interest.

Supplemental Material

Table 1. Growth factor array data for 40 growth factors.

For each condition, the concentration of the growth factor was calculated by subtracting the raw sample concentration from the media control baseline (i.e. [sample] = [raw sample] – [media control]). Thus, concentrations in the table represent the mean ± SD concentration of growth factor contributed by the presence of the MSC in pg/mL. Concentration values that were either below the media control baseline or the Assay Detection Limit (DL) are labeled '< DL'. If the media control was < DL, then no subtraction was performed on the sample concentration for the given growth factor. Each growth factor was measured 4 times and if 3 of the 4 measurements were below the detection limit, they were listed as '<DL'. For each growth factor, a one-way ANOVA with Sidak correction for multiple comparisons was performed to compare cryo-MSC to fresh MSC under stimulated and unstimulated conditions. A p-value <.05 was considered significant and multiplicity adjusted p-values are provided in the table.

		Increase in concentration above media control								
		Unstimulated		Fresh vs Cryo Unstimulated		Stimulated with IFN-γ/TNF-α		Fresh vs Cryo +IFN-γ/TNF-α		
Growth Factor	**Media Control**	**Fresh MSC**	**Cryo MSC**	**Significant?**	**p-value**	**Fresh MSC**	**Cryo MSC**	**Significant?**	**p-value**	**Assay DL (pg/mL)**
BMP-7	< DL	< DL	295 ± 365	NA	-	< DL	474 ± 127	NA	-	54
GDF-15	< DL	24 ± 20	61 ± 17	Yes	0.01	48 ± 8	47 ± 13	No	0.99	3
IGFBP-1	8 ± 3	< DL	48 ± 10	NA	-	11 ± 12	< DL	NA	-	5
IGFBP-2	493 ± 40	821 ± 229	627 ± 291	No	0.32	324 ± 216	190 ± 174	No	0.68	27
IGFBP-3	< DL	1869 ± 130	1445 ± 41	No	0.47	714 ± 776	986 ± 381	No	0.75	270
IGFBP-4	1253 ± 477	159 ± 262	349 ± 264	No	0.39	< DL	< DL	NA	-	270
IGFBP-6	< DL	8563 ± 2102	9397± 1220	No	0.69	7870 ± 428	4931 ± 1663	Yes	0.03	135
Insulin	< DL	< DL	189 ± 123	NA	-	75 ± 139	34 ± 53	No	0.71	27
OPG	< DL	358 ± 31	594 ± 113	No	0.39	1386 ± 449	1540 ± 211	No	0.65	5
PDGF-AA	18 ± 7	11.6 ± 0.7	16 ± 7	No	0.43	7 ± 8	18 ± 2	Yes	0.04	13
PIGF	< DL	9 ± 5	8 ± 4	No	0.83	< DL	< DL	NA	-	5

Table 1 – Continued

SCF R	< DL	< DL	< DL	NA	-	67 ± 22	202 ± 155	No	0.06	27
TGFβ1	< DL	< DL	< DL	NA	-	1403 ± 580	678 ± 584	Yes	0.05	135
VEGF	< DL	620 ± 210	796 ± 214	No	0.30	670 ± 120	703 ± 93	No	0.96	13
AR	< DL	< DL	< DL	NA	-	< DL	< DL	NA	-	13
BDNF	5 ± 2	< DL	< DL	NA	-	< DL	0.29 ± 0.08	NA	-	3
bFGF	420 ± 310	< DL	< DL	NA	-	< DL	< DL	NA	-	27
BMP-4	< DL	< DL	< DL	NA	-	< DL	< DL	NA	-	135
BMP-5	272 ± 57	< DL	< DL	NA	-	< DL	< DL	NA	-	135
β-NGF	< DL	< DL	< DL	NA	-	< DL	< DL	NA	-	13
EGF	< DL	< DL	< DL	NA	-	< DL	< DL	NA	-	0.3
EGF R	< DL	< DL	< DL	NA	-	< DL	< DL	NA	-	13
EG-VEGF	66 ± 51	< DL	< DL	NA	-	< DL	< DL	NA	-	13
FGF-4	862 ± 111	< DL	< DL	NA	-	< DL	< DL	NA	-	135
FGF-7	109 ± 16	< DL	57 ± 57	NA	-	< DL	< DL	NA	-	13
GDNF	29 ± 9	< DL	< DL	NA	-	< DL	< DL	NA	-	5
GH	170 ± 42	< DL	< DL	NA	-	< DL	< DL	NA	-	13
HB-EGF	< DL	< DL	< DL	NA	-	< DL	< DL	NA	-	13
HGF	39 ± 20	< DL	< DL	NA	-	< DL	< DL	NA	-	5
IGF-I	< DL	< DL	< DL	NA	-	< DL	< DL	NA	-	27
MCF R	< DL	< DL	< DL	NA	-	< DL	< DL	NA	-	54
NGF R	35 ± 23	< DL	4 ± 4	NA	-	< DL	< DL	NA	-	13
NT-3	< DL	< DL	< DL	NA	-	< DL	< DL	NA	-	54
NT-4	< DL	< DL	72 ± 12	NA	-	< DL	< DL	NA	-	13
SCF	< DL	< DL	< DL	NA	-	< DL	< DL	NA	-	13
TGFα	< DL	< DL	< DL	NA	-	< DL	< DL	NA	-	13
TGFβ3	< DL	< DL	< DL	NA	-	< DL	55 ± 9	NA	-	54
VEGF R2	< DL	< DL	< DL	NA	-	28 ± 24	< DL	NA	-	13
VEGF R3	< DL	< DL	< DL	NA	-	< DL	< DL	NA	-	54
VEGF-D	< DL	< DL	29 ± 13	NA	-	< DL	< DL	NA	-	27

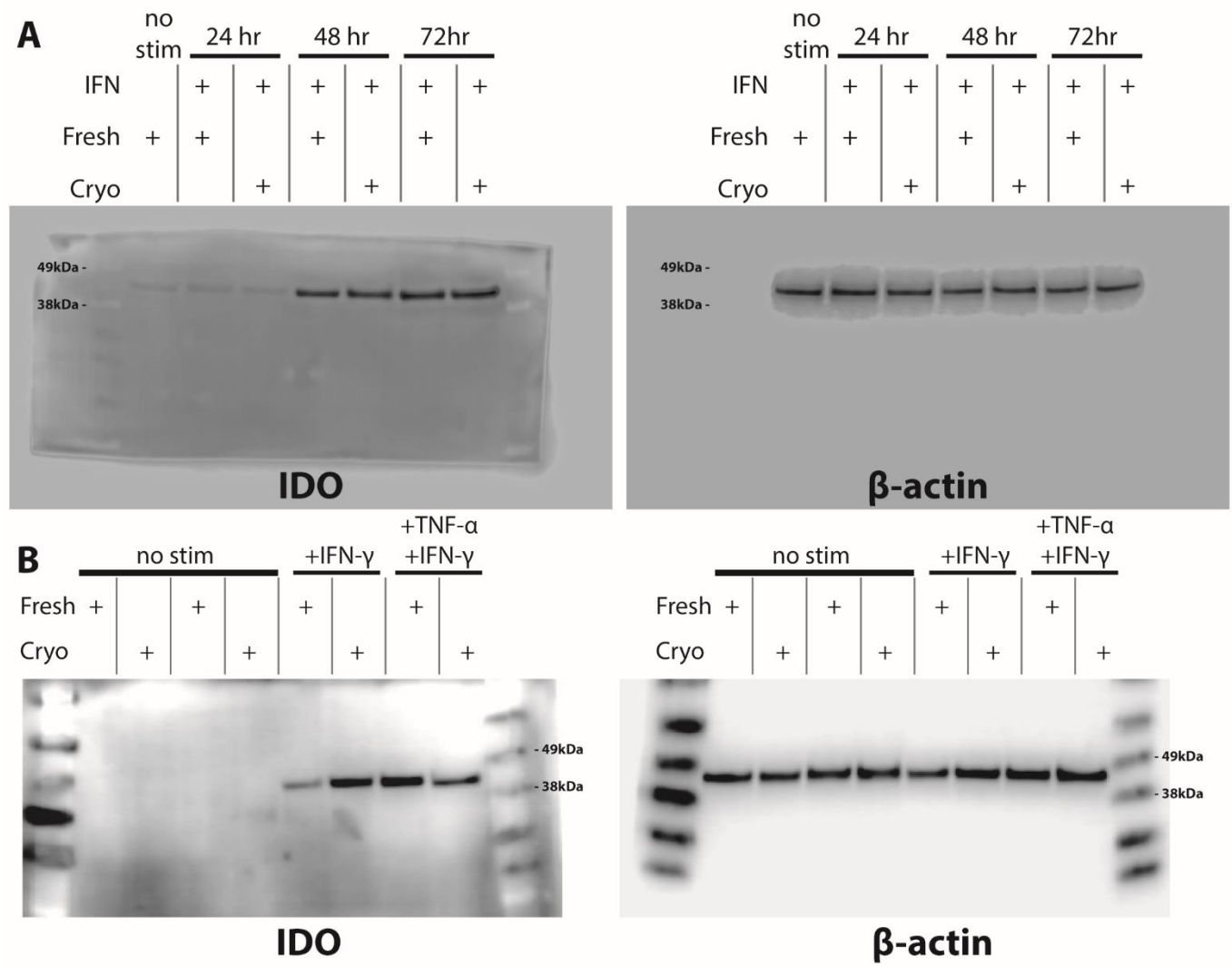

Figure 7. IDO production remains consistent after cryopreservation.

Full length blots from which the cropped blots in (A) Fig 2A and (B) Fig 2B were derived. Molecular weight markers were annotated based on the location of pre-stained molecular weight markers.

2.3. PRELICENSING MSCS WITH IFN-γ HINDERS FUNCTION IN ISCHEMIA/REPERFUSION INJURY

Introduction

Success of mesenchymal stromal cell (MSC) therapies in disease models has sparked hundreds of clinical trials in humans[2]. While the first MSC clinical trials, for pediatric osteogenesis imperfecta[50] and GvHD[51], utilized fresh cultured MSC, the majority of clinical trials and companies developing commercially available MSC-based products today utilize cryopreserved MSCs. Cryopreservation simplifies logistics of cell therapy but is not without potential drawbacks and the full impact of cryopreservation on MSC function in specific disease contexts is not well understood. In recent years, several groups have examined the impact of cryopreservation on MSC function with mixed results.[6–9,43] A particular focus has been around whether or not MSC's diverse immunomodulatory functions remain intact following cryopreservation. Several groups have reported reduced potency of MSCs following cryopreservation[7,9] while others have seen no significant decline in immunosuppressive function[6,52,53]. Some discrepancy can be attributed to poor viability following cryopreservation and differences in PBMC suppression assay protocols that may not be sensitive enough to detect differences in potency.

The excellent paper by Chinnadurai *et al.* adds to the evaluation of the fitness of cryopreserved MSCs by demonstrating that thawed MSCs are susceptible to lysis by cytotoxic T lymphocytes (CTL) in co-culture assays[54]. Cryopreserved MSCs co-cultured with PBMCs in direct contact failed to suppress PBMC proliferation and in some cases mildly enhanced PBMC proliferation while cryopreserved MSCs co-cultured with PBMCs in transwells remained suppressive. As could be expected, allogeneic thawed MSCs were far more sensitive to T cell mediated lysis than autologous MSC after co-culture. Together these results suggest increased allo-reactivity to recently thawed MSCs. To investigate the cause of MSC's failure to suppress PBMCs and avoid lysis by CTLs the authors determined the rate at which MSCs are capable of suppressing degranulation of CD8+ T cells and found cryopreserved MSCs failed to suppress degranulation at all time points while fresh MSCs suppressed degranulation by day 2 of the co-culture. To restore the immunosuppressive potency of cryopreserved MSCs, cells were pre-licensed with IFN-γ for 48 hours before cryopreservation so that upon thawing, MSCs would

already have high levels of IDO, a potent immunosuppressive enzyme. Indeed, pre-licensed cryo-MSCs had high levels of IDO mRNA and protein and avoided CTL mediated lysis while suppressing PBMC proliferation equally as well as fresh MSCs. IDO activity is known to suppress CD8+ CTL[55] and is likely responsible for the improved survival and potency of pre-licensed cryo-MSCs. Thus, they suggest pre-licensing MSCs with IFN-γ may inform strategies to overcome the detrimental effects of cryopreservation on MSC.

In this study we sought to determine if pre-licensing MSCs prior to cryopreservation would enhance their production of IDO. Additionally, we tested whether pre-licensing cryopreserved MSCs increased their effectiveness in rescuing retinal ganglion cells from death in our mouse retinal model of ischemia/reperfusion (I/R) injury.

Materials and Methods

Western blot

MSCs were cultured and cryopreserved as described in Chapter 2.2. Human MSCs pretreated with 100 ng/mL rhIFN-γ for 24 hour or 48 hour prior to cryopreservation (Pre-cryo IFN-γ), followed by re-stimulation for an additional 8, 24, or 48 hour (Post-cryo IFN- γ). Fresh MSC cultures were grown in 100 ng/mL IFN-γ for the same total duration without cryopreservation. β-Actin served as a loading control. Western blots were performed as previously described[52] using primary antibodies for IDO and β-Actin (1:500 rabbit anti-IDO (12006S, Cell Signaling, Danvers, MA), 1:20,000 mouse anti-β -actin (1406030, Ambion, Thermo Scientific, Waltham, MA). Densitometry measurements made with LI-COR ImageStudio software.

In vivo retinal I/R mouse model

Fresh, cryo-, and prelicensed cryo-MSCs were prepared prior to injection. Prelicensed cryo-MSCs were preconditioned in 100ng/mL IFN-γ for 48 hours prior to cryopreservation. Cryopreserved MSCs were thawed, washed to remove DMSO, and then stored in PBS on ice prior to use.

All animal experiments were carried out in accordance with the ARVO Statement for the Use of Animals in Ophthalmology and Vision Research and were approved by the IACUC committee of the University of Iowa. Unilateral retinal damage was induced by

Ischemia/Reperfusion (I/R) injury as described earlier[52]. Two-month old C57BL6/J (The Jackson Laboratory, Bar Harbor, ME) were anaesthetized by intraperitoneal injection of Xylazine/Ketamine (10 mg/kg and 100 mg/kg, respectively). Eyes received 0.5% proparacaine eye drops for topical analgesia, pupils were dilated with 0.5% tropicamide (both Akorn, Lake Forest, IL), and corneas were kept moist until animals had fully recovered (GenTeal, Alcon, Fort Worth, TX). Intraocular pressure was elevated to 80 mmHg for 60 minutes by cannulating the anterior chamber with a sterile 30-gauge needle connected to an elevated saline reservoir. Animals were allowed to rest for 2 hours after IOP elevation to simulate a reperfusion injury after which they were sedated and received intraocular injection of PBS or 30,000 MSCs suspended in 3 µl if PBS. The right eyes of all mice received no manipulation and served as controls. After 7 days, animals were euthanized and RGC survival was quantified by staining for γ -synuclein, a marker for retinal ganglion cells (RGC), and the number of surviving RGC was determined. Briefly, retinas where incubated overnight with mouse anti-γ -synuclein primary antibody solution (1:400, Abnova Corporation, Walnut, CA, USA), followed by several rinses in PBS and incubation with an Alexa Fluor 488 donkey anti-mouse secondary antibody (1:300, Life technologies, Grand Island, NY). After another PBS wash, retinas were whole-mounted, cover slipped and imaged. Twelve images (318 × 318 µ m, 40X magnifications) were taken at predetermined mid-peripheral locations using a Nikon Eclipse i80 confocal microscope (Nikon Instruments Inc, Melville, NY). γ -synuclein positive RGC were counted in a masked fashion by an independent observer using the cell counter plugin in ImageJ software (NIH).

Results and Discussion

We recently reported that cryopreserved MSCs maintain viability, responsiveness to inflammatory stimuli, and growth factor secretion and showed a small and not-significant decline in their ability to suppress PBMCs in co-cultures *in vitro*[52]. In addition, cryopreserved MSCs performed equally as well as fresh MSCs when used to rescue retinal ganglion cells (RGC) following an ischemia reperfusion injury to the eye [52]. We then sought to improve the therapy further by pre-licensing MSCs with IFN-γ prior to freezing. Using a similar strategy to Chinnadurai, we pretreated MSCs with IFN-γ for 24 or 48 hours and froze the MSCs as reported[52]. We then examined the level of IDO expression after thawing and plating MSC in IFN-γ containing media. Both batches of primed MSCs were evaluated for IDO protein content

8, 24, and 48 hours after thaw or until they had been exposed to IFN-γ for a total of 72 hours (Figure 8A). At 8 and 24 hours after thawing, the 24-hour pre-licensed group had less IDO content compared to fresh MSC but the discrepancy in IDO content was no longer noticeable at 48 hours after thawing (72 hours of total IFN-γ exposure). The 48-hour pre-licensed group performed considerably better in this assay, displaying comparable levels of IDO content at both 8 and 24 hours after thawing. We then took the 48-hour pre-licensed cryo-MSC and tested to see if they would outperform fresh MSCs in an ischemia/reperfusion model *in vivo*. To our surprise, the IFN-γ pre-licensed cryo-MSCs lost effectiveness *in vivo*, rescuing fewer RGC than either fresh or unlicensed cryopreserved MSC (Figure 8B,C).

While MSCs licensed with IFN-γ are known to increase expression of immunosuppressive factors, treatment also dramatically increases surface expression of MHC-I and MHC-II molecules[21] which may accelerate the detection and clearance of MSC via xeno-recognition. Notably, in our ischemia/reperfusion model all human MSC were cleared from the mouse eyes by day 7.[52] Further analysis is needed to determine if the reduced effect of pre-licensed MSC was due to hastened immune detection and clearance of MSC or changes in secreted factors that support RGC survival. While a syngeneic or autologous transplant model would allow for analysis of the fate of pre-licensed cryo-MSC independent of rejection mechanisms, it would not be without significant drawbacks. Notably, MSC biology diverges significantly between human and mice, with documented differences in chemokine receptors[56] as well as their use of central immunomodulatory mechanisms, with murine MSC utilizing iNOS while human MSC employ IDO.[57] In addition, since the goal of our work was to move toward an off-the-shelf therapy for I/R injury that can be administered within hours of the onset of an ischemic event, the analogous human application would likely employ allogeneic MSC, and thus MSC would likely suffer from enhanced allo-recognition in a pre-licensed state. Our current data is insufficient to fully conclude that pre-licensed cryo-MSC have no place in the world of cell-therapy but highlight the need for future work in this area to proceed cautiously with careful attention paid toward *in vivo* immune detection and clearance.

Chinnadurai et al.'s report[54] that cryopreserved MSCs can be killed via CTL mediated lysis is further evidence that MSCs are immune evasive in nature, but only evade destruction if their immunosuppressive facilities are intact[2]. Both the Chinnadurai et al. report[54] and our

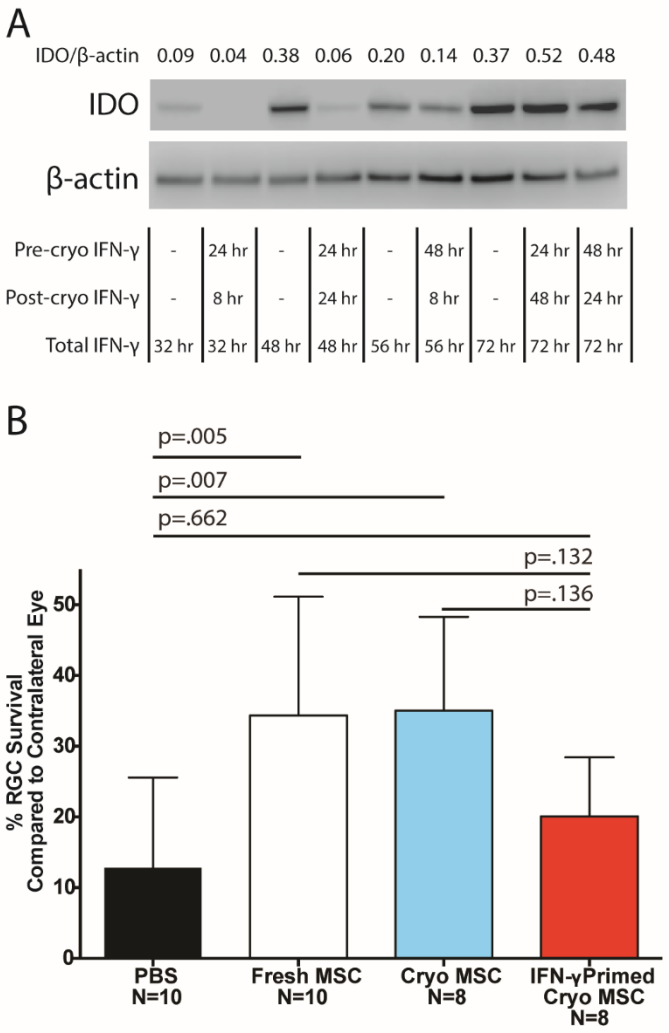

Figure 8. IFN-γ priming enhances IDO expression of cryopreserved MSCs *in vitro* but is detrimental to MSC performance in an ischemia/reperfusion injury *in vivo*.

(A) Representative Western blot of IDO protein in human MSCs pretreated with 100 ng/mL rhIFN-γ for 24 hour or 48 hour prior to cryopreservation (Pre-cryo IFN-γ), followed by re-stimulation for an additional 8, 24, or 48 hour (Post-cryo IFN- γ), compared to fresh MSC cultures grown in 100 ng/mL IFN-γ. (B) Quantitative analysis of RGC survival in eyes after retinal I/R injury revealed a significant rescue effect after transplantation of fresh MSC and cryo-MSC, while cryo-MSC preconditioned in 100ng/mL IFN-γ for 48 hours show diminished rescue of RGCs (mean ± SD, One-way ANOVA with Tukey honest significant difference post hoc test to correct for multiple comparisons, $p < 0.05$ considered significant).

observed negative impact of pre-licensing on MSCs *in vivo* (Figure 8B) highlight the need to understand in greater detail the multiple mechanisms by which MSCs are cleared *in vivo* and how cryopreservation and other preconditioning regimens extend or shorten their persistence *in vivo*. In addition, our observation that pre-licensed cryopreserved MSCs performed worse in the retinal ischemia/reperfusion model demonstrates the need to evaluate the suitability of cryopreserved or otherwise manipulated MSCs in a disease specific context. MSC exert multiple mechanisms including immune suppression, secretion of growth factors[58], and even donation of mitochondria[59]. However, each can be differentially impacted by cryopreservation and preconditioning strategies and the appropriateness of such strategies cannot be determined outside of the context of a specific pathology.

Studies in animal models to date have shown that cryopreserved MSC are effective in treating disease models of colitis[60], allergic airway inflammation[53], and ischemia/reperfusion injury to the eye[52]. In contrast, cryo-MSC failed to induce a chondrogenic response in a mouse-based chondrocyte-responsive bioassay suggesting cryo-MSC may be unsuitable for treatment of osteogenesis imperfecta[61]. In humans, cryopreserved MSC have elicited positive responses in clinical trials for critical limb ischemia[62] while retrospective analysis of GvHD patients receiving fresh versus thawed MSC suggest fresh MSC are more efficacious[9]. Thus, cryopreserved MSCs may be suboptimal and inappropriate for the treatment of some conditions, while being adequate and necessary for others (Figure 9). As our understanding of the disease specific therapeutic mechanisms employed by MSCs grows, so too will our ability to identify culture conditions and cryopreservation techniques that maintain or enhance rather than hinder MSC potency.

Acknowledgements

MSC obtained from Texas A&M Health Science Center College of Medicine Institute for Regenerative Medicine at Scott & White through a grant from NCRR of the NIH, Grant # P40OD011050, resource ID SCR_005522. Financial support for this work was provided in part by the NIDDK Diabetic Complications Consortium (DiaComp,www.diacomp.org), grant DK076169 to J.A.A. and start-up funding provided by the Fraternal Order of Eagles Diabetes Research Center to J.A.A..

Author Contributions

A.J. Burand, OWG, and A.J. Brown: Conception and design and manuscript writing. JAA: conception and design, manuscript writing, and final approval of manuscript.

Author Conflicts of Interest

The authors indicate no potential conflicts of interest.

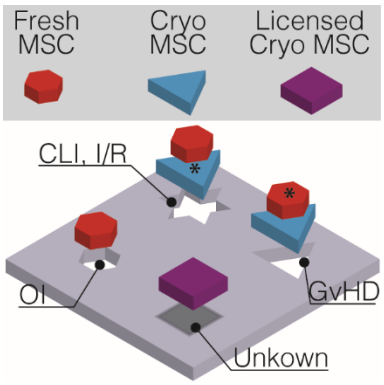

Figure 9. Tailoring MSCs to fit the disease.

Fresh, cryopreserved and, pre-licensed cryopreserved MSC are all being explored to treat numerous diseases, but all are not suitable to treat all conditions. CLI: Critical limb ischemia, OI: osteogenesis imperfecta, GvHD: graft versus host disease, I/R: ischemia reperfusion (I/R) injury. '*' denotes preferred therapeutic strategy when both fresh MSC and cryo-MSC have shown utility in treating the disease but one is more efficacious or logistically suitable.

2.4. REFERENCES

1. Ankrum, J. & Karp, J. M. Mesenchymal stem cell therapy: Two steps forward, one step back. *Trends Mol. Med.* **16**, 203–209 (2010).
2. Ankrum, J. a, Ong, J. F. & Karp, J. M. Mesenchymal stem cells: immune evasive, not immune privileged. *Nat. Biotechnol.* **32**, 252–260 (2014).
3. da Silva Meirelles, L., Chagastelles, P. C. & Nardi, N. B. Mesenchymal stem cells reside in virtually all post-natal organs and tissues. *J. Cell Sci.* **119**, 2204–2213 (2006).
4. Stolzing, A., Jones, E., McGonagle, D. & Scutt, A. Age-related changes in human bone marrow-derived mesenchymal stem cells: Consequences for cell therapies. *Mech. Ageing Dev.* **129**, 163–173 (2008).
5. Murphy, M. B., Moncivais, K. & Caplan, A. I. Mesenchymal stem cells: environmentally responsive therapeutics for regenerative medicine. *Exp. Mol. Med.* **45**, e54–e54 (2013).
6. Luetzkendorf, J. *et al.* Cryopreservation does not alter main characteristics of Good Manufacturing Process–grade human multipotent mesenchymal stromal cells including immunomodulating potential and lack of malignant transformation. *Cytotherapy* **17**, 186–198 (2015).
7. François, M. *et al.* Cryopreserved mesenchymal stromal cells display impaired immunosuppressive properties as a result of heat-shock response and impaired interferon-γ licensing. *Cytotherapy* **14**, 147–152 (2012).
8. Chinnadurai, R. *et al.* Actin Cytoskeletal Disruption following Cryopreservation Alters the Biodistribution of Human Mesenchymal Stromal Cells In Vivo. *Stem Cell Reports* **3**, 60–72 (2014).
9. Moll, G. *et al.* Do Cryopreserved Mesenchymal Stromal Cells Display Impaired Immunomodulatory and Therapeutic Properties? *Stem Cells* **32**, 2430–2442 (2014).
10. Dominici, M. *et al.* Minimal criteria for defining multipotent mesenchymal stromal cells. The International Society for Cellular Therapy position statement. *Cytotherapy* **8**, 315–317 (2006).
11. Davies, L. C. *et al.* Oral Mucosal Progenitor Cells Are Potently Immunosuppressive in a Dose-Independent Manner. *Stem Cells Dev.* **21**, 1478–1487 (2012).

12. Kuehn, M. H., Kim, C. Y., Jiang, B., Dumitrescu, A. V. & Kwon, Y. H. Disruption of the complement cascade delays retinal ganglion cell death following retinal ischemia-reperfusion. *Exp. Eye Res.* **87**, 89–95 (2008).
13. Kambhampati, S. P. *et al.* Systemic and Intravitreal Delivery of Dendrimers to Activated Microglia/Macrophage in Ischemia/Reperfusion Mouse Retina. *Investig. Opthalmology Vis. Sci.* **56**, 4413 (2015).
14. Joachim, S. C. *et al.* Effect of Ischemia Duration on Autoantibody Response in Rats Undergoing Retinal Ischemia-Reperfusion. *Ophthalmic Res.* **48**, 67–74 (2012).
15. Ding, Q. J., Cook, A. C., Dumitrescu, A. V & Kuehn, M. H. Lack of Immunoglobulins Does Not Prevent C1q Binding to RGC and Does Not Alter the Progression of Experimental Glaucoma. *Investig. Opthalmology Vis. Sci.* **53**, 6370 (2012).
16. Gramlich, O. W. *et al.* Adoptive transfer of immune cells from glaucomatous mice provokes retinal ganglion cell loss in recipients. *Acta Neuropathol. Commun.* **3**, 56 (2015).
17. He, F. *et al.* Ion transport through dimethyl sulfoxide (DMSO) induced transient water pores in cell membranes. *Mol. Membr. Biol.* **29**, 107–113 (2012).
18. Fallarino, F. *et al.* Tryptophan catabolism generates autoimmune-preventive regulatory T cells. *Transpl. Immunol.* (2006). doi:10.1016/j.trim.2006.09.017
19. Van der Sluijs, K., Singh, R., Dijkhuis, A., Snoek, M. & Lutter, R. Indoleamine-2,3-dioxygenase activity induces neutrophil apoptosis. *Crit. Care* **15**, P208 (2011).
20. Nauta, A. J. & Fibbe, W. E. Immunomodulatory properties of mesenchymal stromal cells. *Blood* **110**, 3499–3506 (2007).
21. Ankrum, J. a, Dastidar, R. G., Ong, J. F., Levy, O. & Karp, J. M. Performance-enhanced mesenchymal stem cells via intracellular delivery of steroids. *Sci. Rep.* **4**, 4645 (2015).
22. Deng, Y. Bin *et al.* Intravenously administered BMSCs reduce neuronal apoptosis and promote neuronal proliferation through the release of VEGF after stroke in rats. *Neurol. Res.* **32**, 148–156 (2010).
23. Johnson, T. V *et al.* Identification of retinal ganglion cell neuroprotection conferred by platelet-derived growth factor through analysis of the mesenchymal stem cell secretome. *Brain* **137**, 503–519 (2014).

24. Zhukareva, V., Obrocka, M., Houle, J. D., Fischer, I. & Neuhuber, B. Secretion profile of human bone marrow stromal cells: Donor variability and response to inflammatory stimuli. *Cytokine* **50**, 317–321 (2010).
25. Paradisi, M. *et al.* Human mesenchymal stem cells produce bioactive neurotrophic factors: Sourse, individual variability and differentiation issues. *Int. J. Immunopathol. Pharmacol.* **27**, 391–402 (2014).
26. Lee, R. H. *et al.* TSG-6 as a biomarker to predict efficacy of human mesenchymal stem/progenitor cells (hMSCs) in modulating sterile inflammation in vivo. *Proc. Natl. Acad. Sci.* **111**, 16766–16771 (2014).
27. Kummer, M. P., Abbott, J. J., Dinser, S. & Nelson, B. J. Artificial Vitreous Humor for In Vitro Experiments. in *2007 29th Annual International Conference of the IEEE Engineering in Medicine and Biology Society* 6406–6409 (IEEE, 2007). doi:10.1109/IEMBS.2007.4353822
28. Moriscot, C. *et al.* Human Bone Marrow Mesenchymal Stem Cells Can Express Insulin and Key Transcription Factors of the Endocrine Pancreas Developmental Pathway upon Genetic and/or Microenvironmental Manipulation In Vitro. *Stem Cells* **23**, 594–603 (2005).
29. Tucker, B. A. *et al.* Patient-specific iPSC-derived photoreceptor precursor cells as a means to investigate retinitis pigmentosa. *Elife* **2**, 824 (2013).
30. Lalu, M. M. *et al.* Safety of Cell Therapy with Mesenchymal Stromal Cells (SafeCell): A Systematic Review and Meta-Analysis of Clinical Trials. *PLoS One* **7**, e47559 (2012).
31. Yong, K. W. *et al.* Cryopreservation of Human Mesenchymal Stem Cells for Clinical Applications: Current Methods and Challenges. *Biopreserv. Biobank.* **13**, 231–239 (2015).
32. Yong, K. W. *et al.* Assessment of tumourigenic potential in long-term cryopreserved human adipose-derived stem cells. *J. Tissue Eng. Regen. Med.* **11**, 2217–2226 (2017).
33. Yong, K. W. *et al.* Phenotypic and Functional Characterization of Long-Term Cryopreserved Human Adipose-derived Stem Cells. *Sci. Rep.* **5**, 9596 (2015).
34. Tokumoto, S., Sotome, S., Torigoe, I., Omura, K. & Shinomiya, K. Effects of cryopreservation on bone marrow derived mesenchymal cells of a nonhuman primate. *J. Med. Dent. Sci.* **55**, 137–43 (2008).

35. Zhu, X. *et al.* Evaluation of Canine Bone Marrow-derived Mesenchymal Stem Cells After Long-term Cryopreservation. *Zoolog. Sci.* **30**, 1032–1037 (2013).
36. Liu, G., Shu, C., Cui, L., Liu, W. & Cao, Y. Tissue-engineered bone formation with cryopreserved human bone marrow mesenchymal stem cells. *Cryobiology* (2008). doi:10.1016/j.cryobiol.2008.02.008
37. Shen, H., Kreisel, D. & Goldstein, D. R. Processes of Sterile Inflammation. *J. Immunol.* **191**, 2857–2863 (2013).
38. Rock, K. L., Latz, E., Ontiveros, F. & Kono, H. The Sterile Inflammatory Response. *Annu. Rev. Immunol.* **28**, 321–342 (2010).
39. Iyer, S. S. *et al. Necrotic cells trigger a sterile inflammatory response through the Nlrp3 inflammasome*.
40. Chen, G. Y. & Nuñez, G. Sterile inflammation: sensing and reacting to damage. *Nat. Rev. Immunol.* **10**, 826–837 (2010).
41. Kono, H. & Rock, K. L. How dying cells alert the immune system to danger. *Nat. Rev. Immunol.* **8**, 279–289 (2008).
42. Marquez-Curtis, L. A., Janowska-Wieczorek, A., McGann, L. E. & Elliott, J. A. W. Mesenchymal stromal cells derived from various tissues: Biological, clinical and cryopreservation aspects. *Cryobiology* **71**, 181–197 (2015).
43. Alaminos, M. *et al. Cryopreserved hMSCs maintain comparable in vitro functional activity compared to fresh hMSCs*. *Journal of Cytotherapy* **17**, (2015).
44. Sanes, J. R. & Masland, R. H. The Types of Retinal Ganglion Cells: Current Status and Implications for Neuronal Classification. *Annu. Rev. Neurosci.* **38**, 221–246 (2015).
45. Kaur, C., Foulds, W. S. & Ling, E.-A. Hypoxia-ischemia and retinal ganglion cell damage. *Clin. Ophthalmol.* **2**, 879–889 (2008).
46. Osborne, N. N. *et al.* Retinal ischemia: mechanisms of damage and potential therapeutic strategies. *Prog. Retin. Eye Res.* **23**, 91–147 (2004).
47. D'Onofrio, P. M. & Koeberle, P. D. What can we learn about stroke from retinal ischemia models? *Acta Pharmacol. Sin.* **34**, 91–103 (2013).
48. Baker, M. L., Hand, P. J., Wang, J. J. & Wong, T. Y. Retinal Signs and Stroke. *Stroke* **39**, 1371–1379 (2008).

49. Johnson, T. V *et al.* Neuroprotective Effects of Intravitreal Mesenchymal Stem Cell Transplantation in Experimental Glaucoma. *Investig. Opthalmology Vis. Sci.* **51**, 2051 (2010).
50. Horwitz, E. M. *et al.* Transplantability and therapeutic effects of bone marrow-derived mesenchymal cells in children with osteogenesis imperfecta. *Nat. Med.* **5**, 309–313 (1999).
51. Le Blanc, K. *et al.* Treatment of severe acute graft-versus-host disease with third party haploidentical mesenchymal stem cells. *Lancet* **363**, 1439–1441 (2004).
52. Gramlich, O. W. *et al.* Cryopreserved Mesenchymal Stromal Cells Maintain Potency in a Retinal Ischemia/Reperfusion Injury Model: Toward an off-the-shelf Therapy. *Sci. Rep.* **6**, 26463 (2016).
53. Cruz, F. F. *et al.* Freshly Thawed and Continuously Cultured Human Bone Marrow-Derived Mesenchymal Stromal Cells Comparably Ameliorate Allergic Airways Inflammation in Immunocompetent Mice. *Stem Cells Transl. Med.* **4**, 615–624 (2015).
54. Chinnadurai, R. *et al.* Cryopreserved MSCs are susceptible to T-cell mediated apoptosis which is partly rescued by IFNγ licensing Raghavan. *Stem Cells* **34**, 2429–2442 (2016).
55. Liu, H. *et al.* Reduced Cytotoxic Function of Effector CD8+ T Cells Is Responsible for Indoleamine 2,3-Dioxygenase-Dependent Immune Suppression. *J. Immunol.* **183**, 1022–1031 (2009).
56. Chamberlain, G., Wright, K., Rot, A., Ashton, B. & Middleton, J. Murine Mesenchymal Stem Cells Exhibit a Restricted Repertoire of Functional Chemokine Receptors: Comparison with Human. *PLoS One* **3**, e2934 (2008).
57. Ren, G. *et al.* Species Variation in the Mechanisms of Mesenchymal Stem Cell-Mediated Immunosuppression. *Stem Cells* **27**, 1954–1962 (2009).
58. Ranganath, S. H., Levy, O., Inamdar, M. S. & Karp, J. M. Harnessing the Mesenchymal Stem Cell Secretome for the Treatment of Cardiovascular Disease. *Cell Stem Cell* **10**, 244–258 (2012).
59. Islam, M. N. *et al.* Mitochondrial transfer from bone-marrow–derived stromal cells to pulmonary alveoli protects against acute lung injury. *Nat. Med.* **18**, 759–765 (2012).

60. Castelo-Branco, M. T. L. *et al.* Intraperitoneal but Not Intravenous Cryopreserved Mesenchymal Stromal Cells Home to the Inflamed Colon and Ameliorate Experimental Colitis. *PLoS One* **7**, e33360 (2012).
61. Otsuru, S. *et al.* Genomic and functional comparison of mesenchymal stromal cells prepared using two isolation methods. *Cytotherapy* **17**, 262–270 (2015).
62. Gupta, P. K. *et al.* A double blind randomized placebo controlled phase I/II study assessing the safety and efficacy of allogeneic bone marrow derived mesenchymal stem cell in critical limb ischemia. *J. Transl. Med.* **11**, 143 (2013).

CHAPTER 3: AGGREGATION OF MESENCHYMAL STROMAL CELLS MODULATES THEIR FUNCTION

3.1. OVERVIEW

As described in Chapter 1, MSCs are used in several disease settings for their immunomodulatory and regenerative effects, however, when delivered locally, MSC phenotype dramatically shifts due to cell aggregation. In this chapter, we outline the effects of aggregation on MSC gene expression, signaling, secreted factor production, and response to a T2D environment though an *in vitro* model of MSC aggregation (e.g. spheroid formation). Herein, we show that there are there are gene expression changes to PGE2 receptor expression indicating the possibility of an autocrine feedback loop, however, when blocked this feedback loop does not broadly alter immunomodulatory gene expression. We found that there are drastic gene expression changes in immunomodulatory, growth factor, and signaling proteins, some of which were transient. Several of these genes were upregulated >2-fold from adherent controls including ER stress genes. These changes in spheroid MSCs also lowered their metabolic function. Finally, we demonstrate that palmitate, a commonly upregulated fatty acid in obesity known to have deleterious effects *in vivo*, has a detrimental effect on metabolic function and viability of spheroid MSCs.

Chapter 3.2 is an adaptation of an abstract published on May 9, 2018 in *Molecular Therapy*. Adapted with permission.

Burand AJ, Di L, Boland L, Ankrum JA. (2018). Poster 458: Aggregation of MSCs Leads to a Shift in Secretome Due to Activation of an Ep Receptor-PGE2 Pathway from ASGCT 21st Annual Meeting Abstracts. **Molecular Therapy**, 26(5), 214-215. https://doi.org/10.1016/j.ymthe.2018.05.001

3.2. MSCS ACTIVATE A PGE2-EP RECEPTOR AUTOCRINE FEEDBACK LOOP

Introduction

Upon local injection *in vivo*, MSCs form 3D aggregate structures, which exhibit vastly different gene expression profiles compared to 2D cultured MSCs.[1] These differences lead to significant changes in cell behavior *in vivo* compared to what would be predicted by *in vitro* experiments with 2D cultured cells.[2] Understanding the MSC post-transplant spheroid phenotype is critical to ensuring MSC function and consistency as a cell therapy. Upon aggregate formation, transcriptional changes lead to changes in secreted molecules, cell surface receptors, extracellular matrix molecules, and transcription factors. One of the largest changes is in prostaglandin E2 (PGE2), a small molecule synthesized by COX-2 and PGE synthase which is significantly upregulated in spheroids.[2–5] PGE2 has four receptors (EP1-4), the expression which dictates the effect of PGE2 signaling on cell phenotype. Despite, spheroid MSCs producing high levels of PGE2[2] and expressing PGE2 receptors (EP1, EP2, and EP4)[6], little is known about how MSCs regulate their EP receptors or the role autocrine signaling through the PGE2-EP pathway plays in controlling MSC phenotype.

Materials and Methods

MSC culture

We used *in vitro* MSC spheroids, formed through a hanging droplet method, as a way to mimic *in vivo* aggregation that occurs after local injections of concentrated cell suspensions. This allowed for detailed analysis of the transcriptional and secretory changes that occur upon MSC aggregation into spheroids and examination of the mechanisms that control the shift in MSC phenotype. We cultured, formed, and disassociated MSC spheroids as described in Appendix A.2 using MEM-α supplemented with 10% FBS and 1% penicillin, streptomycin, and L-glutamine. In order to block PGE2 production or signaling through EP2, we treated cells with 50 μM indomethacin or 1 μM TG4-155, respectively 72 hours prior to RNA collection. For spheroid disassociation experiments, we disassociated spheroids and cultured MSCs on tissue culture plastic for 1, 3, or 5 days prior to RNA analysis.

Viability staining

Spheroids allowed to form for 3 days were transferred into low-attachment 24-well plates and treated with 1 μL Hoechst and PI per mL of media. Cells were incubated on ice for 15 minutes prior to imaging. Z-stack images were acquired on a fluorescent microscope and 3D deconvolution software (Leica) was used to de-blur images prior to z-projection.

Statistics

All graphs were prepared using GraphPad Prism 7 software. PCR analysis was done in Excel using GAPDH as the housekeeping gene.

Results and Discussion

To test what impact MSC aggregation had on their PGE2 receptor expression, we formed spheroids using the hanging droplet technique (Figure 10A,B). We have made the novel discovery that PGE2 production increased over 30-fold in spheroids and transcripts for the PGE2 receptors EP2 and EP4, increased by over 20-fold and 3-fold respectively in spheroids (Figure 10C). Blockade of the PGE2-EP2 pathway within spheroids led to a slight downregulation in expression of EP1, EP2, EP3, and PTGS2 (COX-2) genes (Figure 10D). However, other immunomodulatory genes such as TGF-β remained unchanged. To determine if signaling factors produced by spheroids induced the phenotypic switch between the 2D and spheroid MSCs, we performed a series of inhibitor and add-back studies. We found that the addition of spheroid secreted products such as IL-1β and PGE2 or antagonism of the cAMP signaling pathway using forskolin alone did not recapitulate the changes in spheroid MSC EP receptor expression in 2D cultured cells (data not shown). While the spheroid phenotype is stable over seven days and produces high expression of VEGF, HGF, and TGF-β, the phenotype rapidly reverts to that of 2D cells when spheroid MSCs are disassociated and plated on tissue culture plastic (Figure 10E). Collectively this provides evidence that spheroid formation may induce an EP-PGE2 autocrine feedback loop in MSCs. However, this feedback loop is initiated and maintained by the 3D structure of the spheroid and not single soluble factors alone.

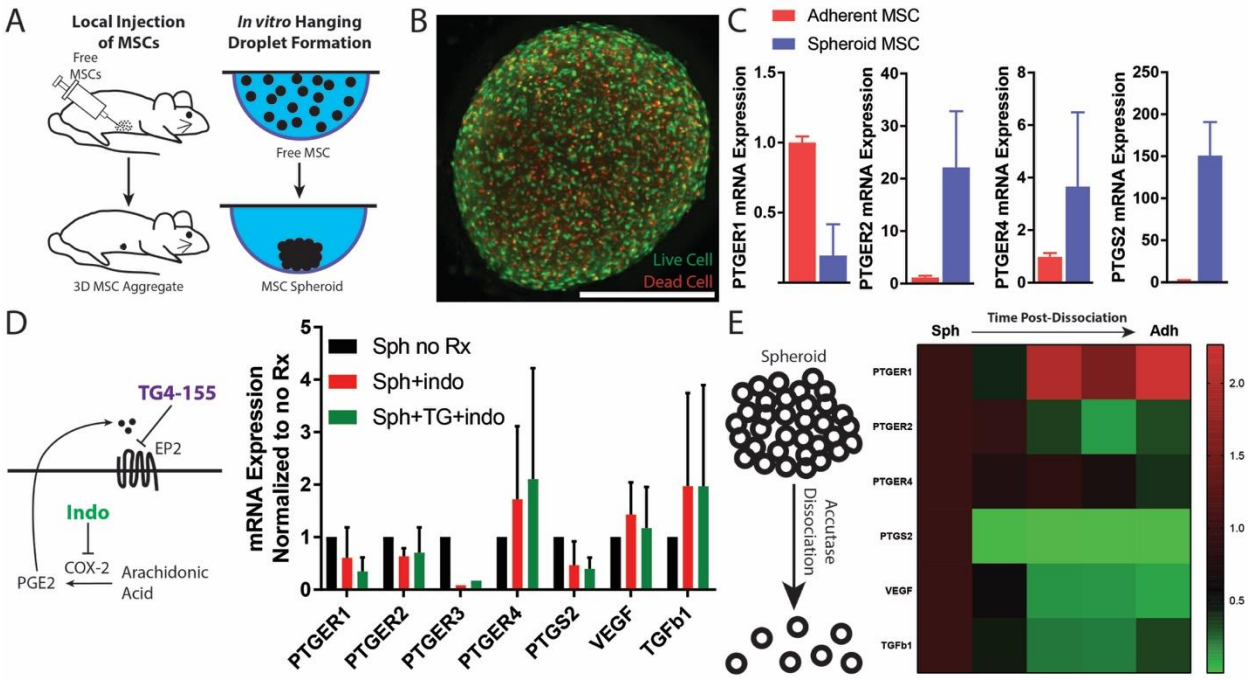

Figure 10. *In vitro* MSC spheroid aggregation leads to upregulation of PGE2 receptors 2/4 to detect synthesized PGE2.

(A) 3D aggregation of MSCs *in vivo* can be modeled with by *in vitro* spheroids. (B) Hoechst/PI staining of spheroid. Scale bar = 250 μm (C) RT-PCR analysis of EP receptors and COX-2 gene expression. (D) Gene expression of spheroids after indomethacin or indomethacin/TG4-155 treatment. (E) Gene expression of MSC spheroids, 2D MSCs, and MSCs after at 1, 3, and 5 days after spheroid dissociation.

Conclusions

The increased PGE2 and EP2/4 expression in spheroid MSCs play a role in regulation of EP receptor and COX-2 expression, but the mechanism which leads to the initial upregulation of these genes is not fully explained by increased PGE2 signaling alone. This suggests, additional factors inherent in the spheroid structure, such as cell-cell contact or hypoxia, play integral roles in the development of the spheroid MSC phenotype.

3.3. MSC AGGREGATES ALTER THROPHIC FACTOR EXPRESSION, INCREASE ER STRESS, DECREASE METABOLIC FUNCTION, AND INCREASE SUSCIPTABILITY TO PALMITATE DAMAGE

Authors: Anthony J. Burand Jr., Lin Di, Lauren Boland, and James A. Ankrum

Abstract

MSCs can aggregate *in vivo* leading to divergent behavior of these cells from adherent MSCs cultured on tissue culture plastic. While pathways for upregulation of PGE2 and other trophic factors have been explored, little research has been done on gene expression kinetics, ER stress, or metabolic function in aggregated MSCs. We show that while some MSC genes are only transiently upregulated, several such as PTGS2, IL6, TWIST1, and HGF were still at least 4-fold increased at 9 days after spheroid culture. Additionally, we show that ER stress gene XBP1, ATF4, and IDDT3 were all significantly upregulated upon MSC aggregation. Finally, spheroid MSCs showed decreased metabolic function compared to adherent MSCs. This demonstrates that there are significant adaptive changes that result from aggregation stress in spheroid MSCs that warrant further exploration so that strategies for manipulating aggregation stress in spheroids can be developed.

Introduction

MSC aggregates are gaining interest in research due to their ability to replicate phenotypic changes that result from local injection into tissue. Spheroid MSCs exhibit a widely altered gene expression profile in immunomodulatory factor, growth factor, and ECM production when compared to MSCs grown on tissue culture plastic.[2] While many groups have studied gene and protein changes in these spheroids, little study has been given to understanding why these changes occur. It has been shown that upon aggregation *in vitro*, aggregated or spheroid MSCs upregulate activation of caspase and Notch signaling. Caspases cleave pro-IL1 into IL-1α and IL-1β which can then signal through IL-1R on MSCs in an autocrine fashion.[2] This signaling leads to upregulation of NFκB signaling which drives upregulation of factors like PGE2, TSG6, and STC-1.[2,7] While these factors play important roles in MSC potency, the full impact of

aggregation on MSC phenotype and the mechanisms by which aggregation stress leads to these alterations remains unknown.

One proposed mechanism by which gene expression and function may be altered is through biomechanical cues present within the spheroid environment including stiffness and mechanical strain due to compaction. MSCs have been traditionally cultured on tissue culture plastic, typically manufactured from polycarbonate. However, this tissue culture plastic has an elastic modulus approximately 5 orders of magnitude higher than what cells experience in spheroids.[8] Stiffer substrates have been shown to increase MSC proliferation, alter their differentiation[9], and gene expression[10,11]. Additionally, during compaction of MSCs into aggregates, cells encounter compression which can lead to alterations in mechanoreceptor signaling. MSCs under fluid shear stress upregulated gene expression of NFkB1, TGFB1, VEGFA, IL1A, and TGFB2 all of which we and others have shown are upregulated in spheroid MSCs. Fluid shear led to increases in COX-2 and PGE2, prominent components of the spheroid MSC secretome, and demonstrated greater suppression of LPS activated splenocytes.[12] Together this data suggests that compaction and substrate stiffness differences observed between spheroid culture and 2D MSC monolayers may explain why gene expression changes occur during cell aggregation. However, further characterization of this phenotypic change in spheroid MSCs is needed in order to understand what impact cell aggregation during local MSC delivery may have in treatment of inflammatory disease.

Herein, we sought to determine if gene expression changes in MSCs resulting from this aggregation event were stable over time. Additionally, since consequences and mechanisms of aggregation stress have been understudied, we tested if this aggregation stress affected ER stress and metabolic function in spheroid MSCs.

Methods

MSC culture

MSCs isolated commercially from bone marrow or previously isolated from umbilical cords were grown in complete minimal essential medium with the alpha modification (MEM) supplemented with 15% fetal bovine serum, 1% L-glutamine, and 1% penicillin/streptomycin. Adherent MSCs were plated on tissue culture plastic at 2,700 – 5,400 cell/cm^2 and 20,000 MSC spheroids were formed using the hanging droplet method as described in Chapter 2.2. Bone

marrow MSCs were used at passages 3-6 post-manufacturing and umbilical cord MSCs were used at passages 6-10 post-isolation. Adherent cells were passaged when they became 70-90% confluent. Briefly, adherent MSCs were washed 3x with PBS, incubated with Accutase at 37°C to detach the cells, spun down at 500g for 5 minutes in a centrifuge, and resuspended in complete MEM prior to counting and plating.

Gene expression profiling

In order to determine how spheroid gene expression changed during initial aggregation and after aggregation, spheroids were cultured as described above for 0, 1, 3, 6, 24, 48, 72, 120, 168, and 216 hours after plating as hanging drops. MSCs were cultured as hanging droplets for up to 72 hours and then were transferred into low-attachment plates (Corning) with a media change after 3 days post-transfer. 200,000-400,000 spheroid MSCs were collected in tubes, washed with PBS, and lysed in Trizol. For the 0, 1, 3, 6, and 24-hour time points, spheroids were collected, spun down at 500g for 5 minutes, washed with PBS, spun again, and resuspended in 0.4 mL of Trizol with gentle pipetting to break up the cell pellets as the spheroids had not fully formed. For spheroids harvested 48 hours and later, spheroids were resuspended in 0.4 mL Trizol and homogenized to disrupt the spheroids as described in Chapter 2.3. RNA was extracted according to the manufacturer protocol and converted into cDNA. RT-PCR was run PTGS2, IL6, TGFB1, VEGF, HGF, TWIST1, and ROCK. The GAPDH gene served as the housekeeping gene to normalize cDNA content post-analysis.

To compare ER stress marker gene expression between adherent and spheroid MSCs, both adherent and spheroid MSCs cultured for 72 hours, were washed and lysed in Trizol prior to RNA extraction and conversion into cDNA. Gene expression for XBP1, ATF4, and IDDT3 was measured using GAPDH as the housekeeping gene.

ROS detection

In order to measure ROS production in spheroid and adherent cells, cells were harvested at 24 or 72 hours and washed with PBS. Adherent cells were lifted as described above and spheroid MSCs were dissociated as described in Chapter 2.2. Briefly, spheroids were incubated at 37°C for 4 minutes, pipetted to break up some spheroids, incubated for another 4 minutes at 37°C, and then pipetted until obtaining a single cell suspension. Cell staining buffers of 10 μM

dihydroethidium (DHE) and cell-permeant 2',7'-dichlorodihydrofluorescein diacetate (DCF) were prepared in cell staining buffer (BD). 70,000 cells from either adherent or spheroid MSCs were stained with both ROS indicators for 30 minutes at 37°C in the dark. Cells were then spun down at 500g for 5 minutes and resuspended in cell staining buffer prior to flow cytometry analysis. Adherent cells were treated with or without 2 μM staurosporine or 5 mM hydrogen peroxide for 4 hours prior to cell harvest to serve as positive controls for DHE and DCF staining.

XTT measurement of metabolic function

In order to measure metabolic function, spheroid or adherent MSCs were harvested after 72 hours in culture, made into a single cell suspension as described above, and plated at 0, 1,000, 5,000, 10,000, or 20,000 cells in a 96-well plate. Cells were allowed to attach overnight (~16 hours) and then 50 μL of XTT reagent (BI), prepared according the manufacturer's instructions, was added to each well. Samples were incubated at 37°C for 2 hours prior to reading absorbance on a plate reader. XTT absorbance was measured at 475 nm with a background correction wavelength of 660 nm. Absorbance from no cell control wells were subtracted from all sample wells to account for non-cell specific XTT signal. For experiments with palmitate, palmitate conjugated to BSA[13] was added to 20,000 adherent or spheroid MSCs at 0, 0.1, 0.2, or 0.4 mM.

Nuclear staining

In order to confirm that similar numbers of adherent and spheroid MSCs were present at each cell dose after XTT analysis, cells used in the XTT analysis were stained with Hoechst ???. Briefly, a solution of 1 μL Hoechst per 1 mL of media was prepared. XTT reagent was aspirated out of the plate and 100 μL of nuclear staining buffer was added. Samples were incubated for 15 minutes at 37°C prior to imaging. After staining, the nuclear staining buffer was removed and replaced with warm MEM. Cells were then fluorescently imaged using a Leica DMI6000 microscope in the tile scan mode. For experiments with palmitate, palmitate conjugated to BSA[13] was added to 20,000 adherent or spheroid MSCs at 0, 0.1, 0.2, or 0.4 mM.

Statistical analysis

All statistical analysis was done in GraphPad Prism 8 using paired t-tests to compare between adherent and spheroid MSC groups. Unless otherwise noted, 3 independent MSC

donors were used for experiments. P-values < 0.05 were considered significant. 3D gene expression plots were created in Excel.

Results

Gene expression during spheroid formation is highly dynamic

First, we wanted to understand if gene expression was stable during spheroid formation. We analyzed gene expression of spheroids over 9 days of several immunomodulatory (PTGS2 and IL6), growth (VEGF, TGFB1, and HGF), and signal transduction factors (TWIST1 and ROCK1). Peak gene expression initially occurred in TGFB1 and HGF occurred within 24 hours, PTGS2 and IL6 peaked after 3 hours, and TWIST1, VEGF, TGFB1, and ROCK1 peaked after 5 days (Figure 11A). PTGS2, IL6, TWIST1, and HGF were greater than 4-fold increased after 9 days. After 72 hours, PTGS2, VEGF, and TGFB1 were all significantly upregulated over adherent MSCs (Figure 11B).

ER stress genes are upregulated upon spheroid formation

Since upregulation of some trophic factors like PTGS2 have been directly linked to cell stress pathways such as caspase activation, we wanted to determine if there were stress pathways which may account for these changes in trophic factor expression. During spheroid formation, cells compact and aggregate together. We wanted to determine if this stress lead to alterations in ER stress genes which can affect a variety of cell pathways including caspase activity. We looked at RNA expression of XBP1, ATF4, and IDDT3 which play a role in ER stress signaling (Figure 12). We found that in spheroids MSCs, all three transcripts were significantly upregulated compared to adherent MSC controls (Figure 12).

Since ER stress genes were upregulated in spheroids and it has been shown that spheroid MSCs upregulate ROS scavenging proteins including STC-1, we wanted to determine if upregulation of ER stress genes could be in response to increased ROS species present in spheroid MSCs. To test this, we cultured adherent and spheroid MSCs for either 24 or 72 hours. While spheroids are not fully formed for 48-72 hours, we wanted to determine if there was an early induction of ROS in the spheroid aggregation process. We stained cells using both dihydroethidium (DHE) also known as hydroethidine and DCF, which stain for the presence of superoxide and other ROS species and analyzed them by flow cytometry (Figure 13). While both

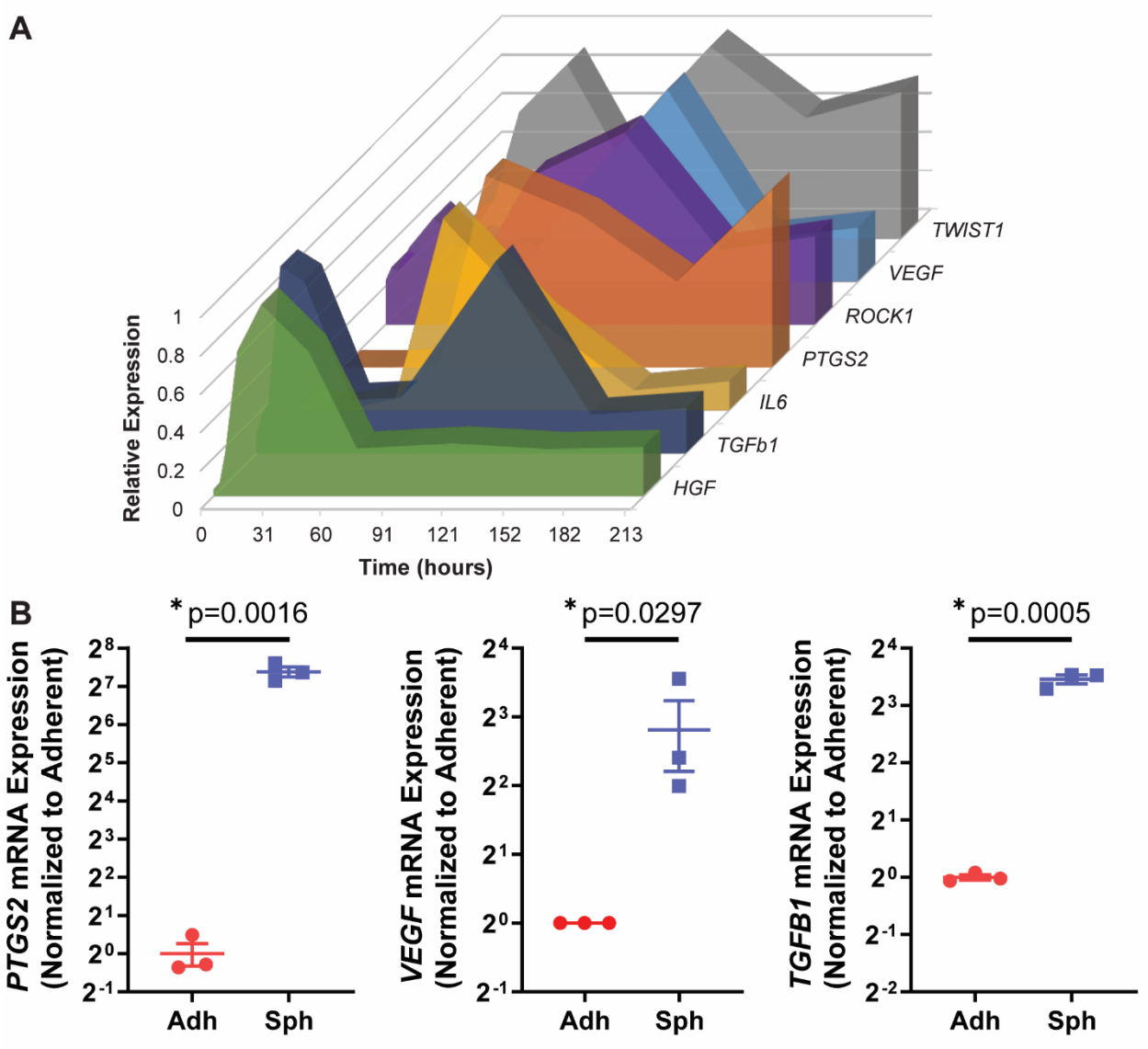

Figure 11. MSC spheroids alter gene expression over time.

(A) Spheroid MSC gene expression over 9 days measured by RT-PCR. Gene expression was normalized to the 0-hour time point. Individual gene expression kinetic profiles are shown in Figure 18. (B) Spheroid MSC expression of PTGS2, VEGF, and TGFB1 at 3 days of aggregation. *p<0.05

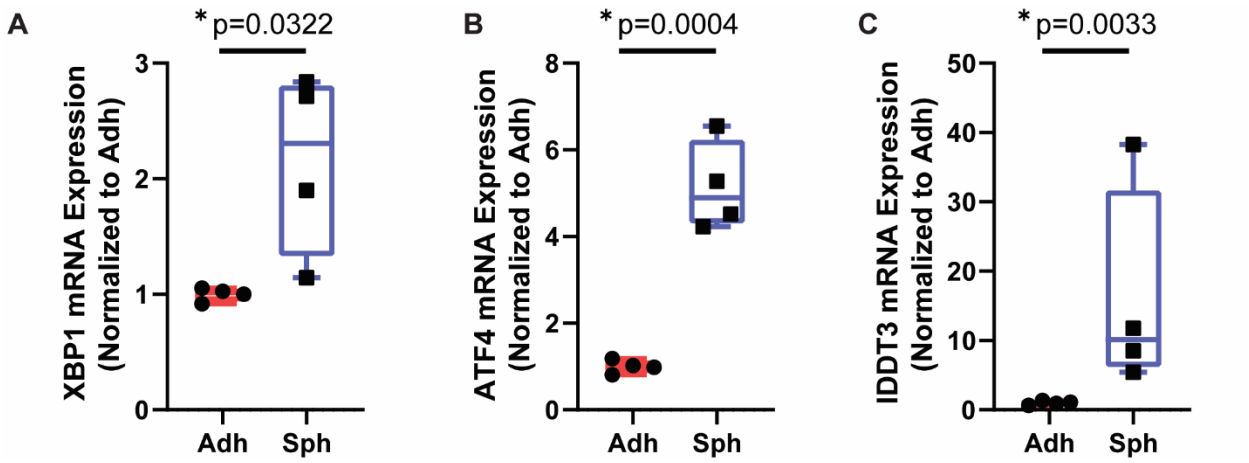

Figure 12. Spheroid MSCs upregulate ER stress genes.

Adherent and spheroid MSCs were culture for 3 days and then RNA was extracted and analyzed by RT-PCR for expression of ER stress markers XBP1 (A), ATF4 (B), and IDDT3 (C). Gene expression was normalized to the adherent control. *$p<0.05$

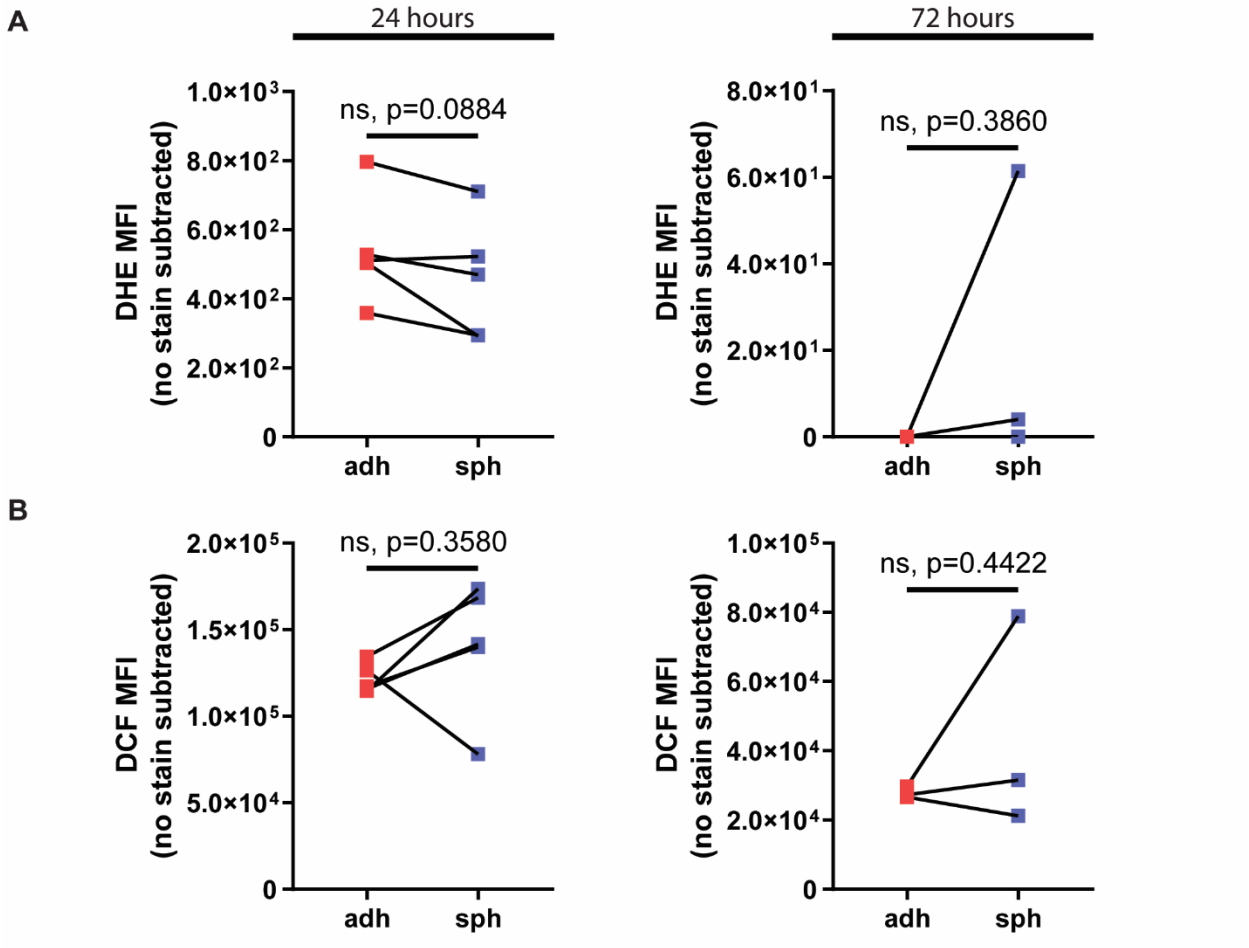

Figure 13. ROS is not significantly upregulated in spheroid MSCs.

Adherent (adh) or spheroid (sph) MSCs were cultured for 24 or 72 hours. Cells were harvested or dissociated and then stained with DHE (A) or DCF (B) to observe changes in ROS. Each experiment was background subtracted from the adherent with no stain control. *p<0.05

target ROS species, we found that the dyes are more sensitive to certain stressors. Specifically, we saw that upon staurosporine treatment in adherent cells, DHE showed a large change from non-treated cells, while DCF staining showed little change (Figure 13). Which challenged with hydrogen peroxide, DCF staining showed the greatest change from baseline, while DHE a smaller shift. When we compared adherent to spheroid cells, we discovered that there was no significant difference between the two at either the 24- or 72-hour time point (Figure 13). While there was no statistical difference between the two groups, we observed a shift from a trending decrease in spheroid DHE staining to a trending increase at 72 hours compared to adherent MSCs.

DHE is more selective for superoxide ROS species and therefore may be more indicative of changes in the electron transport chain function in the mitochondria, which is critical in cellular metabolism. However, DHE measures total intracellular superoxide, not only that present within mitochondria. Because we observed a trending, but not statistically significant change in the DHE staining in spheroids, we tested whether there were any changes in metabolic function of spheroid MSCs. XTT detects relative reduction of NAD+ to NADH in the citric acid cycle, a major component in MSC metabolism. Therefore, we used XTT to assess spheroid MSC metabolic function after spheroid formation (72 hours). As we have observed XTT reagent to aggregated in spheroids as shown in Chapter 2.2, we first disassociated spheroids into single cell suspensions and plated 1,000, 5,000, 10,000, or 20,000 cells with the same number of adherent control cells 16 hours prior to running the XTT assay. We found that there was a drastic decline in XTT signal from spheroid MSCs compared to adherent MSCs (Figure 14). As cell number can drastically affect XTT signal, we stained for nuclei and found that there were a similar number of cells between adherent and spheroid in each cell dose at the time of analysis (Figure 20).

Palmitate impairs spheroid MSC metabolic function and increases cell death

Increasing numbers of patients being treated with MSC therapies have co-morbidities including obesity and type-2 diabetes. Many metabolites are altered in these co-morbidities, including palmitate which has been implicated in disease progression[14,15]. Palmitate has known effects on cell metabolic health and has been shown to lead to cell apoptosis[16,17]. These detrimental effects make high levels palmitate potentially problematic for MSC therapies due to its alteration of cell phenotype and strategies such as pre-licensing must be used to rescue MSC

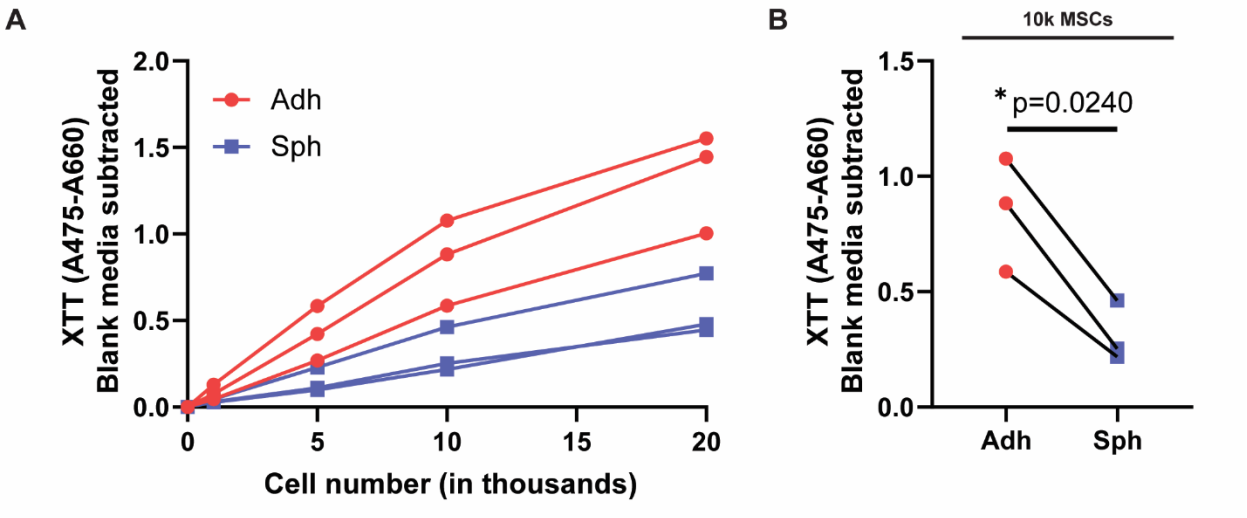

Figure 14. Spheroid formation lowers metabolic function in MSCs.

(A) Adherent (Adh) or disassociated spheroid (Sph) MSCs ranging from 0-20,000 cells were analyzed with XTT 24 hours after plating. Each experiment is shown separately with an individual line. Each experiment was background subtracted to the no cell media alone control. XTT signal from (A) at 10,000 cells are shown for both adherent and spheroid MSC experimental pairs in (B). *$p<0.05$

phenotype[13]. It has been shown that there are substantial effects of palmitate on adherent MSCs[13,18], but little is known about if palmitate has similar effects on spheroid MSCs. In order to determine how palmitate affects spheroid function and viability, we disassociated spheroid into a single cell suspension and cultured with a physiologic range of palmitate[19] (0-0.4 mM palmitate-BSA) for 96 hours. Nuclear staining (Figure 15) and an XTT assay (Figure 16) were used to assess the alterations to MSC viability and metabolic function, respectively. We found that consistent with previous results shown in Figure 20, adherent cells had greater metabolic function than spheroid MSCs. While this increased metabolic function seen in this assay may partly be due to cell proliferation over the 96-hour culture, cells were plated at near confluence to minimize MSC proliferation (Figure 15). We found that increased palmitate concentration resulted in lower metabolic function of both spheroid and adherent MSCs (Figure 16). While both adherent and spheroid MSCs were affected by palmitate, spheroid MSC metabolic function was affected at lower concentrations (Figure 16). At higher palmitate concentrations, there were fewer spheroid MSCs compared to adherent MSCs after the palmitate exposure (Figure 15).

Spheroid MSCs do not increase uptake of palmitate

Since we saw that spheroid MSCs were affected at lower palmitate concentrations than adherent MSCs, we wanted to test if this was due to increased uptake of palmitate. Additionally, we wanted to determine if there were differences in palmitate uptake in spheroid during initial formation of spheroids at 24 hours after plating and after they were fully formed at 72 hours. We treated spheroid and adherent MSCs with BODIPY C16, a fluorescent palmitate analog to see if there were differences in uptake of the fatty acid at both 24 and 72 hours of cell culture. However, we found that surprisingly there was a small, but statistically significant decrease in palmitate uptake in spheroid MSCs at 24 hours (Figure 17A). At 72 hours, there was a trending, but non-significant decrease from adherent MSCs (Figure 17B).

Discussion

We have seen that there are large transcriptional changes that occur within spheroids and some of these changes are transient (Figure 11A). These transcriptional changes result in a dramatically altered MSC secretome and changes their interaction with other cells in inflammatory and ischemic conditions. While many effects of this altered secretome have been

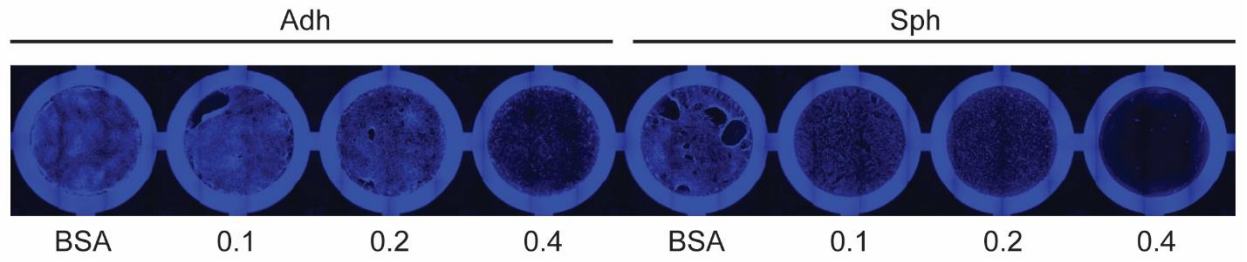

Figure 15. Palmitate negatively affects spheroid MSC viability.

Adherent and disassociated spheroid MSCs were plated at 20,000 cells per well and treated with 0, 0.1, 0.2, and 0.4 mM palmitate-BSA for 4 days. Cells were stained with Hoechst and imaged.

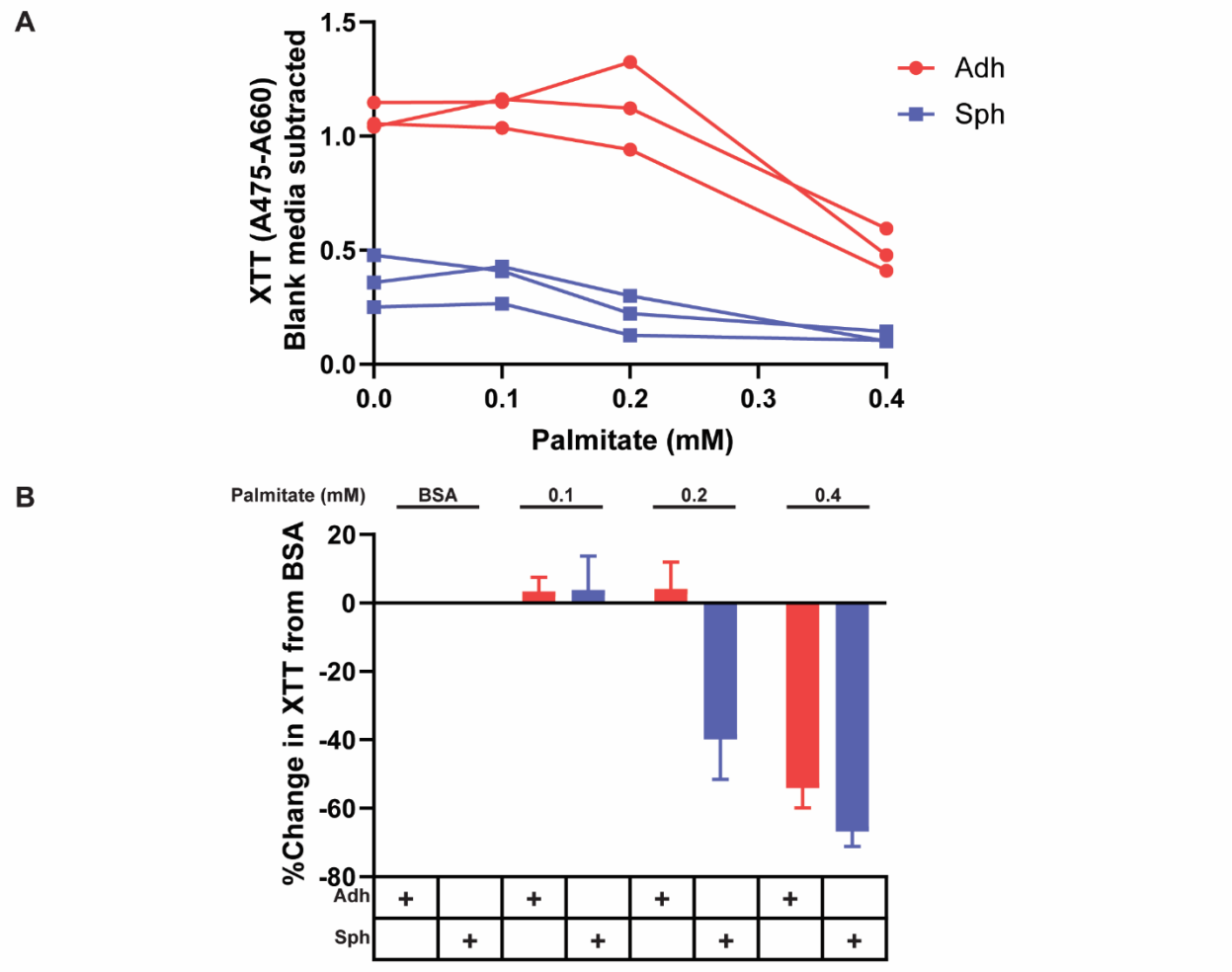

Figure 16. Palmitate affects spheroid MSCs metabolic function more than adherent MSCs. (A) XTT signal from adherent (Adh) and dissociated spheroids (Sph) treated for 48 hours with 0-0.4 mM palmitate. Signal was background subtracted from no cell media only controls. Each trace represents an experiment. (B) XTT data in (A) processed as % change from 0 mM palmitate condition for both adherent and spheroid MSCs.

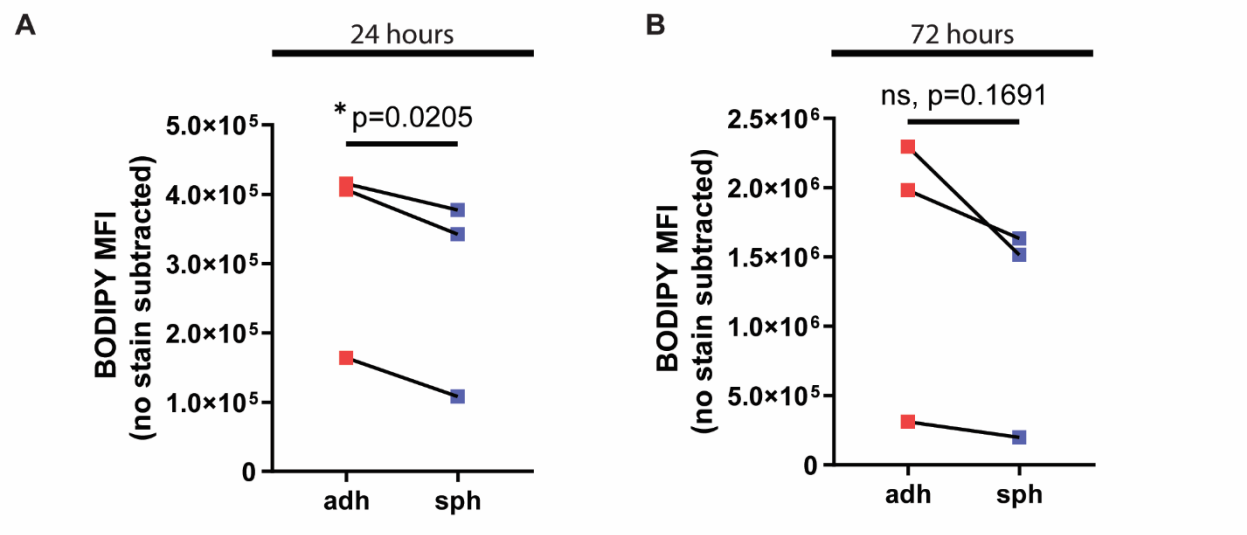

Figure 17. Spheroid MSCs show altered uptake of palmitate.

Adherent and spheroid MSCs were collected at 24 hours (A) or 72 hours (B) after formation and stained with BODIPY C16. Spheroid MSCs were dissociated with Accutase. Data represents N=3 MSC preparations. *p<0.05

observed, little research has been done to understand how MSC aggregation may lead to these alterations and how it can be modulated.

MSC aggregation results is a mechanical environment that is significantly different from that of tissue culture plastic. The 3D structure of MSC spheroids significantly impacts transport of oxygen, small molecules, and proteins both in and out of the spheroid. Additionally, the proximity of cells to one another can alter cell-cell signaling events compared to MSC in monolayers. All three of these changes in the MSC microenvironment can contribute to the observed phenotype. Increased production of factors like PGE2, IL-1, STC-1, caspases, and IL-8 have all been identified with cellular stress.[20–24] Looking at ER stress RNA transcripts for the proteins CHOP, ATF4, and XBP1, we discovered that all of them were elevated in spheroid MSCs compared to adherent MSCs. ER stress response can selectively up- and down-regulate genes to enhance cell survival. Therefore, it is possible that aggregation is a stressful process for MSCs and the gene changes that occur are in response to this stressful environment.

Classic activation of ER stress genes occurs due to the misfolded proteins present in the ER and one mechanism which can drive this is oxidative damage to proteins.[25] Since spheroid cells, upregulate the ROS scavenging protein STC-1[2], we sought to determine if increased oxidative damage may drive this ER stress response. However, in this study we did not see any consistent changes in ROS species present within spheroid compared to adherent MSCs potentially due to ROS species being localized to a specific compartment of the cell, such as the mitochondria. We did see a trending change from 24 to 72 hours of cell culture between adherent and spheroid cells. This led us to examine downstream function of mitochondria through a metabolic activity assay. We found that there was a significant decline in metabolic function of spheroid MSCs. Therefore, there is evidence to support that mitochondrial stress in spheroid MSCs may some phenotypic changes. While ER stress marker expression correlated with metabolic function and gene expression alterations, further study is needed to determine if there these changes in MSC are directly linked to ER stress like they are in other cells types.[26] Additionally, while mitochondrial ROS can induce ER stress, there are a number of other factors that are known to induce the ER stress responses such as hypoxia, low glucose, and inflammatory cytokines, all of which are present within the spheroid microenvironment.[2,25] Therefore, while this study was unable to find a direct link between MSC aggregation and

changes to gene expression, it does point to the fact that further investigation is needed to confirm this hypothesis.

Lastly, we observed that these changes collectively have direct impact on spheroid MSC interaction with their environment. Specifically, in the setting of high levels of palmitate, we saw a greater impact on spheroid MSC viability and metabolic function than seen with adherent MSCs. This observation requires further investigation because in our method, spheroid MSCs were disassociated prior to palmitate exposure, which may make them more susceptible to environmental insults when not in their protective 3D structure. Despite this, spheroid formation has a substantial effect on MSC function even after they return to an adherent state further emphasizing the need to understand the consequences of this phenotype in the context of their immunomodulatory and regenerative capacities. MSC aggregation and its effects on immunomodulatory potential will be further discussed in Chapter 4.2.

Conclusion

Aggregation of MSCs affects gene expression, ER stress, and metabolic function of the cells and can impact how MSCs respond to environmental insults such as palmitate. Understanding the consequences of aggregation is critically important as these alterations to MSC phenotype can impact cell performance *in vivo*. Additionally, understanding the changes can provide insight into the mechanism which drives the phenotypic change and subsequently how this cellular response can be modified. In this study, we provided a path for further investigation into alterations in spheroid MSC secretome and metabolic function and how aggregation of the cells may lead to this phenotypic shift.

Supplemental Figures

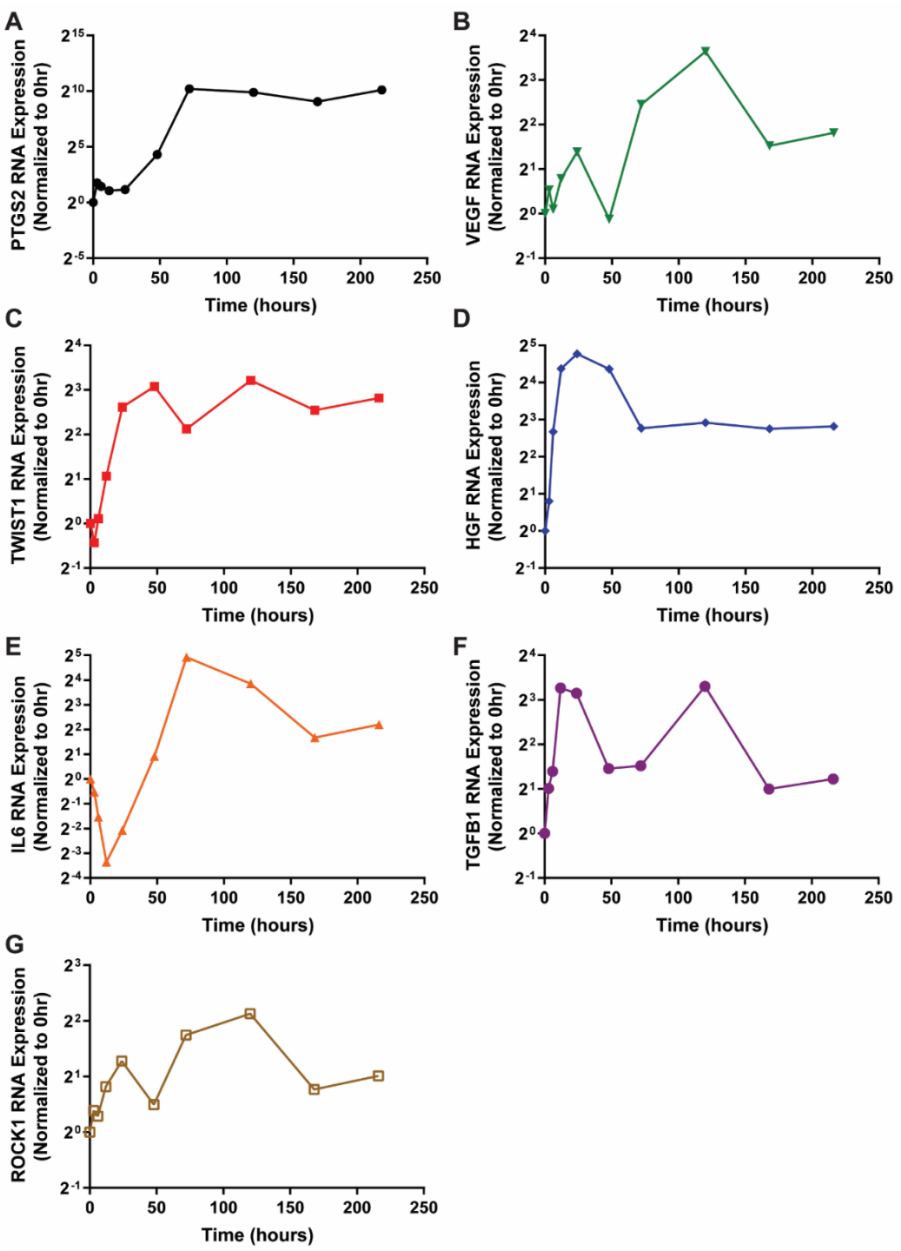

Figure 18. MSC spheroid gene expression varies over time.

Spheroid MSC gene expression profiles over 9 days of culture for PTGS2 (A), VEGF (B), TWIST1 (C), HGF (D), IL6 (E), TGFB1 (F), and ROCK1 (G). All gene expression profiles are normalized to the 0-hour control.

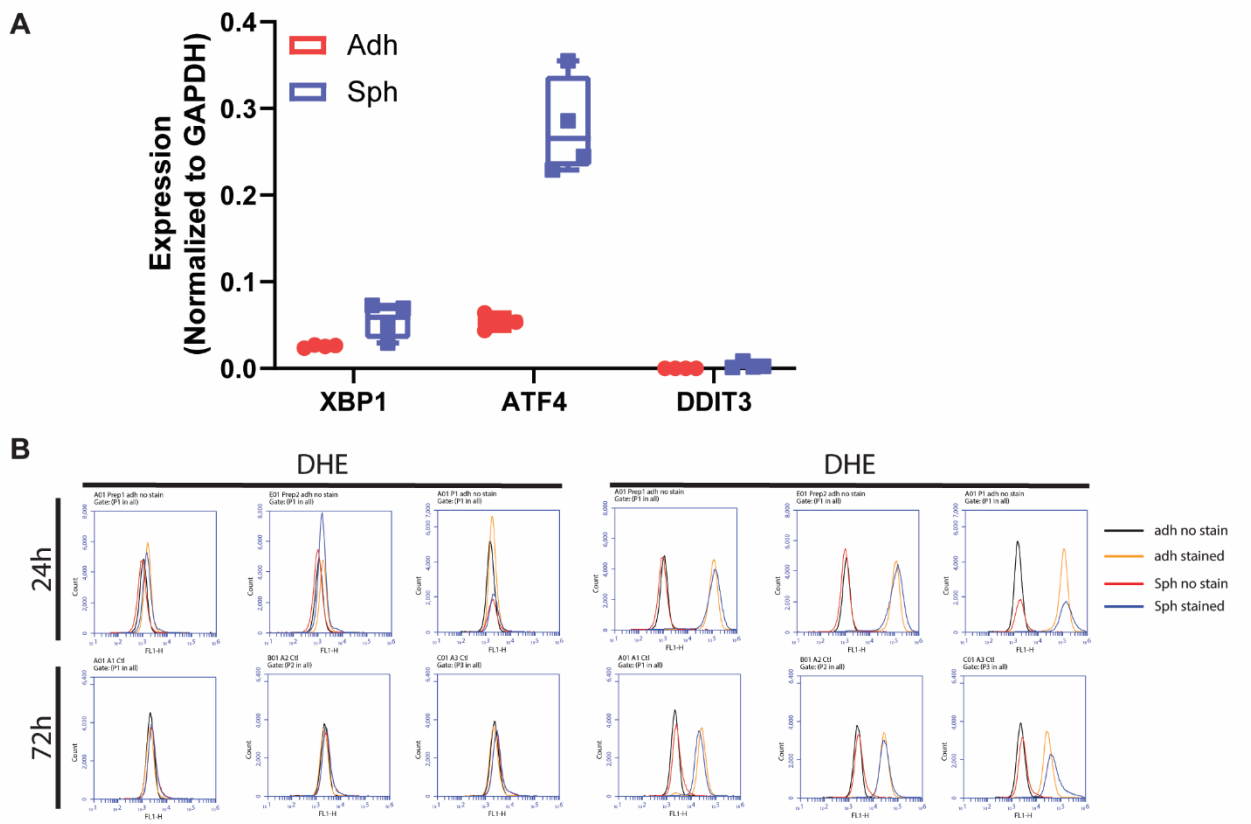

Figure 19. Adherent and spheroid MSC expression or ER stress genes and ROS.

(A) Gene expression data normalized to GAPDH expression prior to normalization as shown in Figure 12. (B) Representative flow cytometry plots of adherent or spheroid MSCs stained with DHE or DCF. Quantified data is displayed in Figure 13.

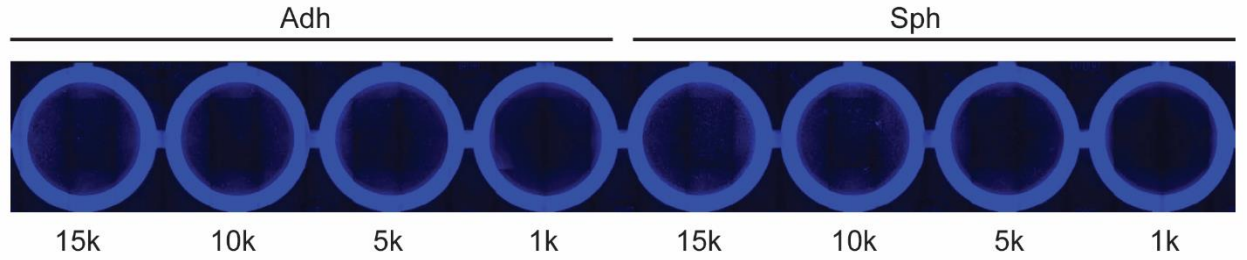

Figure 20. Similar numbers of adherent and spheroid MSCs attach to tissue culture plastic. Adherent (Adh) and dissociated spheroid (Sph) MSCs were stained with Hoechst and imaged after overnight attachment.

3.4. REFERENCES

1. YlÖstalo, J. H., Bartosh, T. J., Coble, K. & Prockop, D. J. Human Mesenchymal Stem/Stromal Cells Cultured as Spheroids are Self-activated to Produce Prostaglandin E2 that Directs Stimulated Macrophages into an Anti-inflammatory Phenotype. *Stem Cells* **30**, 2283–2296 (2012).
2. Bartosh, T. J., Ylöstalo, J. H., Bazhanov, N., Kuhlman, J. & Prockop, D. J. Dynamic compaction of human mesenchymal stem/precursor cells into spheres self-activates caspase-dependent IL1 signaling to enhance secretion of modulators of inflammation and immunity (PGE2, TSG6, and STC1). *Stem Cells* **31**, 2443–2456 (2013).
3. Bartosh, T. J. & Ylostalo, J. H. Preparation of Anti-Inflammatory Mesenchymal Stem/Precursor Cells (MSCs) Through Sphere Formation Using Hanging-Drop Culture Technique. *Curr. Protoc. Stem Cell Biol.* **28**, 2B.6.1-2B.6.23 (2014).
4. Ylostalo, J. H., Bartosh, T. J., Tiblow, A. & Prockop, D. J. Unique characteristics of human mesenchymal stromal/progenitor cells pre-activated in 3-dimensional cultures under different conditions. *Cytotherapy* **16**, 1486–1500 (2014).
5. Xie, L., Mao, M., Zhou, L., Zhang, L. & Jiang, B. Signal Factors Secreted by 2D and Spheroid Mesenchymal Stem Cells and by Cocultures of Mesenchymal Stem Cells Derived Microvesicles and Retinal Photoreceptor Neurons. *Stem Cells Int.* **2017**, 1–13 (2017).
6. Lee, B.-C. *et al.* PGE2 maintains self-renewal of human adult stem cells via EP2-mediated autocrine signaling and its production is regulated by cell-to-cell contact. *Sci. Rep.* **6**, 26298 (2016).
7. Bartosh, T. J. *et al.* Aggregation of human mesenchymal stromal cells (MSCs) into 3D spheroids enhances their antiinflammatory properties. *Proc. Natl. Acad. Sci.* **107**, 13724–13729 (2010).
8. Skardal, A., Mack, D., Atala, A. & Soker, S. Substrate elasticity controls cell proliferation, surface marker expression and motile phenotype in amniotic fluid-derived stem cells. *J. Mech. Behav. Biomed. Mater.* **17**, 307–316 (2013).

9. Sun, M. *et al.* Effects of Matrix Stiffness on the Morphology, Adhesion, Proliferation and Osteogenic Differentiation of Mesenchymal Stem Cells. *Int. J. Med. Sci.* **15**, 257–268 (2018).
10. Sarem, M., Otto, O., Tanaka, S. & Shastri, V. P. Cell number in mesenchymal stem cell aggregates dictates cell stiffness and chondrogenesis. *Stem Cell Res. Ther.* **10**, 10 (2019).
11. Darnell, M., Gu, L. & Mooney, D. RNA-seq reveals diverse effects of substrate stiffness on mesenchymal stem cells. *Biomaterials* **181**, 182–188 (2018).
12. Szymanski, C. J. *et al.* Shifts in oxidation states of cerium oxide nanoparticles detected inside intact hydrated cells and organelles. *Biomaterials* **62**, 147–154 (2015).
13. Boland, L. *et al.* IFN-γ and TNF-α Pre-licensing Protects Mesenchymal Stromal Cells from the Pro-inflammatory Effects of Palmitate. *Mol. Ther.* **26**, 860–873 (2018).
14. Dasu, M. R. & Jialal, I. Free fatty acids in the presence of high glucose amplify monocyte inflammation via Toll-like receptors. *Am. J. Physiol. Metab.* **300**, E145–E154 (2011).
15. Lu, J. *et al.* Palmitate Causes Endoplasmic Reticulum Stress and Apoptosis in Human Mesenchymal Stem Cells: Prevention by AMPK Activator. *Endocrinology* **153**, 5275–5284 (2012).
16. Ertunc, M. E. & Hotamisligil, G. S. Lipid signaling and lipotoxicity in metaflammation: indications for metabolic disease pathogenesis and treatment. *J. Lipid Res.* **57**, 2099–2114 (2016).
17. Yan, L.-J. Pathogenesis of Chronic Hyperglycemia: From Reductive Stress to Oxidative Stress. *J. Diabetes Res.* **2014**, 1–11 (2014).
18. Boland, L. K. *et al.* Nature vs. Nurture: Defining the Effects of Mesenchymal Stromal Cell Isolation and Culture Conditions on Resiliency to Palmitate Challenge. *Front. Immunol.* **10**, 1–15 (2019).
19. Trombetta, A. *et al.* Increase of Palmitic Acid Concentration Impairs Endothelial Progenitor Cell and Bone Marrow-Derived Progenitor Cell Bioavailability: Role of the STAT5/PPAR Transcriptional Complex. *Diabetes* **62**, 1245–1257 (2013).
20. Verhasselt, V., Goldman, M. & Willems, F. Oxidative stress up-regulates IL-8 and TNF-α synthesis by human dendritic cells. *Eur. J. Immunol.* **28**, 3886–3890 (1998).
21. Kannan, K. & Jain, S. K. Oxidative Stress and Apoptosis. *Pathophysiology* **7**, 153–163 (2000).

22. Sheikh-Hamad, D. Mammalian stanniocalcin-1 activates mitochondrial antioxidant pathways: new paradigms for regulation of macrophages and endothelium. *Am. J. Physiol. Physiol.* **298**, F248–F254 (2010).
23. Kowluru, R. A., Mohammad, G., Santos, J. M., Tewari, S. & Zhong, Q. Interleukin-1β and mitochondria damage, and the development of diabetic retinopathy. *J. Ocul. Biol. Dis. Infor.* **4**, 3–9 (2011).
24. Cherian, P. P. *et al.* Effects of Mechanical Strain on the Function of Gap Junctions in Osteocytes Are Mediated through the Prostaglandin EP 2 Receptor. *J. Biol. Chem.* **278**, 43146–43156 (2003).
25. Oslowski, C. M. & Urano, F. Measuring ER stress and the unfolded protein response using mammalian tissue culture system. in *Methods in Enzymology* (2011). doi:10.1016/B978-0-12-385114-7.00004-0
26. Wang, X. *et al.* ER stress modulates cellular metabolism. *Biochem. J.* **435**, 285–296 (2011).

CHAPTER 4: AGGREGATED MESENCHYMAL STROMAL CELLS DEMONSTRATE ALTERED INTERATIONS WITH IMMUNE CELLS

4.1. OVERVIEW

In Chapter 3, we observed several significant changes to MSCs upon aggregation into spheroids. In this chapter, we show that these phenotypic changes lead to a complete loss of T cell suppressive capability, even though spheroid MSCs remain suppressive of inflammatory macrophages. We also show that in our *in vitro* model of local injection, we see significant alterations to the MSCs immunomodulatory protein profile and activity of these proteins. Additionally, we demonstrated that these phenotypic changes in spheroids are not benign but drive inflammation in PBMC co-cultures. However, we found that MSC suppression of activated T cells can be partly restored with co-administration of the glucocorticoid steroid, budesonide. This spheroid-budesonide synergy is mediated through a PGE2-EP2/4 signaling pathway in activated T cells. This demonstrates that the immunomodulatory changes in aggregated MSCs impact their function and therefore bioengineering strategies must be used to enhance their potency for inflammatory diseases.

This is an adaptation of an article that has been submitted to *Stem Cells*.

4.2. AGGREGATED HUMAN MESENCHYMAL STROMAL CELLS LOSE THE ABILITY TO SUPPRESS T CELLS BUT REGAIN IT VIA SYNERGY WITH BUDESONIDE

Abstract

Mesenchymal stromal cells (MSCs) are used to treat several inflammatory diseases, some necessitating localized injection at sites of inflammation. Locally delivered MSCs aggregate into 'spheroids', which alters gene expression. While adherent MSCs demonstrate potency in immunomodulatory assays, spheroid MSCs' suppression of T cells, which are critical drivers of inflammation, has not been extensively studied. In this study, we discovered that although spheroid MSCs suppress inflammatory macrophages, they are unable to suppress activated T cells. Notably, adding the glucocorticoid steroid, budesonide, with spheroids restored suppression of T cells. We determined budesonide acts synergistically with spheroid MSC PGE2 to suppress T cell proliferation through the PGE2 receptors, EP2 and EP4. These findings highlight critical differences between adherent and spheroid MSC interactions with immune cells and uncover a mechanism through which spheroid suppression of T cells can be partly restored. By understanding drug synergy with spheroid MSCs, we can engineer immunosuppressive MSCs for localized delivery.

Significance statement

When locally delivered, human mesenchymal stromal cell (MSC) have been reported to aggregate into spheroids. In this study, we demonstrate that aggregation into spheroids drastically alters MSCs' immunomodulatory phenotype. This altered phenotype includes the loss of the ability to suppress activated T cells, a key mechanism by which MSCs resolve inflammation. However, this loss of potency is context dependent, as we show that PGE2 produced by spheroid MSCs synergizes with budesonide to suppress activated T cells.

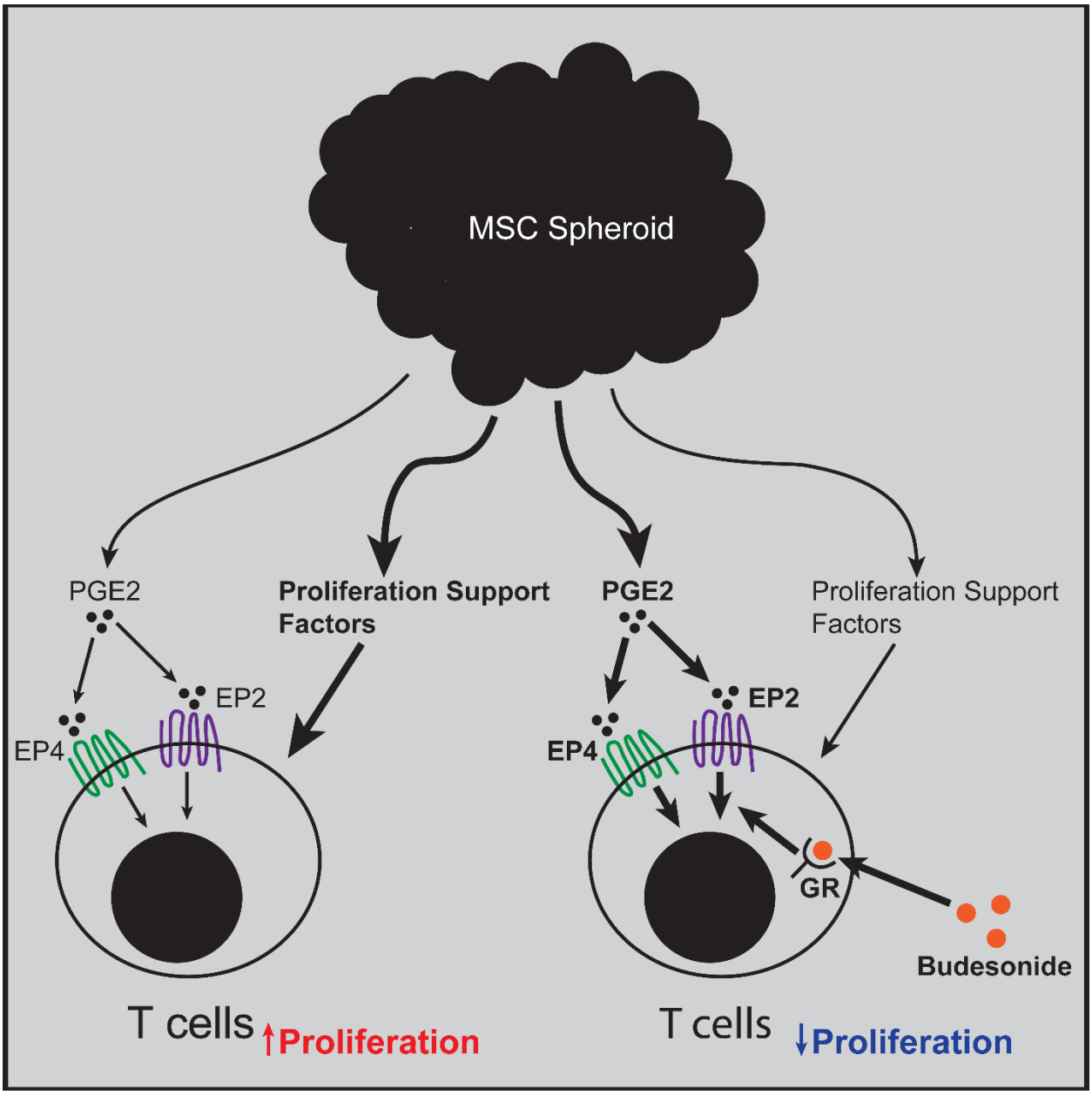

Figure 21. Mechanism of spheroid MSC-budesonide synergistic suppression of T cells. Aggregation of human mesenchymal stromal cells (MSCs) into spheroids perturbs the balance of immunomodulatory factors produced by MSCs ultimately leading to a loss in the suppression of activated human T cells. While spheroid MSC produced PGE2 is not alone suppressive, when combined with budesonide, a glucocorticoid steroid, it works in synergy to inhibit the proliferation of activated T cells.

Introduction

Mesenchymal stromal cells (MSCs) have been used for decades to treat inflammatory diseases because of their ability to produce a range of immunosuppressive products. IDO[1], kynurenine[2], PGE2[3,4], CD73[5,6], TGF-β[7], IL-6[8], and TSG-6[9], amongst others, enable MSCs to modulate the behavior of T cells, B cells, macrophages, natural killer cells, dendritic cells, and neutrophils[10]. The ability of MSCs to both dampen inflammation and promote an anti-inflammatory tolerogenic phenotype in multiple subsets of immune cells has made them candidates to treat complex inflammatory diseases such as graft vs host disease, Crohn's disease, multiple sclerosis, asthma, chronic wounds, and rheumatoid arthritis.

Currently, about 50% of clinical trials employ local injection of MSCs to place them at the site of inflammation[11]. Localized delivery of MSCs is often desirable as it avoids the risk of emboli formation in the lungs and capillary beds[12,13], while placing the cells near sites of injury and inflammation. However, MSCs injected locally into spatially constricted sites aggregate to form spheroids. This aggregation phenomenon has been observed in mice after peritoneal[14], intramuscular[15], peri-implant[16], and intraventricular[17] injections, prompting the study of the spheroid MSC phenotype. MSCs in spheroids dramatically shift their gene expression and phenotype upon local injection[14]. The frequent utilization of local injection and evidence of transcriptional changes raises questions regarding whether the immunomodulatory properties of adherent MSCs displayed in *in vitro* potency assays persist once MSCs aggregate into spheroids.

Alterations in secretome change MSCs interactions with immune cells. Studies to date have shown aggregation into spheroids causes MSCs to upregulate PGE2, TSG-6, IL-1α/β, STC1, as well as several matrix factors[14,18,19]. In transwell experiments with immortalized mouse macrophages, human spheroid MSCs reduced macrophage production of TNF-α and increased IL-10 more than adherent MSCs[14,18,20]. Similar enhanced interactions of spheroid MSCs with macrophage populations have been observed with THP-1 derived macrophages as well as a mouse model of peritonitis[14,18]. In addition to immunomodulatory factors, other groups have demonstrated that when MSCs aggregate *in vivo*, they persist for longer[15], making understanding their post-aggregation phenotype all the more critical. In animal models, spheroid MSCs have been shown to reduce spontaneous limb loss in a hind limb ischemia model[21], lower infarct volume in a stroke model[22], rescue kidney cells from apoptosis[23], and enhance bone regeneration[24], possibly due to enhanced levels of growth factor secretion[25]. While appearing

beneficial in several settings, the full impact of aggregation on MSCs' immunomodulatory phenotype, which is critical both for suppression of inflammation and, in allogeneic uses, immune evasion[26], is still not fully understood.

Many of the disease indications in which localized injection of MSCs occur are mediated, in part, by T cell recruitment and effector function. There is a strong base of literature showing that adherent MSCs suppress activated T cells, PBMCs, and mixed lymphocyte reactions (MLR) *in vitro*[1,2,27–30]. However, few studies to date have looked at the interactions of non-differentiated spheroid MSCs with T cells. To translate MSCs to the clinic, we must know if spheroid MSCs have comparable immunomodulatory potency to their adherent counterparts, or if they display an entirely different, not necessarily superior, immunomodulatory profile. If these profiles are distinct, it makes little sense to study MSC potency under adherent conditions, since their behavior shifts rapidly upon local injection.

Herein, we aimed to elucidate the effect that aggregation has on MSCs' ability to suppress T cells within PBMC populations to more fully understand spheroid MSCs' immunomodulatory phenotype. Insight into these phenotypic changes can then be used to inform the logical design and application of localized MSC therapies for the treatment of inflammatory conditions.

Materials and Methods

MSC spheroid culture

In this study, human bone marrow-derived MSCs, characterized and obtained from RoosterBio (MSC-001 Lot: 00082, MSC-003 Lot: 00055, and MSC-003 Lot: 00022) and isolated human umbilical cord MSCs, characterized in house were used in experiments (Figure 22). MSCs from each donor were expanded, aliquoted, and cryopreserved allowing vials to be outgrown for use in experiments. Cells were cultured in MEM-α (Fisher Scientific, Cat # BW12-169F) supplemented with 15% fetal bovine serum (VWR, Cat # 059B18), 1% L-glutamine (Life Technologies, Cat # 25030081), and 1% penicillin-streptomycin (Life Technologies, Cat # 15140122). Cells were seeded at a density of 4,000-6,000 cells/cm^2 and grown until 70-90% confluent. For experiments, 2D adherent MSCs (Adh) were plated at 5,300 MSCs/cm^2 in T-75 flasks and incubated at 37°C for 3 days. 3D MSC spheroids (Sph) were

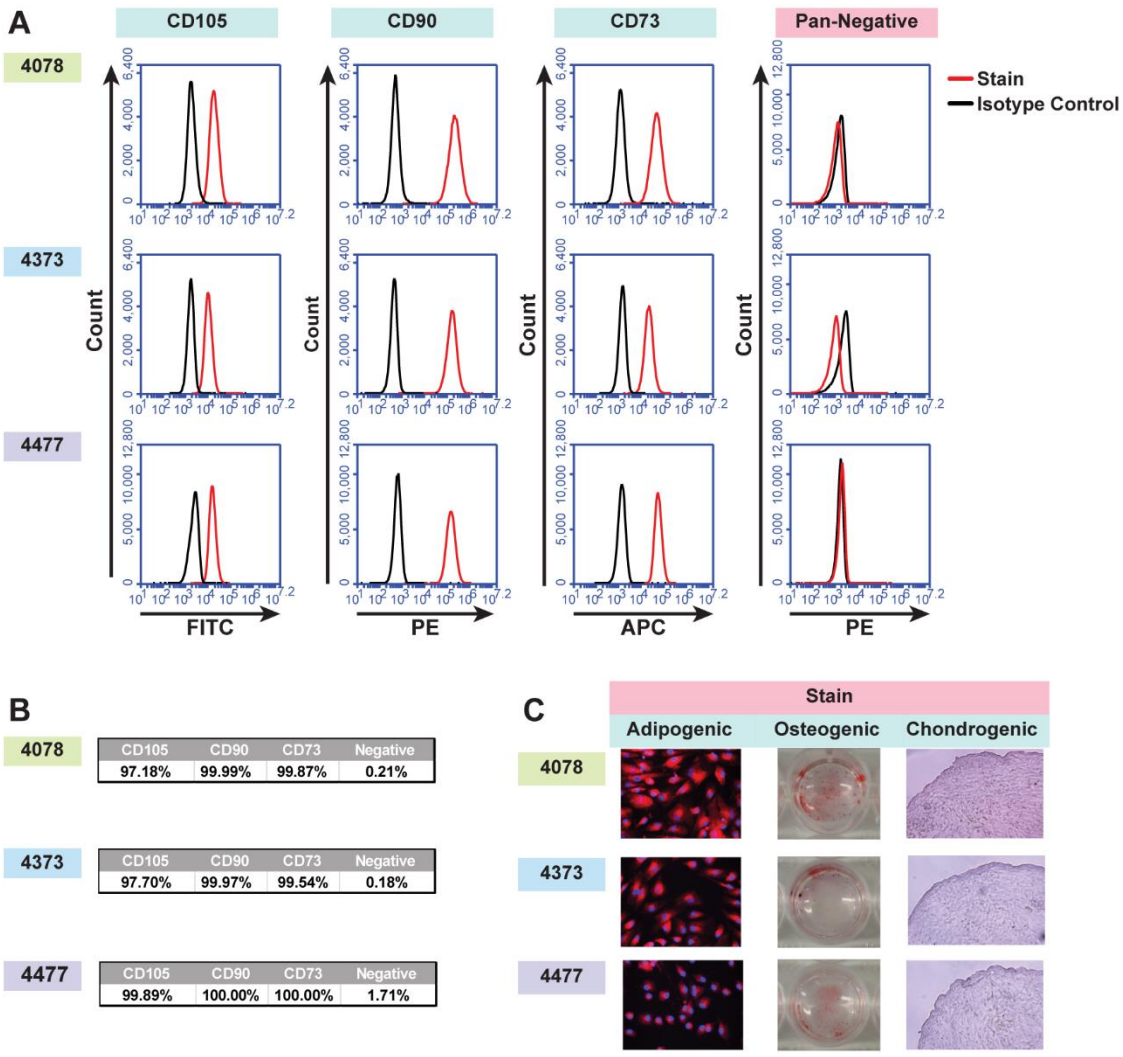

Figure 22. Isolated umbilical cord cells meet the minimal MSC criteria.

(A) Flow cytometry analysis of MSC markers CD105, CD90, CD73, and negative cocktail (CD34, CD11b, CD19, CD45, and HLA-DR) for isolated umbilical cord MSCs. (B) Quantification of MSC marker expression in (A). (C) Differentiated umbilical cord MSCs stained with AdipoRed, Alizarin Red, and Safranin-O for confirmation of adipogenic, osteogenic, and chondrogenic differentiation potential.

formed using a hanging droplet technique as previously described by Ylostalo *et al*[31]. Briefly, MSCs were resuspended to 1 million cells/mL and 20 μL droplets of cell suspension were plated on petri dish lids. Sacrificial droplets of media were placed around the cell droplets and PBS was added to the base of the petri dish to minimize evaporative loss during the spheroid formation process. Lids were inverted and incubated at 37°C for 3 days. A detailed description of the umbilical cord isolation protocol is provided in the Supplemental Materials and Methods.

Adherent and spheroid MSC production of immunomodulatory factors such as IDO, COX-2, CD73, and TGF-β were analyzed at the RNA, protein, or enzymatic product levels. Detailed protocols on RT-PCR, western blot, immunohistochemistry, ELISA, and enzyme activity assays are provided in the Supplemental Materials and Methods. For experiments using the same MSC donor, multiple vials of MSCs were thawed and independently outgrown to provide cells for experimental replicates.

PBMC and T cell co-culture with Sph and Adh MSCs

Isolated PBMCs or T cells, as described in the Supplemental Materials and Methods, were stained with CSFE (Biolegend, Cat # 423801) as described by the manufacturer. Briefly, PBMCs or T cells were thawed and placed in warm complete RPMI containing 10% FBS, 1% penicillin/streptomycin, and 1% L-glutamine for at least 1 hour prior to the staining process. Cells were counted and resuspended in PBS at 1 million cells/mL. 2 μL of 5 mM CSFE in DMSO per 10 million PBMC or T cells was vortexed into the cell suspension to obtain a final dye concentration of 1 μM. The PBMCs or T cells were incubated at 37ºC in the dark for 15 minutes. CFSE was then neutralized with complete RPMI, spun down at 500g for 5 minutes, and resuspended in complete RPMI. The cells were then allowed to incubate for 30 minutes at 37ºC. Cells were spun and resuspended at 2 million cells/mL in complete RPMI. PBMCs or T cells for the unstimulated control were removed prior to human CD3/CD28 Dynabead (Thermo Fisher, Cat # 11132D) addition and adjusted to a final concentration of 1 million cells/mL. 250,000 PBMCs with or without Dynabeads were added to their respective wells in a 24-well plate.

Adherent MSCs or spheroids were plated 3 days prior to the co-culture. Adherent cells were harvested, resuspended at 1 million cells/mL and then 60,000 MSCs were plated (~1:4 MSC:PBMC). 20,000-cell spheroids were then transferred into the wells in equal number to adherent MSCs unless otherwise noted. Visual confirmation was used to ensure an accurate

number of spheroids in each well. After 6 days in co-culture, PBMCs or T cells were collected, and their proliferation was analyzed by flow cytometry. CD3/CD28 Dynabead Stimulated and unstimulated PBMC only controls were used to set proliferation gates. All negative controls without Dynabead stimulation showed no proliferation. Additional PBMC generational analysis was performed using the FlowJo v10 software and normalized proliferation is described in the Supplemental Materials and Methods.

MSC co-culture in transwells

Adherent and spheroid MSCs were platted into the bottom of 24-well plates in 700 µL of complete RPMI (formulated as described above). PBMCs were stained with CSFE and combined with CD3/CD28 Dynabeads to yield a final concentration of 1 million PBMCs/mL. Transwell inserts with 3 µm pores (Corning, Cat # 07-200-148) were added to MSC loaded wells and 250 µL of Dynabead-PBMC solution was placed in the inserts. Cells were then cultured for 6 days prior to analysis by flow cytometry as described above.

PBMC proliferation with BUD, PGE2, EP2/4 inhibitors

PBMCs isolated from three independent de-identified blood donors were thawed from a cryo-stock. After recovery, cells were stained with CFSE as described above and activated with CD3/CD28 Dynabeads. 250,000 activated PBMCs with Dynabeads were plated in each experimental well. Each PBMC donor was plated in duplicate with non-treated activated controls on each plate (one plate to determine synergistic effect of budesonide and PGE2 on preventing PBMC activation; one plate used to determine the ability of EP Receptor inhibitors to prevent the synergistic effect). The final working concentrations of all tested compounds were as follows: Budesonide (10 µM), PGE2 (1 µM, Tocris, Cat # 2296), TG4-155 (10 µM, Tocris, Cat # 5052), and L-161,982 (10 µM, VWR, Cat # 75844-788). The same concentrations were used for experiments with and without MSCs.

Statistics

All statistics and graphs were prepared in GraphPad Prism 8. Error bars on graphs are represented as mean ± SEM (standard error of the mean) unless otherwise stated in the figure

legends. Specific statistical tests and descriptions of pooled data are provided in the figure legends. $p<0.05$ was considered significant.

Results

Spheroids cannot suppress activated PBMCs

In order to test the immunomodulatory properties of aggregated MSCs, we used a previously developed protocol[14] to aggregate MSCs into spheroids over 3 days *in vitro* prior to co-culture with human immune cells (Figure 23A-B). Previous studies have shown spheroid MSCs display superior anti-inflammatory actions toward immortalized or mouse macrophages[18,32–34]. In agreement, we found that in co-cultures with primary human macrophages, spheroids enhance production of anti-inflammatory markers in M2c M-CSF/BUD polarized macrophages (Figure 24B,D). However, in contrast to what had previously been seen with mouse or immortalized macrophage interactions, spheroids in direct contact with M1 LPS/IFN-γ polarized primary human macrophages did not provide superior suppression of inflammatory M1 macrophages (Figure 24A,C). Next, we sought to understand how aggregation of MSCs altered their interaction with activated T cells, another immune cell population known to drive inflammation. Adherent MSCs are well known to suppress the proliferation of PBMCs activated with CD3/CD28 Dynabeads or through MLRs. Because of variability between MSC donors, we used different MSC donors, derived from commercial bone marrow sources and umbilical cords isolated and characterized in house (Figure 22). As expected, adherent MSCs from each donor showed a robust ability to suppress PBMC proliferation. Surprisingly, for all 4 MSC donors, aggregation into spheroids completely eliminated their immunosuppressive potency, despite having the same number of MSCs in both adherent and spheroid conditions (Figure 23C-D).

Spheroid dose and contact factors are not responsible for the loss of PBMC suppression

The dramatic loss in potency we observed just 3 days after spheroid formation was unexpected, so we sought to understand why spheroid MSCs lose immunosuppressive potency. We had seen a substantial fraction of MSCs die upon aggregation (up to 25% PI+, Figure 25), which is consistent with previous reports[18,33,35]. This led us to hypothesize that the loss in potency was an artifact due to a reduction in the number of viable MSCs. To test this hypothesis,

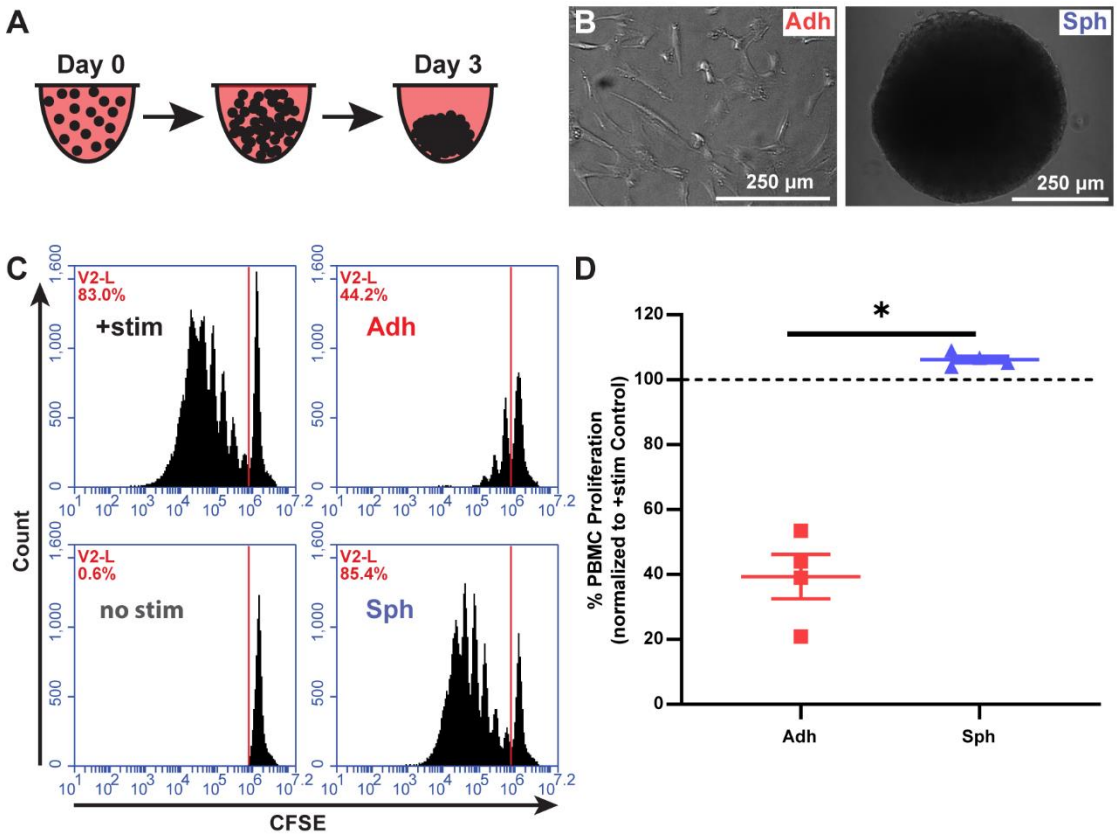

Figure 23. MSC spheroids do not suppress activated PBMCs.

(A) Schematic of spheroid formation. 20,000 MSCs in hanging droplets form spheroid structures within 3 days of culture. (B) Schematic of MSCs in immunomodulatory potency assays. (C) Representative flow cytometry plots of CSFE stained PBMCs with adherent (Adh) or spheroid (Sph) MSCs. (D) Quantification of % proliferated PBMCs for N=4 independent MSC donors (3 bone marrow and 1 umbilical cord MSC donors). Groups in D were analyzed with t-test with Welch's correction for unequal standard deviations. All data is represented as mean ± SEM. *$p<0.05$.

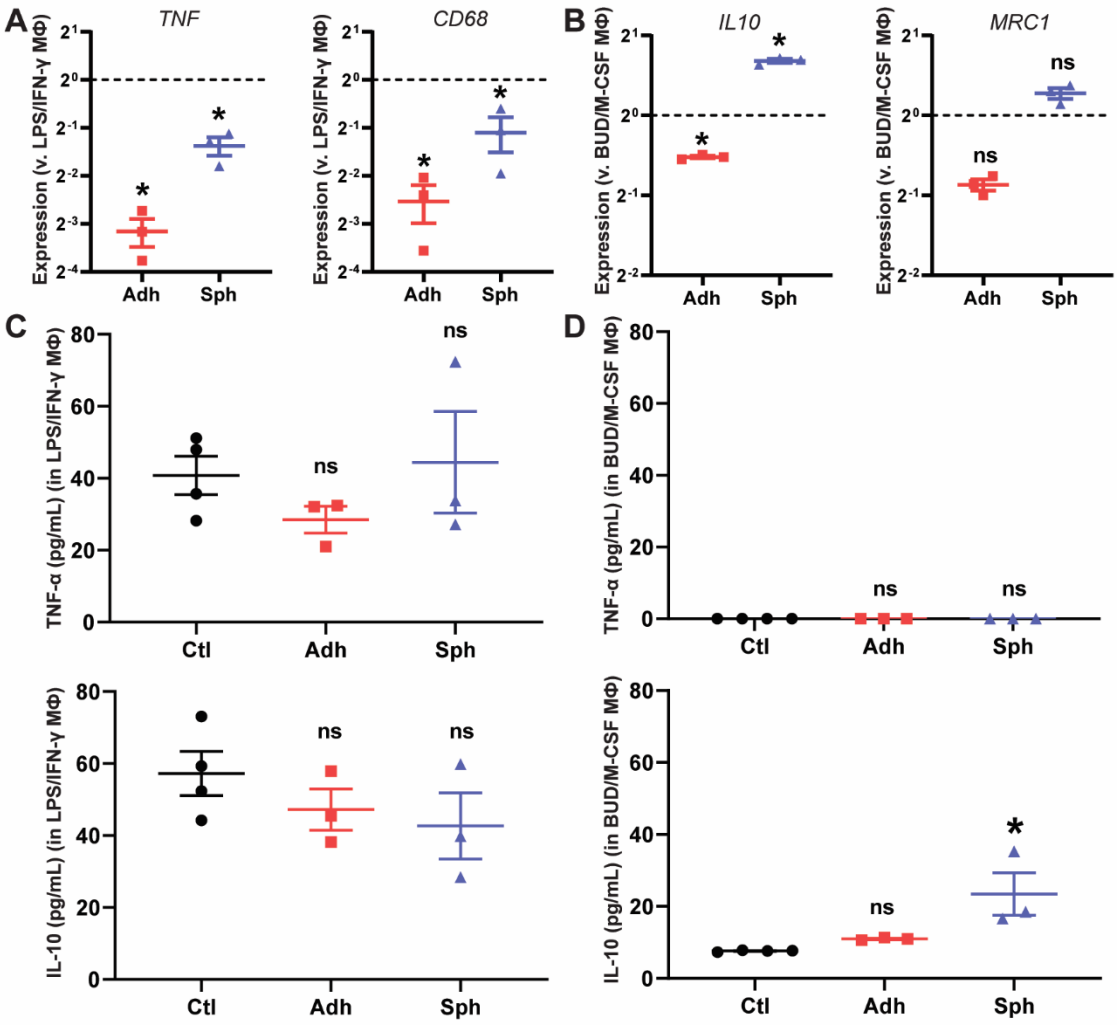

Figure 24. Spheroid MSCs alter macrophage phenotype.

(A) Gene expression of primary human macrophages differentiated with LPS/IFN-γ (M1 like) normalized to the no cell control (indicated by the dashed line). Data represents N=3 independent experiments using MSC0082 with the same macrophage donor. (B) Gene expression of primary human macrophages differentiated with M-CSF/BUD (M2c like) normalized to the no cell control (indicated by the dashed line). Data represents N=3 independent experiments using MSC0082 with the same macrophage donor. (C) TNF-α and IL-10 bead ELISA data from the co-culture conditioned media in (A). N=3 independent media samples from each MSC preparation in (C). (D) IL-10 bead ELISA data from the co-culture conditioned media in (B). N=3 independent media samples from each MSC preparation in (D). Data was analyzed with One-Way ANOVA with Sidak correction for multiple comparisons.

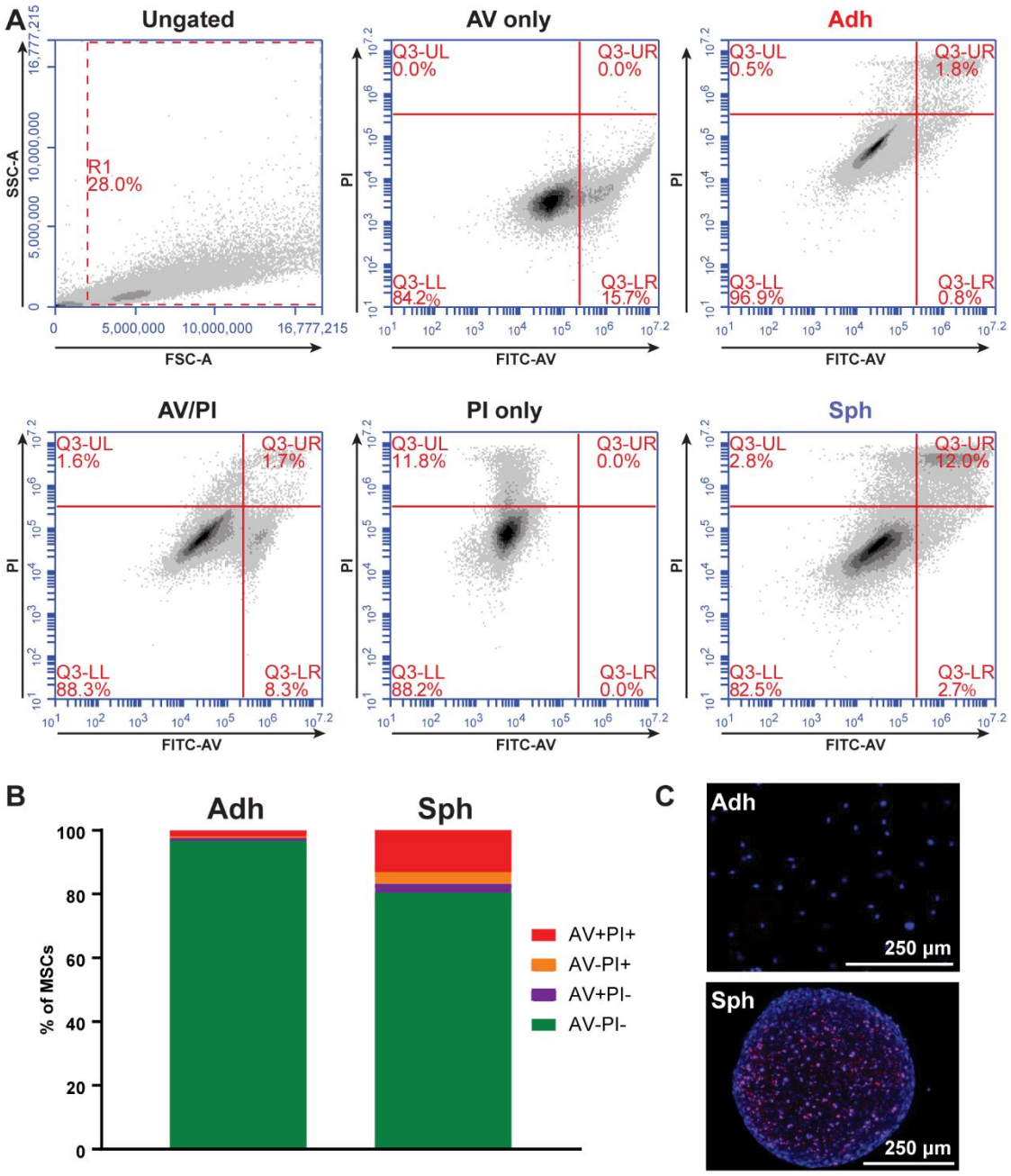

Figure 25. Spheroid MSCs show decreased viability compared to adherent MSCs.

(A) Representative flow cytometry plots for annexin/PI stained adherent and spheroid MSCs. AV only, PI only, and AV/PI controls were run using staurosporine treated adherent cells. (B) Quantification of annexin (AV) and PI staining from flow cytometry analysis in (A). (C) Representative images of adherent or spheroid MSCs stained with PI and Hoechst.

we cultured PBMCs with escalating doses of spheroid MSCs from our original dose of 1:4 (MSCs to PBMCs) to a dose 8X higher of 2:1. Regardless of dose, spheroid MSCs completely failed to suppress PBMC proliferation (Figure 26A).

An alternative explanation was that spheroid MSCs were being eliminated by contact with cytotoxic T cells. Aggregation can cause stress, and stressed cells can upregulate Fas and notch which signal to immune cells to clear them. Therefore, we sought to determine if contact factors, of any kind, were responsible for spheroid MSCs complete loss of potency. We used a transwell to allow for exchange of secreted factors between PBMCs and spheroid MSCs but prevent direct contact. Despite the separation of cells, spheroid MSCs still failed to suppress PBMC proliferation while adherent MSCs remained suppressive (Figure 26B).

Spheroid MSCs produce immunomodulatory factors

Finding that the loss of potency could not be attributed to a reduction in the number of cells or cell contact mediated factors, we next wanted to determine if spheroid MSCs were actually promoting, rather than inhibiting, PBMC proliferation. To test this, we cultured CD3/CD28 Dynabead activated PBMCs with either adherent MSCs alone or a combination of adherent and spheroid MSCs (1:5 ratio of Adh to Sph MSCs). As expected, adherent cells alone were suppressive, but when spheroids were added to adherent co-cultures, PBMC proliferation significantly increased (Figure 27A-B). Thus, spheroid MSCs appear to actively support PBMC proliferation, even when adherent MSCs are present.

As it appeared that PBMC supportive factors were overpowering the immunosuppressive factors produced by adherent MSCs, we next wanted to determine if spheroid MSCs produced the immunosuppressive factors commonly associated with MSCs. Adherent and spheroid MSCs were analyzed for gene expression and production of known immunomodulatory mediators (Figure 27C). We measured mRNA levels of *TGFB1* encoding for TGF-β, *IDO1* encoding for indolamine 2,3-deoxgenase, and *PTGS2* encoding for COX-2 which is a critical enzyme in the prostaglandin synthesis pathway (Figure 27C). Since IDO is an inducible protein, we treated MSCs with or without rhIFN-γ to turn on IDO transcription. We found that *TGFB1* and *PTGS2* transcripts were increased 2 and 500-fold respectively in spheroids compared to their adherent counterparts. With rhIFN-γ stimulation, *IDO1* was expressed at a similar level in both adherent and spheroid MSCs. However, while *IDO1* was not detectable in adherent MSCs without

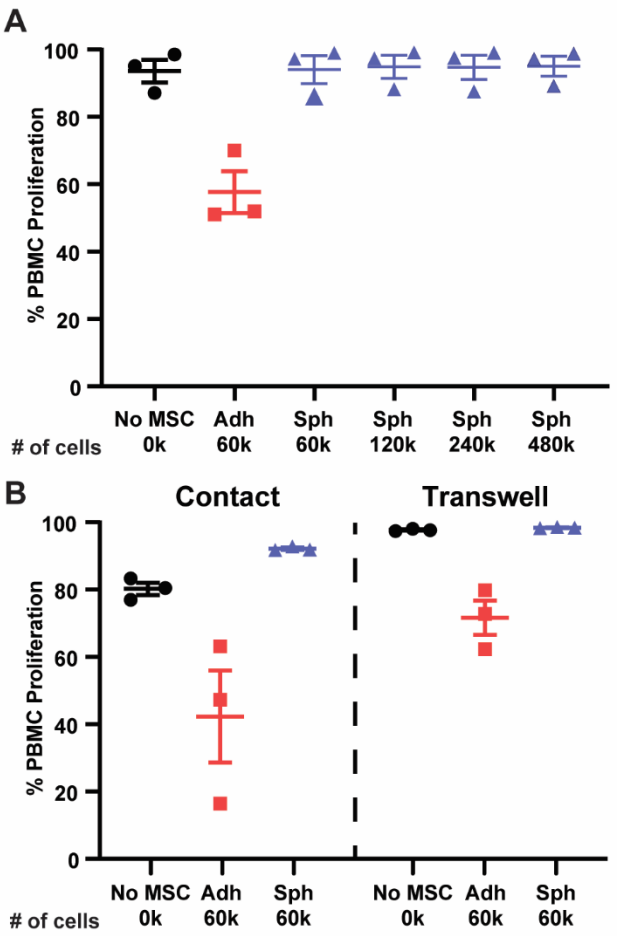

Figure 26. Spheroid dose and contact factors do not explain lack of PBMC suppression. (A) % proliferation of activated PBMCs with escalating doses of MSC spheroid. N=3 independent experiments with 3 different outgrowths of the same MSC donor (UC4373) with thawed aliquots of PBMCs from two different PBMC donors (one aliquot of one PBMC donor and two aliquots of the other). Statistical analysis done with Pearson correlation analysis of spheroid dose vs proliferation ($r=0.8$ and $p=0.10$). (B) PBMC proliferation in response to co-culture with adherent or spheroid MSCs at a 1:4 MSC to PBMC ratio with MSCs and PBMCs in direct contact or separated with a transwell. Experiment was performed in N=3 experiments using outgrowths of the same MSC donor (UC4373) paired with thawed aliquots of the same PBMC donor. Statistics were performed on (B) using a One-Way ANOVA with Tukey correction for multiple comparisons. All data is represented as mean ± SEM with *$p<0.05$.

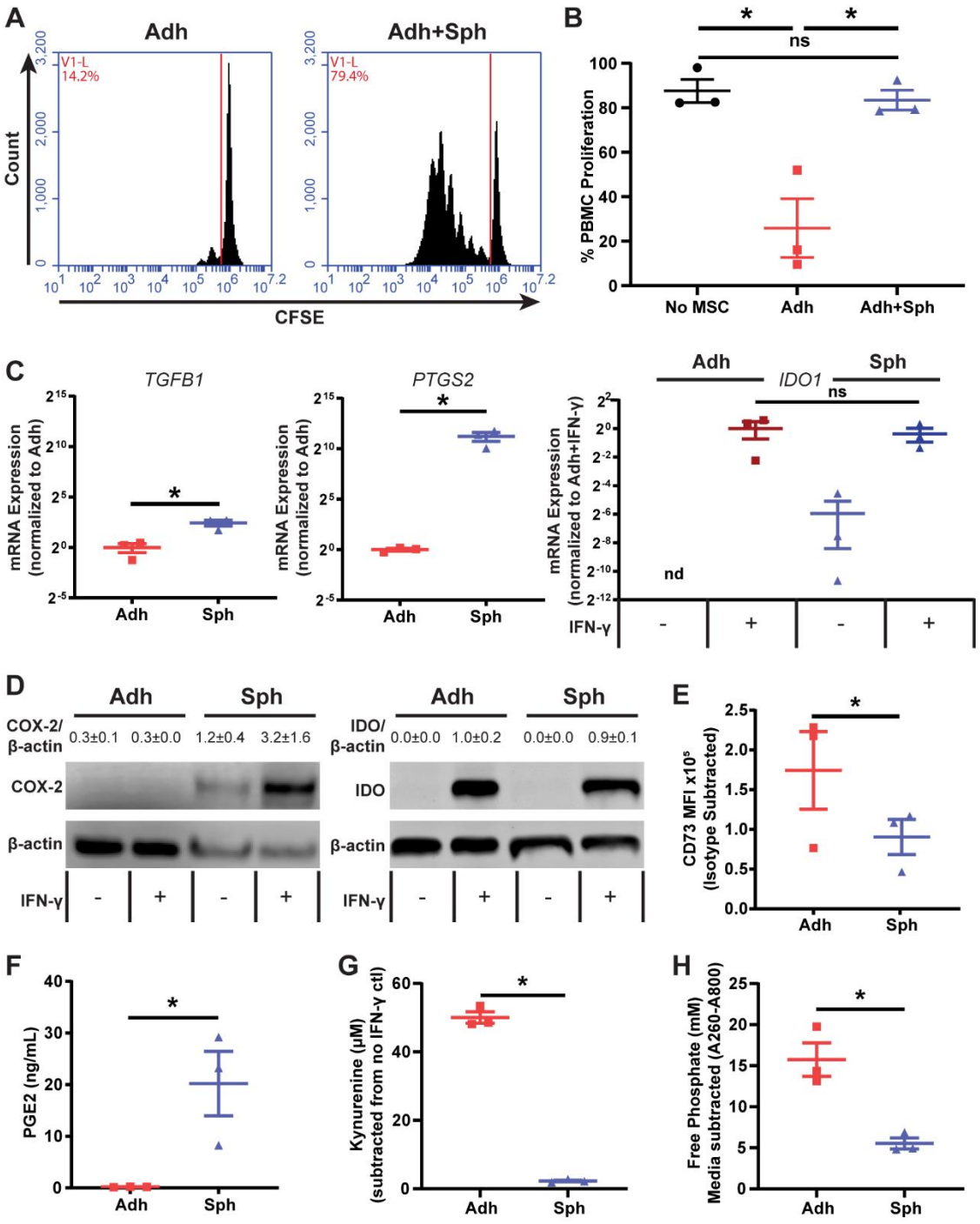

Figure 27. Spheroid MSCs display an altered immunomodulatory profile.

Representative flow cytometry plots of activated PBMC co-cultures with adherent MSCs or adherent MSCs with spheroids added in at a 1:5 adherent to spheroid ratio (A) with quantification of % proliferation in (B). Data in (B) was from N=3 independent experiments using outgrowths of the same MSC donor (UC4373) paired with thawed aliquots of the 2 PBMC

Figure 27 – Continued

donors. Data was analyzed using a One-Way ANOVA with Tukey correction for multiple comparisons. (C) RT-PCR gene expression data for *TGFB1*, *PTGS2*, and *IDO1* in adherent and spheroid MSCs alone. MSCs used for *IDO1* RNA were stimulated with 100 ng/mL IFN-γ for 3 days prior to analysis. N=3 independent experiments were performed with outgrowths of the same MSC donor (MSC00082). RNA data for *TGFB1* and *PTGS2* was analyzed with a T-test with Welch's correction for unequal standard deviations. (D) Protein quantification by western blot of COX-2 and IDO for adherent and spheroid MSCs with and without IFN-γ treatment. Reported protein ratios were averaged across N=3 independent experiments with outgrowths of the same MSC donor (MSC00082). (E) Flow cytometry analysis of CD73 expression on adherent and spheroid MSCs. N=3 independent experiments using outgrowths of the same MSC donor (MSC00082). Statistics were performed using a t-test with Welch's correction for unequal standard deviations. PGE synthase, IDO, and CD73 enzyme products PGE2 (F), kynurenine (G), and free phosphate (H), respectively, measured for spheroid and adherent MSCs. N=3 independent experiments using outgrowths of the same MSC donor (MSC00082 for F-G or UC4373 for H). Statistical analysis in (F-H) were performed using a t-test with Welch's correction for unequal standard deviations. All data is represented as mean ± SEM with *$p<0.05$.

rhIFN-γ stimulation, spheroid MSCs showed small but detectable *IDO1* expression even without rhIFN-γ stimulation.

With both *PTGS2* and *IDO1* showing differences at the RNA level, we next measured the abundance of the enzymes they encode, COX-2 and IDO, respectively (Figure 27D). COX-2 protein was much greater in spheroid compared to adherent MSCs, while IDO expression for both rhIFN-γ stimulated conditions were at similar levels, consistent with mRNA measurements. However, in both groups without rhIFN-γ, there was no IDO protein detected. Additionally, we examined CD73 (ecto-5′-nucleotidase), a surface marker for hMSCs that also has immunomodulatory function through the conversion of AMP to adenosine and free phosphate. Since CD73 is expressed by all MSCs (Figure 22), we looked at changes in surface protein levels of the enzyme after aggregation. Unlike IDO and COX-2, surface expression of CD73 was significantly lower in spheroid compared to adherent MSCs (Figure 27E).

We next measured the activity of the three immunomodulatory enzymes, COX-2, IDO, and CD73 in spheroid MSCs. PGE2, the product of COX-2 and prostaglandin E synthase, was found to be produced by spheroid MSCs at levels ~100-fold higher than adherent MSCs (Figure 27F). In contrast to PGE2, the levels of enzymatic products of IDO and CD73, kynurenine and free phosphate, were dramatically reduced in spheroid MSC cultures (Figure 27G-H). While expected for CD73, since surface expression was reduced in spheroids, these results showed an unexpected disconnect between levels of IDO protein and the activity of the enzyme. Thus, spheroid MSCs loss of PBMC suppressive potency is associated with a dramatic increase in the production of PGE2 and a significant reduction of activity in both IDO and CD73, revealing a distinct immunomodulatory phenotype of spheroid MSCs.

Spheroid MSC suppression of PBMCs can be partly restored in the presence of budesonide

While loss of PBMC suppression is concerning, MSCs are often not administered alone but in combination with standard of care therapies. For inflammatory conditions like GvHD, Crohn's disease, and ulcerative colitis, locally administered glucocorticoid steroids are preferred to treat lesions[36]. Budesonide is a commonly used glucocorticoid steroid for local applications due to its poor systemic absorption and high first-pass metabolism[36]. Thus, we wanted to determine if MSC spheroids would suppress PBMCs in the presence of budesonide (Figure 28A). We found that spheroids or budesonide (10 μM) alone were not capable of suppressing

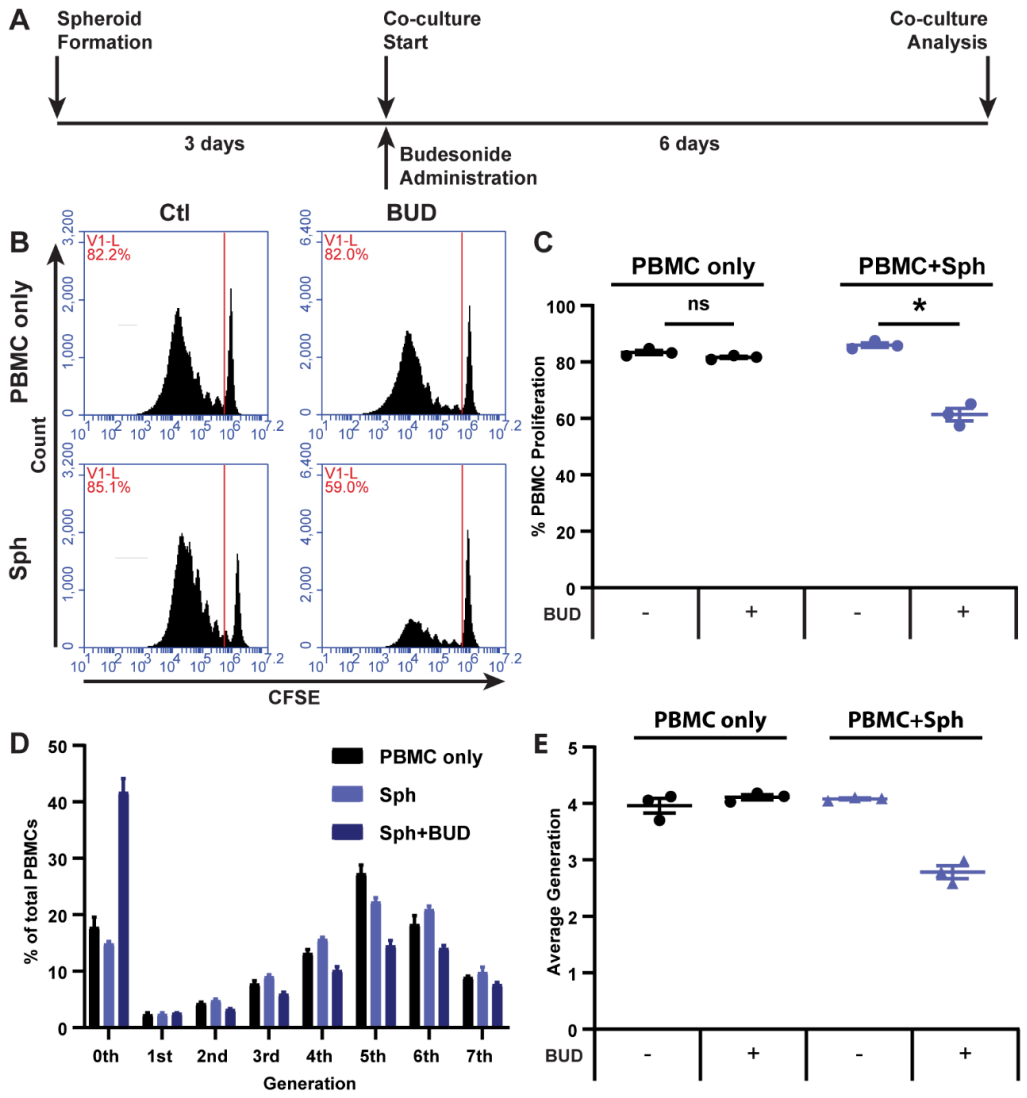

Figure 28. Budesonide synergizes with spheroids to suppress PBMC proliferation. (A) Timeline schematic for spheroid co-culture with budesonide administration. Representative flow cytometry plots (B) for spheroid-PBMC co-culture with and without 10 μM budesonide treatment with quantification of % PBMC proliferation (C). N=3 independent MSC preparations (outgrowths of UC4078) with thawed aliquots of the same PBMC donor. Statistics were performed in (C) with a Two-Way ANOVA with Sidak correction for multiple comparisons between control and budesonide groups. (D) PBMC generational analysis using FlowJo v10 proliferation software from flow cytometry data collected in (C). % of total PBMCs is displayed for each generation (8 peak model). (E) Average generation of PBMCs was calculated from (D) as described in the Supplemental Materials and Methods. All data is represented as mean ± SEM with *$p<0.05$.

CD3/CD28 stimulated PBMCs, but the combination of spheroids with budesonide worked synergistically to increase suppression of PBMC proliferation (Figure 28B-C). Additionally, we examined whether this synergy affected secretion of effector cytokines, specifically IFN-γ, IL-10, and granzyme B. We saw no significant difference between IFN-γ and granzyme B produced from PBMCs alone and PBMCs with spheroids, but there was a significant decline for IL-10 (Figure 29). Budesonide alone had a significant suppressive effect on PBMC production of both IFN-γ and granzyme B (Figure 29A,C), but had no significant effect on IL-10 secretion (Figure 29B). While there was a suppressive effect of budesonide alone, budesonide with spheroid MSCs led to an even greater reduction in IFN-γ and granzyme B levels (Figure 29A,C). Interestingly, in the presence of spheroid MSCs, IL-10 levels in the co-culture also decreased (Figure 29B). Thus, budesonide synergy with MSC spheroids affects both PBMC proliferation as well as the resultant cytokine environment.

While suppression was enhanced with the combination of budesonide with spheroid MSCs, qualitatively the suppressive profile of spheroid MSCs with budesonide was different from that of adherent MSCs. From analysis of the CFSE generation peaks, we found the proportion of proliferated cells within each generation was similar between the spheroid MSC:PBMC co-cultures with and without budesonide (Figure 28D). However, the proportion of non-proliferative to proliferative cells, regardless of generation, was shifted to the non-proliferative gate when budesonide was added with spheroid MSCs yielding an overall lower average generation (Figure 28D-E). This suppression profile was surprising, as adherent MSCs typically halt proliferation after 0-2 doubling events (Figure 23C). Thus, unlike adherent MSCs, spheroid MSCs in combination with budesonide display a distinct pattern of suppression. As this suppression profile was distinct from adherent MSCs, we hypothesized that it was not driven by kynurenine. To test this hypothesis, we treated spheroid MSCs with and without budesonide in the presence of the inflammatory cytokine IFN-γ to determine if budesonide increased spheroid MSC production of kynurenine. We found that budesonide had no effect on spheroid MSC production of kynurenine (Figure 30), suggesting there is likely another suppressive factor dominating the synergistic effect seen with spheroid MSCs and budesonide in co-culture.

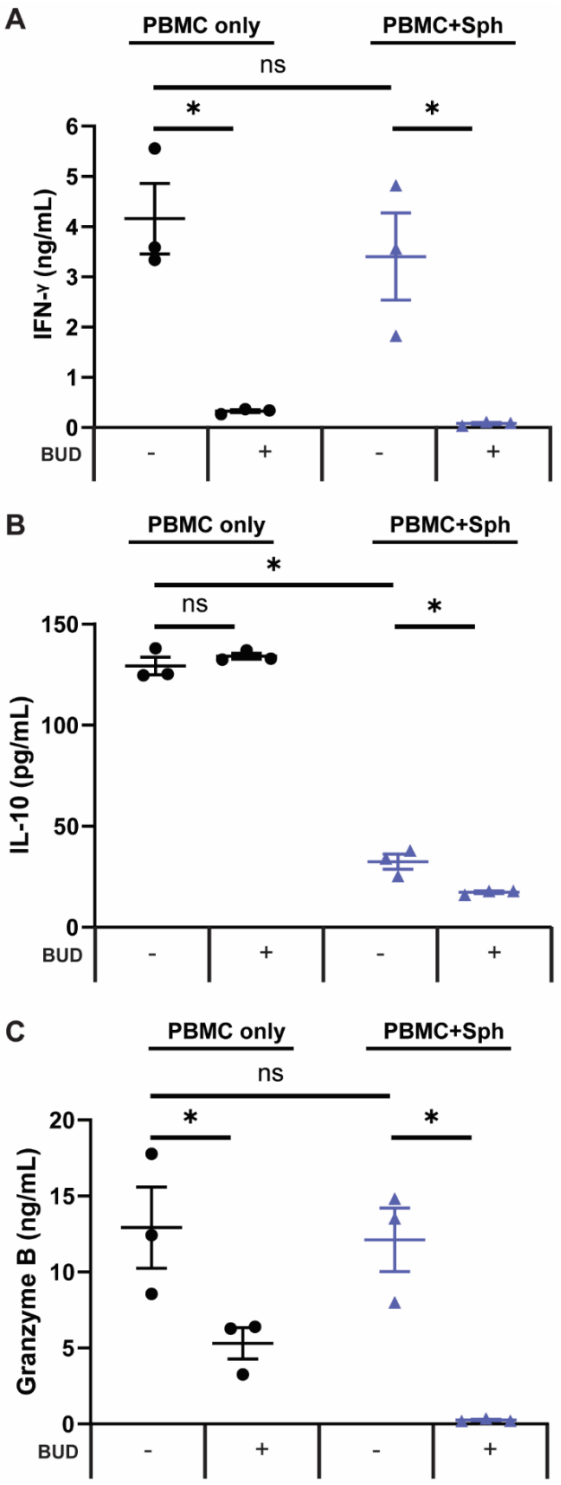

Figure 29. Spheroid MSCs with budesonide affect PBMC production of cytokines.

Media collected from Figure 28C co-culture (N=3 outgrowths of 4078) was assayed for IFN-γ (A), IL-10 (B), and granzyme B (C). Statistics were performed using a Two-Way ANOVA with Tukey correction for multiple comparisons. *$p<0.05$

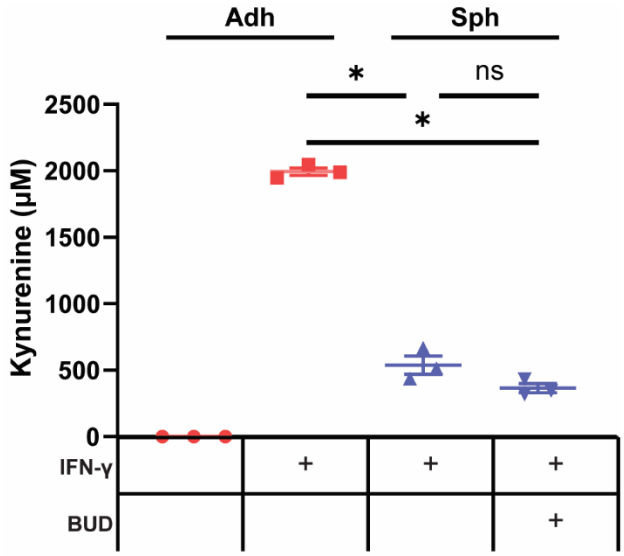

Figure 30. Budesonide treatment of spheroid MSCs does not restore kynurenine production. 20,000-cell spheroid MSCs were treated with 250 μM tryptophan and 100 ng/mL IFN-γ with or without 10 μM budesonide for 72 hours. Media was collected and analyzed for kynurenine. N=3 outgrowths of UC4373 were used. Adherent MSCs with or without 100 ng/mL IFN-γ served as positive and negative controls. Statistics were performed using a One-Way ANOVA with Tukey correction for multiple comparisons. *$p<0.05$

Spheroid produced PGE2 is not sufficient to suppress PBMC proliferation

Because PGE2 was the most highly up-regulated factor we observed (Figure 27), we wanted to determine if PGE2 alone could induce suppression of PBMC proliferation. Therefore, we measured PGE2 in MSC-PBMC co-culture and found that PGE2 was elevated in co-cultures containing spheroids reaching a peak of 85 nM (Figure 31A). As expected, PGE2 levels were higher without budesonide, but PGE2 from both spheroid MSC groups were far higher than the levels measured in the stimulated PBMC controls (Figure 31A). To determine the IC50 of PGE2 required to suppress PBMCs by itself, we treated activated PBMCs with escalating doses of synthetic PGE2 and measured proliferation of the cells. PGE2 alone did have a suppressive effect on PBMCs, however, suppression only occurred at high doses with IC50 values falling between 10-25 μM for 3 different PBMC donors, over 100X higher than the peak PGE2 concentration measured in our co-cultures with MSCs (Figure 31B). As the levels of PGE2 produced from MSC spheroids was far too low to account for PBMC suppression by itself, we theorized spheroid produced PGE2 might be synergizing with budesonide to yield a suppressive effect.

Spheroid MSCs secrete PGE2 that synergizes with budesonide to suppress activated T cells

We wanted to determine if there was synergy between PGE2 from spheroid MSCs and budesonide in our PBMC potency assay and if this synergy could be broken by blocking PGE2 signaling. To test this, we treated PBMCs with MSC spheroids and budesonide and added in selective antagonists for PGE2 receptors EP2 and EP4 (TG4-155 and L-161,432), which have been implicated as critical for PGE2 suppression of PBMCs[37]. As before, spheroids and budesonide synergized to suppress PBMCs (Figure 32A). However, when the EP2/4 inhibitors were added, this suppressive effect was lost. As none of the inhibitors or budesonide combinations impacted PBMC proliferation (Figure 33A), these results suggest that synergy between spheroid MSCs and budesonide is due at least in part to signaling by PGE2 mediated through EP2/EP4 receptors.

We next wanted to determine if the synergy observed between spheroid MSCs and budesonide could act directly on T cells or if the suppressive effect was dependent on non-T cell bystanders within the PBMC population. We used a negative selection kit to remove non-T cell populations from PBMCs and co-cultured spheroid MSCs with the remaining T cells. Addition

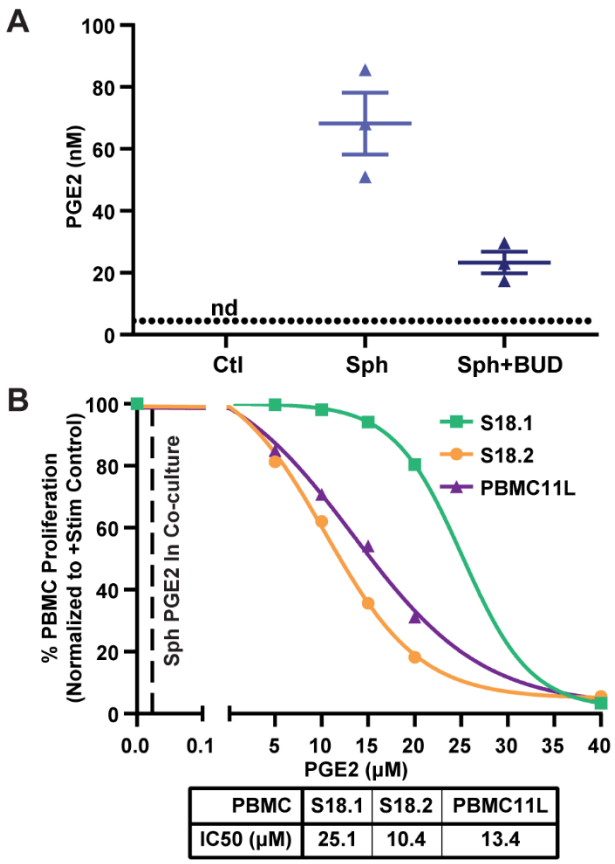

PBMC	S18.1	S18.2	PBMC11L
IC50 (μM)	25.1	10.4	13.4

Figure 31. Spheroid produced PGE2 levels alone are not sufficient to suppress PBMCs. (A) PGE2 measured by competitive ELISA in co-cultures with spheroid MSCs with and without 10 μM budesonide. Media samples were analyzed from Figure 28. Dotted line represents the assay detection limit. All PBMCs alone media samples fell beneath the detection limit. (B) Synthetic PGE2 was added at escalating doses from 0-40 μM with activated PBMCs and proliferation was measured along with IC50 values. Technical replicates for each PBMC donor were averaged and the mean is displayed. Each curve represents one of 3 different PBMC donors used for this experiment. IC50 values were calculated from a 4-parameter log(inhibitor) vs response model in GraphPad Prism 8 for each PBMC donor independently. Dashed line represents average PGE2 concentration from spheroid with budesonide group in (A). Data in (A) is represented as mean ± SEM.

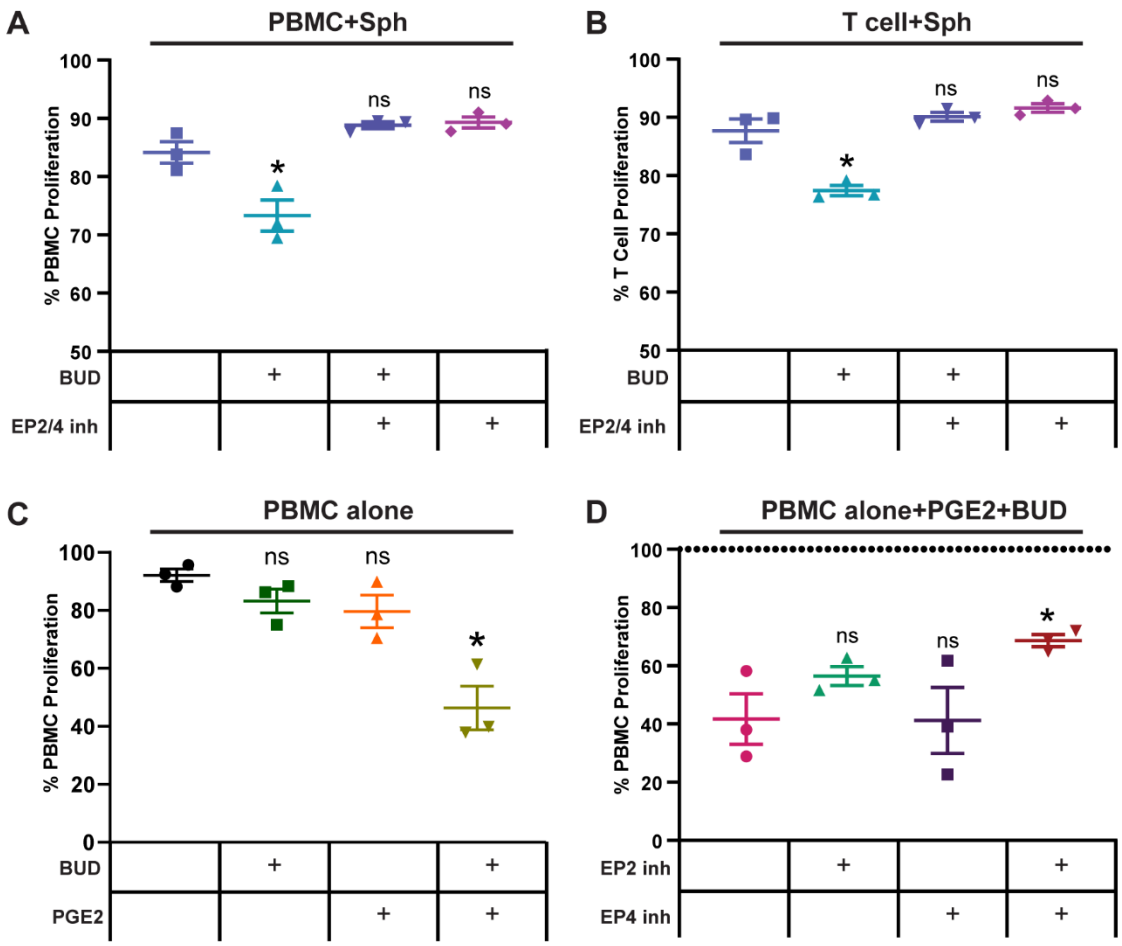

Figure 32. Spheroid PGE2 synergizes with budesonide via EP2/4 receptors on T cells. (A) PBMC proliferation response to spheroids with or without 10 μM budesonide or EP2/4 inhibitors TG4-155/L161,982 (10 μM). Data from N=3 independent experiments using outgrowths from MSC donor: UC4373 with thawed aliquots of one PBMC donor. Statistical analysis was done using One-Way ANOVA with Sidak correction for multiple comparisons to the untreated PBMC with spheroid group. (B) Drug treatments as in (A), but N=3 independent experiments using outgrowths of MSC donor UC4373 in co-culture with T cells isolated from the single PBMC donor in (A). Pooled data was from N=3 independent experiments using outgrowths of MSC donor: UC4373 with thawed aliquots of the same PBMC donor. Statistical analysis was done using One-Way ANOVA with Sidak correction for multiple comparisons to the untreated T cell with spheroid group. (C) PBMC culture with 1 μM synthetic PGE2 and 10 μM budesonide. PBMC proliferation from N=3 different PBMC donors. Statistical analysis was done using One-Way ANOVA with Sidak correction for multiple comparisons to the untreated PBMC alone group. (D) PBMCs treated with budesonide and synthetic PGE2 as in (C) with or

Figure 32 – Continued

without EP2 and EP4 inhibitors TG4-155 and L-161,982 at 10 μM. N=3 independent PBMC donors. Statistical analysis was done using One-Way ANOVA with Sidak correction for multiple comparisons to the control group. All data is represented as mean ± SEM with *p<0.05.

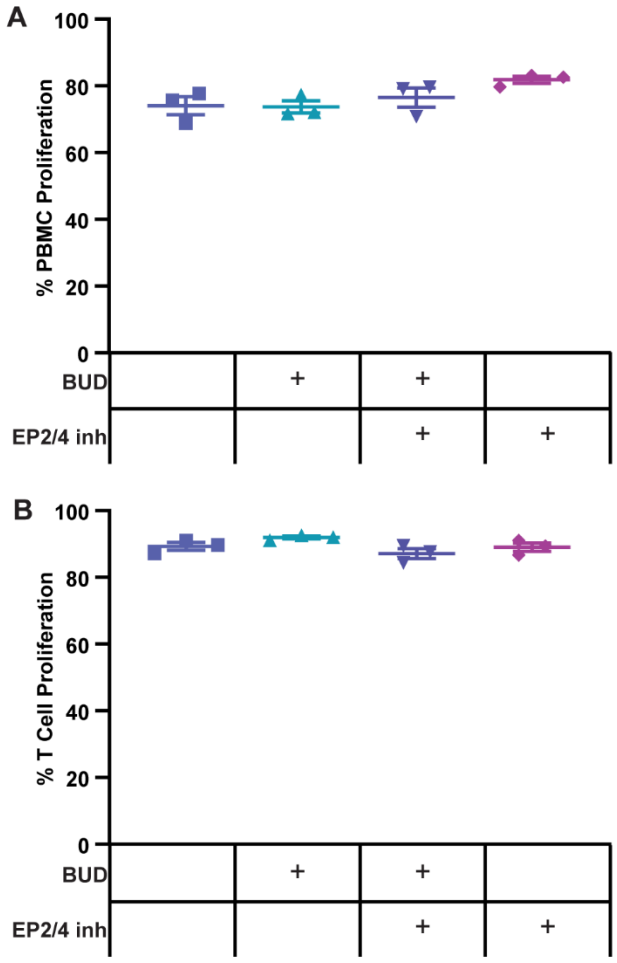

Figure 33. Budesonide and EP inhibitors do not affect PBMC proliferation alone.
(A) Flow cytometry proliferation analysis of PBMC alone with 10 μM budesonide and/or 10 μM TG4-155/L-161,982 targeting EP2/4. (B) Flow cytometry analysis of isolated T cell proliferation with drugs as in (A). Statistical analysis was performed using a One-Way ANOVA with Sidak correction for comparison to the no drug control. *$p<0.05$

of spheroids and budesonide to CD3/CD28 Dynabead activated T cells resulted again in a suppressive effect, which was blocked by addition of EP2/4 inhibitors (Figure 32B). As with PBMCs, drug combinations alone did not have any significant impact on T cell proliferation (Figure 33B). This data suggests, budesonide and spheroid MSC-produced PGE2 can act directly on T cells without requiring a non-T cell bystander to mediate the suppressive effect.

Budesonide works synergistically with PGE2 to suppress PBMC proliferation

Finally, while the secretome from MSCs is complex and contains components critical for non-immunomodulatory functions, we wanted to determine if the synergy observed between spheroid MSCs and budesonide could be replicated using synthetic PGE2 without MSCs. We treated PBMCs with a low dose of PGE2, that had previously been shown insufficient to suppress PBMCs, with or without budesonide. As hypothesized, while neither PGE2 or budesonide alone suppressed PBMC proliferation, their combination led to a large and significant reduction in proliferation (Figure 32C). As with co-cultures with MSC spheroids, addition of EP2/EP4 inhibitors to PBMCs treated with synthetic PGE2 and budesonide resulted in loss of suppression and increased PBMC proliferation (Figure 32D). Blockade of EP2 alone only partially blocked the suppressive effect, while inclusion of both inhibitors together led to a more substantial decrease in the suppression of PBMC proliferation.

Discussion

MSC immunomodulatory phenotype has been studied for years using 2D adherent culture on tissue culture plastic, however, MSCs administered *in vivo* experience a very different environment than seen when cultured in 2D. Specifically, local delivery of MSCs results in aggregation *in vivo*[14,17] that alters the repertoire of trophic factors the cells produce[18,19,38]. This begs the question, are spheroid MSCs more immunomodulatory potent than their adherent counterparts, or do they simply have a different, not necessarily superior, immunomodulatory profile?

Suppression of PBMCs, T cells, or MLRs have long been used as *in vitro* assays to assess the potency of human MSCs[3,27,28,39]. In this study, we examined adherent and spheroid MSC potency in a series of *in vitro* assays using exclusively primary human cells. We expected spheroid MSCs to suppress activated PBMCs in a dose dependent manner but were surprised to

find spheroid MSCs displayed no suppressive potency at all, as measured by PBMC proliferation, IFN-γ, and granzyme B assays. This complete and rapid loss of potency was unexpected, and initially thought to be an artifact of our potency assays or choice of donors. However, the same loss in potency upon spheroid formation was seen with 4 independent human MSC donors, regardless of their tissue of origin. Furthermore, potency could not be restored even after increasing the dose of spheroid MSCs 8X. This finding would seem to be in contrast to work done by Zimmermann *et al.* which showed that untreated spheroid MSCs suppressed activated PBMCs at 3:1 MSC:PBMC ratio[40]. However, the size of the spheroids studied are critically different. While we used 20,000 MSCs in our aggregates, Zimmermann *et al.* used spheroids containing only 500 cells and aggregate size has been shown to substantially affect spheroid secretome[19,40]. While such small sizes are controllable in the lab, we chose larger aggregates to more closely approximate spontaneous aggregation that would occur *in vivo*[14].

Follow up analysis of the expression and production of immunomodulatory factors showed an overall shift in the immunomodulatory phenotype between adherent and spheroid MSCs. While MSCs are known for their anti-inflammatory properties, some of these immunomodulatory factors are not highly upregulated until MSCs are exposed to inflammatory factors, including IFN-γ which has been shown to upregulate IDO and COX-2 protein expression. We used IFN-γ to induce expression of both IDO and COX-2 in order to characterize differences between adherent and spheroid MSC responses to a controlled inflammatory stimulus. Expression of *TGFB1*, protein levels of CD73, and activity of both IDO and CD73 were different between adherent and spheroid MSCs. The most striking observed change in spheroids, however, was the increase in *PTGS2* expression, COX-2 protein, and PGE2 secretion in spheroid MSCs compared to their adherent counterparts.

Not only were spheroids not able to suppress T cell proliferation, but they actually supported proliferation, likely due to a shift in balance between production of anti- versus pro-inflammatory factors. While best known for their anti-inflammatory properties, MSC constitutively express an array of classically pro-inflammatory cytokines and chemokines[41]. In addition, specific environmental factors, such as LPS[42], TNF-α[41,43], and palmitate[27,44], have been shown to polarize MSCs toward a pro-inflammatory state. In spheroids, Bartosh *et al.* have shown MSCs also produce pro-inflammatory cytokines, such as IL-1α/β[14], which can promote T cell expansion[45]. While not addressed in this study, more research is needed to understand how

combinations of different stimuli control the balance of anti-inflammatory and pro-inflammatory products produced by MSCs.

Other stimuli that affect MSC interactions with immune cells are the standard of care immunosuppressants patients receive prior to MSC therapy. Glucocorticoid steroids are commonly used on patients with inflammatory diseases and can impact both the recipient's immune cells as well as the transplanted MSCs. Studies of steroids effects on MSCs have been limited but suggest this interaction requires more extensive investigation and understanding. For example, Chen *et al.* showed that mouse MSCs treated with dexamethasone decreased their suppression of anti-CD3 activated splenocytes[46]. When they then examined human MSCs, they found dexamethasone reduced MSC expression of inflammation-inducible immunomodulatory proteins. However, there is evidence that steroid treatment may have a beneficial effect on MSC function as well. Dexamethasone treated MSCs suppress IFN-γ, perforin, and CD69 expression in NK cell populations[47]. In addition, we have previously shown that loading MSCs with intracellular microparticles containing budesonide enhances their suppression of peripheral blood mononuclear cells (PBMCs)[2]. In this study, we used budesonide, a commonly used steroid for local administration, to understand glucocorticoid's impact on spheroid MSC:PBMC interactions. To our surprise, while neither spheroid MSCs nor budesonide suppressed T cell proliferation alone, together they synergized to suppress T cell proliferation. While many spheroid MSC-based factors could synergize with steroids, we focused on understanding the role spheroid produced PGE2, the most highly upregulated factor in spheroid MSCs, played in the observed synergy. PGE2, while present in MSC spheroid:PBMC co-culture media, was at a concentration far too low to induce suppression by itself. We found intact PGE2 signaling was found to be critical for synergy with budesonide, as inhibition of EP2/4 receptors eliminated the synergy entirely. Furthermore, the synergy between PGE2 and budesonide appears to not rely on non-T cell populations, as their depletion left the synergy between spheroid PGE2 and budesonide intact. Thus, synergy appears to act directly on T cells and be reliant on intact EP2/4 signaling. We confirmed that kynurenine production from spheroid MSCs was not enhanced through budesonide treatment, further supporting our data showing that MSC suppression of PBMC proliferation had shifted from a kynurenine dominated mechanism to a PGE2-budesonide mechanism.

Interestingly, both PGE2 and glucocorticoids have known effects on TCR signaling. PGE2 signaling via EP2/4 increases cAMP levels which activate PKA, which in turn can phosphorylate LCK[505], which is critical in the initial formation of the TCR/CD3 signaling complex[48]. Thus, PGE2 signaling could be enhanced by glucocorticoids as they can bind to cytoplasmic glucocorticoid receptor (GR) and also activate PKA leading to inhibition of LCK[49]. This signaling then precipitates disassociation of the LCK/FYN complex reducing TCR signaling[49]. In addition to direct action on TCR signaling, both PGE2 and glucocorticoids can modulate T cell phenotype though transcriptional regulation. PGE2 has been shown to inhibit expression of inflammatory mediators such as IFN-γ and IL-17 via transcriptional regulation[3]. The glucocorticoid-GR acts as a transcription factor to modulate activation of inflammatory genes, often inhibiting NFκB signaling, which is critical for expression of cytokines upon T cell activation[50].

In our system, we have shown that PGE2 signaling through the EP2/4 receptors is critical for spheroid MSC-budesonide synergy in the suppression of human T cells. With signaling downstream of both PGE2 and budesonide impinging upon the PKA/LCK/TCR pathway, together they appear capable of a suppressive effect that neither can achieve alone. Furthermore, by replacing MSC spheroids with synthetic PGE2 we were able to replicate this synergistic effect, suggesting PGE2 from spheroids is indeed the predominant signaling molecule produced by MSCs that works synergistically with budesonide to suppress T cell proliferation.

While this study provides significant insight into spheroid MSC interaction with T cells, there are limitations which should be considered when interpreting the data. Firstly, all the PBMC suppression work has been performed using immune cells isolated from peripheral blood. However, upon local injection, MSCs would interact with both tissue resident as well as recruited T cells. Tissue resident T cells can have significant differences in response including gene expression, proliferation, and motility[51]. Additionally, our study solely looked at PBMC proliferation response. While proliferation has been shown to correlate with inflammatory cytokine secretion under certain circumstances, proliferation and effector functions including cytokine secretion, cytotoxic killing, and T cell polarization are not always correlated[2,44].

Conclusion

Aggregated human MSCs lose the ability to suppress activated T cells and show a stimulatory effect on T cell proliferation. While alone, spheroid MSCs do not suppress T cell proliferation, when placed in an environment with budesonide, a glucocorticoid steroid, they regain suppressive potency. Using a series of inhibitor and add-back studies, we found spheroid MSC-produced PGE2 acts on EP2/EP4 receptors on T cells in synergy with budesonide to suppress T cell proliferation. While synthetic PGE2 is sufficient to replicate the spheroid-budesonide suppression, this does not mean MSC spheroids are therapeutically unnecessary. The advantage of cell therapy over synthetic drugs has always been their ability to produce a host of factors in a coordinated fashion to resolve inflammation and promote tissue regeneration. In this study, we focused on spheroid MSCs immunomodulatory properties but did not assess their production of antimicrobial, growth, neuroprotective, or anti-apoptotic factors. Depending on the needs of a specific disease indication, spheroid MSCs may retain a sufficient repertoire of therapeutic mediators to justify their use and the choice of MSC therapy must always be made within the context of the disease process and required mechanisms of action[52]. For inflammatory conditions, suppression of T cells is a critical part of resolving inflammation and this study highlights the importance of understanding the effect of cell aggregation on MSCs' immunomodulatory phenotype and how that phenotype's efficacy depends on the presence of other environmental cues.

Acknowledgements

A.J.B. was supported through an NIH training grant (#1T32NS045549) and L.B. was supported in part by NIH training grant #5T32GM007337. Support from the Straub Foundation, Diabetes Action Research and Education Foundation, and the Fraternal Order of Eagles Diabetes Research Foundation awarded to J.A.A. were used to complete the project. Several of the chemical/media reagents used for this work were provided through a BD Immunology Grant and a Biological Industries USA Research Award to J.A.A.. Additional D.S. was supported by the American Heart Association Strategically Focused Research Network [grant numbers 15 SFRN 23730000, 18679000, 18679001, 18679002, 18679003]. The Women's Health Tissue Repository is supported by the Carver College of Medicine, the Department of Obstetrics & Gynecology,

and the National Center For Advancing Translational Sciences of the National Institutes of Health under Award Number UL1TR002537.

Disclosures

The authors indicate no potential conflicts of interest.

Supplemental Materials and Methods

MSC isolation from umbilical cords

MSCs were outgrown from umbilical cord pieces. Briefly, umbilical cords were obtained with patient consent from the University of Iowa Women's Health Tissue Repository. Briefly, 1 cm pieces were cut cross-sectionally from the umbilical cords, washed in PBS, and cut into smaller pieces. These pieces were placed into dry petri dishes and left to adhere prior to media addition. MEM-α (Invitrogen, Cat # 12561072) supplemented with 15% (v/v) fetal bovine serum (FBS, VWR, Cat # 059B18), 1% (v/v) L-glutamine (Cat # 25030081, Life Technologies), 1% (v/v) penicillin-streptomycin (Life Technologies, Cat # 15140122), and 2% (v/v) Amphotericin B (Sigma Cat # A2942) was added to cover the bottom of the dish and media was changed every 2-3 days for 9 days. Tissue pieces were removed, cells were washed with PBS, and then detached with Accutase (Innovative Cell Technologies, Cat # AT-104). Harvested cells were then plated, further expanded, and frozen down at 1 million cells/mL in CryoStor CS5 freezing media (Sigma, Cat # C2999) at 1°C/min in CoolCell LX freezing containers (Corning, Cat # BCS-405). After cells were cooled for at least 3 hours at -80°C, they were transferred to liquid nitrogen for long term storage. MSC identity was confirmed using tri-lineage differentiation and surface marker assessment as described below. For this study, three umbilical cord donors UC4477, UC4373, and UC4078 were used (Figure 22).

Umbilical cord cells were confirmed to meet the minimal MSC criteria for differentiation by differentiating cells into adipocytes, osteocytes, or chondrocytes, using adipogenic (Biological Industries, Cat # 05-330-1B), osteogenic (Biological Industries, Cat # 05-440-1B), or chondrogenic (R&D systems, Cat # SC006) differentiation medias. For adipogenic and osteogenic differentiation, cells were plated in 24-well plates at a cell density of 60,000 cells per well until 80% confluence. Media was exchanged for adipogenic or osteogenic media and the cells were allowed to culture for 14 days with media exchanged every 3 days. Adipogenic

lineage was confirmed by fluorescent microscopy after AdipoRed staining for lipid droplets. Osteogenic lineage was confirmed by brightfield imaging after Alizarin Red staining for mineral deposition. For chondrogenic differentiation, MSCs were transferred to a 15 mL conical tube at 250,000 cells per tube. The cells were washed and resuspended in chondrogenic differentiation media, then centrifuged. The pelleted cells were grown for 14 days and media was exchanged every 2-3 days. The pellet was fixed, cryosectioned, and stained with Safranin-O prior to brightfield imaging.

Umbilical cord cells were also confirmed to meet the minimal MSC criteria for surface markers as established by the ISCT by staining for the presence of CD73, CD90, and CD105 and the absence of CD11b, CD19, CD34, CD45, and HLA-DR. PE.Cy7-CD73 (BD Biosciences, Cat # 561258), PE-CD90 (BD Biosciences, Cat # A15794), and FITC-CD105 antibodies (BD Biosciences, Cat # 561443) with corresponding isotype controls (PE.Cy7 Mouse lgG1k (BD Biosciences, Cat # 557872), PE Mouse lgG1 (Invitrogen, Cat # GM4993), and FITC Mouse lgG1k (BD Biosciences, Cat # 556649)) were used to assess positive markers. PE hMSC Negative Cocktail (BD Biosciences, Cat # 562530) was used to assess the negative markers and included appropriate isotype controls. Cells were analyzed on a BD Accuri C6 flow cytometer.

PBMC and macrophage isolation from leukocyte reduction cones

Leukocyte reduction cones were obtained from the DeGowin Blood Center, University of Iowa Hospital and Clinics. Patient information was de-identified according to Institution Review Board regulations and the Usage Agreement. The sample was diluted to 50 mL with base RPMI 1640 (Life Technologies, Cat # 11835030). 16 mL of Ficoll (GE Healthcare, Cat # 17-5442-02) was added into 50 mL LeucoSep tubes (Greiner Bio, Cat # E140933Y) and centrifuged at 500g for 1 minute to partition the Ficoll beneath the filter. Half of diluted blood was then transferred into each LeucoSep tube and centrifuged for 30 minutes at 600g with acceleration of 5 and brake off. After spin, the buffy coat which contained peripheral blood mononuclear cells (PBMCs) was collected and washed twice with 10 mL of PBS containing 2% FBS. To remove the remaining red blood cells, the cell pellet was resuspended with 5 mL of RBC Lysis Buffer (Biolegend, Cat # 420301) diluted to 1x in water and incubated on ice for 5 minutes. The suspension was diluted to 30 mL with PBS containing 2% (v/v) FBS, centrifuged at 500g for 5 minutes, and resuspended

with 30 mL of complete RPMI containing 10% FBS, 1% L-glutamine, and 1% penicillin-streptomycin.

To cryopreserve the PBMCs, PBMCs were resuspended at 20 million cells/mL in complete RPMI. A 2X freezing solution was prepared made of 20% DMSO and 80% FBS. This freezing solution was then mixed 1:1 with the cells to obtain a 10 million cell/mL solution containing 10% DMSO and 45% FBS. Cells were then immediately aliquoted into 2mL cryo-tubes and placed in a CoolCell (Biocision, Cat # BCS-405). Cells were placed at -80C overnight and then transferred to liquid nitrogen for storage until use. PBMCs used for macrophage differentiation were immediately plated without freeze down.

To prepare macrophages for co-culture with MSCs, T-175 flasks were coated with 20 mL 2% (w/v) type A gelatin (Fisher Scientific, Cat # G8-500) for 2 hours. The gelatin was then aspirated leaving approximately 1 mL of gelatin solution adsorbed to the flask. Flasks were then allowed to dry at 37°C overnight. Immediately prior to starting the monocyte isolation, 15 mL of CELLstart (Invitrogen, Cat # A1014201) was added to each gelatin coated flask and incubated for 1 hour at 37°C. CELLstart was then removed and 15 mL of PBMC suspension obtained from the PBMC isolation was plated into each of the flasks, and the cell solution was incubated at 37°C for 1 hour to allow monocyte attachment to the flask. Non-adherent cells were then washed out of the flasks with PBS twice. The hM media was prepared with RPMI base supplemented with 10% human AB Serum (VWR, Cat # 45001-062), 10% FBS, 1% L-glutamine, and 1% penicillin-streptomycin. The monocytes were lifted with sterile filtered PBS containing 5 mM EDTA (Quality Biological, Cat # 351-027-721) and resuspended at 1 million cells/mL with hM media supplemented with 25 ng/mL of recombinant human M-CSF (PeproTech, Cat # 300-25) prior to plating.

Macrophage co-culture

1 million monocytes, isolated as described in the above, were resuspended in hM media containing RPMI 1640 (Life Technologies, Cat # 11835030) supplemented with 10% human AB Serum (VWR, Cat # 45001-062), 10% FBS, 1% L-glutamine, 1% penicillin-streptomycin, and 25 ng/mL of recombinant human M-CSF (PeproTech, Cat # 300-25) were added to 24-well plates. Cells were differentiated for 6 days, with a media change after 3 days. After differentiation, macrophages were polarized for 2 days in M1 media containing 50 ng/mL LPS

(Sigma, Cat # L6529) and 50 ng/mL IFN-γ (PeproTech, Cat # 300-02) or M2c media containing 10 ng/mL M-CSF and 100 nM of budesonide (Tocris, Cat # 2671), the polarizing media was replaced 2 days prior to the co-culture.

For MSC-macrophage co-cultures, either 100,000 adherent MSCs or five-20,000-cell spheroids were added to M1 or M2c macrophages isolated from PBMC monocytes. Co-cultures were incubated at 37°C for 2 days and then processed for mRNA content and protein secretion of TNF-α and IL-10 as found below and Table 2.

T cell enrichment

Fresh PBMCs isolated as described above were enriched for CD3+ T cells using a MojoSort Human CD3 T Cell Isolation Kit (Biolegend, Cat # 480021). 60 million PBMCs were washed and resuspended at $1x10^8$ cells/mL in sorting buffer containing 1X PBS with 0.5% (w/v) BSA and 2mM EDTA according to the manufacturer's protocol. 10 µL Biotin-Antibody cocktail and 10 µL streptavidin nanobeads were added per 10 million cells and incubated for 15 minutes on ice. After 8 minutes in a magnet, the supernatant containing unlabeled cells was collected, the remaining beads were resuspended in sorting buffer, and separated again using a magnet as before to increase T cell yield. The collected supernatant was combined, placed in a new tube, and placed in a magnet for an additional 5 minutes to remove any residual nanobeads. The resultant negatively selected T cells were then counted, stained with CFSE, and plated as described above for PBMCs.

Proliferation analysis

Percent proliferation normalized to the positive control was calculated by the formula: % proliferation sample / % proliferation positive control. For Peak fitting analysis of PBMC proliferation, FlowJo v10 was used. Exported FCS flow cytometry files were fit using the Proliferation Modeling module. An 8 peak model was used with fixed ratio, CV, and background parameters. According to the developer's instruction, parameters were optimized using the RMS of the model on the PBMC alone with and without Dynabead conditions. The software calculated cells per generation were exported, normalized to total PBMC count, and used to calculate the average generation. Average PBMC generation was calculated by the following equation $Ave\ Gen = \sum_{i=0}^{7}(i * \chi_i)$, where "i" is the generation multiplied by χ_i, the fraction of

total PBMCs in the "i-th" generation, summed over all PBMC generations (0^{th} to 7^{th} generations).

PCR for MSC and macrophage mRNA expression

In order to measure changes in inflammatory M1 markers and anti-inflammatory M2 markers, co-cultured macrophages were harvested with 0.4 mL of TRIzol (Thermo Fisher, Cat#15596018). To collect RNA from adherent MSCs, samples were lysed in 0.4mL of TRIzol and collected. Spheroid MSC samples due to difficultly in disrupting the MSC aggregates, were washed in PBS and then homogenized at 33,000 rpm for 5 seconds using a Tissue Master 125 homogenizer with microprobe attachment (VWR, Cat # TMP125-115). Briefly, to extract mRNA from all samples, each sample lysed in TRIzol was added to 80 µL of chloroform (Sigma Aldrich, Cat # C2432), followed by 12,000g centrifugation for 15 minutes at 4°C. The aqueous layer was collected and 200 µL isopropyl (Sigma Aldrich, Cat # 190764-1L) was added to precipitate the RNA. The mixture was centrifuged at 12,000g for 10 minutes at 4°C. The pellet was then washed with 0.4 mL of 75% (v/v) 200-proof ethanol (Fisher Scientific, Cat # BP2818-500) and centrifuged at 7,500g for 5 minutes. The RNA pellet was air dried for 10 minutes and resuspended with 20 µL DNase- and RNase-free UltraPure water (Life Technologies, Cat # 10977-01). RNA concentrations were determined using NanoDrop (NanoDrop 2000 Spectrophotometer, Thermo Scientific). The mRNA sample was converted into cDNA with a High-Capacity cDNA Reverse Transcription Kit with RNase Inhibitor (Thermo Fisher, Cat # 4374966) as described in the manufacturer protocol. Thermocycler (ProFlex PCR System, AppliedBiosystems) was set to heat the samples at 25°C for 10 minutes, 37°C for 2 hours, 85°C for 5 minutes, and cooled down to 4°C. A 10 µL solution of diluted cDNA (2 ng/mL), POWER SYBR Green Master Mix (Applied Biosystems, Cat# 4367659), primer, and ultrapure water at a ratio of (1:10:1:8) was plated in triplicate into a 348-well PCR plate (Applied Biosystems, Cat # 4309849). The data was analyzed using QuantStudio3 software (AppliedBiosystems) to obtain CT values. All gene expression was normalized to GAPDH expression. A list of primers and catalog numbers is given in Table 2.

Table 2. List of human primers.

Gene	IDT Cat #	Primer Sequences
TNF	Hs.PT.58.45380900	TCAGCTTGAGGGTTTGCTAC TGCACTTTGGAGTGATCGG
CD68	Hs.PT.58.2488447.g	CCATGTAGCTCAGGTAGACAAC CCACCTGCTTCTCTCATTCC
IL10	Hs.PT.58.2807216	TCACTCATGGCTTTGTAGATGC GCGCTGTCATCGATTTCTTC
MRC1	Hs.PT.58.15093573	TCCATCTTCCTTGTGTCAGC GGTTTTGGAGTAATATTCACTGTTCT
IDO1	Hs.PT.58.924731	ACGTCCATGTTCTCATAAGTCAG CCTTACTGCCAACTCTCCAA
TGFB1	Hs.PT.58.39813975	GTTCAGGTACCGCTTCTCG CCGACTACTACGCCAAGGA
PTGS2	Hs.PT.58.77266	GCCAATAGTCAGCATTGTAAGTTG GCACTACATACTTACCCACTTCA
GAPDH	Hs.PT.39a.22214836	TGTAGTTGAGGTCAATGAAGGG ACATCGCTCAGACACCATG

Bead ELISA for macrophage/PBMC IL-10/TNF-α/Granzyme B production

To measure cumulative inflammatory and anti-inflammatory factor production, culture media collected from co-cultures was analyzed by bead ELISA and compared to standards of Human TNF (BD Biosciences, Cat # 558273), IL-10 (BD Biosciences, Cat # 558274), and granzyme B (BD Biosciences, Cat # 560304). Capture Beads were mixed with Capture Bead Diluent from the Human Soluble Protein Master Buffer Kit at a ratio of 1:1:48. 50 uL media sample or standard was then added to 50 µL of diluted capture beads and incubated for 1 hour at room temperature. PE Detection Reagents were mixed with Detection Reagent Diluent at a ratio of 1:1:48. After incubation, 50 uL of PE detection mixture was added to each sample and incubated for 2 hours at room temperature, followed by adding 1 mL Wash Buffer. The sample was centrifuged for 5 minutes at 200g. After supernatant removal, each sample was resuspended in 150 µL of the Wash Buffer. The samples were then analyzed on the Accuri C6 cytometer (IL-10/TNF-α) or the Attune NxT flow cytometer (Granzyme B).

Plate ELISA for PBMC co-culture production of IFN-γ/IL-10

Media from PBMC co-cultures were analyzed for IFN-γ and IL-10 content. Briefly, media from PBMC-spheroid co-culture was collected and frozen at -20°C prior to analysis. The day before the analysis, Nunc MaxiSorp ELISA plates (Biolegend, Cat # 423501) were coated with either IFN-γ or IL-10 capture antibody diluted in Coating Buffer (Biolegend, Cat # 421701) and allowed to incubate overnight at 4°C. After the plate was washed 4X with a wash buffer made from PBS containing 0.05% (w/v) Tween-20 (Sigma, Cat # P1379), all wells were blocked using Assay Diluent (Biolegend, Cat # 421203) for 1 hour at room temperature with shaking at 500 rpm on an orbital shaker. Samples for IFN-γ analysis were diluted 20X in Assay Diluent and samples for IL-10 analysis were not diluted. After 4 washes of the plate, 100 µL of samples or standards were added to their respective wells according to the manufacturer's protocol. Plates were allowed to incubate overnight at 4°C. Plates were treated with their respective capture antibodies and biotin-HRP with appropriate shaking and wash steps as indicated in the manufacturer's protocol. 100 µL of substrate F (Biolegend, Cat # 437004) was added to each well and allowed to incubate for 30 minutes at room temperature. 50 µL of Stop Solution (Biolegend, Cat # 423001) was added to each well and the absorbance was measured at 450 nm with a background correction wavelength of 570 nm.

MSC intracellular protein collection

After spheroid formation, adherent and spheroid MSCs from 3 independent preparations of MSCs were cultured for 3 days with or without IFN-γ. MSCs were then washed with PBS and 40 µL of RIPA lysis buffer (Santa Cruz Biotechnology, sc-24948A) was added to each sample. Adherent samples were scraped with a cell scraper (VWR, 89260-222) and spheroid cells were disrupted using a SFX150 Cell Disruptor (Fisher Scientific, Cat # 15-338-528) at a continuous setting of 30% power for 5 seconds. Lysate was spun at 8,000g for 10 minutes at 4°C. After spinning, 5 µL of lysate sample was diluted in PBS to achieve a 1:40 dilution. A 2 mg/mL bovine serum albumin solution (Thermo Scientific, 23235) was diluted 1:1 with PBS to obtain a protein standard curve from 200 to 3.1 µg/mL total protein. 150 µL of diluted lysate or BSA standard were then added to a 96 well plate and 150 µL of working reagent (Thermo Scientific, 23235) was added. Samples were incubated at 37°C for 12 minutes. After incubation, the plate was read at 562 nm on a plate reader (Molecular Devices, 60139412). The BSA standard curve was then used to interpolate the protein concentration in each sample.

Western blot

Lysate was denatured by adding 38.5 µL of 4X LDS sample buffer (Thermo Fisher, B0007) and 15.5uL of 10X Bolt reducing agent (Invitrogen, B0009) per 100 µL of lysate and heated at 95°C for 2 minutes. The gel electrophoresis apparatus (Life Technologies, A25977) was loaded with 4-12% gradient, 10-well bis-tris gels (Bolt, NW04120BOX) and filled with running buffer diluted from 20x stock (Invitrogen, b0002). 10 µg of protein was added for each sample as well as a precision plus protein Kaleidoscope (Bio-Rad, 1610375). The gel was then run at 200V for 20 minutes. Transfer buffer was prepared with 700 mL of milli-Q, 200 mL methanol (Fisher Scientific, A414P-4), and 100 mL 10X Tris-glycine buffer (Amresco, M114-1L). PVDF blotting membrane (GE Healthcare, 10600023) was activated in methanol for two minutes. After running the gel, the gel transferred to the membrane at 10V for 2 hours.

After transfer, the membrane was removed from the cassette and blocked in 5% non-fat dried milk for 1 hour. After blocking, primary antibody was added which consisted of 5% (w/v) BSA (Sigma-Aldrich, A9647-10G), 1:1,000 IDO primary antibody (Cell Signaling, 86630S), 1:10,000 β-actin primary antibody (Thermofisher Scientific, AM4302), and 1:250 COX-2 primary antibody (BD Biosciences, 610203). Primary antibody staining was performed overnight

at 4°C with gentle rocking. After primary antibody staining, the appropriate secondary antibody was then added and incubated at room temperature. 1:10,000 Goat anti-rabbit antibody (BD Pharmingen, 554021) was used for IDO while 1:5,000 goat anti-mouse antibody (BioLegend, 405306) was utilized for COX-2 and β-actin. HRP substrate, a WesternBright Quantum mix (Advansta, K-12042-D10), was added to the membrane and scanned on a C-DiGit Blot Scanner (LI-COR Biosciences, 3600-00).

Kynurenine measurement

In order to measure IDO enzymatic activity, we directly measured conversion of tryptophan to kynurenine. Cells were cultured in 250 μM Tryptophan supplemented MEM-α with or without 100 ng/mL rhIFN-γ for 3 days after which media was collected and used in the activity assay. A 1 mM kynurenine stock was diluted 1:1 with media to obtain a standard curve ranging from 200 μM to 3.1 μM. 200 μL of kynurenine standards or media samples were then added to a 96 well plate. 100 μL of 30% (w/v) trichloroacetic acid (Sigma-Aldrich, T9159-100G) was added to each active well to precipitate proteins. The plate was then heated at 52°C for 30 minutes to convert N-formylkynurenine to kynurenine. After heating, the plate was spun at 1,200g for 15 minutes. 75 μL of supernatant was then collected and mixed 1:1 with 0.8% (w/v) p-dimethylaminobenzaldehyde (Sigma-Aldrich, 156447-25G). Absorbance was measured on a plate reader at 492 nm. Absorbance values of the known kynurenine standards were used to interpolate media kynurenine concentrations.

PGE2 ELISA

The concentration of Prostaglandin E2 (PGE2) in cell culture media was determined by Prostaglandin E2 Human ELISA Kit (Life Technologies, Cat # KHL1701) as described in the manufacture's protocol. Briefly, the standard was prepared by serial 1:1 dilutions from 2,500 to 39.1 pg/mL. Calibrator diluent alone was added as a non-specific binding control. 150 μL of standards or samples were added into pre-coated 96 well plate. 50 μL of primary antibody solution was added to all wells except the well for non-specific binding, followed by a 1-hour incubation at room temperature on orbital shaker with 500 rpm. After incubation, reagents were aspirated, and each well was washed with 300 μL of Wash Buffer 4 times. 200 μL substrate solution was then added to all wells, followed by incubation at room temperature for 30 minutes

in dark. 100 µL of stop solution was added to every well after incubation and the plate was read at 570 nm and 450 nm to perform wavelength correction.

CD73 expression and activity

To evaluate CD73 expression at cell surfaces, adherent cells were lifted using Accutase. Spheroid MSCs were collected, washed in PBS, and incubated with Accutase at 37°C. Spheroids were incubated for 4 minutes, followed by vigorous pipetting to disrupt the spheroids. The suspension was incubated at 37°C for another 4 minutes to ensure complete dissociation of spheroids. 200,000 cells from both adherent and spheroid MSC suspensions were spun down and resuspended in 100 µL of Cell Staining Buffer. For each sample, 5 µL of PE-Cy7 anti-CD73 (BD Biosciences, Cat # 561258) or 5 µL of PE-Cy7 Mouse IgG1K Isotype Control (BD Biosciences, Cat # 557872) was added. The samples were incubated on ice for 30 minutes, followed by flow cytometry analysis. Reported CD73 MFI values were baseline corrected using the MFI of the isotype control.

To evaluate CD73 expression in both adherent MSCs and spheroid MSCs, 20,000 cells per well were plated in either standard or spheroid (Corning, Cat # 4515) 96-well plates, respectively, with 100 µL of MEM-α complete. After culturing for 3 days, media was swapped to 75 µL of base MEM-α supplemented with 25 µL 1.2 mM AMP (Fisher Scientific, Cat # 50-490-075), followed by incubation at 37°C for 48 hours. The culture media was then collected for free phosphate measurement. Malachite Green Assay (Sigma Aldrich, Cat # MAK307-1KT) was performed as described in manufacturer protocol to quantify free phosphate. Briefly, reagent A and B were mix with ratio of 100:1 to form working reagent. 80 µL of 400x diluted sample and 20 µL of working reagent were added to a 96-well plate. The plate was incubated at 37°C for 30 minutes, followed by measurement of absorbance readings at 620 nm and 800 nm on a plate reader. 800 nm readings were used for background subtraction.

4.3. REFERENCES

1. François, M., Romieu-Mourez, R., Li, M. & Galipeau, J. Human MSC Suppression Correlates With Cytokine Induction of Indoleamine 2,3-Dioxygenase and Bystander M2 Macrophage Differentiation. *Mol. Ther.* **20**, 187–195 (2012).
2. Ankrum, J. a, Dastidar, R. G., Ong, J. F., Levy, O. & Karp, J. M. Performance-enhanced mesenchymal stem cells via intracellular delivery of steroids. *Sci. Rep.* **4**, 4645 (2015).
3. Rozenberg, A. *et al.* Human Mesenchymal Stem Cells Impact Th17 and Th1 Responses Through a Prostaglandin E2 and Myeloid-Dependent Mechanism. *Stem Cells Transl. Med.* **5**, 1506–1514 (2016).
4. Kalinski, P. Regulation of Immune Responses by Prostaglandin E2. *J. Immunol.* **188**, 21–28 (2012).
5. Dominici, M. *et al.* Minimal criteria for defining multipotent mesenchymal stromal cells. The International Society for Cellular Therapy position statement. *Cytotherapy* **8**, 315–317 (2006).
6. Shin, E. Y. *et al.* Adenosine Production by Biomaterial-Supported Mesenchymal Stromal Cells Reduces the Innate Inflammatory Response in Myocardial Ischemia/Reperfusion Injury. *J. Am. Heart Assoc.* **7**, (2018).
7. English, K. *et al.* Cell contact, prostaglandin E2 and transforming growth factor beta 1 play non-redundant roles in human mesenchymal stem cell induction of CD4 + CD25 High forkhead box P3 + regulatory T cells. *Clin. Exp. Immunol.* **156**, 149–160 (2009).
8. Sivanathan, K. N. *et al.* Interleukin-17A-Induced Human Mesenchymal Stem Cells Are Superior Modulators of Immunological Function. *Stem Cells* **33**, 2850–2863 (2015).
9. Lee, R. H. *et al.* TSG-6 as a biomarker to predict efficacy of human mesenchymal stem/progenitor cells (hMSCs) in modulating sterile inflammation in vivo. *Proc. Natl. Acad. Sci.* **111**, 16766–16771 (2014).
10. Ma, S. *et al.* Immunobiology of mesenchymal stem cells. *Cell Death Differ.* **21**, 216–225 (2014).
11. Moll, G. *et al.* Intravascular Mesenchymal Stromal/Stem Cell Therapy Product Diversification: Time for New Clinical Guidelines. *Trends Mol. Med.* **25**, 149–163 (2019).

12. Liu, Y.-Y. *et al.* Hypoxia-preconditioned mesenchymal stem cells ameliorate ischemia/reperfusion-induced lung injury. *PLoS One* **12**, e0187637 (2017).
13. Sugiyama, Y. *et al.* Intravenous Administration of Bone Marrow-Derived Mesenchymal Stem Cell, but not Adipose Tissue-Derived Stem Cell, Ameliorated the Neonatal Hypoxic-Ischemic Brain Injury by Changing Cerebral Inflammatory State in Rat. *Front. Neurol.* **9**, 757 (2018).
14. Bartosh, T. J., Ylöstalo, J. H., Bazhanov, N., Kuhlman, J. & Prockop, D. J. Dynamic compaction of human mesenchymal stem/precursor cells into spheres self-activates caspase-dependent IL1 signaling to enhance secretion of modulators of inflammation and immunity (PGE2, TSG6, and STC1). *Stem Cells* **31**, 2443–2456 (2013).
15. Braid, L. R., Wood, C. A., Wiese, D. M. & Ford, B. N. Intramuscular administration potentiates extended dwell time of mesenchymal stromal cells compared to other routes. *Cytotherapy* **20**, 232–244 (2018).
16. Kanazawa, M. *et al.* The influence of systemically or locally administered mesenchymal stem cells on tissue repair in a rat oral implantation model. *Int. J. Implant Dent.* **4**, 2 (2018).
17. Jungwirth, N. *et al.* Mesenchymal Stem Cells Form 3D Clusters Following Intraventricular Transplantation. *J. Mol. Neurosci.* **65**, 60–73 (2018).
18. Bartosh, T. J. *et al.* Aggregation of human mesenchymal stromal cells (MSCs) into 3D spheroids enhances their antiinflammatory properties. *Proc. Natl. Acad. Sci.* **107**, 13724–13729 (2010).
19. Xie, L., Mao, M., Zhou, L., Zhang, L. & Jiang, B. Signal Factors Secreted by 2D and Spheroid Mesenchymal Stem Cells and by Cocultures of Mesenchymal Stem Cells Derived Microvesicles and Retinal Photoreceptor Neurons. *Stem Cells Int.* **2017**, 1–13 (2017).
20. YlÖstalo, J. H., Bartosh, T. J., Coble, K. & Prockop, D. J. Human Mesenchymal Stem/Stromal Cells Cultured as Spheroids are Self-activated to Produce Prostaglandin E2 that Directs Stimulated Macrophages into an Anti-inflammatory Phenotype. *Stem Cells* **30**, 2283–2296 (2012).
21. Li, Y. *et al.* Primed 3D injectable microniches enabling low-dosage cell therapy for critical limb ischemia. *Proc. Natl. Acad. Sci.* **111**, 13511–13516 (2014).

22. Li, Y. *et al.* Three-dimensional spheroid culture of human umbilical cord mesenchymal stem cells promotes cell yield and stemness maintenance. *Cell Tissue Res.* **360**, 297–307 (2015).
23. Xu, Y., Shi, T., Xu, A. & Zhang, L. 3D spheroid culture enhances survival and therapeutic capacities of MSCs injected into ischemic kidney. *J. Cell. Mol. Med.* **20**, 1203–1213 (2016).
24. Yamaguchi, Y., Ohno, J., Sato, A., Kido, H. & Fukushima, T. Mesenchymal stem cell spheroids exhibit enhanced in-vitro and in-vivo osteoregenerative potential. *BMC Biotechnol.* **14**, 105 (2014).
25. Rettinger, C. L. *et al.* In vitro characterization of scaffold-free three-dimensional mesenchymal stem cell aggregates. *Cell Tissue Res.* **358**, 395–405 (2014).
26. Ankrum, J. a, Ong, J. F. & Karp, J. M. Mesenchymal stem cells: immune evasive, not immune privileged. *Nat. Biotechnol.* **32**, 252–260 (2014).
27. Boland, L. *et al.* IFN-γ and TNF-α Pre-licensing Protects Mesenchymal Stromal Cells from the Pro-inflammatory Effects of Palmitate. *Mol. Ther.* **26**, 860–873 (2018).
28. Kim, D. S. *et al.* Enhanced Immunosuppressive Properties of Human Mesenchymal Stem Cells Primed by Interferon-γ. *EBioMedicine* **28**, 261–273 (2018).
29. Prasanna, S. J., Gopalakrishnan, D., Shankar, S. R. & Vasandan, A. B. Pro-Inflammatory Cytokines, IFNγ and TNFα, Influence Immune Properties of Human Bone Marrow and Wharton Jelly Mesenchymal Stem Cells Differentially. *PLoS One* **5**, e9016 (2010).
30. Ryan, J. M., Barry, F., Murphy, J. M. & Mahon, B. P. Interferon-γ does not break, but promotes the immunosuppressive capacity of adult human mesenchymal stem cells. *Clin. Exp. Immunol.* **149**, 353–363 (2007).
31. Ylostalo, J. H., Bazhanov, N., Mohammadipoor, A. & Bartosh, T. J. Production and Administration of Therapeutic Mesenchymal Stem/Stromal Cell (MSC) Spheroids Primed in 3-D Cultures Under Xeno-free Conditions. *J. Vis. Exp.* **55126**, (2017).
32. Bartosh, T. J. & Ylostalo, J. H. Preparation of Anti-Inflammatory Mesenchymal Stem/Precursor Cells (MSCs) Through Sphere Formation Using Hanging-Drop Culture Technique. *Curr. Protoc. Stem Cell Biol.* **28**, 2B.6.1-2B.6.23 (2014).

33. Ylostalo, J. H., Bartosh, T. J., Tiblow, A. & Prockop, D. J. Unique characteristics of human mesenchymal stromal/progenitor cells pre-activated in 3-dimensional cultures under different conditions. *Cytotherapy* **16**, 1486–1500 (2014).
34. Zimmermann, J. A. & Mcdevitt, T. C. Pre-conditioning mesenchymal stromal cell spheroids for immunomodulatory paracrine factor secretion. *Cytotherapy* **16**, 331–345 (2014).
35. Costa, M. H. G., McDevitt, T. C., Cabral, J. M. S., da Silva, C. L. & Ferreira, F. C. Tridimensional configurations of human mesenchymal stem/stromal cells to enhance cell paracrine potential towards wound healing processes. *J. Biotechnol.* **262**, 28–39 (2017).
36. O'Donnell, S. & O'Morain, C. A. Therapeutic benefits of budesonide in gastroenterology. *Ther. Adv. Chronic Dis.* **1**, 177–186 (2010).
37. Sreeramkumar, V., Fresno, M. & Cuesta, N. Prostaglandin E2 and T cells: friends or foes? *Immunol. Cell Biol.* **90**, 579–586 (2012).
38. Jeon, S. *et al.* Shift of EMT gradient in 3D spheroid MSCs for activation of mesenchymal niche function. *Sci. Rep.* **7**, 6859 (2017).
39. Burand, A. J., Gramlich, O. W., Brown, A. J. & Ankrum, J. A. Function of Cryopreserved Mesenchymal Stromal Cells With and Without Interferon-γ Prelicensing is Context Dependent. *Stem Cells* **35**, 1437–1439 (2017).
40. Zimmermann, J. A., Hettiaratchi, M. H. & McDevitt, T. C. Enhanced Immunosuppression of T Cells by Sustained Presentation of Bioactive Interferon-γ Within Three-Dimensional Mesenchymal Stem Cell Constructs. *Stem Cells Transl. Med.* **6**, 223–237 (2017).
41. Ranganath, S. H. *et al.* Controlled Inhibition of the Mesenchymal Stromal Cell Pro-inflammatory Secretome via Microparticle Engineering. *Stem Cell Reports* **6**, 926–939 (2016).
42. Waterman, R. S., Tomchuck, S. L., Henkle, S. L. & Betancourt, A. M. A New Mesenchymal Stem Cell (MSC) Paradigm: Polarization into a Pro-Inflammatory MSC1 or an Immunosuppressive MSC2 Phenotype. *PLoS One* **5**, e10088 (2010).
43. Bernardo, M. E. & Fibbe, W. E. Mesenchymal Stromal Cells: Sensors and Switchers of Inflammation. *Cell Stem Cell* **13**, 392–402 (2013).

44. Boland, L. K. *et al.* Nature vs. Nurture: Defining the Effects of Mesenchymal Stromal Cell Isolation and Culture Conditions on Resiliency to Palmitate Challenge. *Front. Immunol.* **10**, 1–15 (2019).
45. Ben-Sasson, S. Z. *et al.* IL-1 enhances expansion, effector function, tissue localization, and memory response of antigen-specific CD8 T cells. *J. Exp. Med.* **210**, 491–502 (2013).
46. Chen, X. *et al.* The interaction between mesenchymal stem cells and steroids during inflammation. *Cell Death Dis.* **5**, e1009–e1009 (2014).
47. Michelo, C. M. *et al.* Added effects of dexamethasone and mesenchymal stem cells on early Natural Killer cell activation. *Transpl. Immunol.* **37**, 1–9 (2016).
48. Chemnitz, J. M. *et al.* Prostaglandin E 2 Impairs CD4 + T Cell Activation by Inhibition of lck: Implications in Hodgkin's Lymphoma. *Cancer Res.* **66**, 1114–1122 (2006).
49. Löwenberg, M. *et al.* Glucocorticoids cause rapid dissociation of a T-cell-receptor-associated protein complex containing LCK and FYN. *EMBO Rep.* **7**, 1023–1029 (2006).
50. Petta, I. *et al.* The Interactome of the Glucocorticoid Receptor and Its Influence on the Actions of Glucocorticoids in Combatting Inflammatory and Infectious Diseases. *Microbiol. Mol. Biol. Rev.* **80**, 495–522 (2016).
51. Schenkel, J. M. & Masopust, D. Tissue-Resident Memory T Cells. *Immunity* **41**, 886–897 (2014).
52. Yin, J. Q., Zhu, J. & Ankrum, J. A. Manufacturing of primed mesenchymal stromal cells for therapy. *Nat. Biomed. Eng.* **3**, 90–104 (2019).

CHAPTER 5: LOCALLY INJECTIONED CELLS LABELED WITH A FLUORESCENT DYE CAN BE TRACTED WITH A LOW-COST INTRAOPERATIVE TECHNIQUE

5.1. OVERVIEW

One critical component of local injection of MSCs into animal models is validation of consistent injections and tracking the cell retention over time. However, papers which do this are often few and far between due to the cost-prohibitive and time-intensive nature of many cell tracking technologies. Herein, we outline a low-cost technique which can detect, and track cells injected into the skin of mice. This technique uses fluorescent labeling of MSCs with a handheld fluorescent camera to quickly image cells immediately after injection. This chapter also outlines the limitation in sensitivity and image quality of this technique compared to a fluorescent bed scanner. Ultimately this technique can be used determine consistency of cell injections into animals and can give researchers a general picture of how long cells persist in the site.

This chapter is an adaptation of a peer-reviewed article published on December 1, 2017 in *Advances in Wound Care*. Reprinted with permission.

Burand AJ Jr, Boland L, Brown AJ, Ankrum JA. A Low-Cost Technique for Intraoperative Imaging of Cell Delivery and Retention in a Model of Delayed Wound Healing. **Adv Wound Care (New Rochelle).** 2017 Dec 1;6(12):413-424. doi: 10.1089/wound.2017.0751. PubMed PMID: 29279805; PubMed Central PMCID: PMC5734161.

5.2. A LOW-COST TECHNIQUE FOR INTRAOPERATIVE IMAGING OF CELL DELIVERY AND RETENTION IN A MODEL OF DELAYED WOUND HEALING

Abstract

Techniques to validate successful delivery of cell products are expensive, time consuming, and require transport of the animal to imaging facilities preventing their widespread use as documentation tools. The goal of this study was to determine if a low-cost, portable, microscope could provide sufficient performance to be used to document delivery of cell products and track retention over time. A Dino-Lite fluorescent microscope and an Odyssey CLx whole animal scanner were compared on the basis of resolution, sensitivity, and linearity. The impact of different injection profiles on image quality was also compared and the system was used to track cells, injected freely or on scaffolds, in a model of diabetic wound healing. Both systems were able to detect 50 fluorescently labeled cells and there was a linear relationship between fluorescent signal and cell number *in vitro*. *In vivo*, both systems were found to be non-linear, but correlated highly with one another. The Dino-Lite system was able to distinguish between depth of injection, diffuse injections, subcutaneous injections, and failed injections. In contrast to traditional imaging systems, the technique presented here is affordable, rapid enough that it can be used to validate every injection and can be brought to the animal, reducing handling and stress that may interfere with wound healing processes. Collectively, we found the speed, affordability, and portability of hand-held microscopes combined with their technical capabilities make them a valuable and accessible tool for routine validation, documentation, and tracking of cell products delivered to wounds.

Introduction

When refining wound healing therapies that incorporate living cellular products, ensuring consistent delivery and retention of the product in the wound site is imperative. If an animal fails to respond to a therapy, researchers need to be able to determine the cause of the failure: insufficient dosing, poor proximity to the wound margins, lack of persistence, or change in cell phenotype. Thus, there is a need for techniques to validate the initial dose and location of cells at the time of administration, either alone or on scaffolds, and to track the persistence of cells in the wound throughout the healing process. While multiple technologies are currently available to

track cells *in vivo*, most require the animal to be taken to an imaging suite, are time-consuming, and remain prohibitively expensive. Herein we present a protocol that utilizes a low-cost handheld fluorescent microscope to rapidly validate and record cell transplantation within an operative environment and demonstrate its utility in monitoring the *in vivo* location and persistence of cells transplanted into a TallyHo excisional wound model. The technical capability of the system combined with its logistical advantages make it attractive for routine validation and tracking of cell transplantation into the wound environment.

Clinical problem addressed

Diabetic wounds are the leading cause of non-traumatic lower extremity amputations[1] and are estimated to afflict 25% of diabetic patients over the course of their lifetime[2]. Due to the large number of patients and shortcomings of current therapies, there is a tremendous need for more efficacious therapies. The complexity of the disease environment and the severity of the dysfunction of resident cells make tissue engineering and regenerative medicine solutions that utilize healthy living cells attractive candidates for new therapies. However, pre-clinical animal testing of these living therapeutics are limited due to different responses to therapy between animals, inconsistency in therapy application, and animal manipulation of the therapeutic. Therefore, it is imperative to document delivery of cell products, improving the relevance of data collected from pre-clinical models and the assessment of novel cell therapies. Unfortunately, cell tracking techniques used today are expensive, time consuming, and require transport of the animal to imaging facilities preventing their widespread use as documentation tools.

Materials and Methods

Cell culture

Human mesenchymal stem cells also known as mesenchymal stromal cells or MSCs were obtained from RoosterBio and cultured in MEM-alpha media supplemented with 15% FBS, 1% L-glutamine, and 1% penicillin/streptomycin. MSCs from RoosterBio are evaluated according to the ISCT minimal criteria[3] and are specifically >95% positive for CD73a, CD90, and CD105, <2% positive for CD11, CD14, CD19, CD34, CD45, CD79a, and HLA-II, and capable of multilineage differentiation. Cell cultures were seeded at 3,000 cells/cm^2 and passaged when

plates reached 70% confluence for all experiments. All cells used in this study were passage 3-6 at time of use.

Adenoviral amplification

Adenovirus expressing the mCherry fluorescent protein was procured from the Viral Vector Core at the University of Iowa (Ad5CMVmCherry, cat# VVC-U of Iowa-537). HEK293A cells grown to 90% confluence in a 150 mm petri dish were infected with 40 µL of Ad5CMVmCherry ($7x10^{10}$ pfu/ml). After cell detachment from the plate and confirmation of cell expression of mCherry, cells were collected and then lysed via freeze/thaw cycling. The media was spun at 800 g for 5 minutes to pellet cell debris. Supernatant was transferred and stored at -80°C (generation 1 virus). HEK293A cells were grown to 90% confluence and infected with 80 µL of generation 1 virus. After confirmation of mCherry expression and detachment from the plate, virus was collected and frozen for labeling of MSCs as before (generation 2 virus). IFU of the adenovirus was calculated by infecting 500,000 HEK293 cells in a 12-well plate with 10 µL, 1 µL, 100 nL, 10 nL, and 1 nL of crude virus. After 48 hours, the cells were visualized on a fluorescent microscope and cells were averaged from the condition which contained on average 10-50 cells expressing mCherry per 20x field of view. The IFU was calculated by averaging the number of mCherry positive HEK293 cells in 20 fields of view with IFU/mL = (average # mCherry+ cells * 597 fields of view per well)/(mL of virus added). In this case, the wells containing 10 nL of virus had an average of 12 mCherry positive cells in them. Therefore, IFU/mL = (24*597)/(1E-5mL) = 1.4E9 IFU/mL.

Cell staining and tracking

To be able to track MSCs both with our handheld fluorescent microscope and the Odyssey CLx whole animal scanner, MSCs were co-labelled with DiR and transduced to express mCherry. For adenoviral induction of mCherry expression, 250 µL of generation 2 adenovirus at a stock concentration of 1.4E9 IFU/mL yielding a MOI of 440 IFU/cell encoding for mCherry was incubated in 4 mL MEM-alpha supplemented with 25 mM $CaCl_2$ (Sigma) for 20 minutes at room temperature. MSCs were washed in PBS and then incubated with the virus solution at 37°C for 30 minutes. Cells were washed in complete MEM-alpha and allowed to recover for at least 4 hours before re-plating. Cells were harvested 2 days after adenoviral transduction to allow for

stable expression of mCherry and then stained with DiR immediately before plating in experimental conditions. MSCs were lifted with accutase, washed in PBS, and incubated with DiR dye (Biotium) diluted to 0.1 mg/mL in media for 20 minutes at 37°C. Cells were then rinsed with PBS, pelleted, and re-suspended in fresh media before use in either *in vitro* or *in vivo* assays. This dose of virus had been confirmed to maintain >95% MSC viability.

Mice and animal care

Animal experiments were approved by the University of Iowa IACUC committee. 8-week male TallyHo mice were purchased from the Jackson Laboratories and housed for an additional 6 weeks on an NIH-31 modified open formula mouse diet (Envigo 7913). At 10-12 weeks, increase in urination became apparent indicating induction of diabetes. At weeks 15, 16 and 17, blood glucose of each mouse was measured and recorded to confirm hyperglycemia followed by wounding procedures to enable *in vivo* tracking of cells administered to the wound bed. After wounding, animals were singly housed to prevent animals from interfering with each other's bandages. Since hyperglycemic phenotype penetrance is less than 100% in the TallyHo mice[4,5], the glucose levels of all were measured prior to surgery and post-surgery to ensure that blood glucose levels of animals used were >200 mg/dL. As the focus on this project was on developing the cell tracking technique in a chronic wound model, only diabetic mice were used for all experiments.

Full thickness excisional wounding and stenting

An adaptation of a previously published protocol was used to create two full excisional wounds on the backs of each mouse (Figure 39A,B)[6]. Mice were anesthetized with isoflurane and maintained at a level of anesthesia to suppress pedal reflexes. Glucose was measured with a handheld meter to ensure all mice were diabetic (plasma glucose >200mg/dL, average 485 ± 144 mg/dL). All mice were shaved and depilated by applying Veet hair removal cream for 5 minutes. The cream was removed thoroughly with 70% ethanol wipes. The site was then sterilized using 3 alternating applications of 70% ethanol and betadine solution prior to wounding. Mice were placed on their side, and a 5 mm biopsy punch was pushed through a dorsal skin fold to create a full thickness excisional wound on each side of the midline near the scapula. To prevent the wound from closing via contraction, each wound was stented by suturing an autoclaved stainless-

steel locking washer (Grainger, item#19NP58) with a 6.5 mm inner diameter around each wound using 5.0 silk sutures.

Intraoperative in vitro and in vivo validation of cell transplantation

For *in vitro* cell dosing, DiR/mCherry labeled MSCs were plated in 20 µL droplets on the bottom of a 150 mm petri dish and allowed to attach overnight. Each 20µL droplet contained $250x10^3$, $150x10^3$, $75x10^3$, $50x10^3$, $25x10^3$,$10x10^3$, $1x10^3$, 500, 100, or 0 cells. Droplets were then imaged with a Dino-Lite Edge Digital Microscope with a filter set optimized to detect mCherry (AM4115T-RFYW) at a working distance of 20.6 mm (40x) with a 250 msec exposure time. The $250x10^3$, $1x10^3$, and 50 cell conditions were also imaged at a working distance of 10.6 mm (60x) and 62.6 mm (20x). The plate was then re-imaged on an Odyssey CLx far-red imaging system (LI-COR) using 21 µm spatial resolution, lowest image quality, L1 700 nm laser power, L2 800 nm laser power, and scanning offset of 0.0 mm. The Odyssey settings were determined in pilot studies used to identify settings that produced, focused, quantifiable signal in a reasonable amount of time. The settings used allowed for detection of the highest dose of cells using our staining protocol without saturating the signal of any one pixel. Note that the quality parameter refers to the scan speed. Higher quality settings result in more data collected however it increases scan time dramatically (ie. >30 min per mouse). In a scenario where there would be movement of the animal (eg. breathing), the quality parameter would have to be set lower or movement artifacts would be picked up by the scanner.

For initial *in vivo* dosing experiments, TallyHo mice were injected with $250x10^3$, $75x10^3$, $25x10^3$, $1x10^3$, 500, 0 MSCs stained with DiR and virally induced with mCherry dyes. Subcutaneous injections were performed on the dorsal side of the mouse to either side of the spine. Varying depth injections of $75x10^3$ MSCs were performed at 0.5 mm, 1.8 mm, 3.1 mm, 4.4 mm, 5.7 mm, and 7.0 mm into the dorsal side of the mouse. Depth of injection was controlled by limiting the length of exposed needle using stiff silicone spacers. At all injections, moderate pressure was applied to the syringe to ensure that the syringe was at the measured depth. Length of exposed needle was measured for each injection using digital calipers. Injection points were imaged with the Dino-Lite at a working distance of 20.6 mm (40x) and exposure of 0.25 seconds. Mice were then place on the Odyssey scanner dorsal side down and imaged with

21 µm spatial resolution, lowest image quality, 700 nm laser power of 1, 800 nm laser power of 3.5, and scanning offset of 4.0 mm.

MSC loading onto gelatin microcarriers

An adaptation to a gelatin microcarrier (MC) protocol was used to create a scaffold system for MSCs[7]. Briefly, gelatin microcarriers were prepared by crosslinking 5% w/v gelatin (Fisher Scientific) with 1.25% v/v glutaraldehyde (25% aqueous solution stock, Alfa Aesar) for 1 day. Residual glutaraldehyde and aldehyde groups were reduced using 2 treatments with 100 mM sodium borohydride (Thermo Fisher) for 24 hours. After neutralization, the crosslinked gelatin changed from a brown to a white color. Crosslinked gelatin was lyophilized, ground, and sieved to generate microcarriers 100-300 µm in diameter. The microcarriers were then rehydrated in media for 24 hours to remove any residual sodium borohydride and allow adsorption of fibronectin onto the gelatin scaffold, rinsed, and then re-lyophilized. To sterilize the gelatin, 200 µL of 70% ethanol was added to each tube and ethanol was evaporated overnight under a UV sterilization light. $400x10^3$ MSCs modified with mCherry were then seeded in 100 µL media onto 15 mg of microcarriers. Cells were allowed to attach for 1 hour, and then 1 mL of media was added incubated overnight.

Serial monitoring of cell retention

TallyHo mice wounded as described above and MSCs modified with mCherry were injected subcutaneously around the wound bed or topically applied at $200x10^3$ cells per wound, one day after wounding. Free MSCs were harvested, washed in PBS, and re-suspended at 4 million cells/mL in PBS. Free MSCs were loaded into insulin syringes and 50 µL total cell suspension was injected in 3-5 areas around the perimeter of the excisional wound site. MSCs on microcarriers were applied directly to the wound bed to achieve delivery of $200x10^3$ cells per wound. All wounds were bandaged after application of cells.

At days 3, 7, and 8 for the PBS and MSC only groups and days 3 and 5 for the MC and MSC/MC groups, the mouse wound bandages were removed, and fluorescent images were taken using the Dino-Lite camera in a dark room. Mice were anesthetized with isoflurane and positioned directly under the Dino-Lite and imaged as described above.

Results

Handheld microscope setup and configuration

The Dino-Lite handheld microscope (Figure 34A) has the ability to acquire both bright field and fluorescent images. The AM4115T-RFYW Dino-Lite configuration is optimized for detection of the mCherry fluorescent protein; however, configurations can be customized to match the excitation and emission characteristics of a variety of fluorophores. To begin, a basic understanding of the relationship between the field of view (FOV), working distance (WD) from the microscope to the focal plane, and sensitivity was examined. FOV and WD from the sample are inversely proportional and both are directly tied to the level of magnification (Figure 34A,B). Depending on the FOV requirements, images from 5.9 mm x 4.7 mm to 19.6 mm x 15.7 mm in size can be acquired with working distances ranging from 0.86-6.26 cm from the focal plane of the sample. The smaller the FOV the greater the resolution and sensitivity of the image (Figure 34C), therefore, the cell detection limit will be higher for larger fields of view. Spatial resolution of the Dino-Lite is dependent on the magnification. At 20x magnification, resolution is 15 µm and spatial resolution at a 40x magnification is 7.6 µm. Thus, care must be taken in selecting the appropriate working distance with the Dino-Lite in order to capture the necessary image area.

Range and sensitivity of detection of fluorescent cells under ideal conditions

To characterize the linearity of the Dino-Lite microscope, we compared its range and sensitivity to a robust whole animal imaging system, the Odyssey CLx infrared scanner. MSCs co-labelled with mCherry (optimal spectral characteristics for the Dino-Lite) and DiR (optimal spectral characteristics for the Odyssey) were plated in 20 µL droplets at concentrations ranging from 50-250,000 cells per droplet and imaged with both imaging systems under pre-optimized settings. Qualitatively, both systems were able to detect small clusters of cells down to the 50 cell condition (Figure 35A) while quantitatively, based on mean fluorescent intensity (MFI), the Odyssey system had a lower limit of detection (50 cells) compared to background. Both the Odyssey and Dino-Lite produced calibration curves with a linear relationship between cell number and MFI (Figure 35B-E). For optimal prediction of cell number, two distinct fit curves were produced, one for the doses ranging from 0-1,000 cells and another for detection of 10,000-250,000 cells. Thus, under ideal acquisition settings in which the sample resides in a single focal

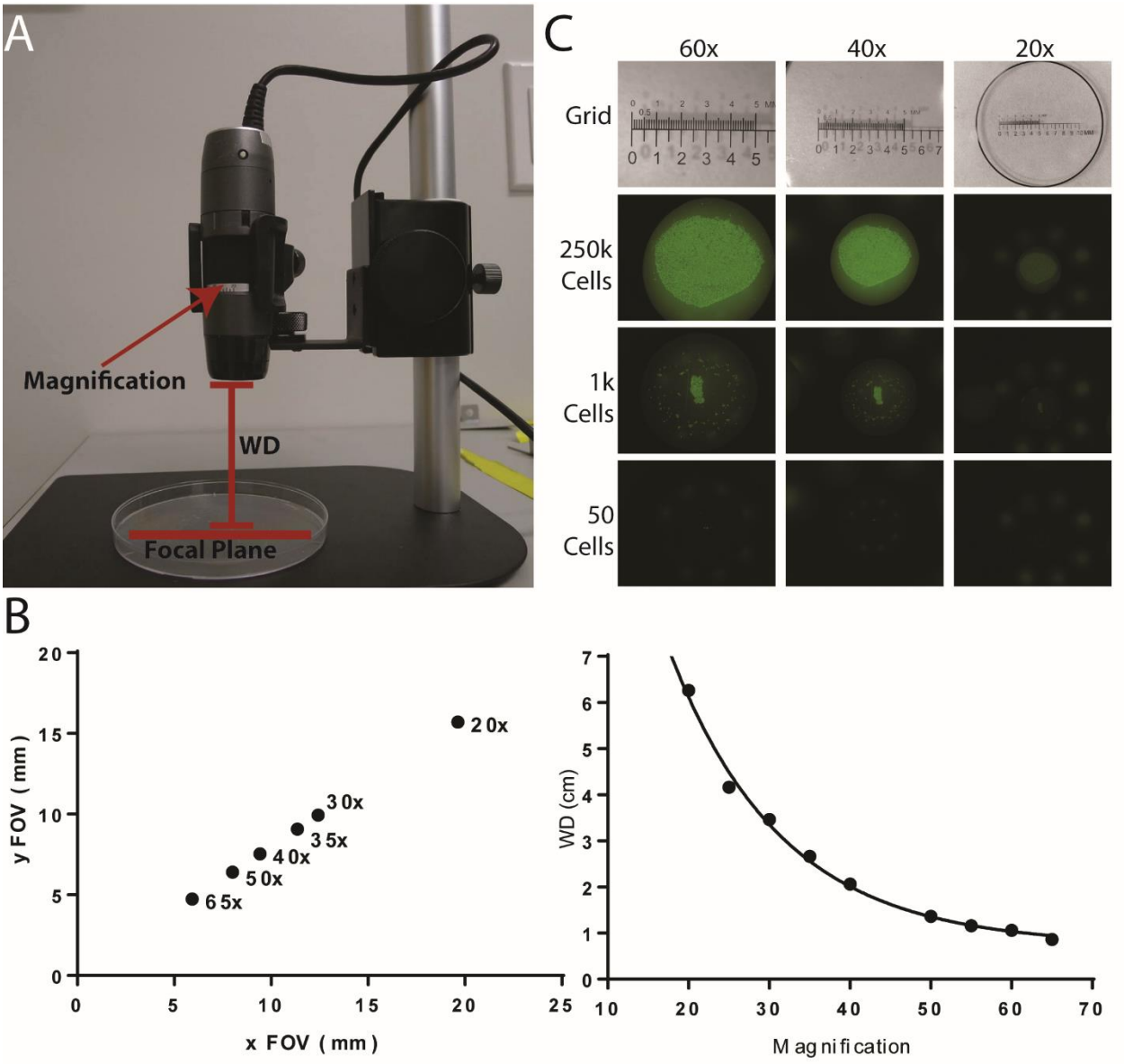

Figure 34. Magnification can be set on the Dino-Lite system to optimize working distance (WD), field of view (FOV), and fluorescent intensity.

Dino-Lite setup (A) where variation in magnification produces a nonlinear relation with working distance and a linear relation with field of view (B). (C) Dino-Lite magnification modulates fluorescent intensity of cells.

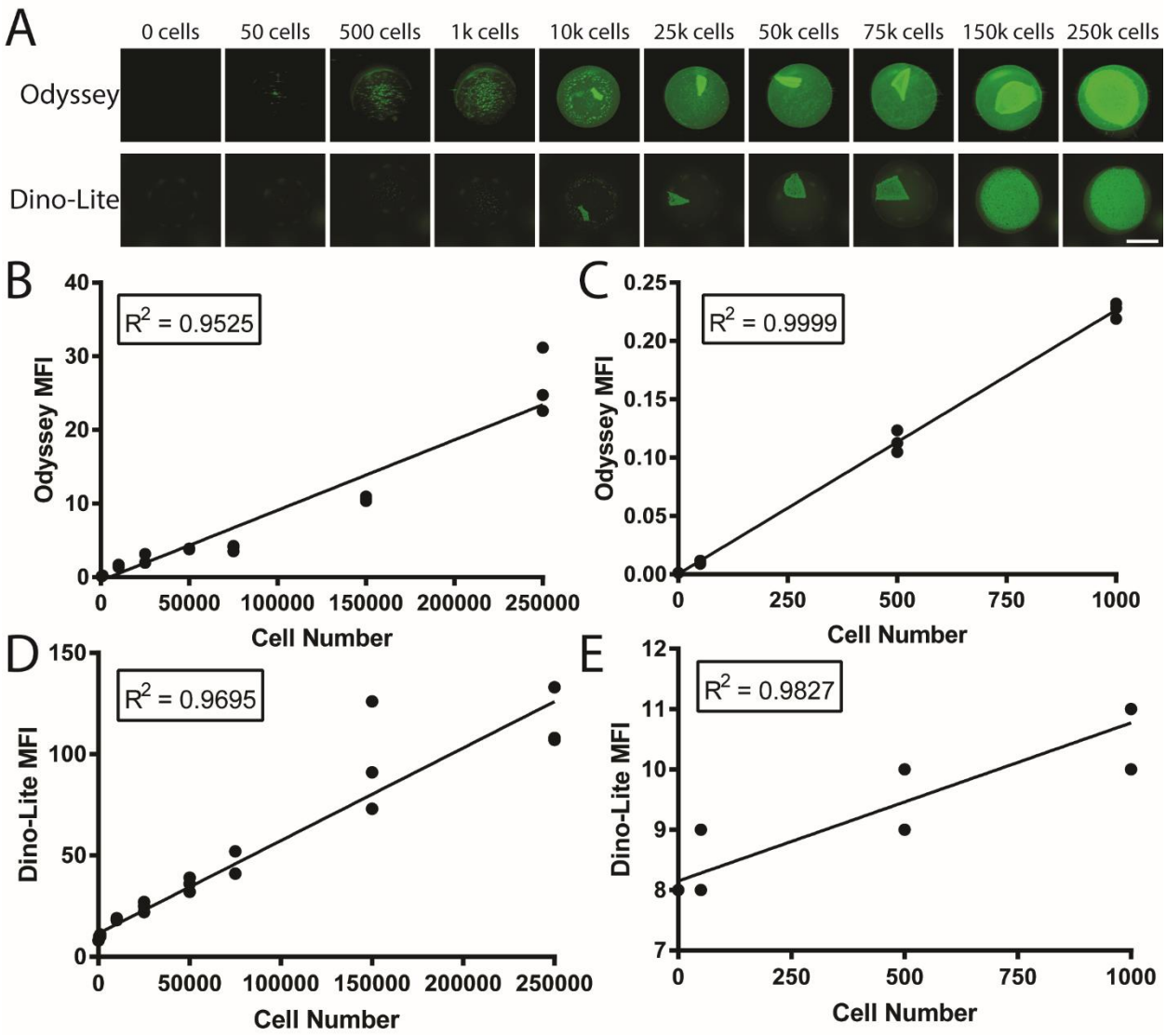

Figure 35. DiR/mCherry stained MSCs display a dose dependent fluorescent signal *in vitro* via both Odyssey and Dino-Lite imaging.

(A) DiR/mCherry stained MSCs in petri dish imaged by Odyssey fluorescent scanner and Dino-Lite (40x magnification). Mean fluorescent intensity (MFI) of MSCs over dosing range (n=3) for Odyssey fluorescent scanner (B,C) and Dino-Lite (D,E). Scale bar 3 mm.

plane, the Dino-Lite and Odyssey imaging systems performed similarly, and both produced a quantitative assessment of cell number over a large range of cell doses.

In vivo relationship between cell number and fluorescent intensity

Due to absorption of light by tissues, as well as differences in the depth of injection and dispersion of cells within a tissue, *quantitative* tracking of cell numbers using light-intensity based modalities is challenging. We wanted to determine if the ability to focus the Dino-Lite on a specific focal plane for each injection site would result in improved quantification of cell number *in vivo* compared to a traditional whole-body scanner. Thus, we subcutaneously injected defined numbers of labelled MSCs into cadaver mice and imaged with both the Dino-Lite and Odyssey system. While DiR fluorescent emission had less interference from the tissue (Figure 36A,B), both systems were able to detect cell numbers as low as 1,000 cells injected subcutaneously. As seen in Figure 36, the Odyssey system can image the entire mouse in one scan, while the Dino-Lite requires a separate image for each injection site. However, most wound healing studies are performed with wounds smaller than 10 mm in diameter, making the field of view of the Dino-lite adequate for use as a documentation camera for wound healing experiments. Because each Dino-Lite image could be individually focused on the injection site, the variability between repeat measurements was lower for the Dino-Lite compared to the Odyssey system. In addition, the acquisition time for the Dino-Lite took seconds, while the Odyssey scan took ~20 minutes per image. To adjust the focus of the Odyssey scanner, by changing the 'scanning offset' parameter, an additional 20-minute acquisition would have been required for each focal plane making real-time focusing logistical impractical. For both the Dino-Lite and Odyssey systems, there was a similar nonlinear relationship between cell number and MFI. Additionally, a high degree of correlation between measurements obtained with the individual systems was achieved (Figure 36C-E). Thus, the Dino-Lite appears to perform equally to the Odyssey scanner with respect to detection limit, as well as the ability to detect cells both *in vitro* and *in vivo*. While robust *in vivo* quantitative assessment is not possible with either system, a qualitative assessment can be obtained with both allowing for confirmation and qualification of each injection as was explored next.

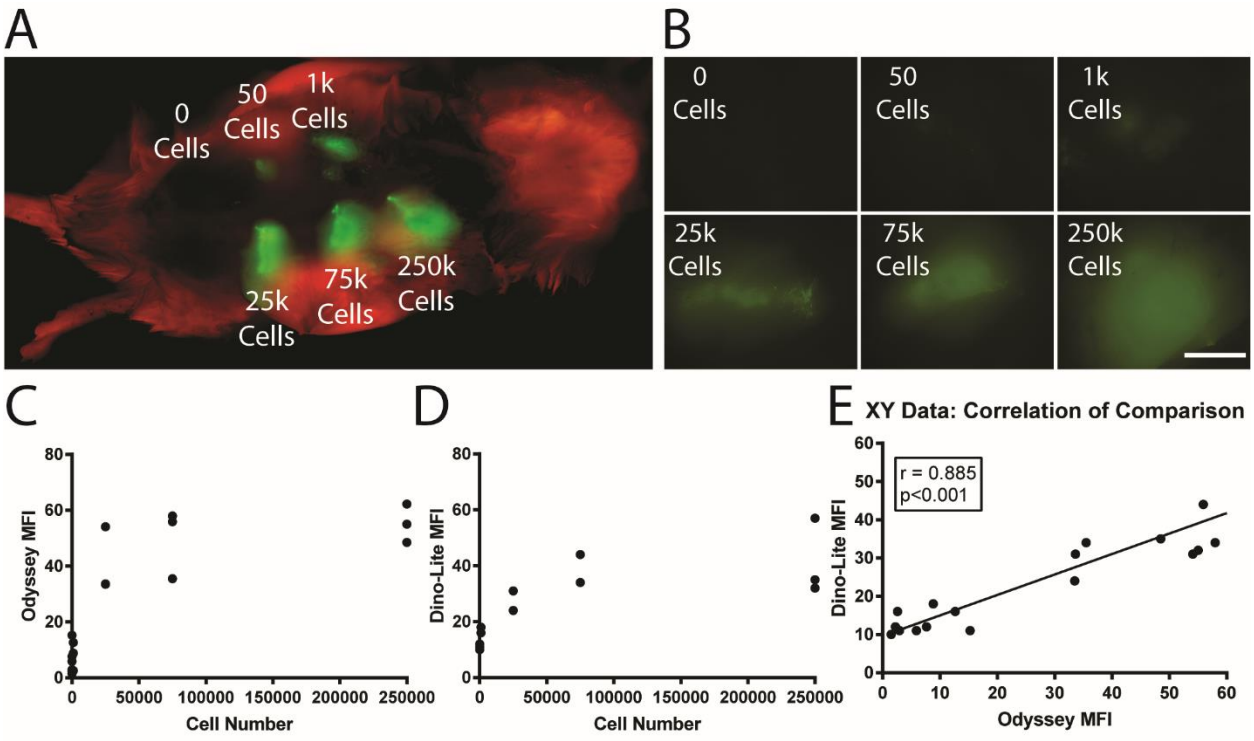

Figure 36. Dino-Lite and Odyssey quantification of MSC fluorescence shows a similar dose dependence *in vivo*.

DiR/mCherry stained MSCs subcutaneously injected into mouse skin imaged by Odyssey scanner (A) and Dino-Lite (B). Quantification of mean fluorescent signal of MSCs for Odyssey scanner (C) and Dino-Lite (D). Spearman correlation comparison of measured intensities from Dino-Lite and Odyssey imaging (E). Scale bar 3 mm.

Validating consistency in cell product delivery

To determine if the Dino-Lite was able to detect changes in fluorescent intensity that arise due to inconsistencies in delivery technique, we took images of 150,000 cells injected at varying depths in TallyHo mice. As seen in Figure 37, injection depth drastically changed the signal acquired by the Dino-Lite. After deep injections, the Dino-Lite detects a well-defined injection track. At medium injection depths, 1.8-4.4 mm, the fluorescent signal transitions from a single point to a less defined point amongst a diffuse fluorescence radiating from the injection track as the Dino-Lite excites and identifies cells that are dispersed under the skin. Finally, at the shallowest depth, 0.5 mm, the majority of the cells flowed out of the tissue leaving a diffuse layer of cells on the surface of the skin. Thus, with the Dino-Lite, we were able to distinguish successful point injections from failed injections in which the cell product flowed out of the injection site.

In addition to failed injections, we hypothesized other manipulations of the mice during handling or deviations in pre-surgical preparation could impact the signal detected by the handheld microscope. Thus, we staged common scenarios known to arise in wound studies including application of pressure on the wound site, presence of hair, and removal of the cell product by mechanical abrasion (Figure 38). While subcutaneous point injections in TallyHo mice have a bright injection point (Figure 38A), application of pressure to the injection site, as might occur during bandaging, causes the injection point to become less distinct (Figure 38C). Failure to completely depilate the surgical site before injection can also lead to variations in the fluorescent profile, as hair can both absorb and scatter the excitation and emission light traveling from the microscope and cells, respectively (Figure 38D). Finally, topically applied cells, whether intentionally or unintentionally due to injection site squirt out creates a bright patterned texture (Figure 38E). However, if cells are removed, to clean the surface after a failed injection or due to activity by the animal, residual cells can still be detected on the skin surface (Figure 38F). While qualitative, the Dino-Lite images were able to validate initial injection success and track the relative decline in remaining cells if the majority of cells are removed by physical abrasion. Combined with the speed and ease of acquisition, these results make the system attractive as a routine documentation system for wound healing studies of cell-based therapies.

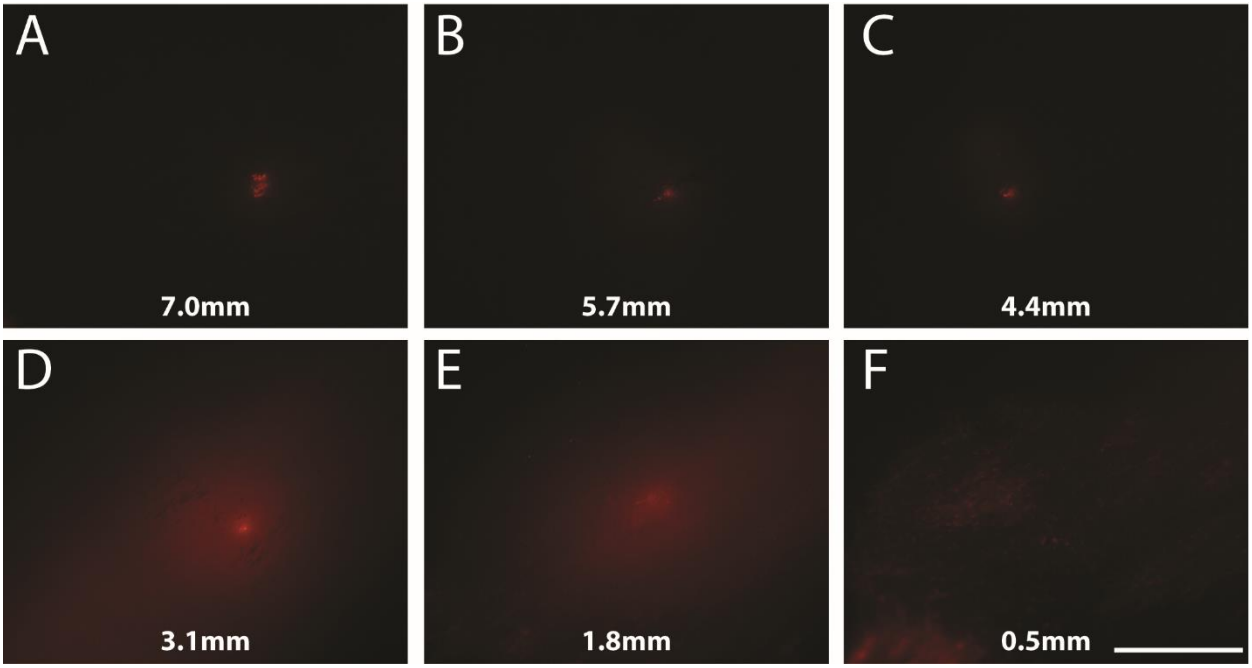

Figure 37. Injection depth impacts MSC fluorescent intensity and distribution of signal. Fluorescent signal from 150,000 mCherry-MSCs as measured by Dino-Lite at 7.0 (A), 5.7 (B), 4.4 (C), 3.1 (D), 1.8 (E), and 0.5 mm (F) depths in mouse skin. Scale bar 3 mm.

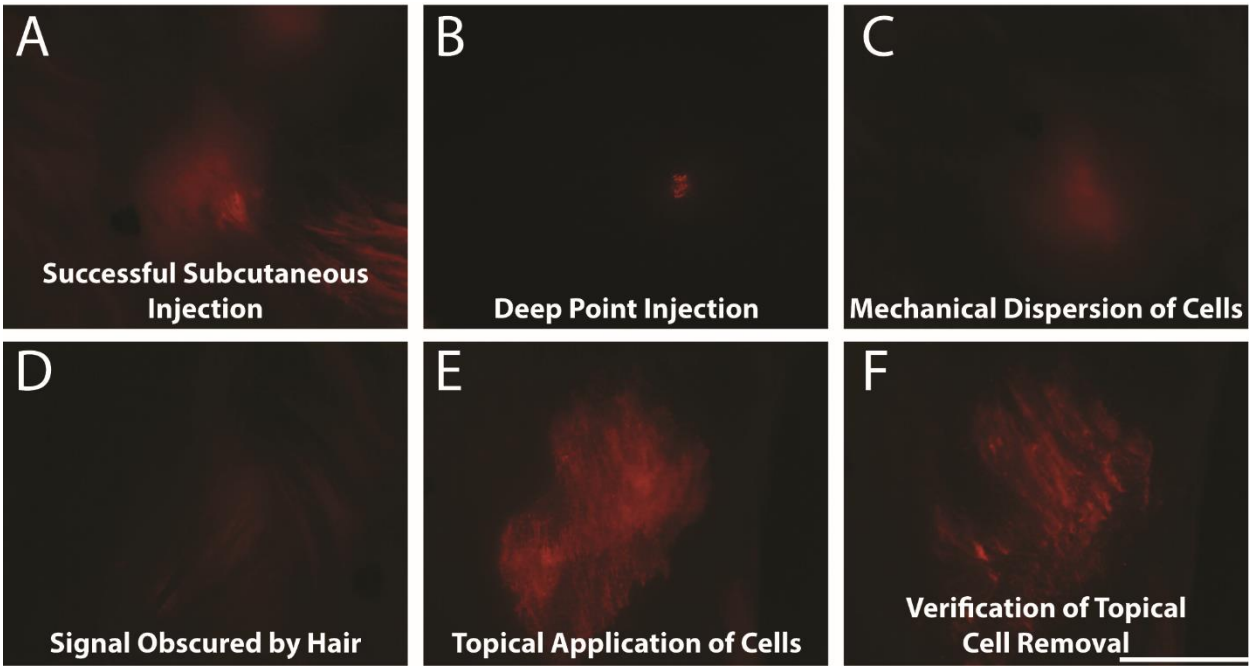

Figure 38. Dino-Lite imaging to document and characterize quality of cell application *in vivo*. (A) Subcutaneous point injection of 150,000 mCherry-MSC. (B) Deep point injection 7 mm into mouse tissue. (C) Point injection of cells with subsequent mechanical stress applied to tissue causing cell dispersion. (D) Point injection where cell signal has been obscured by mouse hair. (E) Topical squirt out of cells onto mouse skin. (F) Verification of topical cell removal. Scale bar 3 mm.

Serial imaging to track persistence of cell product

Validation of initial application of cells is useful but continued tracking of cells over time is also important for verification of relative cell decline throughout the duration of the study, particularly for slow healing models of disease. We sought to determine if we could successfully track MSC decline in TallyHo mice after topical delivery on a gelatin scaffold or via subcutaneous injection in the margins of an excisional wound (Figure 39A,B). 15-week-old TallyHo mice, with advanced hyperglycemia and impaired wound healing (78 ± 12% remaining wound area at day 7 post-wounding), were wounded with two 5 mm full excisional wounds and each wound was stented as shown in Figure 39A. A sub-therapeutic dose of MSCs was administered on a scaffold topically or without a scaffold via subcutaneous injection the day after wounding (Day 1). As can be seen in Figure 39, the PBS and scaffold only groups had minimal background signal while both MSC groups were bright 3 days after injection. In the free MSC groups, fluorescent signal declined over time (Figure 39) whereas MSC signal in the topical scaffold administration remained relatively constant (Figure 39D (i)). However, over the course of study, several mice were able to remove much of the cell-laden scaffold and this was documented with the Dino-Lite fluorescent imaging system (Figure 39D (ii)). Thus, in addition to initial confirmation of cell delivery, the Dino-Lite was useful in tracking the relative decline of cell numbers present within a particular wound site. As the *in vivo* imaging is qualitative, the assessment was most useful in comparing time points within the same animal allowing for detection of cell product removal due to scratching from the mice.

Discussion

In the current study, we have shown when compared side-by-side with an Odyssey scanner, the handheld Dino-Lite microscope performed similarly while providing significant logistical advantages. Several manufacturers sell handheld fluorescent microscopes for less than $1,000 making it an accessible technology for most labs. In addition, the small footprint of the microscope and ability to operate off a laptop allows the microscope to be used in the operating suite, eliminating transport of the animal to an imaging suite. This has significant advantages in reducing the stress experienced by research animals, which can have dramatic effects on the animal's health. This technique can readily be adapted to larger animal models where other imaging modalities may not be available due to scanner size constraints. Finally, while the

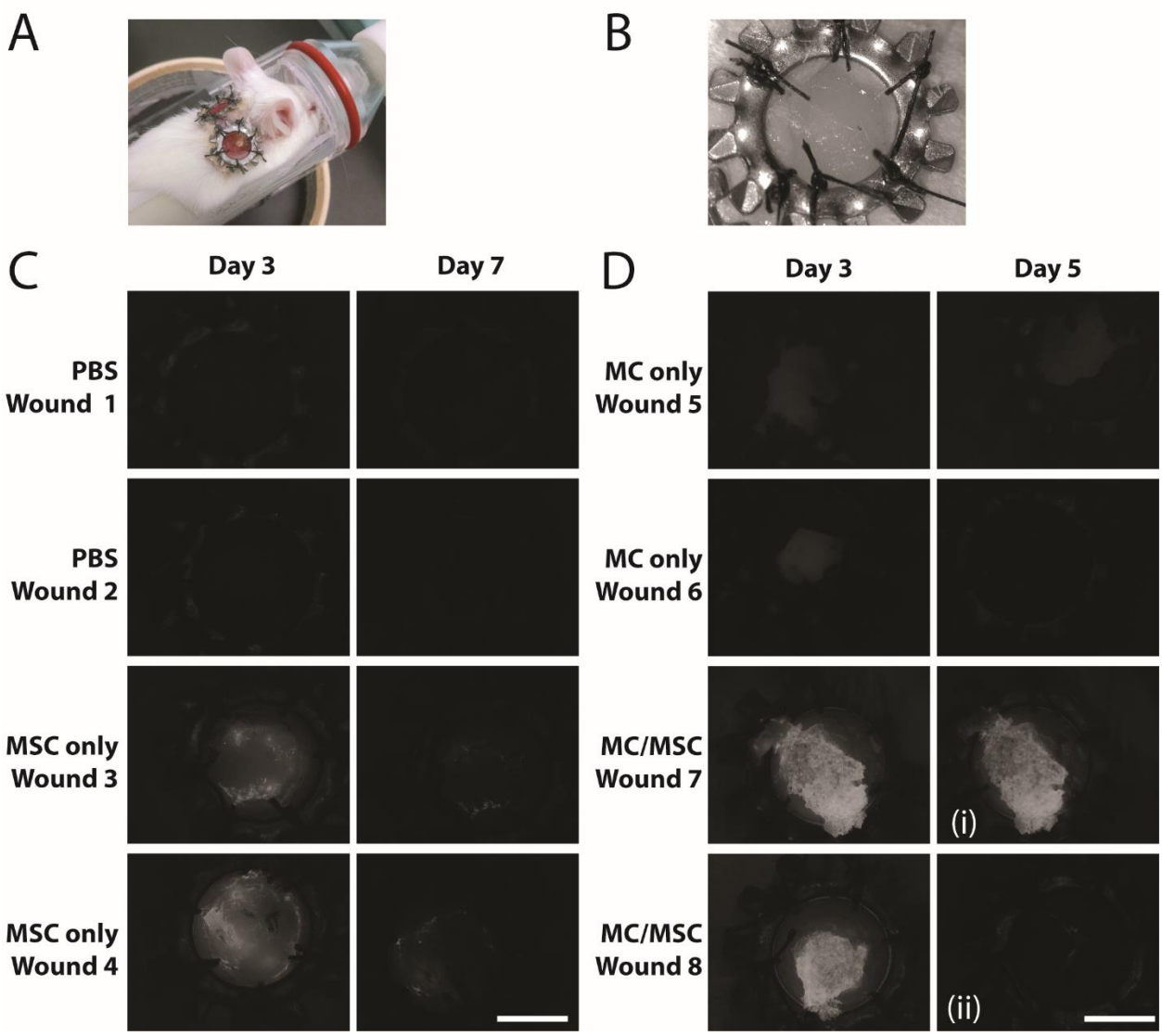

Figure 39. Fluorescently labeled MSCs can be tracked multiple days *in vivo*.

(A) TallyHo mice were wounded, injected with PBS, and wound tissue was harvested on day 7 and 14. After creation of wounds, metal washers (6.5 mm ID) were sutured in place to prevent wound closure and provide an image alignment reference. (C) Representative fluorescent Dino-Lite images of mCherry labeled MSCs (400,000 cells) over study for PBS and MSC only at 3 and 7 days after wounding. (D) Validation of MSC-scaffold scratch out detection; (i) indicates wounds without detected scratch out and (ii) indicates wounds with scratch out detected. Scale bar 3 mm.

maximum range of detection of handheld microscopes is not as large as whole animal imagers like IVIS or Odyssey, the acquisition time is significantly shorter as each wound can be imaged in less than a minute with relatively high resolution and sensitivity (Figure 35). Therefore, bright field and fluorescent images can be acquired on the operating table allowing for immediate feedback on the quality of cell administration. As we have shown, both Dino-Lite and Odyssey systems have a linear relationship between fluorescence and number of cells under ideal conditions (Figure 35) and both systems have a non-linear relationship *in vivo* (Figure 36C,D) due to tissue absorption and cell distribution. With this non-linear monotonically increasing trend, we compared the correlation between the two curves and found that the spearman correlation and p-value were $r = 0.885$ and $p<0.001$, respectively, indicating a high degree of similarity in dose response of both techniques. Table 3 compares and contrasts a fluorescent handheld microscope compared to alternate imaging modalities. Collectively, this data validates that the Dino-Lite is able to detect fluorescently labeled cells with similar sensitivity to the Odyssey system and with the additional logistical benefits outlined in Table 3 and discussed above demonstrates the utility of the Dino-Lite as a valuable tool for validation of cell delivery and tracking of cell retention in dermal wounds.

As handheld microscopes feature a single fixed filter set and exposure durations up to 1 second, advanced planning is required to maximize the performance of the system. Figure 40 outlines the process of designing a study using a hand-held microscope and the discussion below is focused on highlighting options and considerations that will impact the performance of the technique. Parameters such as mouse strain, route of cell delivery, size of wounds, and study duration are dictated based on the hypothesis being tested and should be considered first. The skin color of the mouse and rate of hair growth, which is dependent on strain, will impact the degree of optical interference. While the duration of tracking needed and expected persistence of cells in the wound bed will influence choice of labeling strategy. Wounds <6 mm in diameter can readily be imaged at magnifications of <50x (Figure 34B) but if a lower magnification is used, the sensitivity of the system will drop, which may necessitate an increase in labeling intensity. In addition, as demonstrated above, the dose of cells (Figure 35) and depth of injection (Figure 37) also impact the sensitivity of the imaging system. Thus, in the planning stage, each of these parameters should be considered, and the impact of the therapeutic strategy on the

Table 3. Comparison of imaging modalities.

	IVIS	Odyssey	Handheld Microscope
Resolution	**20-50 microns**	**21-337 microns**	**4.6-15 microns**
Field of View	**3.9-25 cm square**	**Up to 25 cm square**	**Up to 1.95 cm x 1.56 cm**
Setup time	**5-10 minutes**	**5-10 minutes**	**1 min**
Acquisition Time	**1-10 seconds**	**20-30 minutes/animal**	**0-1 second**
Spectral Flexibility	**Bright Field Luminescence Multicolor Fluorescence**	**2-Color Fluorescence: 700-900 nm**	**Bright Field Single Fluorescent Color**
Price Range (depends on configuration)	**>$100,000**	**>$10,000**	**<$1,000**
Portable	**No**	**no**	**yes**

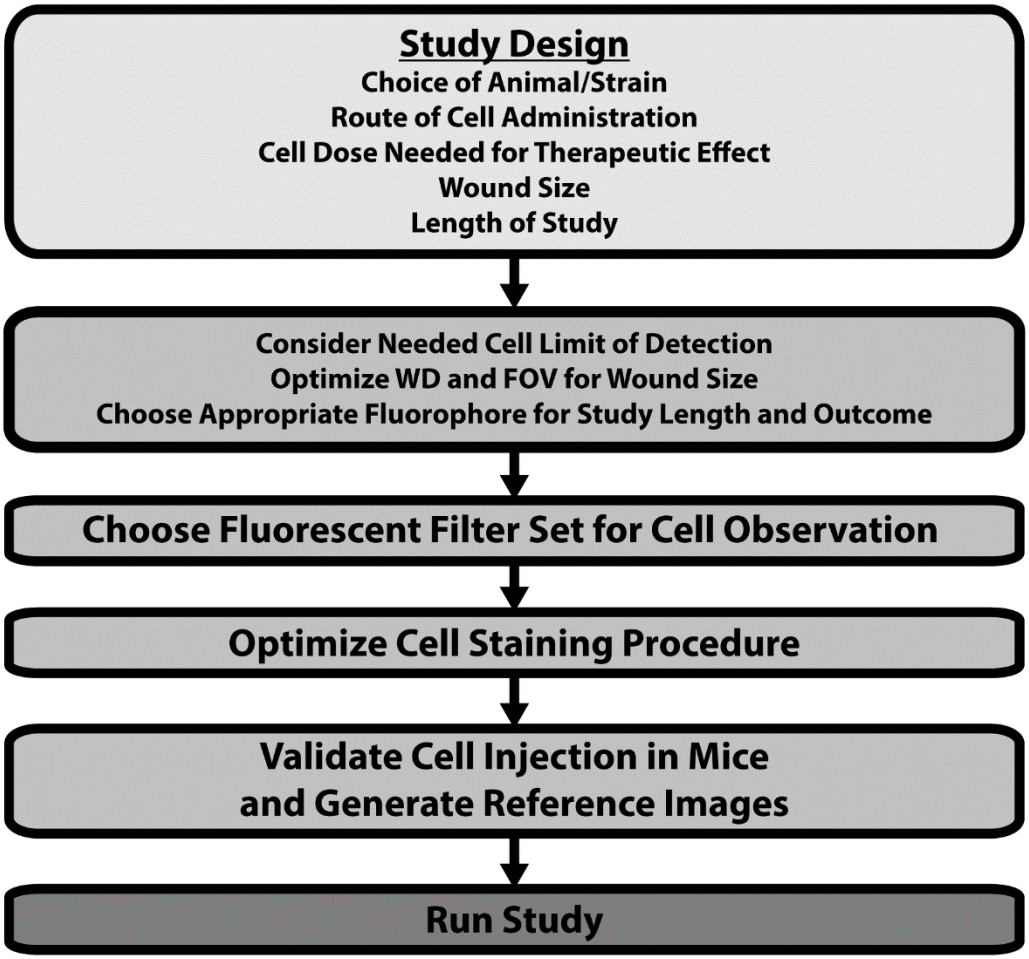

Figure 40. Workflow to tailor cell labeling and handheld microscope parameters to study needs.

ability to image the cells should be considered when selecting the labeling technique to ensure adequate sensitivity is achieved.

Many labeling strategies exist for *in vivo* cell tracking, but each have advantages and disadvantages that need to be considered in light of the overarching goals of the experiment. For cell tracking *in vivo*, far-red emitting dyes allow for minimal light scattering and absorption in the tissue allowing for greater depths of penetration. These dyes mainly fall into three categories: chemical dyes, fluorescent proteins, and quantum dots (Table 4). Chemical dyes consist of membrane dyes (e.g. DiR, PKH26, Claret) and cytosolic dyes (e.g. CellTrace) which have been validated for *in vivo* cell detection[8,9]. These dyes have the advantage of rapid labeling (<1 hour), require no viral or transfection reagents, and dye concentrations can easily be adjusted to gain greater sensitivity. However, these dyes can transfer to other cells and be diluted during cell division making them non-ideal for systems where transplanted cells undergo proliferation or studies where dye transfer events may dominate and cause an overestimation of cell retention. Fluorescent proteins overcome this problem as only living cells with the vector are capable of producing the fluorescent protein and fluorescent transfer is therefore unlikely. The downside of fluorescent proteins is they typically require several days to establish stable expression and many cell types are difficult to transfect and in some instances, fluorescent proteins can have an effect on cell function and immune detection[10]. Alternatively, quantum dots have been developed with UV excitation and emission spectra in the red-NIR wavelengths. Quantum dots are brighter and more photostable than traditional fluorophores and can be functionalized to allow for rapid labeling of cells (<1 hour). Quantum dots are, however, pH sensitive and contain heavy metals, which can cause toxicity issues if they degrade[11]. Since quantum dots are typically attached to the cell membrane or internalized into the cell, like membrane and cytoplasmic dyes, they are diluted in proliferating cells and vulnerable to being transferred to neighboring cells. Regardless of the choice of label, labeling procedures should be tested prior to use to ensure that they do not negatively affect the function and lifespan of the cells *in vivo* when compared to unlabeled cells.

After an appropriate fluorophore is chosen for the study objective and duration, an appropriate handheld microscope which matches the spectral characteristics of the fluorophore can be selected. The Dino-Lite system utilized in the current study has a narrow band-pass excitation filter optimized for mCherry. In situations where biomaterials are auto-fluorescent, custom filter-sets with narrow bandwidths optimized for specific fluorophores can be used to

Table 4. Selection of compatible fluorescent tracers (pros/cons).

Type of Tracer	**Advantages**	**Disadvantages**
Chemical Dyes (e.g. DiD, DIR, PKH26, Claret)	Rapid, viral free, easily titrate intensity.	Signal dilutes with cell division, potential for transfer to neighboring cells
Fluorescent Proteins (e.g. mCherry, mNeptune)	Degraded when cell dies	Potentially interferes with biological processes
Quantum Dots	Multiple far-red emission spectra available. Rapid labeling	Cytotoxic, signal decays in cellular environment.

minimize auto-fluorescence. With a dye and microscope selected, the staining procedure can be optimized to enable detection of a desirable range of cell numbers. Care should be taken during labeling optimization to evaluate both sensitivity of detection, as well as the impact of labeling on cell viability and function. Cell staining can be adjusted to allow for more sensitive detection of cells in higher numbers; however, this optimization comes at the expense of a higher limit of detection.

Prior to data collection, the handheld microscope should be calibrated to ensure the same magnification is used at each time point. Using a calibration grid to measure number of pixels over a known distance or a reference object, such as a metal washer stent, work well to calibrate the microscope. For imaging of stented wounds, the stent helps ensure the region of interest is within the FOV and that the wound is directly facing the camera. During validation, both a cell number standard curve using the optimized labeling strategy and a series of reference images depicting a successful application of cells should be generated in order to judge whether future cell applications have been successful. As seen in Figure 38. Dino-Lite imaging to document and characterize quality of cell application *in vivo*., different profiles of cell distribution generate distinct patterns that can then be used to determine if a cell product has been administered as intended. During the study, not only can relative cell decline be measured by comparing images of the same injection site at different time points, but it can also be determined if the animals disturb or remove part of the treatment (Figure 39).

In this study, a fluorescent handheld microscope could detect cell numbers with similar sensitivity, detection limit, and linear response as a fluorescent whole-body scanner. The handheld microscope's additional logistical advantages, namely portability and speed, made it an accessible and valuable tool to validate and track cell product delivery to wounds. The handheld microscope was affordable, rapidly captured images, and could be brought directly to the surgical suite minimizing transport of animals. Like the traditional whole animal scanner, the handheld microscope quantified changes in cell number under ideal conditions while providing qualitative information *in vivo*. The handheld microscope distinguished between differences in depth of injection, cell number, cell squirt out, and removal of cells. With appropriate planning and preparation to identify fluorophores, staining conditions, and filter sets, the handheld microscope is a powerful technique that makes the routine validation and documentation of cell product delivery to wounds practical and accessible to all labs.

Conclusion

In contrast to traditional imaging systems, the technique presented here is affordable, portable, and fast. This makes it accessible for all labs, reduces animal handling, and is fast enough to be used to validate every injection. The innovation of this technique lies in its ease of use, accessibility, and speed that make it both technically and logistically valuable as a routine documentation system for cell therapy. This is a significant advancement that enables careful, routine documentation of every cell injection in pre-clinical models, leading to significantly increased rigor in the development of cell-based wound therapies.

Key Findings

- The Dino-Lite had a linear response to fluorescently labeled cell number similar to that of the Odyssey system.
- Depth of injection of the cell products produced distinct fluorescent patterns
- The hand-held microscope could detect different types of injections including point injections, topical cell application, and dispersion of cells over time from a point injection.
- Fluorescent microscope imaging could detect cell decline and scratch out of cells in a model of diabetic wound healing.

5.3. REFERENCES

1. Baltzis, D., Eleftheriadou, I. & Veves, A. Pathogenesis and Treatment of Impaired Wound Healing in Diabetes Mellitus: New Insights. *Adv. Ther.* **31**, 817–836 (2014).
2. Singh, N., Armstrong, D. G. & Lipsky, B. A. Preventing Foot Ulcers in Patients With Diabetes. *JAMA* **293**, 217 (2005).
3. Dominici, M. *et al.* Minimal criteria for defining multipotent mesenchymal stromal cells. The International Society for Cellular Therapy position statement. *Cytotherapy* **8**, 315–317 (2006).
4. Kim, J. H. & Saxton, A. M. The TALLYHO Mouse as a Model of Human Type 2 Diabetes. in *Animal Models in Diabetes Research* **933**, 75–87 (Humana Press, 2012).
5. Kim, J. H. *et al.* Phenotypic characterization of polygenic type 2 diabetes in TALLYHO/JngJ mice. *J. Endocrinol.* **191**, 437–446 (2006).
6. Wang, X., Ge, J., Tredget, E. E. & Wu, Y. The mouse excisional wound splinting model, including applications for stem cell transplantation. *Nat. Protoc.* **8**, 302–309 (2013).
7. Li, Y. *et al.* Primed 3D injectable microniches enabling low-dosage cell therapy for critical limb ischemia. *Proc. Natl. Acad. Sci.* **111**, 13511–13516 (2014).
8. Lo Celso, C. *et al.* Live-animal tracking of individual haematopoietic stem/progenitor cells in their niche. *Nature* **457**, 92–96 (2009).
9. Xu, C. *et al.* Tracking Mesenchymal Stem Cells with Iron Oxide Nanoparticle Loaded Poly(lactide-co-glycolide) Microparticles. *Nano Lett.* **12**, 4131–4139 (2012).
10. Ansari, A. M. *et al.* Cellular GFP Toxicity and Immunogenicity: Potential Confounders in in Vivo Cell Tracking Experiments. *Stem Cell Rev. Reports* **12**, 553–559 (2016).
11. Ansell, D. M., Holden, K. a. & Hardman, M. J. Animal models of wound repair: Are they cutting it? *Exp. Dermatol.* **21**, 581–585 (2012).

APPENDIX A: TECHNIQUES FOR CREATING AND ANALYZING MESENCHYMAL STROMAL CELL SPHEROIDS *IN VITRO*

A.1. OVERVIEW

This chapter outlines methods to create and analyze *in vitro* MSC cell aggregates which have been shown to mimic phenotypic shifts that occur *in vivo* in the setting of localized delivery. We show that while hanging droplets have been used for over a decade to produce MSC aggregates or "spheroids", there are several other techniques which can be used to form MSC spheroids including low-attachment plates, encapsulation of cells in alginate, spheroid forming plates, bi-phasic PEG-dextran solutions, and gelatin-alginate gels. Each technique has unique advantages and limitations, which must be considered when choosing a method. Additionally, we provide an optimized method to extract spheroid RNA as well as describing tips and tricks for staining, performing XTT, sectioning, and disassociating spheroid MSCs. Finally, since it is difficult to determine spheroid MSC number in assays and cultures with spheroids and other cells. Therefore, we describe a method to determine spheroid volume which can be used to calculate total cell number using ImageJ.

Appendix A.4 is an adaptation one peer-reviewed article published on October 4, 2018 *Physiological Reports*. Adapted with permission.

Harata, M., Liu, S., Promes, J. A., **Burand, A. J.**, Ankrum, J. A., & Imai, Y. (2018). Delivery of shRNA via lentivirus in human pseudoislets provides a model to test dynamic regulation of insulin secretion and gene function in human islets. **Physiological Reports**, 6(20), e13907. https://doi.org/10.14814/phy2.13907

A.2. METHODS FOR FORMING SPHEROID MSCS

Authors: Anthony J. Burand Jr., Lauren Boland, Lin Di, and James A. Ankrum

Abstract

The study of MSCs *in vivo* has shown that in localized delivery they behave radically different from their adherent counterparts grown on tissue culture plastic. This has led to the advent of 3D *in vitro* MSC culture systems to better mimic the phenotypic changes that occur *in vivo*. While there are many methods available to create these 3D cultures termed spheroids, it can be difficult to compare across different methods of spheroid formation. We demonstrate six different methods for spheroid formation along with an analysis of strengths and weaknesses of each. These techniques differ on scalability, cost, ease of learning the technique, and consistency of MSC spheroids. In addition, this study provides details on how some common cell biology techniques such as immunohistochemistry, XTT, viability staining, and membrane staining can be adapted for a diffusion limited MSC spheroid system.

Introduction

Mesenchymal stromal cell (MSC) spheroids can be formed *in vitro* using several different techniques each with different benefits. One of the most common methods utilizes gravity to force cell-cell compaction into spheroids. This technique known as the hanging drop method utilizes cells in suspension plated onto a lid of a cell culture dish which is then inverted to allow for cells to be drawn down apex of the droplet[1]. Void of other surfaces to attach to, the cells will aggregate together forming a "spheroid" structure. While there have been a number of resources published on the hanging droplet technique, it requires some technique, therefore, several manufacturers have created non-adherent or low-protein binding culture vessels to simplify the spheroid formation process. Additionally, advances in microfluidic and 3D printing technology allows for assembly of cell aggregates with and without the presence of biomaterials. Many of these techniques require specialized equipment or culture materials which can be costly for researchers, but lower-cost options may have result in inconsistencies in spheroid size which can vary their properties and lead to inconsistencies in experimental results.

Following formation of spheroids, common downstream analysis of spheroids includes RNA expression, protein expression, secretome, and interactions with other cells. Analyzing spheroid MSCs presents a challenge for several techniques due to diffusion gradients present within spheroids[2]. While small molecules can easily diffuse into spheroids, larger molecules, proteins, and antibodies do not readily diffuse into the core of spheroids making immunohistochemical analysis difficult. Therefore, optimization of current cell biology techniques and development of new analysis methods are needed for these 3D culture systems.

Herein, we describe six methods which can be used to form spheroids and compare the strengths and weaknesses of each to provide a tool to help researchers choose which spheroid forming technique will work for their system. Additionally, we briefly describe some of the spheroid analysis tools available and where assays used for adherent monolayer culture systems need to be optimized for 3D culture of MSCs.

Materials

Cell culture reagents

- MSC source (we used a commercial bone-marrow source from RoosterBio)
- MEM-α (Fisher Scientific, Cat # BW12-169F)
- FBS (VWR, Cat # 97068085)
- Penicillin/streptomycin (Thermo Fisher, Cat # 15140122)
- PBS without calcium/magnesium (Caisson Labs, Cat # PBL01-6X500ML)
- EDTA (Quality Biological, Cat # 351-027-721)
- Accutase (Fisher, Cat NC9464543)

Spheroid formation materials

- 100 mm petri dishes (Fisher, Cat # FB0875712)
- 96-well spheroid microplates (Corning, Cat # 4515)
- Calcium chloride (Sigma, Cat # C8106)
- Barium chloride (Sigma, Cat # 217565)
- Sodium alginate (Sigma, Cat # A1112)
- Reagent reservoirs (Argos, Cat # EW-04395-27)
- 40 μm cell strainers (Thermo Fisher, Cat # 222363547)
- 6-well low attachment plates (Corning, Cat # CLS3471)
- Polyethylene glycol, 35 kDa (EMD Millipore, Cat # 8.18892.1000)
- Dextran, ~500 kDa (Fisher, Cat # AAJ6370218)
- Gelatin Type A (Fisher, Cat # G8-500)

Procedures

Spheroid MSC Formation

Hanging Droplet Method (HDM)

1. Resuspend cells in growth media at a concentration of 0-5 million cells/mL. For a 20,000-cell spheroid, resuspend at 1 million cells/mL.
2. Pipette 10-50 μL of cell suspension as drops on the inside of a petri dish lid leaving 0.5" around the perimeter. Droplets should be spaced between 0.5-2 droplet diameters apart. For a 20,000-cell spheroid, pipette 20 μL droplets. A 10 cm petri dish can fit fifty to one hundred 20 μL droplets.

   Critical Step: Must be done rapidly to prevent MSCs from becoming stressed and dying.

   Critical Step: Droplets larger than 50 μL are difficult to keep from running off the lid when flipped and droplets smaller than 10 μL will evaporate rapidly killing the MSCs. 20 μL droplets are the easiest to handle.

   Scaleup: May use a 12-channel pipette, but the spacing between droplets will need to be larger to prevent droplets from running together
3. Pipette at least one row of 20 μL sacrificial droplets made of complete growth media around the cell droplets to prevent evaporation and loss of cell viability.

   Critical Step: Media containing some serum must be used as the proteins in the serum increase surface tension and help prevent droplets from running.
4. Add PBS to the bottom of the petri dish. For a 10 cm dish, use 10-20 mL of fluid.

   Optional: Sterile water can be used to reduce cost.
5. Place the petri dish lid in the palm of the hand and invert the petri dish lid using a single fluid arc motion. Place on top of the PBS filled bottom.

   Critical Step: Practice inverting the petri dish lid using media without cells to learn motion and prevent droplets from running together.
6. Carefully place petri dishes in incubator and incubate 1-3 days.

   Critical Step: Spheroids typically become fully formed and compacted in 2-3 days. Manipulating spheroids before 2 days may result in shearing the spheroids into pieces or having high numbers of cells in suspension which will result in a mixture of monolayer and aggregated MSCs in future cultures. Leaving 20,000-cell spheroids for more than 3 days without transferring them into new media can result in cell death.

7. Confirm spheroid formation visually or by microscope. 20,000-cell spheroids are visible to the eye and are approximately 500 μm in diameter.
8. Transfer the spheroids using a 200 μL pipette tip cut partway up to make an orifice large enough to allow for the spheroid to not get lodged.
   Critical Step: The tip should be cut straight with a sharp razor blade to prevent microscopic jagged plastic pieces from catching and retaining spheroids. The tip should not bend or become crazed while cutting.
   Critical Step: Pre-wet cut tip with warm complete media to coat the inside of the tip with proteins and prevent spheroids from sticking.

Low-Attachment Plates (LAP)

9. Warm media in low-attachment dishes.
10. Add MSCs to low attachment dishes. Typically for a 24-well plate a density of 10,000 cells/cm2 will allow for spheroid formation.
11. Allow cells to incubate for 2-3 days. Longer time can result in larger spheroids.
    Critical Step: Moving the low-attachment dish during the spheroid formation step can result in more inconsistent spheroid sizes as spheroids can bump into each other and coalesce together.
12. Media should be changed every 3-4 days depending on cell density.

Alginate Encapsulation (AlgE)

13. Prepare a 100 mM calcium chloride solution and sterile filter with a 0.2 μm syringe filter. Warm solution at 37°C prior to use.
14. Prepare a 2% (w/v) sodium alginate solution in complete growth media and sterile filter with a 0.2 μm syringe filter.
    Critical Step: Ensure alginate is fully dissolved in the media or it will not go through the filter.
15. Resuspend cells at 4-8 million MSCs/mL in complete growth media.
16. Mix the cell suspension with the alginate solution at a ratio of 1:1.
17. Load an insulin syringe with alginate-cell suspension.
18. Add the calcium chloride solution to a reagent reservoir.

19. Dispense fluid slowly until a small droplet appears at the end of the syringe tip.
    Scaleup: An electrostatic bead generator may be used to rapidly produce alginate spheres.
20. Touch droplet to the surface of the calcium chloride solution to allow surface tension to pull droplet off the tip of the syringe. The droplet should sink rapidly to the bottom of the calcium chloride solution.
    Critical step: Extended time in calcium chloride is stressful to MSCs, so every 10-20 minutes collect alginate spheres and transfer them into complete growth media before continuing to make more.
21. Collect alginate spheres by straining them through a 40 μm cell strainer and then using a microspoon to collect spheres from reagent reservoir and cell strainer.
22. After alginate sphere are transferred into growth media, incubate for 1-2 days to form spheroids.
23. Use a microscope to confirm spheroid formation within the alginate spheres.
    Optional: Spheroids may be released from the alginate solution adding 20 μL of a 350 mM EDTA in PBS without calcium/magnesium solution with ~100 μL of alginate spheres and pipetting vigorously. Alginate spheres must be washed well in PBS without calcium/magnesium to remove excess calcium ions.

Spheroid Forming Plates (SFP)

24. Resuspend cells in complete growth media. For 20,000 cell spheroids, resuspend cells at 100,000 cells/mL.
25. Add 200 μL of cell suspension to appropriate wells in 96-well spheroid plate.
    Optional: The plate may be spun at 300-500g for 5 minutes to facilitate spheroid formation.
26. Incubate MSCs for 1-3 days to form spheroids.

PEG/DEX Separation (PDS)

27. Create 4% (w/v) polyethylene glycol (PEG) and 4% (w/v) dextran (DEX) solutions in complete growth media. Sterile filter with a 0.2 μm syringe filter.
    Critical Step: Gently rock solutions to completely dissolve the reagents prior to filtering.

28. Resuspend MSCs in DEX solution.

    Optional: The PEG and DEX solution can be interchanged (i.e. cells can be resuspended in the PEG solution and the DEX solution used in the cell culture plate). Generally, resuspending in DEX, will result in more defined droplets of cells when placed into the PEG solution.
29. Add PEG solution to cell culture plate.
30. Use a 2 µL pipette tip to dispense 0.5-2 µL droplets into the PEG solution.

    Critical step: In order to get the full cell solution out, it works best to submerge the pipette tip before dispensing the cell solution.
31. Place plate in the incubator for 2-3 days for spheroid formation.
32. Use a microscope to verify spheroid formation.

    Optional: To disrupt the bi-phasic solution after spheroid formation, diluted media by a factor greater than 4 with complete media.

Gelatin-Alginate Gel Injection (GAGI)

33. Make a 6% (w/v) gelatin and alginate solution in PBS without calcium/magnesium.

    Critical step: Heat solution to 80°C to dissolve both reagents.

    Optional: Alginate and gelatin concentrations can be varied to meet the desired stiffness and fluidity of the mixture. A 6% gelatin-alginate solution will set firmly when cooled to 37°C.
34. Sterile filter the solution shortly after heating to prevent gelling in the filter unit.
35. Add 3 mL of solution to a 6-well plate and allow gel to cool and set.
36. Resuspend cells in complete growth media and load into insulin syringe.
37. Inject 5-50 µL of cell solution into different parts of the gel.

    Critical Step: For easy imaging, injections should be close to but not on the bottom of the cell culture plate.
38. Add 3 mL of warm growth media to the top of the gel and place in incubator for 1-2 days for spheroid formation. Verify spheroid formation using microscope.

    Optional: If desired, a membrane permeable dye such as Hoechst can be added to the top of the gel and allowed to diffuse and stain the cells.

Spheroid Disassociation into Single Cell Suspension

39. Collect spheroids into a 1.5 mL microcentrifuge tube.
    Critical step: Put no more than 800,000 spheroid MSCs into each tube as exceeding this may reduce the effectiveness of the disassociation reagent.
40. Wash spheroids three times with PBS without calcium/magnesium to remove media.
    Critical step: Do not pipette spheroids into the pipette tip as they will stick to the interior of the pipette tip.
    Critical step: Add PBS vigorously down the side of the tube so that spheroids are dislodged from the bottom of the tube and media gets diluted.
    Critical step: Allow spheroids to settle to the bottom of the tube between washes.
41. Remove as much PBS as possible from the spheroids and add 1 mL of Accutase.
    Optional: A trypsin-EDTA solution may be used as well to disassociate the spheroids.
42. Gently invert the tube and lay on its side in a 37°C incubator so that spheroids line the length of the tube and do not cluster at the bottom of the tube.
43. Incubate for 4 minutes.
44. Remove spheroid tube from the incubator and pipette solution very vigorously with a 1 mL pipette for 30-120 seconds.
    Critical step: Keep pipetting until the spheroid appear considerable smaller than they were initially.
45. Incubate cells for an additional 4 minutes to complete the disassociation.
    Optional: A 40 μm cell strainer can be used to remove larger non-disassociated cell debris.
46. Neutralize, spin cells in a centrifuge, and resuspend cells in complete growth media.
    Optional: Count cells for downstream applications. It is important to note that many spheroid MSCs are sheared and damaged in this procedure so you should only expect a 30-60% recovery of viable cells.
    Optional: As antibodies do not penetrate spheroids well, surface marker or intracellular staining should be done at this point. For staining with a membrane intercalating dye, it is recommended that staining be done prior to spheroid formation as this results in a better cell yield at the end.

Optional: XTT reagent will crystalize and precipitate in spheroids, therefore, after spheroid dissociation, plate dissociated cells for 4-16 hours as adherent cells in a 96-well plate and perform the XTT assay.

Optional: For histological analysis, whole spheroids can be either fixed with 10% (w/v) neutral buffered formalin and mounted in paraffin or mounted in OCT and flash frozen before sectioning. Paraffin embedded samples should be deparaffinized prior to staining. H&E can be performed or if immunohistochemistry is desired, antigen retrieval such as sodium citrate should be used prior to antibody staining.

Troubleshooting

Table A.1. Troubleshooting spheroid formation methods.

Step	Problem	Possible Reason	Solution
5	Droplets run together when the lid is inverted	Droplets are too big	Reduce Droplet volume
		Droplets are too close together	Space droplets further apart
		Too much acceleration or deceleration during lid inversion	Use a circular fluid motion to invert the lid, not starting or stopping abruptly
7-8	Instead of a spheroid, there is a haze of MSCs or when transferring spheroids, they break up into a single cell suspension	Spheroid plating took too long and MSCs became stressed	Make fewer spheroids at a time and keep the rest in the incubator
		There was too much evaporative loss in the droplets causing the cells to dye	Place droplets closer together and place 2-3 rows of sacrificial droplets around the cell containing droplets
8	Even after pre-wetting the pipette tip, spheroids still stick to inside	MSC donor is more adherent to plastic	Pull up fewer spheroids at a time into the pipette and immediate dispense into new container to prevent them from having time to adhere to the tip plastic

Table A.1 – Continued

			Pipette up and down forcefully into the receiving media to dislodge spheroids from the inside of the tip
11	Spheroids are too small or too big	Initial seeding density was not optimized	Try a range of seeding densities to obtain the size spheroid desired
11	Polydispersity is very high	Non-homogenous cell suspension	Ensure the cell suspension in the well is well mixed prior to inserting into the incubator Do not swirl plate as this can result in a high concentration of cells in the center of the well. Instead use a linear shake to distribute cells.
14	Alginate will not go through syringe filter	Alginate is not well dissolved in the media	Sonicate, gently vortex, and heat solution at 37°C to help alginate dissolve
20	Alginate-cell solution will not dispense from syringe or droplets will not release from tip	Alginate is gelling at the syringe tip	Use a wipe to clean off the syringe tip
27	PEG or DEX solution will not filter	PEG or DEX is not fully dissolved into the media	Heat and shake at 37°C. Do not heat at higher temperatures or the media proteins may denature
30	No DEX droplets can be seen	Low contrast microscope PEG or DEX concentration is too low	Use a microscope with phase or DIC option Can increase PEG and DEX concentrations
32	Cells adhered to the plate instead of forming a spheroid	DEX droplets are too small	Increase volume of DEX-cell solution to make each droplet Use a non-tissue culture treated vessel

Table A.1 – Continued

34	Gelatin-Alginate solution will not filter	Solution gelled	Heat solution back up to 80°C and filter sooner after taking it off the heat
37	Cell Solution squirts out of the gel	Too much volume of cell solution added	Lower the volume of cell solution being injected Gently move the needle around to create a larger channel for the cells to sit in
38	No spheroids	Gel was not cool enough when cells were added	Allow gel to cool at room temperature and then warm up for 37°C

Expected Results and Discussion

One of the most commonly described protocols for formation of spheroid formation is the hanging droplet technique. However, there are many different techniques which can be utilized to obtain a similar result. One parameter varied to study spheroids is shape and size. As there are phenotypic differences between different sized spheroids, results can be more reproducible with spheroids of consistent size, but this can be less physiologically relevant. Therefore, to test the variability on spheroid size, we formed spheroids using the hanging droplet method (HDM), spheroid forming plates (SFP), low-attachment plates (LAP), alginate encapsulation (AlgE), bi-phasic polyethylene glycol-dextran separation (PDS), and injection of cells into a gelatin-alginate gel (Figure A.1). We found that spheroid forming plates and the hanging droplet method produced the most consistent spheroids, while low-attachment plates, alginate encapsulation of cells, and injection of cells into an alginate-gelatin gel produced highly variable spheroids. As can be seen in Figure A.1A and C, seeding density can tune spheroid size in formation techniques such as hanging droplets and low-attachment plates.

It is important to note that there are several other *in vitro* spheroid forming technologies available to researchers including microfluidic approaches, PDMS molds, and spheroid formation ECM. There are distinct advantages to these techniques, but here we focused on techniques that are low-cost, are accessible for most MSC researchers, require minimal specialized equipment or reagents, and do not need extensive prior training to execute. As can be

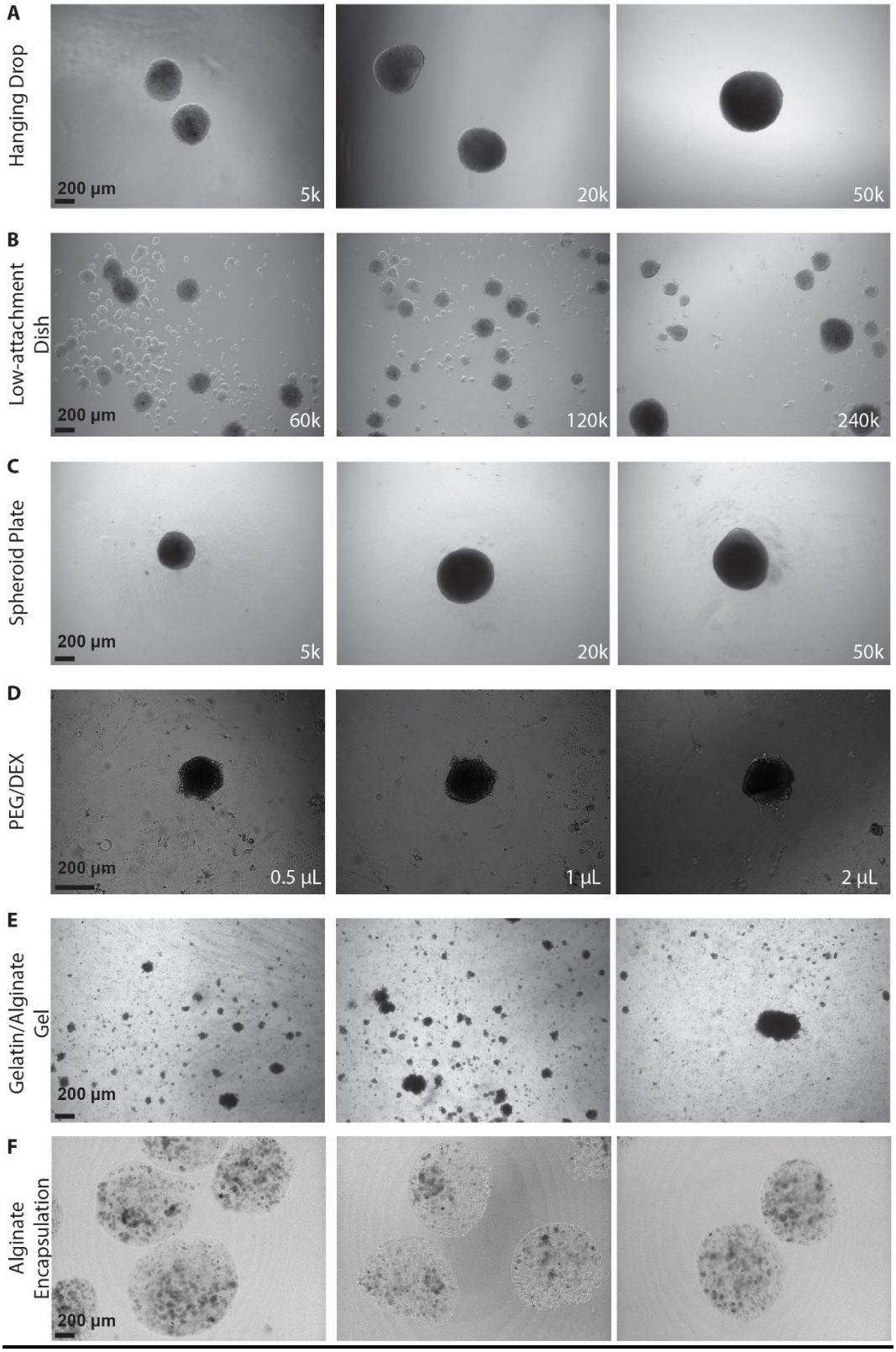

Figure A.1. Spheroids can be made through several methods.

Figure A.1 – Continued

(A) 5,000, 20,000, or 50,000-MSC spheroid form after 72 hours as hanging drops (HDM). (B) 60,000, 120,000, or 240,000-MSCs plated in a 6-well low-attachment plate (LAP) after 72 hours. (C) 5,000, 20,000, or 50,000-MSC spheroid form after 72 hours in a spheroid forming plate (SFP). (D) 10,000-MSC spheroids formed from MSC-dextran solution in polyethylene glycol solution after 72 hours (PDS). (E) Representative images of MSC injected into an alginate-gelatin gel and allowed for form for 72 hours (GAGI). (F) Representative images of MSCs encapsulated in alginate cross-linked with $CaCl_2$/$BaCl_2$ after 24 hours. All images are brightfield images.

seen in Table A.2, there is variation in technique cost, spheroid consistency, scalability, ease of handling, ease of culture, and the learning curve to master the technique.

After spheroid formation, endpoint analysis techniques must be carefully chosen, as there are significant complications to using some common biological assays with 3D culture methods. There is a significant diffusion gradient observed in spheroids preventing the transport of proteins and some molecules that would normally be easily transported to cells in a monolayer. Measuring metabolic function through assays such as XTT, can be an important in understanding how spheroid react to drug treatment. We found that spheroids treated with XTT, instead of the XTT remaining soluble in the media, the XTT reagent was converted and precipitated inside the spheroids (Figure A.2A). One additional complication with transferring spheroids for use in assays like XTT is the possibility of shearing the spheroid into multiple smaller components which may affect the spheroid count at the end (Figure A.2B). This can be mitigated through culturing spheroids in a vessel such as a spheroid plate that does not require movement of the spheroid or through avoiding vigorous pipetting steps which can lead to spheroid shearing.

Antibodies have high molecular weights in addition to electrostatic interactions making it difficult to get even staining in intact spheroids. However, immunohistochemical analysis of surface protein expression can be achieve through disassociation of spheroids into single cell suspensions as outlined in the methods above prior to using antibodies to probe for surface marker expression such as EP2 (Figure A.2C). Because enzymatic dissociation has potential to damage surface proteins, we also tested histological techniques such as fixation and embedding into paraffin as well as snap freezing in optimal cutting temperature compound (OCT). We found that both were able to preserve the spheroid structure and provide even staining for surface proteins and intracellular enzymes using immunofluorescent staining procedures (Figure A.2C,D).

Finally, for *in vitro* and *in vivo* cell tracking, it can be useful to label the cells with a fluorescent reporter such as a membrane intercalating dye. We found that there was a more even stain produced when spheroid MSCs were stained immediately prior to spheroid formation (Figure A.2E-G). It is important to note that these fluorescent aggregates were significantly brighter than stained adherent cells, making it difficult to observe other adherent cells stained with the same reagent mixed with spheroids without saturating our microscope detector. We

Table A.2. Comparison of common *in vitro* spheroid forming techniques.

Criteria	HDM	LAP	AlgE	SFP	PDS	GAGI
Is there a Learning Curve for the Technique?	Yes	No	Yes	No	Yes	No
What is the Minimum Time Needed to Form Spheroids?	2-3 days	2-3 days	1-2 days	1-3 days	2-3 days	1-2 days
What is the Technique Cost to Make 100 Spheroids?	~$2 ($)	~$11 ($$)	~$2 ($)	~$22 ($$)	~$2 ($)	~$2 ($)
Are Materials Needed that are not Standardly Used?	No	Yes	Yes	Yes	Yes	Yes
What are the Upfront Costs for Specialized Culture Reagents?	None	None	Yes, ~$75	None	Yes, ~$140	Yes, ~$70
Is Media Easy Exchange in 3D Culture System?	No	Yes	Yes	Yes	No	No
Are Spheroids Easy to Transfer to Other Cultures?	No	No	No	Yes	Yes	No
Is Caution Needed for Handling During Spheroid Formation?	Yes	No	No	No	Yes	No
Is Spheroid Size Controllable?	Yes	No	No	Yes	Partly	No
Is the Technique Scalable without Specialized Equipment?	No	Yes	No	Yes	No	No

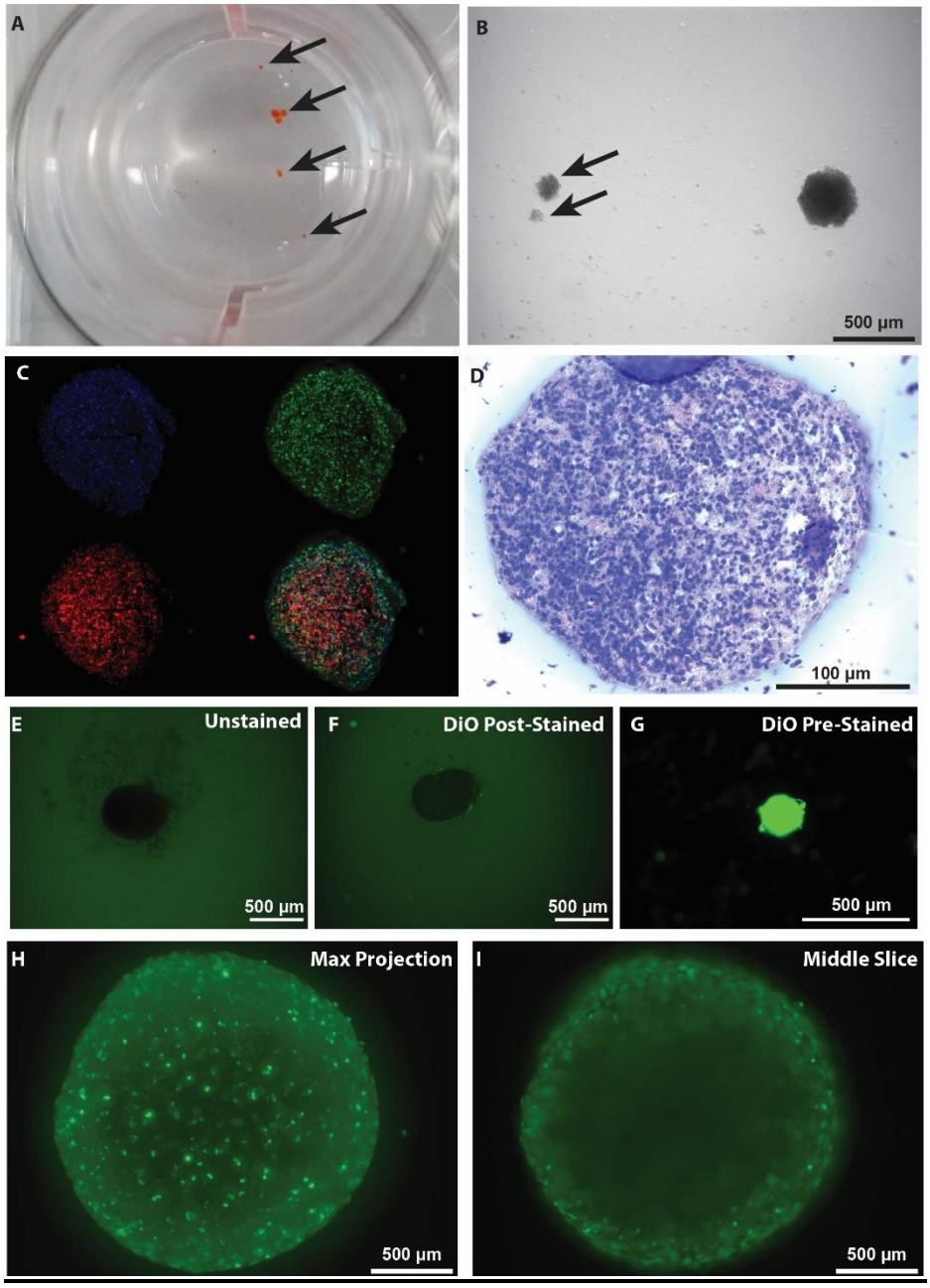

Figure A.2. Assays must be optimized for use with spheroid MSCs.

(A) Representative image of XTT precipitate in MSC spheroids denoted with arrows. (B) Representative image of spheroid sheared apart by pipetting denoted with arrows. (C) Representative image of IHC from a paraffin embedded spheroid. Blue is nuclei stained by Hoechst, green is TUNEL stain, and red is EP2 stain. (D) Representative image of spheroid embedded in paraffin stained with H&E. Representative image of MSC spheroid with no stain (E), with DiO stain after 72-hour spheroid formation (F), or with DiO stain of MSC prior to

Figure A.2 – Continued

spheroid formation (G). (H) Representative image of spheroid stained with Hoechst, z-stack imaged, and max projected. (I) Representative image of middle slice from spheroid in (H).

found that for fluorescent DNA intercalating viability stains such Hoechst and PI, these dyes readily diffuse into intact spheroids (Figure A.2H). However, there are depth limitations in imaging spheroid MSCs with a conventional fluorescent microscope due to scattering of light (Figure A.2I). If a more comprehensive analysis of all cells in spheroid is needed, we recommend dissociating the spheroid or using histological sectioning as described above. While total nuclear counts cannot be easily achieved with fluorescent microscopy, these images of the spheroid capture the cross-section of the spheroid since the cells in the outer layer of the spheroid are not subject to the extreme scattering present for cells near the core of the spheroid. This cross-section can be used to estimate the spheroid size and cell number as described in Appendix A.4.

Conclusion

As the number of techniques for 3D MSC culture continues to grow, researchers must be aware of the trade-offs present between techniques. As we have demonstrated, many of these techniques require different levels of experience and provide different consistencies in spheroid size. As these spheroids have diffusion gradients, care in selecting and adapting endpoint analysis techniques are critical to collection of high-quality data.

A.3. METHODS FOR EXTRACTING RNA FROM SPHEROID MSCS

Authors: Anthony J. Burand Jr., Lauren Boland, Lin Di, Shreya Ghimire, Alejandro A. Pezzulo, and James A. Ankrum

Abstract

3D MSC culture systems have become increasingly used as they can more accurately replicate *in vivo* phenotype of locally delivered cells. *In vitro* analysis of MSCs can be difficult due to cell compaction, loss of cell viability, and diffusion gradients present within the cell aggregates or "spheroids". Therefore, there is a need for optimization of existing molecular biological approaches for analysis of these spheroids. We optimized two RNA isolation protocols, which increases RNA yield from MSC spheroids reducing the number of cells required for gene expression analysis. Additionally, we compared the advantages and limitations of each protocol, showing that availability of reagents, cell disruption equipment, and cell number are important factors to consider when choosing an RNA isolation technique.

Introduction

3D culture systems for mesenchymal stromal cells (MSCs) have gained popularity for modeling *in vivo* phenotype[1]. While there has been substantial development of methods to form and culture MSCs in 3D, only recently have been optimized have many of the standard molecular biology techniques been optimized for these systems. There exists a significant diffusion gradient present in 3D MSC aggregates also known as spheroids[3], preventing rapid diffusion of large molecular weight reagents such as proteins and antibodies into these spheroids compared to their adherent monolayer counterparts. Another complication of spheroids is that upon aggregation, many of the cells upregulate caspase activity[1] indicating a cellular stress response or die[4,5]. This loss in viability can affect RNA extraction[6]. While there have been advances made in optimizing assays for imaging, measuring metabolic activity, viability, and cell cycle analysis in spheroid systems, there is still a need for optimization of RNA extraction techniques.

Herein, we describe parameters that affect RNA yield from spheroid using two different techniques, Trizol extraction and BSA-Igepal direct lysis. We show pitfalls with using these

techniques to extract RNA and how they can be overcome to increase RNA yield from MSCs in spheroids.

Materials

Cell preparation

- Mesenchymal stromal cells; we have used both umbilical cord and bone marrow sources
- MEM-α (Fisher Scientific, Cat # BW12-169F)
- FBS (VWR, Cat # 97068085)
- Penicillin/streptomycin (Thermo Fisher, Cat # 15140122)
- PBS without calcium/magnesium (Caisson Labs, Cat # PBL01-6X500ML)

RNA extraction and PCR

- Micro centrifuge tubes (VWR, Cat # 89000-028)
- Trizol (Thermo Fisher, Cat # 15596018)
- Non-acetylated BSA (Sigma, Cat # B6917)
- Igepal CA 630 (Sigma, Cat # I8896)
- Ultra-pure water (Thermo Fisher, Cat # 10977-015)
- Chloroform (Sigma, Cat # C2432)
- Isopropyl alcohol (Sigma, Cat # 190764)
- 200 proof ethanol (Decon Labs, Cat # 12R1001)
- RNeasy purification columns (Qiagen, Cat # 74104)
- High capacity CDNA kit (Thermo Fisher, Cat # 4368814)
- Power Sybr Green (Thermo Fisher, Cat # 4367659)

Equipment

- Tissue homogenizer (Omni International, Tissue Master 125 with 5 mm probe)
- Probe sonicator (Fisher, Cat # 15-338-528)

Reagent preparation

Igepal lysis reagent: Dissolve 10 mg non-acetylated BSA (0.1% (w/v)) and 30 mg Igepal CA 630 (0.3% (w/v)) in ultra-pure water. Can be stored at 4°C for 1 week.

Procedures

Spheroid RNA collection with Trizol

1. Spheroids should be collected into a 1.5 mL microcentrifuge tube.
2. Wash spheroids 2x with PBS.

   Critical step: Allow spheroids to settle to the bottom of the tube between washes.

3. Add 0.4 mL of Trizol per 100,000-1,000,000 MSCs
4. Homogenize samples at half speed for 10 seconds.
5. Extract RNA using manufacturer's protocol.

   Note: When using the direct lysis method, not further RNA extraction is needed.
6. Measure RNA concentration.

   Optional: RNA purification columns can be used to enrich RNA content and decrease DNA and protein contaminants.
7. Convert RNA to cDNA and run RT-PCR.

RNA extraction with BSA-Igepal direct lysis

8. Remove PBS from washed spheroids in Step 2.

   Critical step: PBS must be mostly removed. Dilution of the Igepal will result in less effective lysing of the cells.
9. Add 50 µL per 200,000-500,000 cells of Igepal reagent to each sample.

   Optional: Igepal reagent volume can be increased for larger number of spheroids.
10. Disrupt cells using a probe sonicator set at 30% power for 3-5 seconds.
11. Centrifuge samples at 8,000g for 10 minutes at 4°C to remove cell debris.

    Optional: Since the samples are highly impure, RNA purification columns can be used to enrich RNA content and minimize DNA and protein contaminants.

    Optional: If samples are purified on RNA purification columns, nanodrop can be performed to measure RNA content. Otherwise, fluorescent-based direct RNA measurement methods must be used due to the presence of DNA and protein in the samples. When using the direct lysis methods, RNA cannot be measured through photospectrometer methods such as NanoDrop due to the presence of DNA and proteins in the sample.
12. Convert RNA to cDNA and run RT-PCR.

Troubleshooting

Table A.3. Troubleshooting spheroid RNA extraction methods.

Step	Problem	Possible Reason	Solution
1, 8	Do not get many spheroids in the bottom of the tube	Spheroids are stuck in bubbles at the top of the meniscus	Close the cap and flick the tube to dislodge the spheroids
		Spheroids are stuck in pipet tip	Prewet the pipet tip with warm media and decrease time that spheroids sit in the pipet tip
3	Homogenizer tip will not fit	Did not use 5 mm micro-probe	Only the smaller probes will fit into the 1.5 mL tubes
		Did not use 1.5 mL microcentrifuge tube	Other tube sizes will not work with the 5 mm probe
4, 10	Spheroids are still present in the tube after homogenization/sonication	Spheroids did not get sheared apart by the homogenizer/sonicator	While homogenizing, move the probe up and down at a moderate speed to ensure disruption of spheroids
6	Low RNA yield	Not enough cells	Increase the number of cells used for RNA extraction
		Spheroids were not disrupted	Make sure spheroids are not visible after homogenization in step 4
12	Low housekeeping gene expression	Not enough cells	Increase the number of cells used for RNA extraction
		Spheroids were not disrupted	Make sure spheroids are not visible after homogenization in step 10
		Lysis reagent was old	Use reagent that is <1-week-old

Expected Results and Discussion

While there are well established techniques for RNA extraction from adherent and suspension cells, we wanted to determine if these standard unoptimized protocols using the Trizol extraction reagent would work for spheroid MSCs. First, we wanted to determine if RNA yield from spheroid and adherent MSCs was similar. We therefore collected RNA from the same number of adherent or spheroid MSCs and found that there was a significant difference in RNA yield between them (Figure A.3A). Since spheroids are large and similar to tissue samples, we used a probe sonicator to break up the spheroid cells. We wanted to test whether disruption of the cells was necessary or if it helped increase RNA yield. We saw that there was a significant improvement in RNA content when a probe sonicator was used to disrupt the spheroids (Figure A.3B). Because the lower RNA yield could be an artifact of the chosen sonicator settings, we varied both the power and duration of the sonication and saw that continuous 30% power setting for 10 seconds did not significantly impact RNA yield compared to sonication at lower power and shorter duration (Figure A.3C). While tissues can be disrupted with a probe sonicator, the sonication can also damage the RNA and therefore some researchers utilize tissue homogenizers to disrupt cells in tissue samples. When homogenized RNA yield and cDNA content of spheroid produced transcripts, GAPDH and PTGS2, were increased in two MSCs donors, but decreased in one donor compared to sonication (Figure A.3D-F).

Since homogenization produced the best RNA and transcript yield in our hands, we then sought to determine how RNA yield increased with spheroid cell number. We took 3, 5, 10, and 25 spheroids containing 20,000 cells and extracted RNA. As expected, more spheroids resulted in increased RNA (Figure A.4A). There was a significant effect of MSC donor on RNA yield (Figure A.4). Additionally, since spheroid size used in studies varies greatly, we sought to understand if there was an effect of spheroid size on RNA yield. Using 200,000 total MSCs, we measured RNA content from 5,000, 20,000, and 50,000 cell spheroids and saw that spheroid size did not seem to consistently impact RNA yield between all MSC donors (Figure A.4B). Therefore, the cell number used in RNA extraction for each MSC donor needs to be optimized for spheroid MSC RNA extraction.

Finally, while Trizol extraction is relatively simple and quick for a small number of samples, it can quickly become time intensive with large numbers of samples. We used a non-acetylated BSA-Igepal 630 solution that has been previously shown to allow for direct extraction

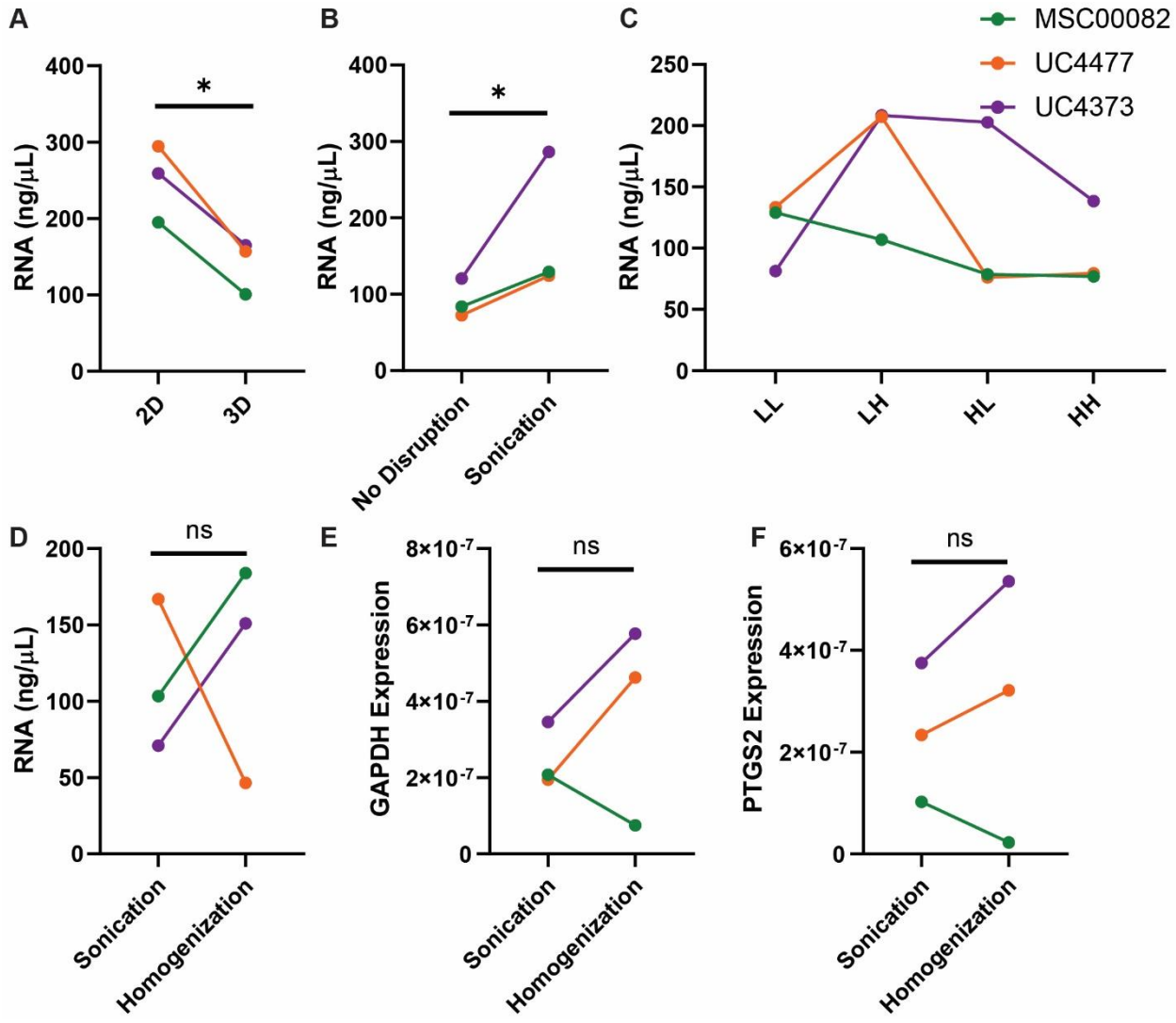

Figure A.3. RNA yield from spheroid MSCs can be improved through cell disruption. (A) Nanodrop measured RNA yield from 200,000 MSCs collected from either adherent (2D) or 20,000 cell-spheroid (3D) formats. (B) RNA concentration from 10-20,000 MSC spheroids in Trizol with or without sonication (30% power, 10 seconds). (C) RNA concentration from 10-20,000 MSC spheroids in Trizol sonicated at 4 different settings: LL (15% power, 3 seconds), LH (15% power, 10 seconds), HL (30% power, 3 seconds), and HH (30% power, 10 seconds). Comparison of RNA concentration (D) and GAPDH (E) or PTGS2 (F) cDNA expression (expression = 2^(-C_t) from 10-20,000 MSC spheroids either sonicated (30% power, 10 seconds) or homogenized (35,000 RPM, 10 seconds). *$p<0.05$

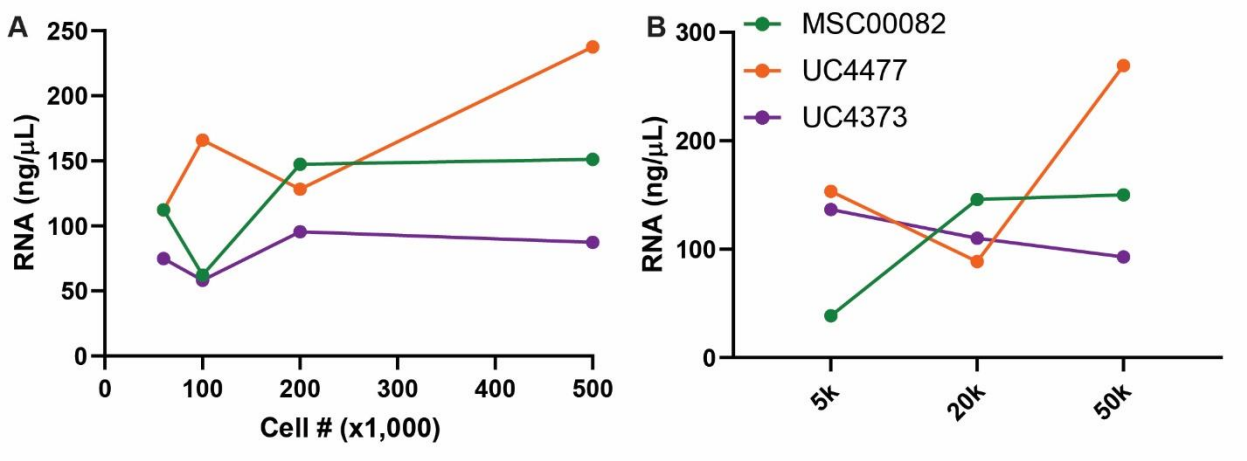

Figure A.4. MSC donor, cell number, and spheroid size lead to variability in RNA yield. (A) RNA concentration measured by NanoDrop for 20,000 MSC spheroids with a total of 60,000, 100,000, 200,000, or 500,000 cells. (B) RNA concentration of 200,000 total MSCs either as 5,000, 20,000, or 50,000-cell spheroids.

of RNA from cell pellets[7] in order to determine if we could reduce the time needed for extracting RNA from spheroid samples. Since previous reports did not utilize mechanical cell disruption[7], we tested whether use of a probe sonicator with the direct cell lysis buffer would improve RNA yield. We determined that probe sonication did significantly increase the transcript yield from spheroid (Figure A.5A) as we had seen when using the Trizol reagent (Figure A.3B). Comparing the direct cell lysis with Trizol extraction, we found that the direct lysis of cells did not yield the same number of transcripts as out optimized Trizol extraction method (Figure A.5B). Despite this, this method did significantly cut down on the RNA extraction time and cost per extraction, making it an attractive method for RNA extraction for high quantities of samples when the spheroid number is not limited (Table A.4). While the RNA extracted using the direct lysis method is highly impure containing proteins and some DNA, commonly available RNA separation columns can be used to further purify RNA for analysis.

Conclusion

RNA extraction for spheroid MSCs is a non-trivial process which requires significant optimization. Using cell disruption in addition to the lysis and RNA extraction buffer is critical in obtaining higher yield of RNA. The MSC donor choice can significantly impact RNA recovery. While Trizol is commonly used as an RNA extraction reagent, we demonstrated that a solution of non-acetylated BSA and Igepal 630 could also be used with an increased number of spheroids to quickly extract RNA from samples at a lower cost. However, even with optimized techniques, RNA yields from spheroids are significantly lower than those of adherent MSCs. While this optimization protocol was developed for MSCs spheroids, it could also easily be applied to other 3D culture systems including organoids.

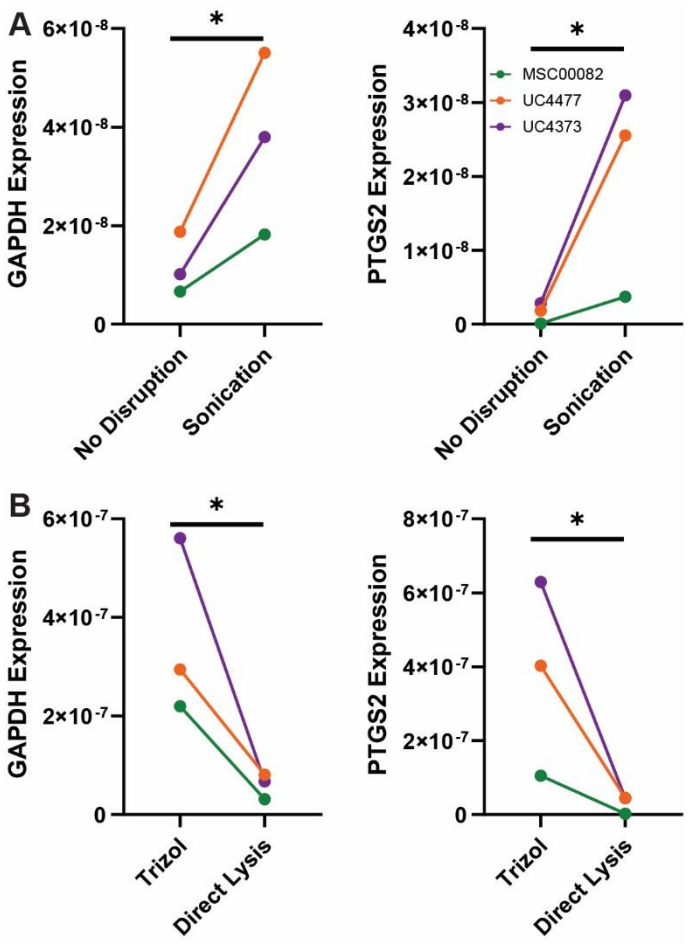

Figure A.5. Direct lysis of spheroid MSCs can be used to extract RNA.
(A) GAPDH or PTGS2 cDNA expression (expression = 2^(-C_t)) for 10-20,000 MSC spheroids in direct lysis buffer with or without probe sonication (30% power, 5 seconds). (B) Comparison of GAPDH and PTGS2 cDNA yields from 10-20,000 MSC spheroids lysed in Trizol with homogenization (35,000 RPM, 10 seconds) or direct cell lysis buffer with sonication (30% power, 5 seconds). *p<0.05

Table A.4. Comparison of Trizol and direct lysis techniques.

	Trizol	**Direct Lysis**
Cost for 200 extractions	~$200 ($$$)	~$23 ($)
Startup reagent cost	~$275 ($$)	~$85 ($)
Procedure time	~60 minutes (++)	~20 minutes (+)
RNA purity	++	-
RNA yield	++	+
Specialized Reagents	No	Yes

A.4. RAPID ESTIMATION OF MSC SIZE AND CELL NUMBER USING IMAGEJ

Abstract

3D culture methods to more accurately represent *in vivo* MSC behavior have grown rapidly in the past decade. While culture systems exist, which provide consistent 3D cell aggregates or spheroids, these techniques can be expensive and require transfer of spheroids to other culture vessels requiring many researchers to use methods which do not result in a consistent number of cells in each spheroid making it difficult to determine if the same number of cells were used in each downstream assay. While cells in a monolayer are easy to count, it can be difficult or impossible to easily count cells in 3D cultures. We developed an ImageJ script which is capable of measuring cross-section area of spheroids and estimating their total volume from an easily acquired fluorescent image of cell nuclei. We demonstrated that consistent with microscopy images, when the script is used to process islet images, intact islets showed greater variability in size compared to disassociated and re-aggregated "pseudoislets". This script could be adapted to work with bright field image in addition to fluorescent stains, further increasing the speed of determining cell content. While developed for estimating the size and number of pseudoislets, this procedure can be adapted for the measurement of spheroid MSCs.

Introduction

MSCs have been primarily characterized as adherent cells on tissue culture plastic since their discovery. However, in recent years, researchers have shown that in certain circumstances, such as local injection, MSCs alter their *in vivo* behavior from standard *in vitro* culturing conditions due to cell aggregation. This discovery to the development of 3D culture systems to replicate the *in vivo* phenotype. There are a host of 3D culturing methods for MSCs as described in Appendix A.2. While some of these methods like spheroid forming plates, microfluidics, and hanging droplets can produce consistent MSC "spheroids", several of these techniques are costly and not sustainable for every lab. Other lower-cost options can result in spheroids which a variable number of cells. Additionally, even with highly consistent spheroid forming methods, spheroids can be delicate. Therefore, manipulation or transferring them into other assays after formation can result in damage to the spheroid and loss of cells. This means that knowing an exact number of cells being added into an assay can be difficult to ascertain. There are a variety

of assays to determine cell content through DNA content, electron transport chain function, and nuclear counting, however many of these assays can be time consuming or are not currently optimized for use in spheroid systems. There is a need in the field for development of methods to inexpensively and rapidly validate spheroid cell number in a variety of assays. In this section, we will demonstrate an easy to use ImageJ script which can estimate islet volume through imaging on a light microscope, which can also be adapted for use in MSC spheroid systems.

Methods

Human islets

Human islets from nondiabetic donors from Integrated Islet Distribution Program or PRODO laboratories with reported viability and purity above 80% were cultured in CMRL1066 containing 1% human serum albumin (HSA), 1% Pen-Strep, and 1% L-Glutamate (1% HSA CMRL) overnight at 37°C and 5% CO2 upon arrival for recovery from shipping. Then, islets were divided into fresh, cultured-intact, or pseudoislets. While fresh islets were harvested on the next day, cultured-intact islets were maintained in CMRL1066 containing 10% heat inactivated FBS, 1% Pen-Strep, and 1% L-Glutamate (10% HI-FBS CMRL) for 1 week at 37°Cand 5% CO2 before harvesting. For pseudoislets preparation (Figure A.6A), single cell suspension was prepared first as follows. Human islets were washed once with PBS, digested with Accutase (A6964, MilliporeSigma, St Louis, MO) at 37°C for 5 min, pipetted through 1 mL tip for 15 times, digested for additional 4 min at 37°C, and passed through 40 μm strainer using a plunger of 1 mL syringe (Butcher et al. 2014). Filtered single cell suspension was counted, washed with PBS once, resus- pended in 10% HI-FBS CMRL at 102 cells/μL, and seeded in a 96-well spheroid microwell plate (Corning, Corning, NY) at 3000 cells/well. The microwell plate was centrifuged at 270g at room temperature for 7 min and cultured after addition of 100 μL/well of 10% HI- FBS CMRL at 37°Cand 5% CO2 until analyses. The study was reviewed by IRB at University of Iowa and approved as nonhuman study.

ImageJ analysis of islet size

Islets in 10% HI-FBS CMRL were incubated with 10 μg/mL Hoechst 33342 for 30 min at 37°C and 5% CO2. Then, Z-stack images captured by Leica DMi8 Microscope (Leica Microsystem, Buffalo Grove, IL) were analyzed with the ImageJ macro “Measure Spheroid

Shape.ijm."
(https://www.researchgate.net/publication/326844033_ImageJ_Macro_to_Quantify_Spheroid_Volume_and_ Size). The maximal intensity Z-stack was converted into a single plane and a binary threshold was applied to create a mask surrounding the islet cell mass. A series of erosions and dilations were performed to remove debris and the ImageJ plugin "Measure Particles" was used to find the dimensions of the islet fit using an ellipse approximation as well as directly measure the "Area" of the max projected islet cross section. The major and minor diameters of the calculated ellipse were then used to estimate the ellipsoidal volume of the islet that was defined as $V = (4/3)*pi*a*b^2$, where (a) is the major ellipse axis and (b) is the minor ellipse axis. Diameter was calculated as 0.5*square root of (area/p). The macro was run with the restrictions of circularity between 0.5 and 1 and islet area <18% of the total image area. Images which did not pass these quality control metrics were flagged, reviewed, and the image threshold was set manually.

Statistics

Data are presented as mean ± SEM or SD as specified. Differences of numeric parameters between two groups were assessed with Student's t-tests. Paired test was used when all values are paired between groups. Welch correction was applied when variances between two groups were significantly different by F test using Prism 7 (Graphpad, La Jolla, CA). A $P < 0.05$ was considered significant

Results

Pseudoislet area and volume can be measured through ImageJ script

As one of the primary advantages of pseudoislets is their relatively uniform size compared to native islets, we first assessed the variability of pseudoislet size compared with native islets for three human donors. Cross-sectional area of pseudoislets and intact islets was measured, and the ellipsoidal volume was estimated from Z-stack images of Hoechst-stained samples (Figure A.6A,B). Cultured-intact islets showed substantial variability in cross-sectional area and volume within each donor as well as between donors (Figure A.6C,D). As expected, pseudoislet size was highly consistent both within and between donors compared to intact islets. The coefficient of variation for cross-sectional area and volume across all donors

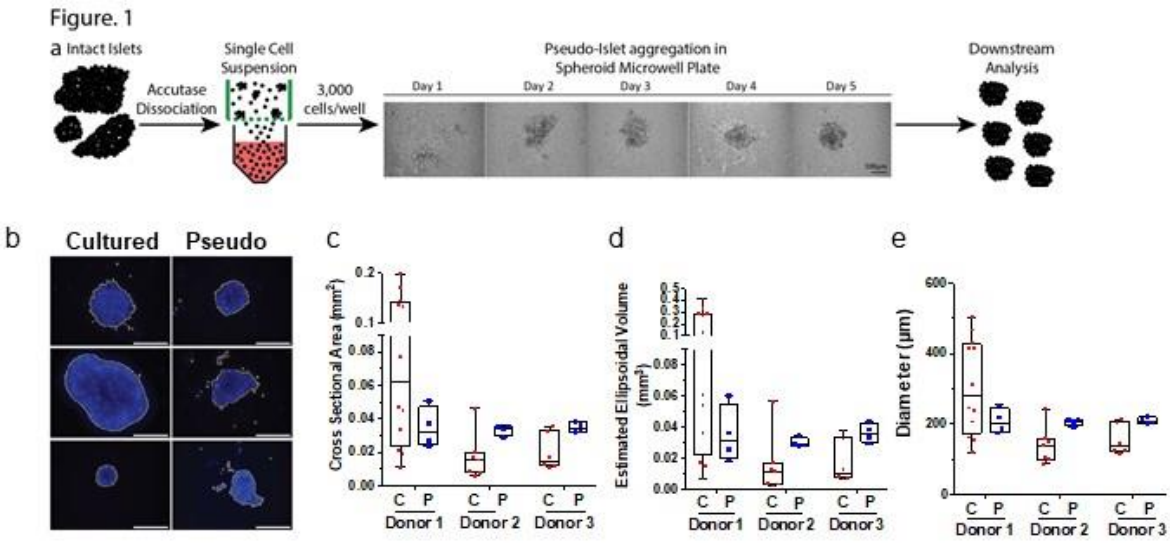

Figure A.6. Pseudoislets exhibit a narrower size distribution compared with cultured-intact islets.

(A) Pseudoislet formation process from fresh islets using spheroid microwell plates. (B) Representative images of pseudo or cultured-intact islets from donor 1 stained with nuclear dye Hoechst 33342 analyzed by ImageJ macro. Analysis marks shown in yellow. Scale bar = 250 μm. (C) Quantified cross-sectional area from cultured-intact C and pseudoislets (P) using max-projected fluorescent images analyzed by ImageJ macro. (D) Estimation of ellipsoidal volume of culture-intact or pseudoislets based on major and minor axis measurements extracted from fluorescent images by ImageJ macro. (E) Diameter of cultured-intact or pseudoislets obtained as in methods. Mean ± SEM, n = 12 (donor 1, culture-intact), 7 (donor 2, culture-intact), 6 (donor 3, culture-intact), 4 (all donors, pseudoislets).

was reduced from 89% (mean ± SD = 0.039 ± 0.035 mm^2) and 123% (mean ± SD = 0.057 ± 0.071 mm^3) for cultured-intact islets to 2.7% (mean ± SD = 0.034 ± 0.001 mm^2) and 9.8% (mean ± SD = 0.034 ± 0.003 mm^3) for pseudoislets. Average diameter of cultured islets from three donors varied from 141 ± 52 μm to 306 ± 134 μm, while that of pseudoislets were tightly distributed ranging from 199 ± 39 to 211 ± 9 μm (all mean ± SD) among three donors (Figure A.6E).

Discussion

Results from this study demonstrate that by using this ImageJ script, human islet size can be quickly and inexpensively measured. This program will take allows the user to select an input folder where the image files are stored and an output folder where data will be saved (Figure A.7). This script uses two quality control metrics to ensure that cell aggregates found are accurate, circularity of the cell aggregate and the percentage of the total image area the cell aggregate occupies (Figure A.7). Any violation of these user dictated quality control metrics will be noted in a log generated by the program and will allow the user to manually threshold the image to get a more accurate aggregate measure on images which do not work well with the default thresholding function in ImageJ (Figure A.8). The script will output the area, perimeter, estimated major ellipse diameter, estimated minor ellipse diameter, and estimated ellipsoid volume for cell aggregates. Additionally, the program outputs a maximum projected image with the outline of what it measured as the cell aggregate (Figure A.9). Current limitations of the script are that it will only process z-stack Leica files. Time courses and multiple channels are not supported, and the user must manually configure all images to fit this format. Additionally, the program finds the largest cell cluster in the image, therefore, there can only be a single cell aggregate in the field of view, else the image must be processed such that there is a single spheroid in each image. Blinded analysis is critical to avoid human bias when processing images. While the program does not require human input, if users review the images and manually adjust the threshold, that may introduce bias since the file names are displayed. It is recommended that users analyzing the data receive files which have been deidentified to prevent bias from occurring.

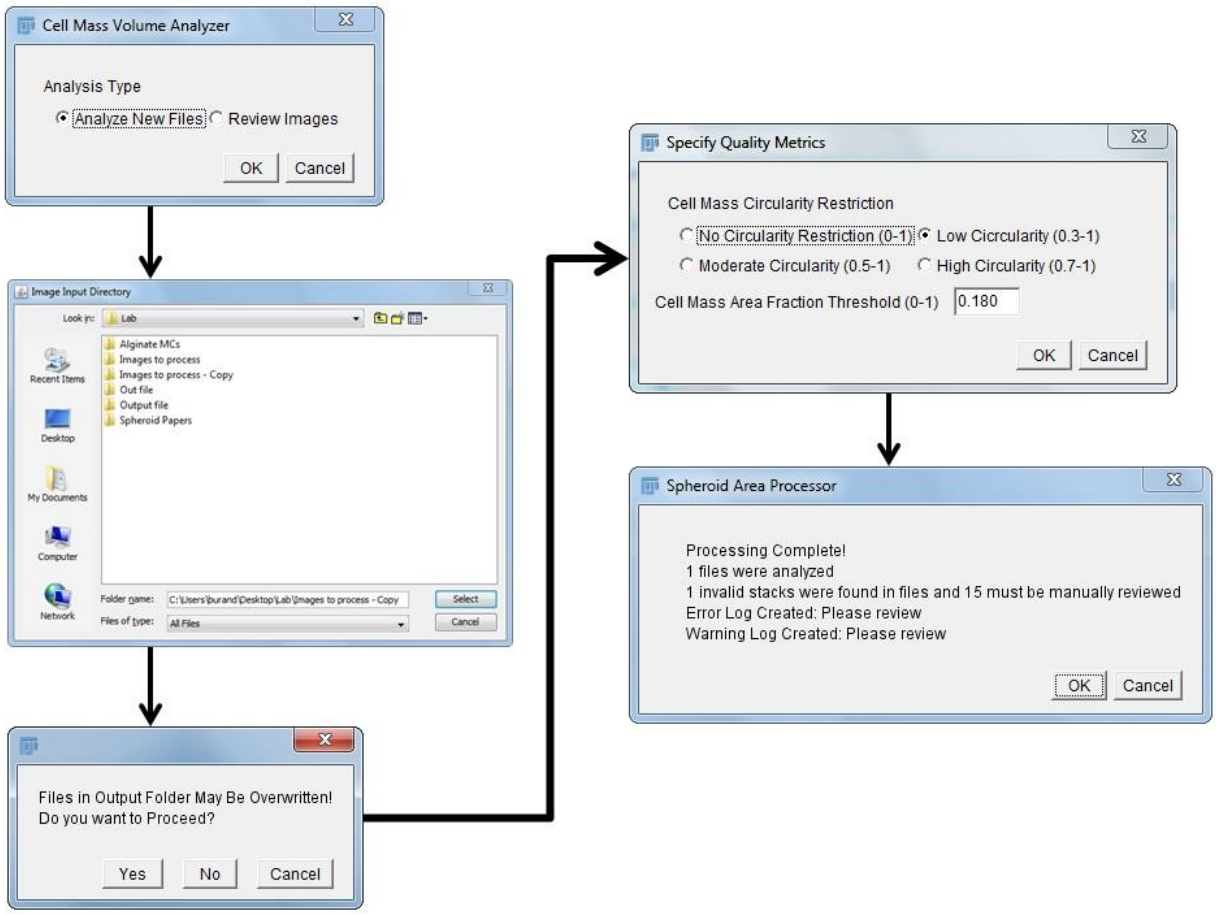

Figure A.7. ImageJ macro measures spheroid size from Leica z-stack .lif files.
Users can start a new analysis or go back to review an old analysis. All images should be deidentified and placed into one folder for analysis. The macro will allow users to define circularity of the cell aggregate and the fraction of the total image area the aggregate will maximally occupy as quality control metrics which the program used to flag images for user review.

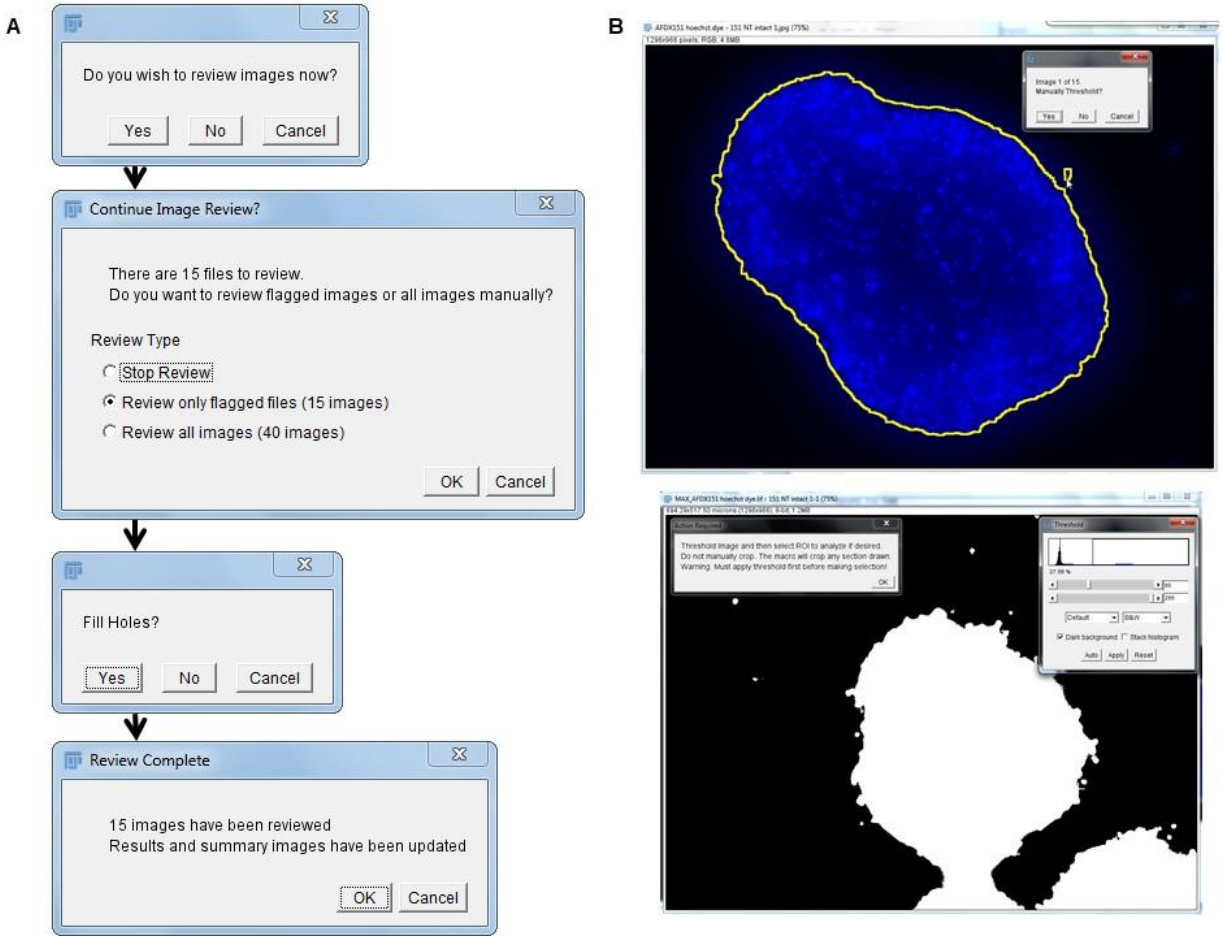

Figure A.8. Macro defined spheroid boundaries can be manually reviewed by the user. (A) During image review, users will have the option to review image which only failed the quality control check inputted during the initial analysis or review all the images. (B) The script will show the user where the cell mass boundaries were found to be (yellow outline), and the user can choose to manually change them. (C) If users manually threshold the image, the new thresholded image will be used in the analysis.

A

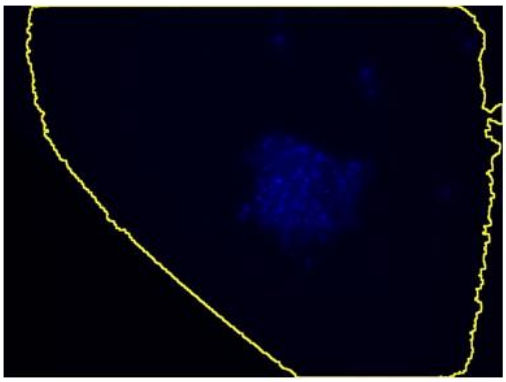

B

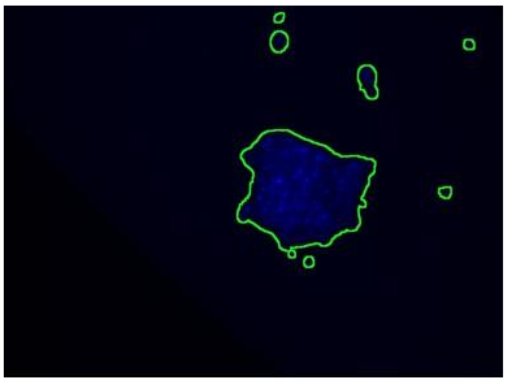

C

	A	B	C	D	E	F	G
1	Index	Area (microns^2)	Perim. (microns)	Major (microns)	Minor (microns)	Ellipsoid Volume (microns^3)	Warning
2	AFDX151 hoechst dye.lif - 151 NT pseudo1	24123.215	731.003	215.256	142.689	18357978.8	
3	AFDX151 hoechst dye.lif - 151 NT pseudo2	37727.106	965.985	267.982	179.25	36067211.1	
4	AFDX151 hoechst dye.lif - 151 NT pseudo3	27329.178	687.962	197.213	176.442	25717461.2	
5	AFDX151 hoechst dye.lif - 151 NT pseudo4	50725.448	1145.482	289.227	223.305	60412156.3	
6	AFDX151 hoechst dye.lif - 151 LV pseudo1	29186.863	998.899	233.265	159.312	24799057.1	
7	AFDX151 hoechst dye.lif - 151 LV pseudo2	31522.673	827.758	258.748	155.116	26078271.6	
8	AFDX151 hoechst dye.lif - 151 LV pseudo3	31524.108	823.374	210.531	190.65	32053708.4	
9	AFDX151 hoechst dye.lif - 151 LV pseudo4	30037.501	753.664	237.739	160.869	25771148	
10	AFDX151 hoechst dye.lif - 151 NT intact 1	144323.728	1582.681	517.587	355.03	273276366	TRUE
11	AFDX151 hoechst dye.lif - 151 NT intact 2	44946.621	856.547	253.422	225.82	54132455.7	
12	AFDX151 hoechst dye.lif - 151 NT intact 3	134016.777	1598.721	424.401	402.062	287376377	TRUE
13	AFDX151 hoechst dye.lif - 151 NT intact 4	11242.826	410.432	124.093	115.355	6916856.1	
14	AFDX151 hoechst dye.lif - 151 AV intact 1						Invalid picture: Couldn't process
15	AFDX151 hoechst dye.lif - 151 AV intact 2	51099.109	895.011	278.172	233.889	63741402.7	
16	AFDX151 hoechst dye.lif - 151 AV intact 3	24463.585	620.794	181.977	171.164	22332120.6	
17	AFDX151 hoechst dye.lif - 151 AV intact 4	33044.293	789.456	218.734	192.35	33899187.2	
18	AFDX151 hoechst dye.lif - 151 NT intact 1-1	82086.259	1551.172	364.448	286.777	125548872	Manual Threshold
19	AFDX151 hoechst dye.lif - 151 NT intact 1-2	174185.879	3008.744	587.564	377.457	350653966	Manual Threshold
20	AFDX151 hoechst dye.lif - 151 NT intact 1-3	20926.436	759.864	168.273	158.34	17671944.1	
21	AFDX151 hoechst dye.lif - 151 NT intact 2-1	197391.587	2521.563	637.742	394.089	414879766	TRUE
22	AFDX151 hoechst dye.lif - 151 NT intact 2-2	47679.338	1086.715	254.866	238.193	60570129.3	
23	AFDX151 hoechst dye.lif - 151 NT intact 3-1	136265.916	1976.245	446.614	388.477	282326448	TRUE
24	AFDX151 hoechst dye.lif - 151 NT intact 3-2	33747.992	843.31	211.802	202.874	36515012.2	
25	AFDX151 hoechst dye.lif - 151 NT intact 4-1	19147.96	613.164	166.072	146.803	14991838.2	

Figure A.9. Auto-threshold misidentification of cell mass can be corrected with a manual threshold.

(A) Example of the auto-threshold incorrectly identifying the islet mass boundary (outlined in yellow). (B) The manually thresholded image is marked in green to distinguish it from the auto-thresholded images. Only the largest aggregate will be used in the analysis. All other smaller cell clusters will be discarded. (C) Example output of islet area, perimeter, major/minor ellipse axis, and estimated ellipsoidal volume for each image. Warnings, errors, and notations for manual thresholding are indicated.

Despite some of these limitations, this script is versatile and can be used with simple modifications to measure cell aggregates in a variety of spheroid and organoid systems. While monolayer cells require brightfield microscopes equipped with phase rings or differential interference contrast (DIC) capabilities in order to clearly define cells, spheroids containing even a few hundred cells dramatically increase their optical density and will appear significantly darker even simply using a conventional brightfield microscope. This script currently is tailored for cell aggregates stained with a fluorescent nuclear dye, but due to the optical properties of cell aggregates, brightfield images could be processed to be usable with this script. Mainly through inverting the brightfield z-stack image before inputting it into the program. This program outputs an estimated aggregate volume based on an ellipse approximation of the cross-sectional area of the cell mass. This volume can be used as a normalizing factor in experiments to ensure similar number of cells were used. In addition, users can create a calibration curve of number of cells in an aggregate and the cross-sectional area to get an estimated number of cells present in each aggregate. Because of the increase in optical density of the cell mass, light is scattered, presenting conventional microscopy from being able to image all nuclei in aggregates containing more than a few hundred cells (see Figure A.2I). While this program cannot count total nuclei in the cell mass, however, the cross-sectional area of the aggregate is the only metric which can be easily obtained for larger cell masses with conventional microscopy.

Conclusion

As use of 3D culturing systems continues to increase, methods to validate cell number will become increasingly important to provide consistent results in assays. We created an ImageJ macro which allows for the identification and measurement of spheroid, islet, and organoid cell masses. This program can measure aggregate cross-sectional area and estimate aggregate volume using an ellipsoidal approximation. This simple rapid method can be used to further research efforts in 3D cell systems.

A.5. REFERENCES

1. Bartosh, T. J., Ylöstalo, J. H., Bazhanov, N., Kuhlman, J. & Prockop, D. J. Dynamic compaction of human mesenchymal stem/precursor cells into spheres self-activates caspase-dependent IL1 signaling to enhance secretion of modulators of inflammation and immunity (PGE2, TSG6, and STC1). *Stem Cells* **31**, 2443–2456 (2013).
2. Egger, D., Tripisciano, C., Weber, V., Dominici, M. & Kasper, C. Dynamic Cultivation of Mesenchymal Stem Cell Aggregates. *Bioengineering* **5**, 48 (2018).
3. Li, Y. *et al.* Three-dimensional spheroid culture of human umbilical cord mesenchymal stem cells promotes cell yield and stemness maintenance. *Cell Tissue Res.* **360**, 297–307 (2015).
4. Bartosh, T. J. *et al.* Aggregation of human mesenchymal stromal cells (MSCs) into 3D spheroids enhances their antiinflammatory properties. *Proc. Natl. Acad. Sci.* **107**, 13724–13729 (2010).
5. Ylostalo, J. H., Bartosh, T. J., Tiblow, A. & Prockop, D. J. Unique characteristics of human mesenchymal stromal/progenitor cells pre-activated in 3-dimensional cultures under different conditions. *Cytotherapy* **16**, 1486–1500 (2014).
6. Nguyen, Q. H., Pervolarakis, N., Nee, K. & Kessenbrock, K. Experimental Considerations for Single-Cell RNA Sequencing Approaches. *Front. Cell Dev. Biol.* **6**, 1–7 (2018).
7. Viet-Phuong Le, A., Huang, D., Blick, T., Thompson, E. W. & Dobrovic, A. An optimised direct lysis method for gene expression studies on low cell numbers. *Sci. Rep.* **5**, 12859 (2015).

APPENDIX B: CELLULAR ENGINEERING METHODS CAN ALTER MSC PHENOTYPE

B.1. OVERVIEW

The synergy between budesonide and spheroids shown in Chapter 4 appeared to be independent of direct modulation of MSC phenotype and acted directly on T cells. In this appendix, we test how prelicencing with the inflammatory cytokines and use of biomaterial scaffolds can directly modulate MSC phenotype. We found that prelicencing with IFN-γ did not alter expression of chemoattractant and growth factor production in spheroid MSCs consistent with the results seen in Chapter 2.3. However, we discovered that encapsulation of MSCs in an alginate scaffold induced a spheroid-like phenotype, which could be partly modulated using chemical modification of the alginate.

B.2. MSC PHENOTYPE CAN BE MODULATED WITH BIOMATERIALS

Authors: Anthony J. Burand Jr. and James A. Ankrum

Abstract

In local injection, MSC phenotype and secretome dramatically changes. While these changes have been shown to be beneficial, there are also cases where spheroid phenotype can be detrimental to their function. Despite this, there are a host of tools including prelicensing with inflammatory cytokines and biomaterial scaffolds which have been used to enhance elements of the MSC phenotype prior to transplant to improve their function in treating ischemic and inflammatory disease. We demonstrate that while IFN-γ treatment did not affect spheroid secretome, use of alginate and alginate chemically linked to gelatin could skew MSC secretome towards spheroid and adherent respectively. This study provides a framework for future research into engineering MSC phenotype pre-transplant for local injections.

Introduction

Mesenchymal stromal cells (MSCs) are influenced by environmental and chemical factors present both during cell culture and after transplant into patients. While some of these factors have minimal influence, a growing body of literature shows that there are several factors which can dramatically alter MSC efficacy *in vivo*. While MSCs produce many anti-inflammatory factors which can reduce inflammation, we and other have shown that environmental cues can shift MSCs to a pro-inflammatory phenotype, including LPS[1], palmitate[2], and inflammatory cytokines[3,4]. Because of the significant influence the host environment has on MSC phenotype, there has been a significant effort in discovering methods to polarize MSCs into an anti-inflammatory pro-regenerative phenotype to increase their efficacy as a cell therapy.

Two common methods to control MSC phenotype are through polarizing factors such as inflammatory cytokines and use of biomaterial scaffold. While many cytokines have been used to prelicense MSCs, the most common cytokine is IFN-γ as it has been shown to directly upregulate anti-inflammatory factors such as IDO, PGE2, TGF-β, and HGF.[5,6] Prelicensing with IFN-γ has been shown to improve MSC suppression of immune cells[7], mitigate proinflammatory

effects on MSCs due to palmitate[2], and increase mouse survival of GvHD[8]. Many biomaterials have been used to increase MSC survival and function *in vivo*. Gelatin microcarrier systems have been shown to prolong MSC presence in mice and reduce spontaneous limb amputation after a critical limb ischemic event.[9] Alginate has been used to encapsulate MSCs because it has low immunogenicity *in vivo* and it prevents direct interactions with immune cells.[10] There are many biomaterials and surface modifications to enhance cell attachment, substrate stiffness, cell viability, and cell proliferation to provide a more hospitable transplant environment in which MSCs can work. Both prelicensing and biomaterial scaffold are powerful tools to enable MSC phenotype control.

While chemical cues have been shown to modify MSC phenotype, biomechanical factors such as aggregation during local injection also substantially influence MSC properties as discussed in Chapters 3 and 4. Aggregated MSCs have been shown to upregulate immunomodulatory factors such as PGE2 and TSG-6.[11] Additionally, they have been shown to improve outcomes in mice which experienced ischemic stroke[12] or kidney damage[13]. However, as we have shown in Chapters 3 and 4, aggregated or spheroid MSCs can also exhibit a pro-inflammatory phenotype, which hinders their use as a cell therapy. The benefit of aggregated MSCs is context dependent. Therefore, further study in phenotype control of MSCs for local injection must been done to ensure a therapy which will benefit and not harm patients.

In this study, we wanted to test if these cell engineering tools could be utilized to control MSC phenotype in the setting of localized delivery. We tested the effect of IFN-γ prelicensing out affect inflammatory factor expression of spheroid MSCs. Additionally, we used modified alginate to encapsulate MSCs and test whether we could push the cell phenotype towards that of adherent or spheroid MSCs.

Methods

MSC culture

MSCs obtained from Rooster Bio (Lot #00082) were cultured in MEM-α supplemented with 15% FBS and 1% penicillin, streptomycin, and L-glutamine. Adherent cells were plated at 2,000-4,500 cells/cm^2 on tissue culture plastic. Adherent cells were harvested using accutase and used for experiment between passages 4-6. 20,000-cell spheroid were formed over 3 days using the hanging droplet methods as described in Appendix A.2.

IFN-γ prelicencing

20,000 MSC spheroids were formed as described above and then 60,000 total cells were transferred into a 6-well low-attachment plate (Corning) with 3 mL of media and then treated with or without 100 ng/mL IFN-γ. Spheroids were incubated at 37°C for 3 days prior to collection of the media.

Alginate preparation

A 2% (w/v) sodium alginate solution was prepared in media. To get alginate to dissolve, alginate in media was sonicated in a water bath sonicator for 30 minutes with occasional vortexing. In order to chemically link gelatin with alginate, we used a 1-Ethyl-3-(3-dimethylaminopropyl)-carbodiimide (EDC) and N-hydroxysuccinimide (NHS) reaction. Briefly, 0.5 mL of 4% (w/v) sodium alginate and 2% (w/v) gelatin were dissolved in HBSS buffer in separate microcentrifuge tubes. 20 mg of EDC and 12 mg of NHS were then dissolved in the sodium alginate solution and incubated for 15 minutes at room temperature. The alginate solution was then added to the gelatin solution and incubated with shaking for 2 hours. 500 µL of MEM was then added to quench the reaction and allowed to incubate for 2 hours. Another 4% (w/v) alginate solution was prepared in media. The chemically linked alginate-gelatin solution was added to the alginate solution at a ratio of 3:1. A control, non-linked solution of alginate and gelatin was prepared by dissolving 2% (w/v) alginate and 1% (w/v) gelatin in media. All solutions were filtered through a 0.4 µM syringe filter and stored at 4°C prior to use.

Alginate encapsulation

A MSCs were harvested and resuspended at 8 million cells/mL in the alginate or alginate-gelatin solutions. A cross-linking solution was prepared using 50 mM $CaCl_2$ and 1 mM $BaCl_2$. A repeating pipette was used to dispense 0.5 µL droplets containing 4,000 cells into the cross-linking solution as described in Chapter 2.2. A total of 100,000 cells or 25 alginate spheres were collected and transferred into 2 mL of warm media containing 100 ng/mL IFN-γ and 250 µM L-tryptophan in a 12-well plate for each condition. Equal numbers of adherent MSCs or 20,000-cell spheroid MSCs were plated as controls and treated with IFN-γ and tryptophan.

Secreted factor analysis

Media collected from prelicensed MSCs was analyzed using VEGF, bFGF, and IL-8 bead based ELISAs (BD) according to the manufacturer's protocol. For the VEGF and IL-8 bead ELISAs, media was diluted 5x and 50x respectively in assay diluent prior to running the assay. Standards were prepared for each analyte from 0 to 2,500 pg/mL. 50 µL of diluted (VEGF and IL-8) media, undiluted (bFGF) media, or standards was added to 50 µL of capture beads in microcentrifuge tubes and incubated for 1 hour at room temperature on an orbital shaker set at 500 rpm. Then, 50 µL of detection reagent was added to their respective tubes and the samples were shaken for an additional 2 hours. Beads were then diluted in 1 mL of wash buffer and spun at 200g for 5 minutes. Beads were resuspended in 150 µL of wash buffer before running them on an Accuri C6 flow cytometer. Sample concentrations were determined by fitting the mean fluorescent intensity of the standards to a 4-parameter logistic curve model and then back calculating concentrations based on the dilution factor.

PGE2 (R&D) and IL-1β (Biolegend) plate based ELISAs were used to measure factor concentrations in media collected from alginate encapsulated MSCs. Neither samples were diluted prior to the assay. PGE2 and IL-1β ELISAs were run according to the manufacturer's protocol with standards ranging from 0-2,500 pg/mL and 0-500 pg/mL respectively. Sample absorbances were read on a plate reader at 450 nm with a background correction at 570 nm. The background corrected absorbances for the standard curve was fit via linear regression to interpolate the sample concentrations.

A kynurenine assay was performed on the alginate-MSC media. In a 96-well plate, 200 µL of media or L-kynurinine standard (0-300 µM) prepared in media was added to 100 µL of 30% trichloroacetic acid (TCA) in water to precipitate proteins. The samples were heated for 30 minutes at 50°C to convert back to L-kynurenine. Samples were spun at 3,000g for 10 minutes and then 75 µL of sample was removed and placed into a new 96-well plate in duplicate. Samples were then mixed with 1.2% (w/v) 4-dimethylaminobenzaldehyde in acetic acid and incubated at room temperature for 10 minutes. Absorbance was read at 492 nm on a plate reader. Absorbances of the standards were fit with a linear regression curve to interpolate kynurenine concentrations.

Data processing

Data display and interpolation of standard curves for the bead based ELISAs was done using GraphPad Prism 7 and 8. A SpectraMax i3 plate reader from Molecular Devices was used to measure absorbances from the kynurenine and PGE2 assays. Data from the kynurenine assay was fit using linear regression on the plate reader. Interpolation of all other standard curves was done in GraphPad Prism.

Results

IFN-γ prelicensing does not alter the spheroid phenotype

There are numerous reports demonstrating the benefits of IFN-γ prelicensing of MSCs to produce a more anti-inflammatory and pro-regenerative phenotype, but we have seen that the benefit or prelicensing is context dependent. We wanted to determine if IFN-γ would increase growth factor production and decrease chemoattractant production in spheroid MSCs. We cultured spheroid and adherent MSCs and treated spheroid MSCs with a high dose of IFN-γ for 3 days to see whether prelicencing would alter their phenotype. We found that there was a difference between adherent and spheroid production of VEGF (Figure B.1A), a growth factor important in angiogenesis, and IL-8 (Figure B.1B), a known chemoattractant of neutrophils. There was no difference between adherent and spheroid MSC production of bFGF (Figure B.1C). When spheroids were prelicenced with IFN-γ, spheroids did not increase production of VEGF or decrease production of IL-8 (Figure B.1).

Biomaterials can alter MSC phenotype

While IFN-γ treatment did not affect spheroid phenotype, there is a large body of literature supporting the use of biomaterials to alter cell phenotype. Therefore, we wanted to determine if MSCs could be engineered through encapsulation in alginate to behave similar to spheroid MSCs. We encapsulated MSCs and tested their production of IL-1β, PGE2, and kynurenine. We have shown that spheroid MSCs decrease their production of kynurenine while increasing PGE2 production as described in Chapter 4.2 and other researchers have previously confirmed that IL-1β is produced by spheroid MSCs. We found that when MSCs were encapsulated in alginate, their secretome became similar to that of spheroid MSCs (Figure B.2A). However, we did not have enough data to confirm this by statistical analysis.

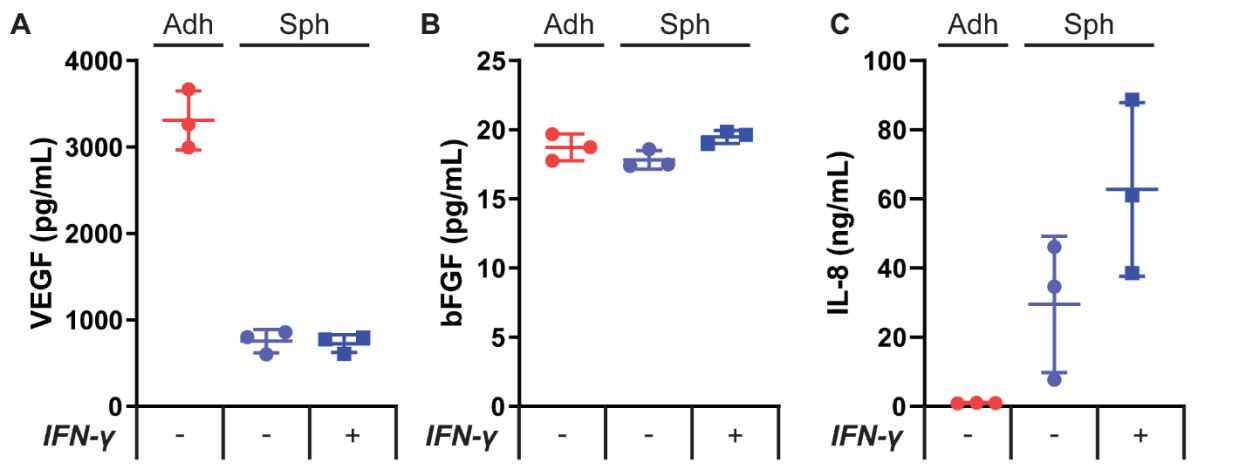

Figure B.1. Spheroid MSCs do not alter secretion of factors in response to IFN-γ. Spheroid MSCs were treated with 100 ng/mL IFN-γ for 72 hours prior to media collection. Media from adherent, spheroid, and IFN-γ treated spheroid MSCs was analyzed via a bead-based ELISA for VEGF (A), bFGF (B), and IL-8 (C).

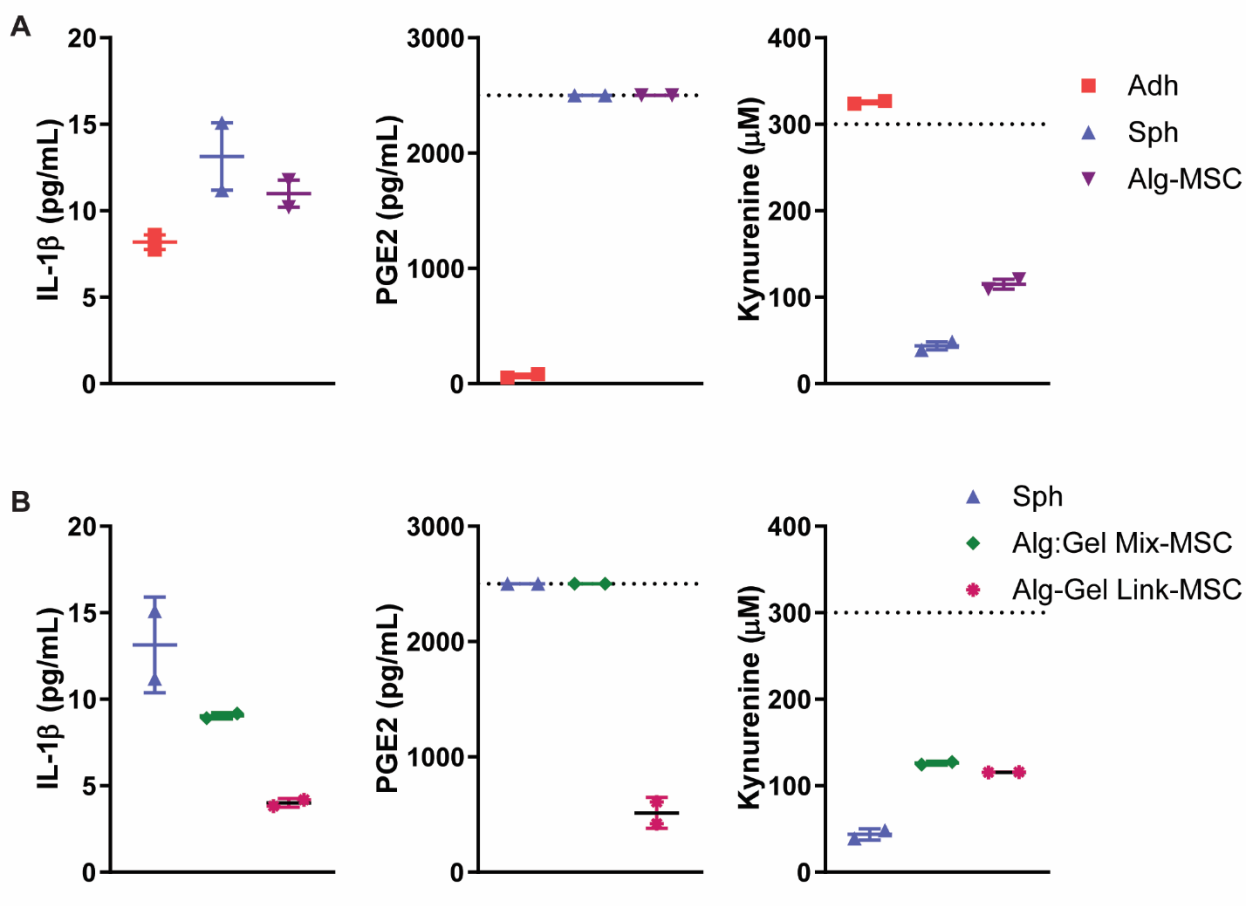

Figure B.2. Alginate encapsulation of MSCs modulates their phenotype.

(A) Measurement of IL-1β, PGE2 and kynurenine production from adherent, spheroid, and alginate encapsulated MSCs after 72 hours of culture with 100 ng/mL IFN. (B) MSCs were encapsulated in alginate covalently linked to alginate (Alg-Gel Link-MSC) or an alginate-gelatin mixture (Alg:Gel Mix-MSCs). MSCs were cultured in IFN-γ containing media for 72 hours prior to analysis of secreted factors.

We next wanted to see if we could further manipulate the phenotype of these alginate encapsulated MSCs to engineer their secretome to look like that of adherent MSCs. We hypothesized that since alginate does not have peptide sequences which allowed for cell attachment, we could provide those sequences by covalently linking alginate chemically to gelatin. We also wanted to control for gelatin alone (not covalently linked) having an effect so we also encapsulated MSCs in an alginate-gelatin mixture. We discovered that while the alginate-gelatin mixture did not produce a large change in the MSC secretome, when gelatin was linked to alginate, there was a dramatic reduction in IL-1β and PGE2 from the alginate-gelatin mixture, but the kynurenine levels remained unchanged (Figure B.2B). Again, we did not obtain a large enough sample size to verify this result through statistical analysis.

Discussion

Prelicensing with inflammatory cytokines like IFN-γ has been used in several MSC systems to increase production of growth factors and anti-inflammatory factors. Previously we have found that while IFN-γ may increase production of anti-inflammatory factors such as kynurenine, in the context of local cryopreserved MSC delivery to treat ischemia/reprofusion injury in the eye, IFN-γ did not increase MSC ability to rescue retinal ganglion cells as described in Chapter 3.4. Consistent with those results, in this study, we saw that IFN-γ prelicencing did not reverse the phenotype change that occurred in spheroids *in vitro*. Therefore, we sought to determine if encapsulation could be used as a bioprocessing method to tune MSC phenotype in local delivery of cells.

Several groups have used biomaterials to deliver MSCs to local environments such as wounds and ischemic limbs. They have shown that these microcarriers can be used to enhance MSC therapeutic effects *in vivo*. Additionally, there is a growing body of literature looking at the use of alginate for encapsulation of MSCs because alginate can be modified to minimize foreign body reactions while protecting MSCs from direct contact and recognition by host immune cells.[10] In our study, we found that in alginate, MSCs secreted factors at similar levels to spheroid MSCs. This alginate environment prevented significant contact between MSCs, therefore it is possible that the lack of attachment factors, material stiffness, the diffusion gradient present within the microcarrier, or factors secreted by dying cells could be responsible for this shift in phenotype. We tested if attachment factors may play a role in this altered

phenotype and found that when alginate was chemically linked with gelatin through an EDC-NHS reaction, this restores some aspects of the secretome observed by adherent MSCs.

Conclusion

More work is needed to determine way to manipulate spheroid MSC phenotype, but we have shown that IFN-γ prelicencing does not increase trophic factors or reduce chemoattractant factors produced by spheroid MSCs. In addition, we have suggested that modified biomaterials can be used to push MSCs to secrete factors like spheroids or preserve their adherent secretome. In different contexts, spheroid and adherent MSC phenotypes may provide benefit in treatment of disease, therefore, there is benefit in determining how direct treatment of MSCs and manipulation with biomaterials can be leveraged to produce these distinct phenotypes.

B.3. REFERENCES

1. Waterman, R. S., Tomchuck, S. L., Henkle, S. L. & Betancourt, A. M. A New Mesenchymal Stem Cell (MSC) Paradigm: Polarization into a Pro-Inflammatory MSC1 or an Immunosuppressive MSC2 Phenotype. *PLoS One* **5**, e10088 (2010).
2. Boland, L. *et al.* IFN-γ and TNF-α Pre-licensing Protects Mesenchymal Stromal Cells from the Pro-inflammatory Effects of Palmitate. *Mol. Ther.* **26**, 860–873 (2018).
3. Ranganath, S. H. *et al.* Controlled Inhibition of the Mesenchymal Stromal Cell Pro-inflammatory Secretome via Microparticle Engineering. *Stem Cell Reports* **6**, 926–939 (2016).
4. Bernardo, M. E. & Fibbe, W. E. Mesenchymal Stromal Cells: Sensors and Switchers of Inflammation. *Cell Stem Cell* **13**, 392–402 (2013).
5. Ryan, J. M., Barry, F., Murphy, J. M. & Mahon, B. P. Interferon-γ does not break, but promotes the immunosuppressive capacity of adult human mesenchymal stem cells. *Clin. Exp. Immunol.* **149**, 353–363 (2007).
6. Prasanna, S. J., Gopalakrishnan, D., Shankar, S. R. & Vasandan, A. B. Pro-Inflammatory Cytokines, IFNγ and TNFα, Influence Immune Properties of Human Bone Marrow and Wharton Jelly Mesenchymal Stem Cells Differentially. *PLoS One* **5**, e9016 (2010).
7. François, M., Romieu-Mourez, R., Li, M. & Galipeau, J. Human MSC Suppression Correlates With Cytokine Induction of Indoleamine 2,3-Dioxygenase and Bystander M2 Macrophage Differentiation. *Mol. Ther.* **20**, 187–195 (2012).
8. Polchert, D. *et al.* IFN-γ activation of mesenchymal stem cells for treatment and prevention of graft versus host disease. *Eur. J. Immunol.* **38**, 1745–1755 (2008).
9. Li, Y. *et al.* Primed 3D injectable microniches enabling low-dosage cell therapy for critical limb ischemia. *Proc. Natl. Acad. Sci.* **111**, 13511–13516 (2014).
10. Veiseh, O. *et al.* Size- and shape-dependent foreign body immune response to materials implanted in rodents and non-human primates. *Nat. Mater.* **14**, 643–651 (2015).
11. Bartosh, T. J., Ylöstalo, J. H., Bazhanov, N., Kuhlman, J. & Prockop, D. J. Dynamic compaction of human mesenchymal stem/precursor cells into spheres self-activates caspase-dependent IL1 signaling to enhance secretion of modulators of inflammation and immunity (PGE2, TSG6, and STC1). *Stem Cells* **31**, 2443–2456 (2013).

12. Guo, L. *et al.* Three-Dimensional Spheroid-Cultured Mesenchymal Stem Cells Devoid of Embolism Attenuate Brain Stroke Injury After Intra-Arterial Injection. *Stem Cells Dev.* **23**, 978–989 (2014).
13. Xu, Y., Shi, T., Xu, A. & Zhang, L. 3D spheroid culture enhances survival and therapeutic capacities of MSCs injected into ischemic kidney. *J. Cell. Mol. Med.* **20**, 1203–1213 (2016).